Seismic Study of Building Frames with Added Energy-Absorbing Devices

by

W.S. Pong[1], C.S. Tsai[2] and G.C. Lee[3]

June 20, 1994

Technical Report NCEER-94-0016

NCEER Task Number 92-5202B

NSF Master Contract Number BCS 90-25010
and
NYSSTF Grant Number NEC-91029

1 Research Assistant, Department of Civil Engineering, State University of New York at Buffalo
2 Research Assistant Professor, Department of Civil Engineering, State University of New York at Buffalo
3 Professor and Dean of Engineering, Department of Civil Engineering, State University of New York at Buffalo

NATIONAL CENTER FOR EARTHQUAKE ENGINEERING RESEARCH
State University of New York at Buffalo
Red Jacket Quadrangle, Buffalo, NY 14261

PREFACE

The National Center for Earthquake Engineering Research (NCEER) was established to expand and disseminate knowledge about earthquakes, improve earthquake-resistant design, and implement seismic hazard mitigation procedures to minimize loss of lives and property. The emphasis is on structures in the eastern and central United States and lifelines throughout the country that are found in zones of low, moderate, and high seismicity.

NCEER's research and implementation plan in years six through ten (1991-1996) comprises four interlocked elements, as shown in the figure below. Element I, Basic Research, is carried out to support projects in the Applied Research area. Element II, Applied Research, is the major focus of work for years six through ten. Element III, Demonstration Projects, have been planned to support Applied Research projects, and will be either case studies or regional studies. Element IV, Implementation, will result from activity in the four Applied Research projects, and from Demonstration Projects.

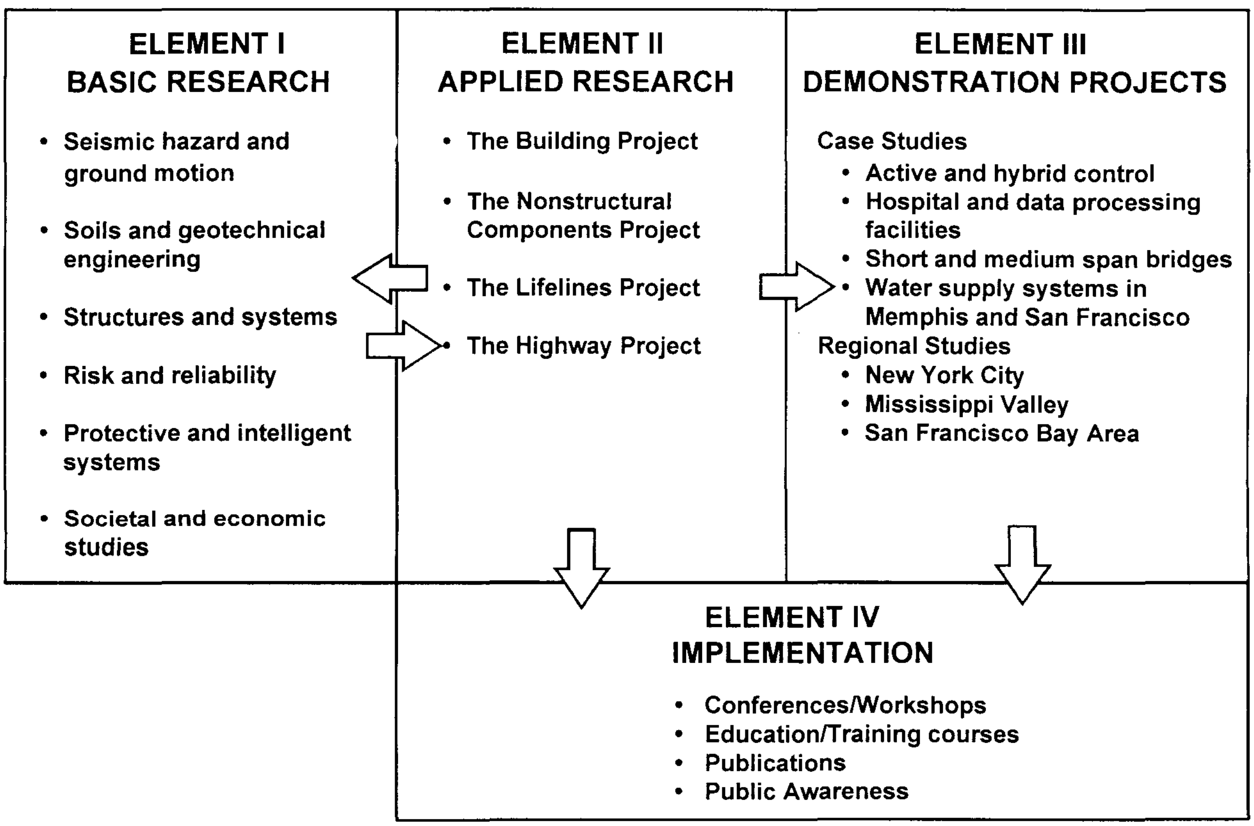

Research in the **Building Project** focuses on the evaluation and retrofit of buildings in regions of moderate seismicity. Emphasis is on lightly reinforced concrete buildings, steel semi-rigid frames, and masonry walls or infills. The research involves small- and medium-scale shake table tests and full-scale component tests at several institutions. In a parallel effort, analytical models and computer programs are being developed to aid in the prediction of the response of these buildings to various types of ground motion.

Two of the short-term products of the **Building Project** will be a monograph on the evaluation of lightly reinforced concrete buildings and a state-of-the-art report on unreinforced masonry.

The **protective and intelligent systems program** constitutes one of the important areas of research in the **Building Project**. Current tasks include the following:

1. Evaluate the performance of full-scale active bracing and active mass dampers already in place in terms of performance, power requirements, maintenance, reliability and cost.
2. Compare passive and active control strategies in terms of structural type, degree of effectiveness, cost and long-term reliability.
3. Perform fundamental studies of hybrid control.
4. Develop and test hybrid control systems.

Passive energy dissipation with building applications is considered in this report. The focus is placed on two combined devices - a combination of tapered-plate energy absorbers (TPEA) and viscoelastic dampers and a combination of TPEA and fluid dampers. Simulation results show that these combined devices can compensate for possible shortcomings associated with each device when used singly and they provide a strong safe-failure mechanism as reliable energy absorbing devices. They also can sustain a wide range of loadings from minor to severe earthquake and wind loads.

ABSTRACT

The concept behind passive vibration control is to add energy dissipating devices to a structure so that energy dissipation can be primarily constrained to the designed location of these passive control devices instead of the main load-carrying members. Since these passive control devices are separated from the main structures, they can be easily replaced if extensively damaged. The use of these energy-absorbing devices to dissipate the seismically induced energy is one of the most economical and effective ways to mitigate the effects of earthquakes on structures.

This report is concerned with a study of two different devices, a combination of tapered-plate energy absorber (TPEA) and viscoelastic dampers and a combination of TPEA and fluid dampers. It starts with a general review of the developments in various energy dissipating devices. Then a finite element formulation for fluid dampers is developed for this study. A comparison is made between numerical solutions and experimental results when a 2/5 scale steel structure is equipped with added viscoelastic dampers. The structural response of high-rise buildings mounted with three energy-absorbing devices, tapered-plate energy absorber (TPEA), viscoelastic dampers, fluid dampers, and two combined devices, TPEA and fluid dampers and TPEA and viscoelastic dampers, respectively, have been investigated. Next, a parametric study of TPEA devices for high-rise buildings is conducted. The selected response parameters in this study include: (1) story shear force; (2) floor displacement; (3) base shear force and (4) ductility ratio.

Finally, two combined devices, TPEA and viscoelastic dampers and TPEA and fluid dampers are examined. Results show such combined devices provide a strong safe-failure mechanism as reliable energy absorbing devices. They also can sustain a wide range of loadings from minor to severe earthquake ground motion and wind loads. The combined devices can compensate for each other's shortcomings so that a satisfactory design for wind loads and seismic hazard mitigation of the structures can be achieved.

ACKNOWLEDGEMENT

The study is jointly supported by the National Science Foundation through the National Center for Earthquake Engineering Research (ECE8607591 and NCEER Project NO. 925202B) and the State University of New York at Buffalo.

TABLE OF CONTENTS

Preceding page blank

TABLE OF CONTENTS (Cont'd)

LIST OF ILLUSTRATIONS

LIST OF ILLUSTRATIONS (Cont'd)

LIST OF ILLUSTRATIONS (Cont'd)

LIST OF ILLUSTRATIONS (Cont'd)

LIST OF ILLUSTRATIONS (Cont'd)

LIST OF ILLUSTRATIONS (Cont'd)

LIST OF ILLUSTRATIONS (Cont'd)

LIST OF ILLUSTRATIONS (Cont'd)

LIST OF ILLUSTRATIONS (Cont'd)

LIST OF ILLUSTRATIONS (Cont'd)

LIST OF ILLUSTRATIONS (Cont'd)

LIST OF ILLUSTRATIONS (Cont'd)

LIST OF TABLES

SECTION 1
Introduction

1.1 Background and Motivation

Earthquakes strike with little notice, often with severe ground shaking, claiming many lives and causing much damage to property every year. The design and construction of earthquake-resistant structures has been a continuous goal of researchers and structural engineers.

The Mexico City earthquake on September 19, 1985 caused over 10,000 deaths from building failures and at least 100,000 persons were left homeless. More than 400 buildings were destroyed and an additional 3200 buildings were damaged in this populous city. The resulting economic loss was measured at four billion dollars; this tremendous damage was done in only three minutes [1]. The Richter magnitude of the Mexico City earthquake was 8.1. The earthquake contained at least 20 sustained cycles of vibration with a dominant period of about two seconds. Ground accelerations ranged from 5 to 20 percent of gravity in a period range of 1.5 to 3 seconds [68]. The sustained shaking continued for about three minutes. Because of the long duration of this shaking, deep soil deposits were excited resulting in amplified ground movements.

Two major dams, La Villita and El Infiernillo, the latter holding one of the world's largest reservoirs, were within 70 km of the epicenter. La Villita has a height of 60 m and an impoundment of 710,000,000 m^3 and El Infiernillo has a height of 146 m and an impoundment of 12,000,000,000 m^3. Both dams were built with the knowledge that a magnitude 8 earthquake was expected to occur [1]. The dams survived the earthquake with only cosmetic damages, which demonstrates that engineers can design and construct safe structures to withstand severe earthquakes.

1.2 Essence of Conventional Seismic Design

A basic principle in structural design against severe earthquakes is to allow the structure to absorb and dissipate energy through ductility. Ductility is obtained in typical civil engineering structures through inelastic deformation of the material developed in carefully chosen regions. However, ductile structures can result in very large inelastic deformations so that they may not be used after the earthquake from the viewpoints of cost and safety. In recent years, more emphasis has been given to the development of cost effective devices for dissipating seismically induced energy in the structure while keeping the structure's responses as much as possible in the elastic range of the material.

1.3 Essence of Structural Control

To add energy dissipating devices to a structure or to isolate the structure from earthquake ground motion is generally known as structural control. Considerable progress has been made over the last two decades in structural control. Based on the nature that the energy is dissipated, two control systems are categorized: passive control and active control [59]. Some of the specific structural control approaches are briefly reviewed in the following sections.

The amount of energy imparted to a structure depends on several factors, some of which are related to the characteristics of the ground motion, such as its amplitude and frequency content. Others are related to the properties of the structure, such as natural period, damping and resistance (or load-deformation) properties [76].

To facilitate subsequent discussion, the amount of input energy imparted to a structure from earthquake ground motion E_I [2] is expressed as

$$E_I = E_K + E_S + E_H + E_\xi = E_E + E_D \tag{1.1}$$

where, E_K is the absolute kinetic energy, E_S is the elastic strain energy, E_H is hysteretic energy dissipated by the structural system through inelastic or other actions, and E_ξ is the energy of viscous damping. E_E is the elastic vibrational energy which is the sum of E_K and E_S. E_D is the dissipated energy which is the sum of E_H and E_ξ. From Eq.(1.1), the use of supplemental damping devices can increase the energy dissipation capacity, E_D, so that the response of the building during the earthquake can be improved.

1.3.1 Active Control

An active control system relies on the ability to reuse the response information of the structure and the availability of an external energy supply that can generate corrective forces to reduce the undesirable responses [3]. These devices include the Active Mass Damper (AMD), Active Tendons (AT), and Active Variable Stiffness (AVS). The ground acceleration and the system's response (displacement, velocity, and acceleration) at chosen locations are continuously monitored and the control forces are properly applied to the structure through actuators [4,5]. An active control system can change the dynamic characteristics of a structure. Compared to passive control systems, an active system is a more flexible strategy, but considerable further studies are required before it can be used in routine engineering practice.

An active structural control device with a linear optimal feedback control algorithm has been tested experimentally using tendon control [6]. On the basis of the analytical and experimental studies carried out thus far, one may conclude that active control has the potential to be a successful structural control method for seismic hazard mitigation, particularly when it is used in conjunction with a passive device (hybrid control). Two active mass driver systems were installed at the top of a 10-story office building in 1989 [7,8]. Such AMD system is also very effective in reducing vibrations induced by wind [9]. In 1990, a full-scale active bracing system (ABS) was designed and installed in a dedicated test structure for performance verification of the system under actual seismic ground motions [70]. The observed performance of the full-scale active bracing system shows that significant strides have been made in the implementation of active control technology.

1.3.2 Passive Control

The concept behind passive control is to add energy dissipating devices to a structure. These passive devices can be easily replaced if extensively damaged. Base isolation, suitable for lighter structures, and energy-absorbing devices are the two major passive control systems.

1.3.2.1 Base Isolation Systems

It is generally accepted that a base-isolated building can perform better than a conventional fixed-base building during moderate or strong earthquakes. The most important feature of seismic isolation is that its added flexibility increases the natural period of the structure. Because the period is increased beyond that of the earthquake, resonance can be avoided and the seismic acceleration response is reduced [10].

Base isolators for buildings are typically shock-absorbing bearings placed between the base plates and columns. They are stiff enough to support the vertical load transmitted by the column; but, they are horizontally flexible enough to absorb energy generated by earthquake ground movements. A building built on an isolation system should have a lower fundamental frequency than both the fixed-base frequency of the structure and the dominant frequency of the ground motion [11].

Most deformations of a base-isolated structure are attributed to the first mode of the isolated structure. The higher modes, causing deformation of the structure, are orthogonal to the first mode, and thus to the ground motion. As a result, if there is high energy in the ground motion at the frequencies corresponding to the higher mode, the energy cannot be imparted to the structure. In this way, the demand on the structural system is minimized and acceleration transmitted to the internal non-structural components can be also reduced [12]. Base isolators also provide additional damping to the structure. Normally, the acceleration response of the structure is also reduced. The number of base-isolated structures has grown considerably over the last decade. The most widespread use of the base isolation approach is in Japan. The first application of base isolation in the U.S. was the Foothills Community Law and Justice Center, completed in 1985.

1.3.2.2 Energy-Absorbing Devices

The use of energy-absorbing devices to dissipate the seismically induced energy is considered to be one of the most economical and effective ways to mitigate the effects of earthquakes on buildings.

In recent years, many efforts have been given to the development of energy dissipating devices by various investigators. Relatively speaking, the development of energy absorbing devices is behind that of the base isolation techniques. A more general understanding of the dynamic response of the structures implemented with energy absorbing devices need to be further advanced.

1.4 Practical Development of Energy-Absorbing Devices

Many energy-absorbing devices have been proposed and studied for possible applications for seismic mitigation of buildings. Some of the major energy-absorbing devices currently in use include friction dampers [13,14,15,16,60], metallic energy absorbers [17, 18, 19, 20, 21,22,61], fluid dampers [23,62], and viscoelastic dampers [24, 25, 26, 27, 28,63]. Some of these energy-absorbing devices are briefly reviewed in the following subsections.

1.4.1 Friction Dampers

The study of frictional damping elements for a variety of structural systems, ranging from braced frames [29] to concrete shear wall [30] and panelled structures [31], equipped with damping elements, was first carried out by Pall [29,30,31]. Frictional damping elements have the advantage of being adaptable to a particularly simple form of mechanical modeling and their responses should be repeatable. Furthermore, they are fatigue resistant [14].

Although reductions in story shear force are moderate, by using friction dampers, a large portion of the base shear force can be resisted by bracing or secondary members of the structure in a controlled manner. Friction dampers have unique characteristics. Their behavior is relatively less affected by the amplitude and frequency of the earthquakes, variations in temperature or the number of applied loading cycles [32]. Experimental studies by Filiatrault and Aiken demonstrated that friction devices can improve the seismic resistance of conventional structures with little maintenance [33,34]. Adopting friction dampers as a seismic support for the piping system in nuclear power plants was proposed by Japanese researchers [35]. Their studies revealed the following: (1) the dissipated energy increases proportionally with increases in the exciting displacement. Further, the damping ratio also increases within certain ranges of excitation level; (2) the friction damper can greatly increase the damping of piping systems in nuclear power plants compared to conventional supports such as snubbers; and (3) the friction damper has the potential to be an economical energy-dissipating device for buildings.

1.4.2 Metallic Energy Absorbers

Using metallic energy absorbers amounts to utilizing the ductile behavior of the material concentrated at selected locations of the structure. The resisting force of metallic energy absorbers depends on the nonlinear stress-strain characteristics and geometrical configuration of the material. The two most commonly used materials are mild steel and lead [36]. The steel-plate energy device was first adopted for piping applications in nuclear power plants [18]. Many subsequent studies show that these energy absorbing devices can be applied to improve the seismic resistance of high-rise buildings and other structures. There are several advantages for using these devices to resist earthquake damages: (1) energy dissipation can be constrained to the location of the devices; (2) the main structure can resist earthquake loads under simpler and less severe conditions; (3) a more economical cost is possible in both the design and construction process; (4) a substantial reduction in the energy dissipation demands on the structure; (5) the device can be replaced easily; and (6) these devices can provide the building with stiffness and strength as well as increased energy dissipation capacity.

Extensive experimental tests conducted by Whitaker, et al. [20], indicated that all the tested devices exhibited stable hysteretic behavior without any signs of pinching or stiffness and strength degradation for displacement amplitudes of up to $13.6\Delta_y$, where Δ_y is the yield displacement of the devices. The tests also demonstrated that the devices can sustain an extremely large number of yielding reversals (more than 100 cycles) and accumulate a large amount of plastic deformation without any sign of degradation. The devices were also shown to increase the stiffness and strength of the frames. But the most significant feature of the devices mounted to the test structure was increasing the structure's energy dissipation capacity. These results confirm that the steel-plate energy devices are suitable for use not only in retrofitting flexible ductile moment resisting space frames, but also in the construction of new buildings in regions of high seismic risk.

The tapered-plate energy absorber (TPEA) shown in Figure 1-1 [66] is currently under study by a cooperative research program between State University of New York at Buffalo and the National Taiwan University. The TPEA devices are triangular shaped [22,49]. The advantages of triangular shaped steel-plate energy dissipation devices over rectangular shaped devices can be clearly observed in Figure 1-2 [37]. For rectangular plates, the plastic deformation is limited to occur at a finite region at the ends. The curvature is uniform over the height when a finite displacement is imposed at the top of the triangular plate (see Figure 1-3). Therefore, the yielding occurs simultaneously in the entire plate without curvature concentrations. Because the bending moment at the free end of the plate is equal to zero, a more simplified design of the braces supporting the energy-absorbing devices is possible [66].

1.4.3 Viscoelastic Dampers

The application of viscoelastic material to vibration control has a long history, dating back to the mid-1950's. It was first used on aircraft to control the vibration-induced fatigue of air frames [38,39,40]. Applications of viscoelastic dampers to civil engineering structures began about 20 years later. Civil structures often require 10 to 20% of critical damping while aerospace structures usually need 5 to 6% of critical damping [39,40]. Therefore, effective use of the viscoelastic material is important in vibration reduction in civil engineering structures.

Viscoelastic (VE) dampers are normally made of viscoelastic layers bonded to steel plates under direct shear to dissipate input energy [26,41]. A viscoelastic (VE) material acts partly as a viscous material which dissipates energy and partly as an elastic material which stores energy. Figure 1-4 shows a currently used VE damper which is comprised of two viscoelastic layers bonded by three parallel rigid surfaces [74]. The VE materials are acrylic copolymers manufactured by the 3M Company.

The 3M materials are known to be very stable with acceptable aging properties. They are resistant to environmental pollutants. It has been shown that mounting VE dampers to a structure can be an effective method to reduce wind-induced sway of high-rise buildings [24,42]. The World Trade Center in New York City and the Columbia Center and the Number Two Union Square Building in Seattle are examples. VE dampers are relatively efficient in most high energy damping applications. Recent research [25,26,27,28,43] has demonstrated that VE dampers may also be suitable for enhancing the seismic resistance of buildings if equipped properly.

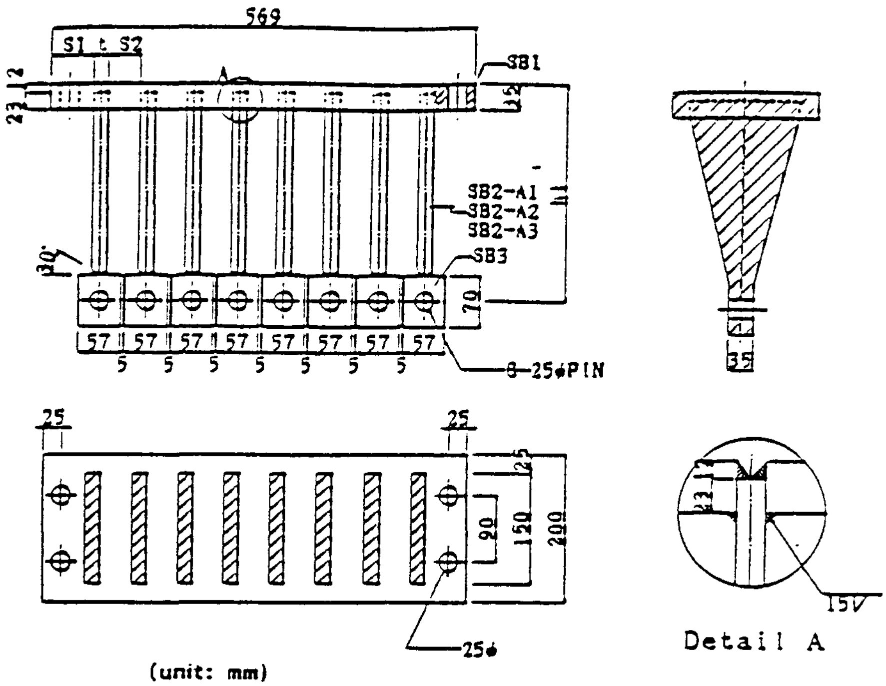

FIGURE 1-1 Details of Specimen [66]

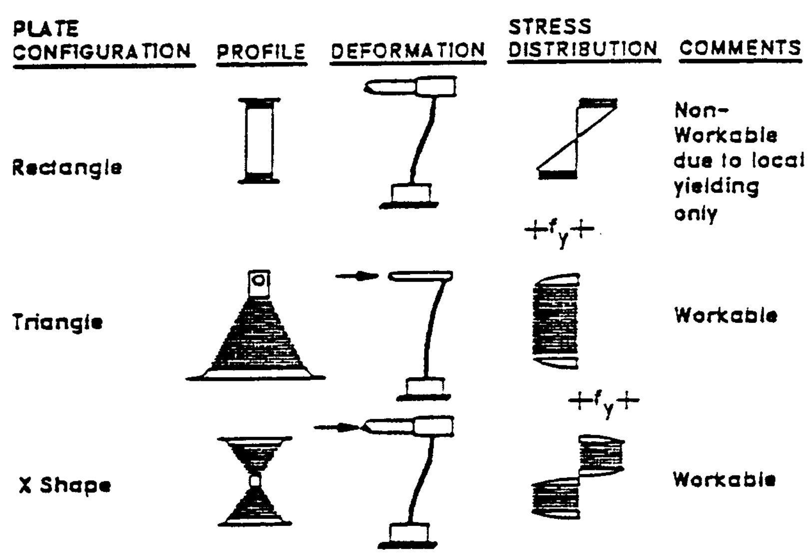

FIGURE 1-2 Steel Plate Energy Absorbers [37]

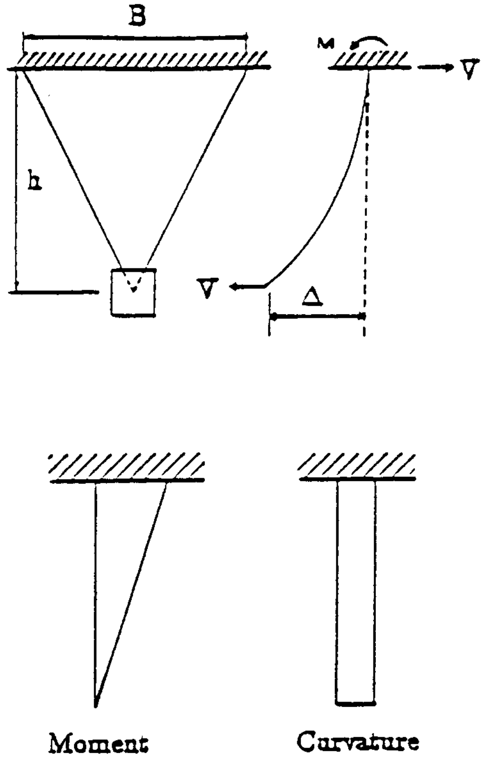

FIGURE 1-3 Basic Behavior of a Triangular Plate Under Load [66]

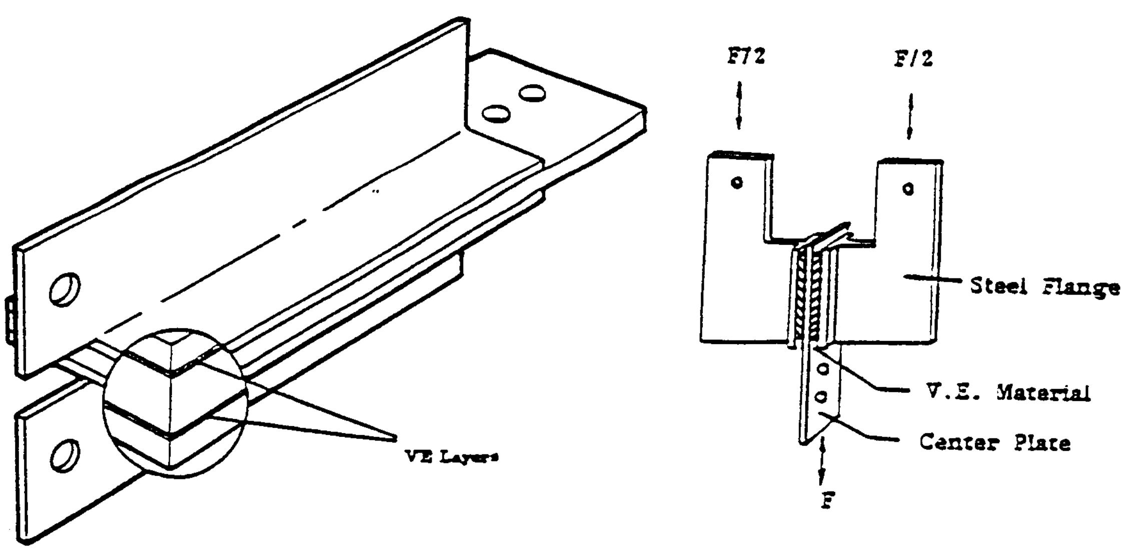

FIGURE 1-4 Typical Viscoelastic Damper Configuration [74]

The number and the thickness of layers, and the cross-section area of the VE dampers determine the amount of damping provided. The location of dampers is a crucially important issue in the design, which is not clearly understood at present. The results of a shaking table test by Chang et al. [43] show that the behavior of the VE damper is dependent on the ambient temperature. Test results, without concerning the locations and numbers of dampers, indicate that, in general, VE dampers are very effective in reducing excessive vibration of the test structure due to seismic excitations. However, the viscoelastic material softens and the effectiveness of the dampers decreases as ambient temperature increases [43].

1.4.4 Fluid Viscous Dampers

Fluid viscous damping devices originated in the early 1960's for use in steel mills as energy absorbing buffers on overhead cranes. Variations of these devices were used as canal lock buffers, as leg suspensions for offshore oil rigs, and mostly as shock isolation systems for aerospace and military hardwares [23]. Recently, there have been several large scale applications of these devices. In the West Seattle Swing Bridge, fluid dampers with a built-in hydraulic logic system provide damping at two predetermined levels. The logical system can determine whether the bridge condition is normal or faulty. The devices have also been installed at the New York Power Indian Point 3 Nuclear Power Plant. Each nuclear generator is connected to the containment building walls by eight fluid dampers of 300 Kips (1.34 MN) each. The dampers have been specially designed for seismic pulse attenuation. The dampers at the Virginia Power North Ana Nuclear Station have 2000 Kips (8.92 MN) capacity and function the same as those at the Indian Point 3 Plant. This type of device has also been used to suppress the wind-induced vibration of launching platforms, such as those for the space shuttle and the Atlas Missile. The dampers' linear viscous behavior and independence over a wide temperature range (-40^{o}C to 70^{o}C) are the two favorable characteristics in seismic design of structures.

Constantinou et al. [23] conducted an experimental study of fluid dampers during which several conclusions were reached. First, fluid viscous dampers may be designed to exhibit an essentially linear viscous behavior for motion frequencies below a certain cutoff frequency. It was also shown that fluid dampers may be modeled as simple linear viscous dampers. The study also revealed that temperature has a minor effect on the mechanical behavior of the fluid dampers that were tested. It was shown that fluid dampers can provide a structure with supplemental damping to enhance its structural seismic resistance. Finally, Constantinou's study proved that fluid dampers reduce drifts and column bending moments because of their viscous nature. At the same time, additional column axial forces, out-of-phase with the bending moments, are introduced. This behavior is beneficial to retrofit applications by preventing the possibility of compression failure of weak columns.

1.5 Objectives

Three energy-absorbing devices, the viscoelastic dampers, the fluid dampers and the TPEA devices were selected for this numerical study of structural response. Two combined systems, TPEA and viscoelastic dampers and TPEA and fluid dampers are examined.

The main objectives of this study are:

(1) Parametric study of a 10-story building frame with fluid dampers, viscoelastic dampers and TPEA devices, respectively.

(2) Investigate the response of the structure equipped with a combination of TPEA and fluid dampers.

(3) Investigate the response of the structure equipped with a combination of TPEA and viscoelastic dampers.

1.6 Scope of Work

The following tasks were carried out:

(1) a finite element formulation for structures equipped with fluid dampers was developed.

(2) a parametric study of a 10-story building frame implemented with fluid dampers.

(3) a parametric study of the same 10-story building frame implemented with viscoelastic dampers.

(4) a comparison between numerical study and experimental results of the structure equipped with viscoelastic dampers.

(5) the effect of stiffness ratio of TPEA on the dynamic response of the 10-story building frames.

(6) the effect of stiffness ratio of braces which support the TPEA devices.

(7) a comparison between a frame with TPEA and a frame with a simple bracing whose stiffness is the same as that of the TPEA.

(8) a numerical study of the 10-story building frame equipped with a combination of TPEA and fluid dampers.

(9) a numerical study of the 10-story building frame equipped with a combination of TPEA and viscoelastic dampers.

A finite element formulation of fluid dampers is developed for the numerical study of the structure equipped with fluid dampers in the first part of Section 2. The seismic behavior of a 10-story building frame equipped with fluid dampers is also presented in Section 2. An analytical model and a finite element program of VE dampers are described first, then the seismic study of the same 10-story building frame equipped with VE dampers is presented in the latter part of Section 2. Section 3 presents the adopted analytical model of TPEA devices and the development of a finite element program of TPEA. It briefly describes the seismic response analysis of a high-rise building equipped with TPEA, where it is shown: (1) the TPEA provides a strong safe failure mechanism; (2) maximum base shear force, roof displacement, and maximum story drifts are significantly reduced by adding TPEA devices to the structure; and, (3) a preliminary study on the location of the TPEA devices. A numerical study of the same frame equipped with viscoelastic dampers is compared to experimental results. Section 4 investigates the response of the structure equipped with a combination of TPEA and VE dampers and a combination of TPEA and fluid dampers. Design implications of the energy-absorbing devices are made at the end of this section. Finally, Section 5 is the summary and conclusions.

SECTION 2
Seismic Study of High-Rise Buildings with Fluid Dampers and with Viscoelastic Dampers

2.1 Current Status of Fluid Dampers Development

Fluid viscous damping devices originated in the early 1960's for use in steel mills as energy absorbing buffers on overhead cranes. Variations of these devices were used as canal lock buffers, as leg suspensions for offshore oil rigs, and mostly as shock isolation systems for aerospace and military hardware [23]. Fluid viscous dampers [23] have been adopted for some large scale applications. Its linear viscous behavior and independence over a wide temperature range (-40°C to 70°C) are the two major characteristics of interest in applications of seismic study.

2.1.1 Description of Fluid Dampers

The fluid damping device under investigation by Constantinou, et al., [23] is shown in Figure 2-1. The device, filled with silicon oil, consists of a stainless steel piston with a bronze orifice head and an accumulator. The fluid damper generates a proportional damping force because a pressure volume is produced by the product of travel distance and piston rod area. The fluid is compressible and also the reduction in fluid volume is accompanied by the development of a resisting (spring-like) force. This is prevented by the use of the accumulator. In Constantinou's study, the tested device showed no measurable stiffness for piston motions with frequency less than about 4 Hz. The cutoff frequency is considered a desirable asset for an energy-absorbing device because additional viscous damping may be provided to the first mode and additional stiffness and damping to the higher modes of the structure resulting in the reduction of the structural response.

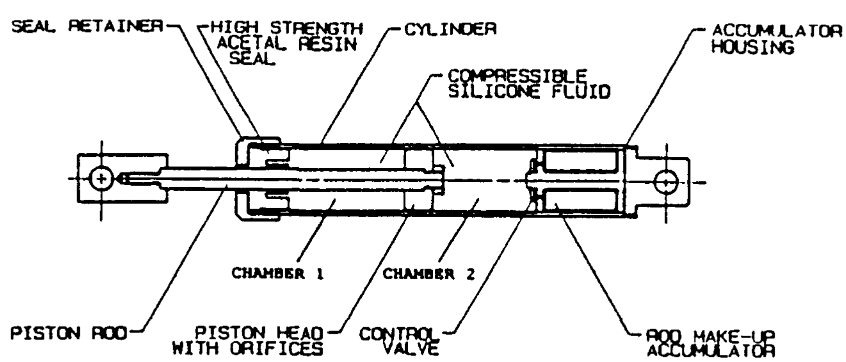

FIGURE 2-1 The ConStruction of the Fluid Viscous Damper [62]

2.1.2 Analytical Model for Fluid Viscous Dampers

The fluid damper exhibits viscoelastic fluid behavior over a large frequency. The simplest model to simulate the mechanical behavior of the fluid viscous damper is the Maxwell model [53] given by

$$P + \lambda \dot{P} = C_o \dot{U} \tag{2.1}$$

where λ is the relaxation time, C_0 is the damping constant at zero frequency, P is the damping force, $\dot{U}$ is the damper position velocity.

A more general Maxwell model may also be considered where the derivatives are of fractional order [54]

$$P + \lambda D^r P = C_o D^q U \tag{2.2}$$

where $D^r f(t)$ is the fractional derivative of order r of the time dependent function f. Eq.(2.2) may provide better results than Eq.(2.1) in simulating the mechanical behavior of complex fluid

dampers. Due to the assumption that the damping coefficient is independent of the velocity over a wide range of values, the parameter q can be set equal to 1. For q=1, the parameter C_0 is the damping constant at zero frequency. If r is also set equal to one, Eq.(2.2) is equal to Eq.(2.1).

2.2 Finite Element Formulation for Fluid Dampers

For convenience, mathematical models for fluid dampers should be easily implemented in computer programs to facilitate their use in engineering practice. Towards this end, a finite element formulation for the fluid dampers is developed and is described in this section.

The global coordinate system x, y, and z, and the local coordinate system ξ, ζ, and η, are depicted in Figure 2-2.

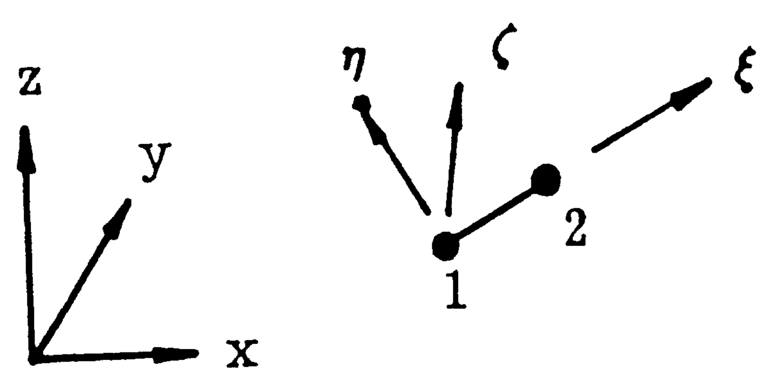

FIGURE 2-2 Two-Node Element

In order to generalize the formulation, dampers are assumed to be applied in the three local directions ξ, ζ, and η, respectively, although only one direction of the dampers along ξ axis was used in the numerical examples. The global displacements at nodal points 1 and 2 shown in Figure 2-2 are $\mathbf{D}_1$(t) and $\mathbf{D}_2$(t), respectively. These global displacements are expressed as

$$\mathbf{D}_1(t) = \begin{bmatrix} u_1(t) \\ u_2(t) \\ u_3(t) \end{bmatrix} \tag{2.3}$$

and

$$\mathbf{D}_2(t) = \begin{bmatrix} u_4(t) \\ u_5(t) \\ u_6(t) \end{bmatrix} \tag{2.4}$$

where u_1(t), u_2(t), and u_3(t) are global displacements at nodal point 1 in the x, y, and z directions, respectively, and u_4(t), u_5(t), and u_6(t) are those at nodal point 2, respectively.

As shown in Figure 2-2, the displacement in local coordinate system. $\bar{\mathbf{D}}_1(t)$, and $\bar{\mathbf{D}}_2(t)$ are expressed as

$$\bar{\mathbf{D}}_1(t) = \mathbf{R}\mathbf{D}_1(t) \tag{2.5}$$

and

$$\bar{\mathbf{D}}_2(t) = \mathbf{R}\mathbf{D}_2(t) \tag{2.6}$$

where R is a transformation matrix related to the local and global coordinate systems. The relative displacements, $\bar{\mathbf{U}}(t)$, between two nodal points 1 and 2 in the local coordinate system ξ, ζ, and η, are defined as

$$\bar{\mathbf{U}}(t) = \bar{\mathbf{D}}_2(t) - \bar{\mathbf{D}}_1(t) = \mathbf{R}\mathbf{D}_2(t) - \mathbf{R}\mathbf{D}_1(t) \tag{2.7}$$

Eq.(2.7) can be rewritten as

$$\bar{\mathbf{U}}(t) = \mathbf{B}\mathbf{U}(t) \tag{2.8}$$

where

$$\mathbf{B} = [-R,R] \tag{2.9}$$

$$\mathbf{U}(t) = \begin{bmatrix} \mathbf{D}_1(t) \\ \mathbf{D}_2(t) \end{bmatrix} = \begin{bmatrix} u_1(t) \\ u_2(t) \\ u_3(t) \\ u_4(t) \\ u_5(t) \\ u_6(t) \end{bmatrix} \tag{2.10}$$

and

$$\mathbf{U}(t) = \begin{bmatrix} U_\xi(t) \\ U_\zeta(t) \\ U_\eta(t) \end{bmatrix} \tag{2.11}$$

Therefore, the relative velocity between points 1 and 2, $\dot{\mathbf{U}}(t)$ can be given a

$$\dot{\mathbf{U}}(t) = \frac{\partial \mathbf{U}(t)}{\partial t} = \mathbf{B}\frac{\partial \mathbf{U}(t)}{\partial t} = B\begin{bmatrix} \dfrac{\partial \mathbf{D}_1(t)}{\partial t} \\ \dfrac{\partial \mathbf{D}_2(t)}{\partial t} \end{bmatrix} \tag{2.12}$$

As a result

$$\dot{\mathbf{U}}(t) = \mathbf{B}\dot{\mathbf{U}} = \mathbf{B}\begin{bmatrix} \dot{u}_1(t) \\ \dot{u}_2(t) \\ \dot{u}_3(t) \\ \dot{u}_4(t) \\ \dot{u}_5(t) \\ \dot{u}_6(t) \end{bmatrix} \tag{2.13}$$

The model for fluid dampers is

$$\mathbf{P}(t) + \lambda\dot{\mathbf{P}}(t) = C_0\dot{\mathbf{U}}(t) \tag{2.14}$$

If linear variation between two time steps, $(n-1)\Delta t$ and $n\Delta t$, is assumed, then the order one fractional derivation of the damping force can be expressed as

$$\dot{\mathbf{P}}(t) = \frac{\mathbf{P}(t) - \mathbf{P}_{n-1}(t)}{\Delta t} \tag{2.15}$$

Applying Eq.(2.15) into Eq.(2.14), one obtains

$$\mathbf{P}(t) + \frac{\lambda}{\Delta t}(\mathbf{P}(t) - \mathbf{P}_{n-1}(t)) = C_o\dot{\mathbf{U}}(t) \tag{2.16}$$

Reorganizing Eq.(2.16), one obtains

$$\left(1 + \frac{\lambda}{\Delta t}\right)\mathbf{P}(t) = C_o\dot{\mathbf{U}}(t) + \frac{\lambda}{\Delta t}\mathbf{P}_{n-1}(t) \tag{2.17}$$

Then

$$\mathbf{P}(t) = \frac{C_o}{1 + \dfrac{\lambda}{\Delta t}}\dot{\mathbf{U}}(t) + \frac{\lambda}{\Delta t}\frac{1}{1 + \dfrac{\lambda}{\Delta t}}\mathbf{P}_{n-1}(t) \tag{2.18}$$

Substitution of Eq.(2.13) into Eq.(2.18) yields

$$\mathbf{P}(t) = \frac{C_o}{1+\frac{\lambda}{\Delta t}}\mathbf{B}\dot{\mathbf{U}}(t) + \frac{\lambda}{\Delta t}\frac{1}{1+\frac{\lambda}{\Delta t}}\mathbf{P}_{n-1}(t) \tag{2.19}$$

Using the virtual work principle, one obtains the equivalent nodal forces, F(t).

$$\mathbf{F}(t) = \mathbf{B}^T\mathbf{P}(t) = \frac{C_o}{1+\frac{\lambda}{\Delta t}}\mathbf{B}^T\mathbf{B}\dot{\mathbf{U}}(t) + \frac{\lambda}{\Delta t}\frac{1}{1+\frac{\lambda}{\Delta t}}\mathbf{B}^T\mathbf{P}_{n-1}(t) \tag{2.20}$$

Introducing a matrix, $\mathbf{C}_f$, as the added damping resulting from fluid dampers, Eq.(2.20) can be rewritten as:

$$\mathbf{F}(t) = \mathbf{C}_f\dot{\mathbf{U}}(t) + \frac{\lambda}{\Delta t}\frac{1}{1+\frac{\lambda}{\Delta t}}\mathbf{B}^T\mathbf{P}_{n-1}(t) \tag{2.21}$$

where

$$\mathbf{C}_f = \frac{C_o}{1+\frac{\lambda}{\Delta t}}\mathbf{B}^T\mathbf{B} \tag{2.22}$$

2.3 A 10-Story Building

A 10-story moment resistant steel frame is shown in Figure 2-3. Both the columns and beams have an elastic modulus and Poisson's ratio equal to $3\text{x}10^7$ psi and 0.3, respectively. The weight of each floor is 25.47 lbs/in. In the analysis, it was assumed that the floors were rigid in their own plan. Three different ground motions are imposed in the lateral direction to the 10-story building. The three selected motion records, shown in Figures 2-4 to 2-6, include the 1940 El Centro Earthquake, the 1971 San Fernando Earthquake, and 1952 Taft Earthquake.As shown in Figure 2.7, fluid dampers are installed on each floor and supported by Chevron braces.

2.4 Design Parameters of Fluid Dampers

The parameters of this study are the number, the position, and the damping coefficient of the fluid dampers. The selected response parameters include: (1) the story shear force, which is the total shear shared by the fluid viscous dampers and the frame; and (2) the floor displacement. The unit of displacement is the inch and the unit of shear force is pounds in all the figures. Table 2-I defines the symbols which represent the selected conditions. For example, if the number of the fluid viscous dampers was selected as 10, 5, 3, 1, they were assigned FD10, FD5, FD3, FD1, respectively. 2FD5(1) means two dampers were mounted at floors 1,2,3,4,5.

2.4.1 The Effect of Damping Coefficients

According to Eq.(2.1), it can be noted that the damping coefficient is a major factor for deciding damping force values. A properly selected damping coefficient can help fluid dampers achieve optimal performance. Figures 2-8 and 2-9 indicate that the curve of roof displacement

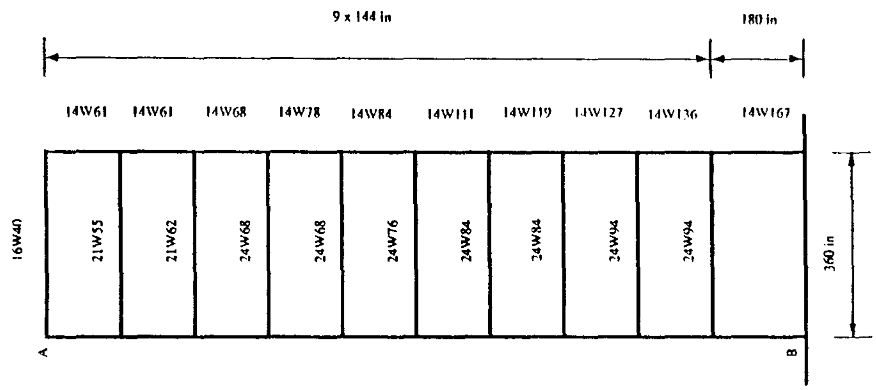

FIGURE 2-3 A 10-Story Building

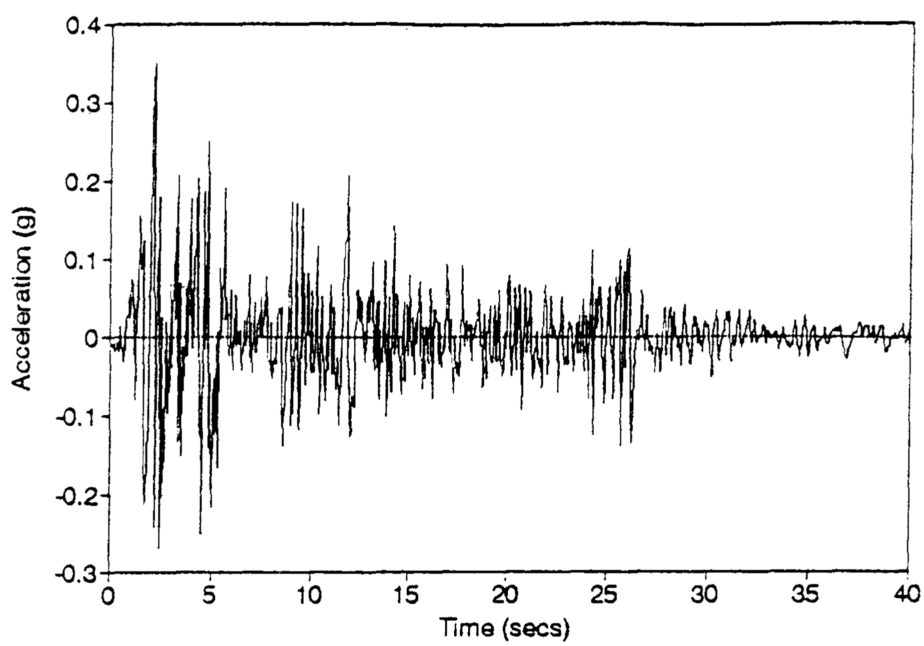

FIGURE 2-4 Component of Ground Motion, El Centro (1940)

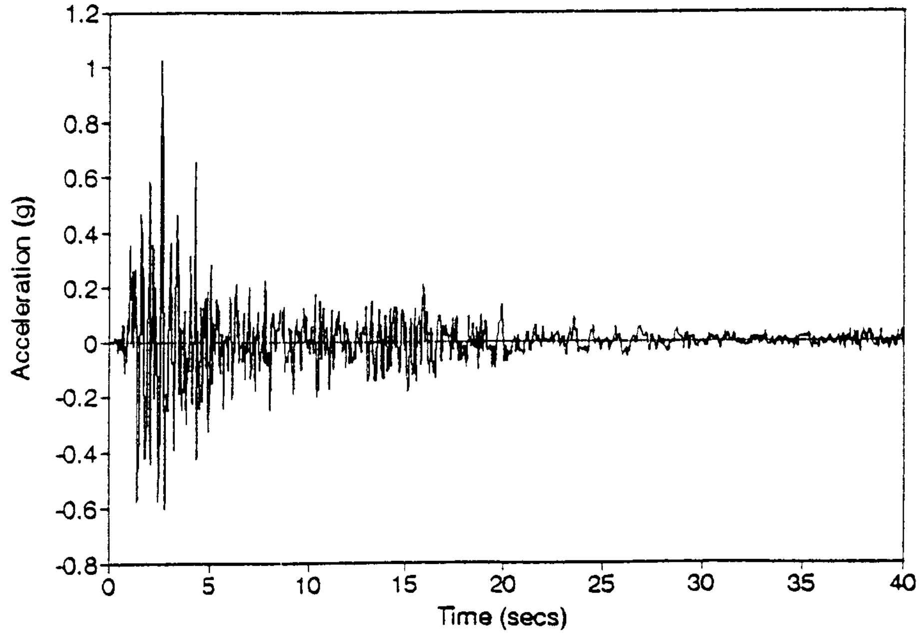

FIGURE 2-5 Component of Ground Motion, San Fernando (1971)

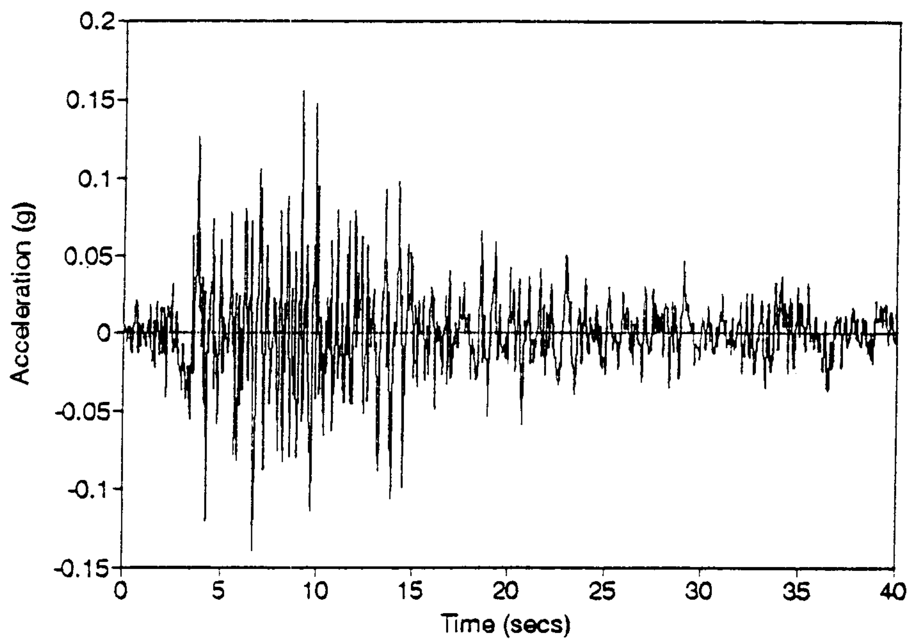

FIGURE 2-6 Component of Ground Motion, Taft (1952)

TABLE 2-I The Explanations of the Symbols

Symbols	Explanations
FD10	Each floor was mounted with a fluid damper
2FD10	Each floor was mounted with wo fluid dampers
FD5(1)	Floors 1,2,3,4,5 were mounted with a fluid damper
2FD5(1)	Floors 1,2,3,4,5 were mounted with two fluid dampers
FD5(2)	Floors 1,3,5,7,9 were mounted with a fluid damper
2FD5(2)	Floors 1,3,5,7,9 were mounted with two fluid dampers
FD1	Floor 1 was mounted with a fluid damper
2FD1	Floor 1 was mounted with two fluid dampers

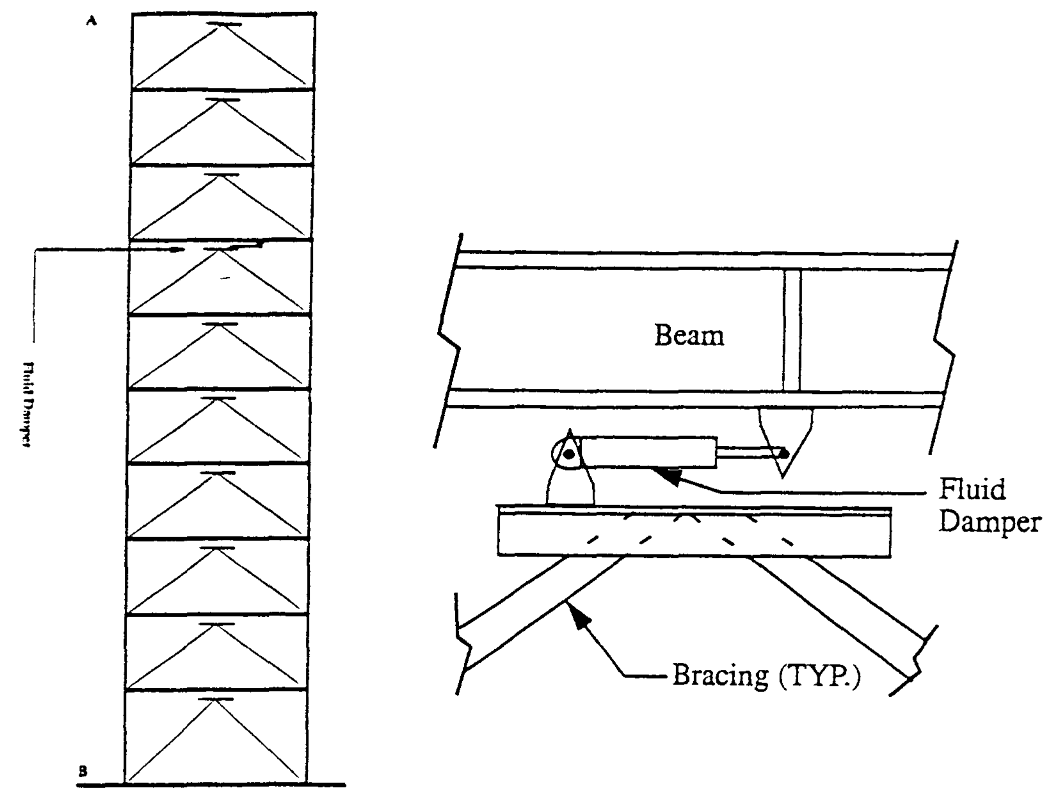

FIGURE 2-7 A 10-Story Building with Proposed Arrangement of Fluid Dampers

decreases while the damping coefficient increases. Because the resisting force of the fluid damping is proportional to the damping coefficient, increasing the damping coefficient increases the damping force so that the roof displacement decreases. Results also show that very small values of damping coefficient could reduce the roof displacement greatly compared to the structure without any device. The time-history response (roof displacement, shear force at column point B, and base shear force) of the structure, with and without fluid dampers, were compared in Figures 2-10 to 2-18 when the values of the damping coefficient, 600 lb-sec/in, 2400 lb-sec/in, and 4800 lb-sec/I, respectively, were adopted to the fluid dampers during the selected ground motions. In Figure 2-10, the structure with fluid dampers has the same number of cycles as the structure without fluid dampers in the same period of time. It can be said that adding fluid dampers to the structure does not change the structure's natural frequency. Furthermore, fluid dampers cannot provide supplemental damping to the structure in the earliest stages of the earthquake excitation. Thus, Figure 2-10 shows that the roof displacement of the structure equipped with fluid dampers is not reduced during the initial ground motion of a seismic event. The addition of damping from fluid dampers eventually increases the structure's energy dissipation capacity so that the roof displacement is significantly reduced after a few cycles of earthquake excitation. The results indicate that the structure with fluid dampers of high damping coefficient has better performance in seismic resistance. But the manufacturing costs of a fluid damping device designed to achieve a higher damping coefficient would be greater. Therefore, selection of a proper damping coefficient plays a major role in seismic design. As shown in Figures 2-10 to 2-18, it can be seen that the damping value of 2400 lb-sec/in reduces about 50% of the roof displacement compared to the structure without fluid dampers.

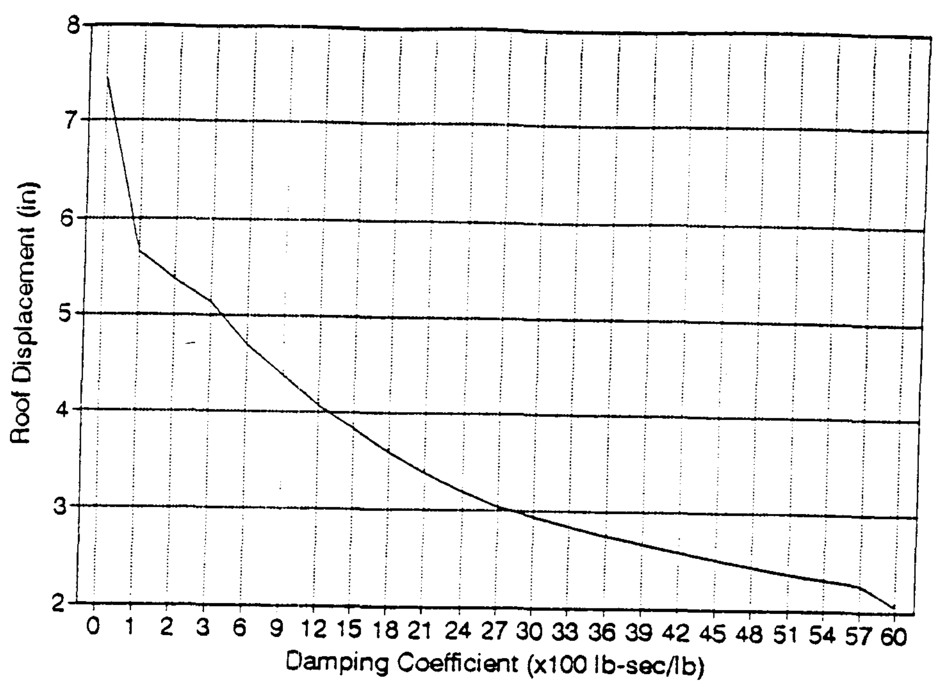

FIGURE 2-8 Relations between Damping Coefficient and Roof Displacement While the Structure is Subjected to El Centro Ground Motion

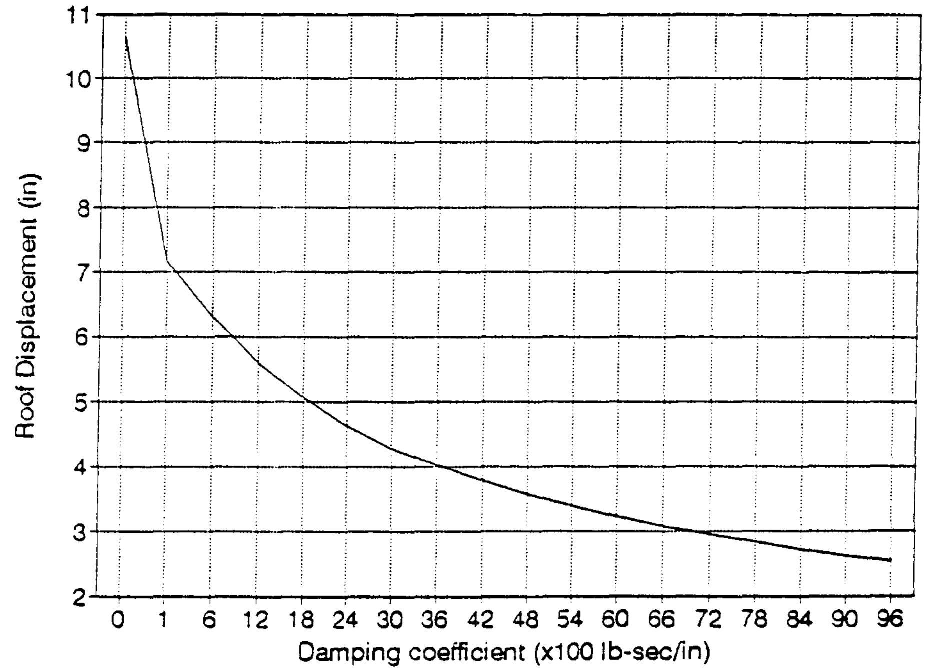

FIGURE 2-9 Relations between Damping Coefficient and Roof Displacement during San Fernando Ground Motion

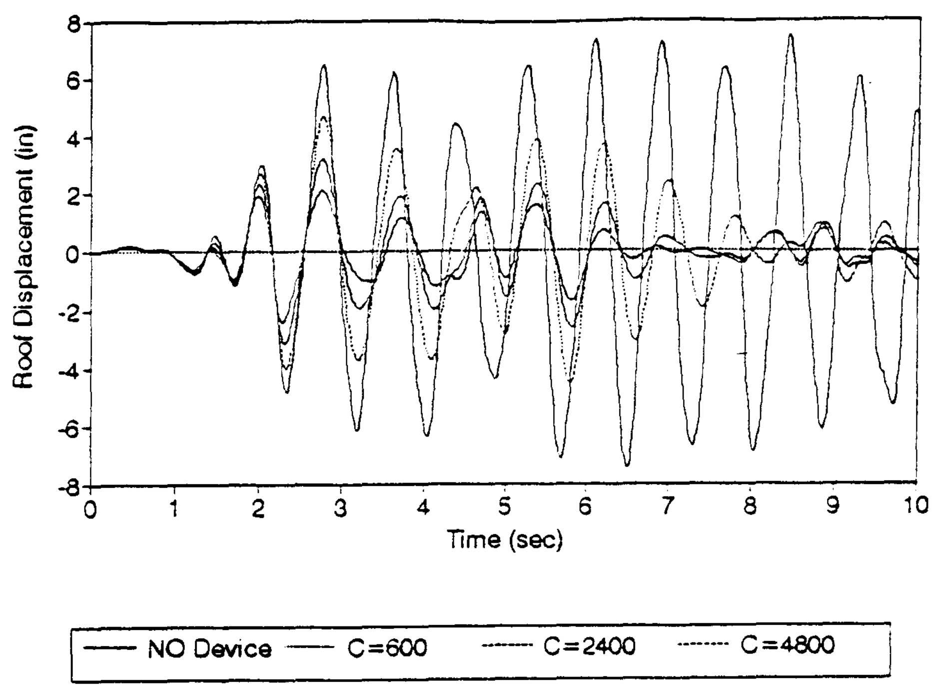

FIGURE 2-10 Comparison of Roof Displacements When the Damping Coefficients (lb-sec/in) are 600, 2400, and 4800, respectively, during El Centro Ground Motion

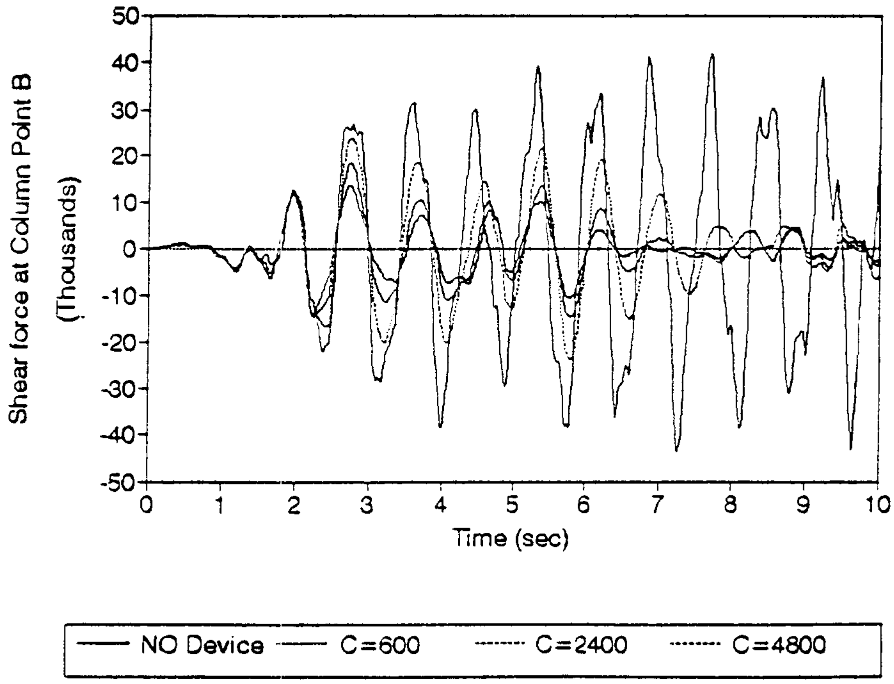

FIGURE 2-11 Comparison of Column Shear Force at Point B When the Damping Coefficients (lb-sec/in) are 600, 2400, and 4800, Respectively during El Centro Ground Motion

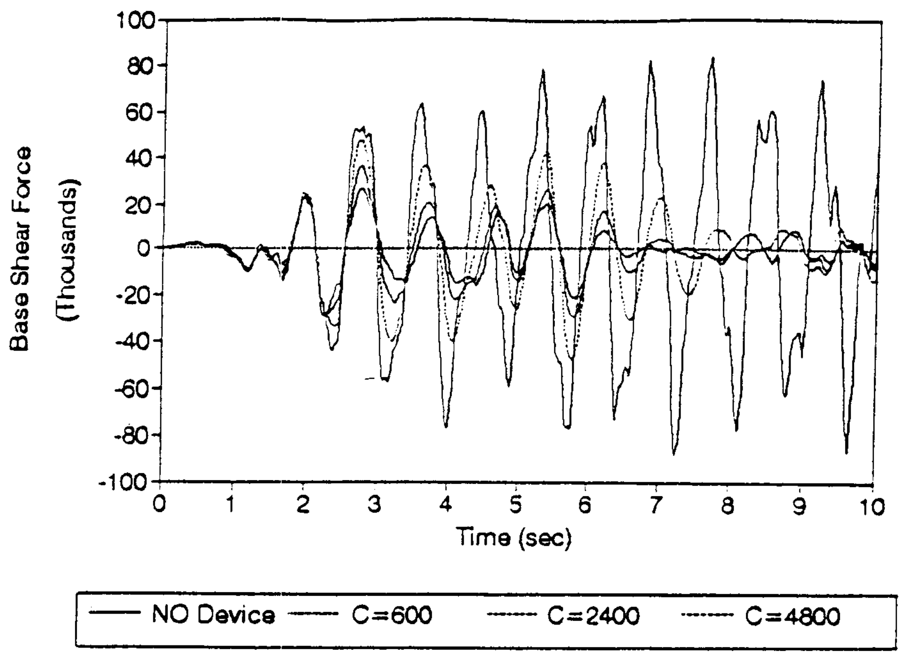

FIGURE 2-12 Comparison of Base Shear Force When the Damping Coefficients (lb-sec/in) are 600, 2400, and 4800, Respectively, during El Centro Ground Motion

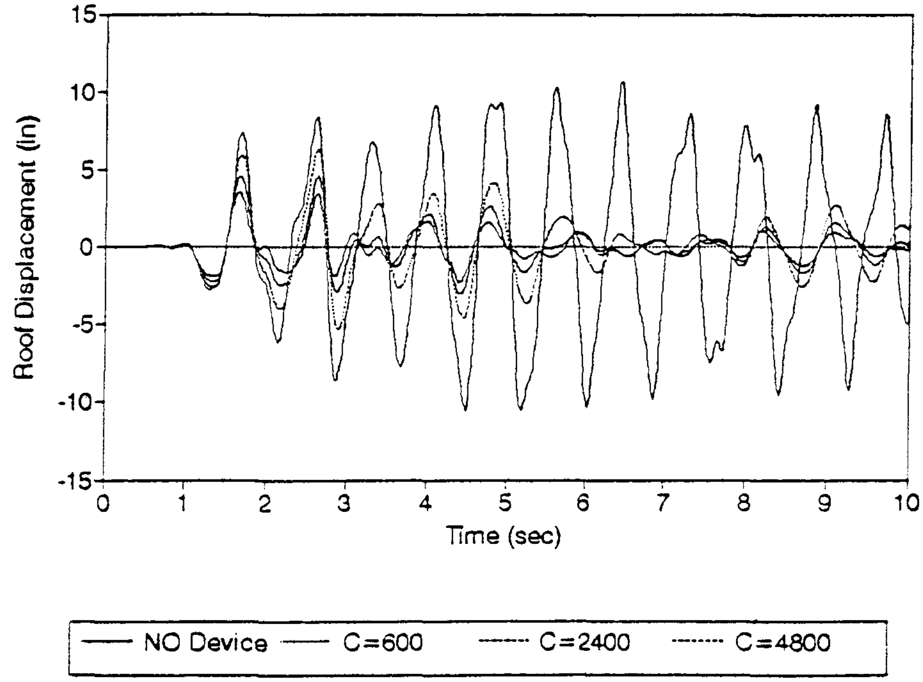

FIGURE 2-13 Comparison of Roof Displacements When the Damping Coefficients (lb-sec/in) are 600, 2400, and 4800, Respectively, during San Fernando Ground Motion

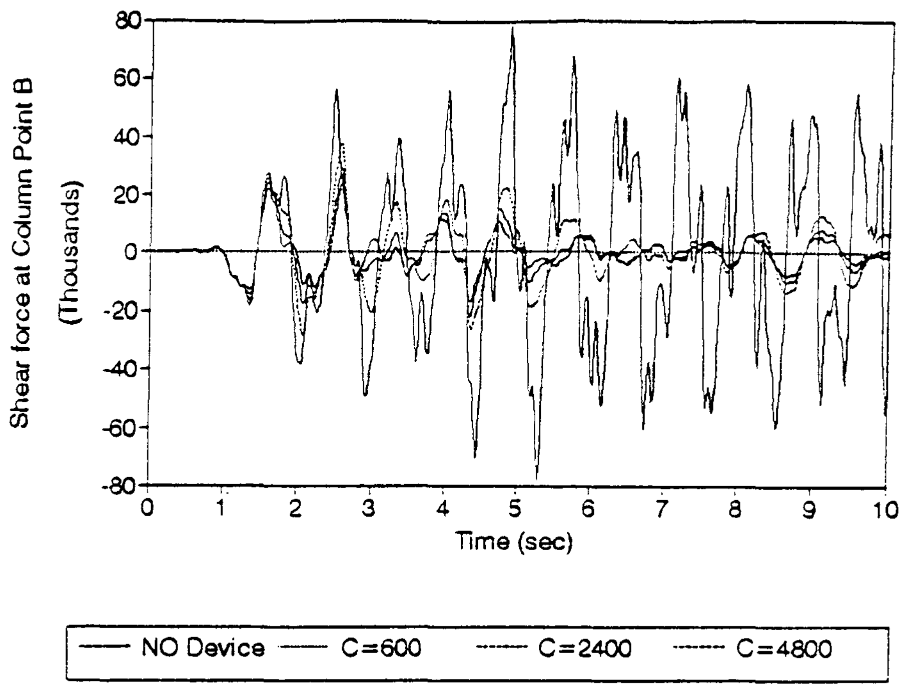

FIGURE 2-14 Comparison of Column Shear Force at Point B When the Damping Coefficients (lb-sec/in) are 600, 2400, and 4800 during San Fernando Ground Motion

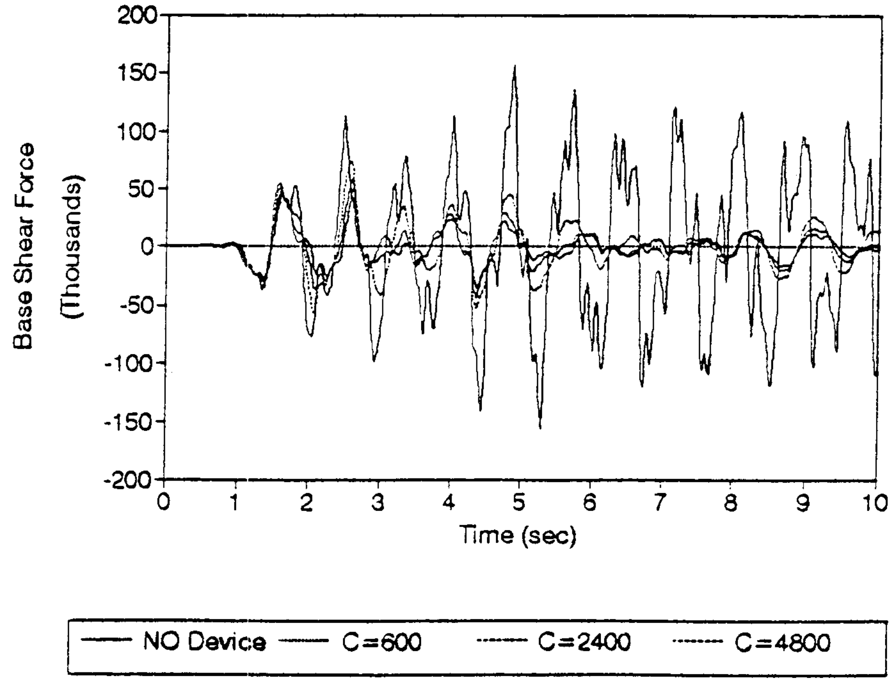

FIGURE 2-15 Comparison of Base Shear Force When the Damping Coefficients (lb-sec/in) are 600, 2400, and 4800, Respectively, during San Fernando Ground Motion

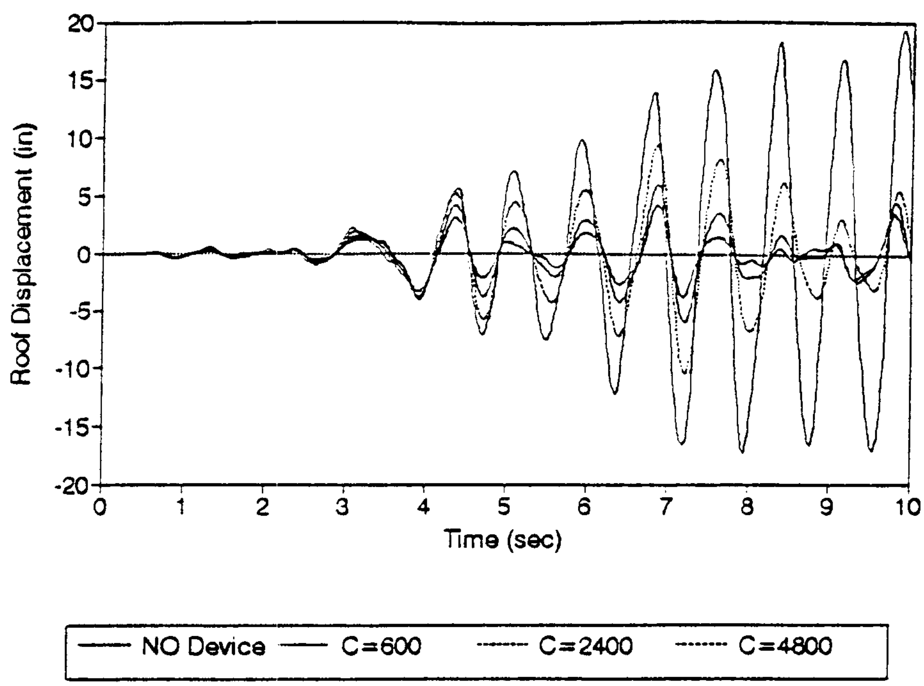

FIGURE 2-16 Comparison of Roof Displacement When the Damping Coefficients (lb-sec/in) are 600, 2400, and 4800, Respectively, during Taft (ERSF=4) Ground Motion

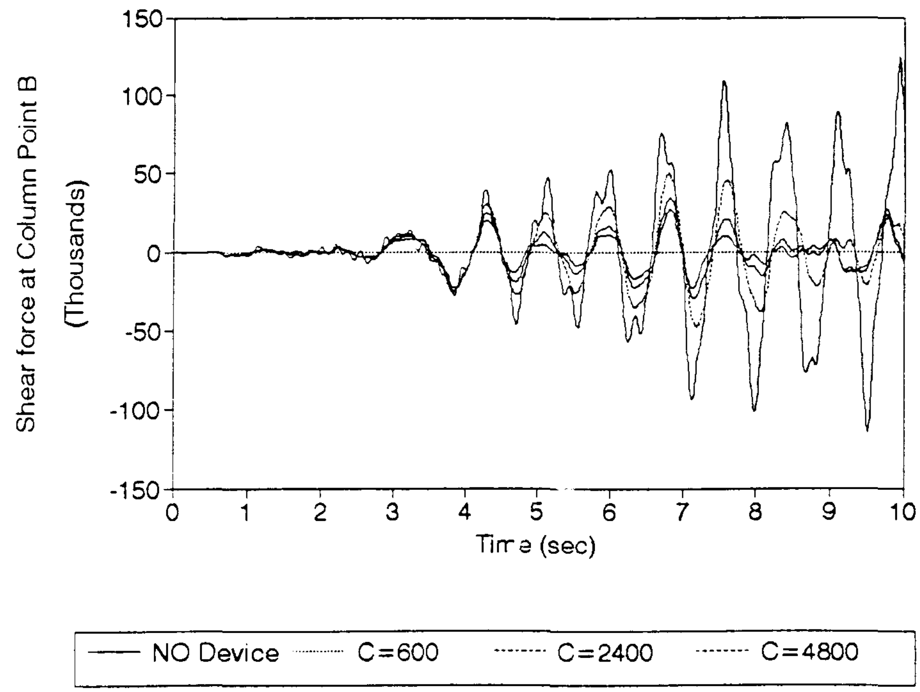

FIGURE 2-17 Comparison of Column Shear Force at Point B When the Damping Coefficients (lb-sec/in) are 600, 2400, and 4800 during Taft (ERSF=4) Ground Motion

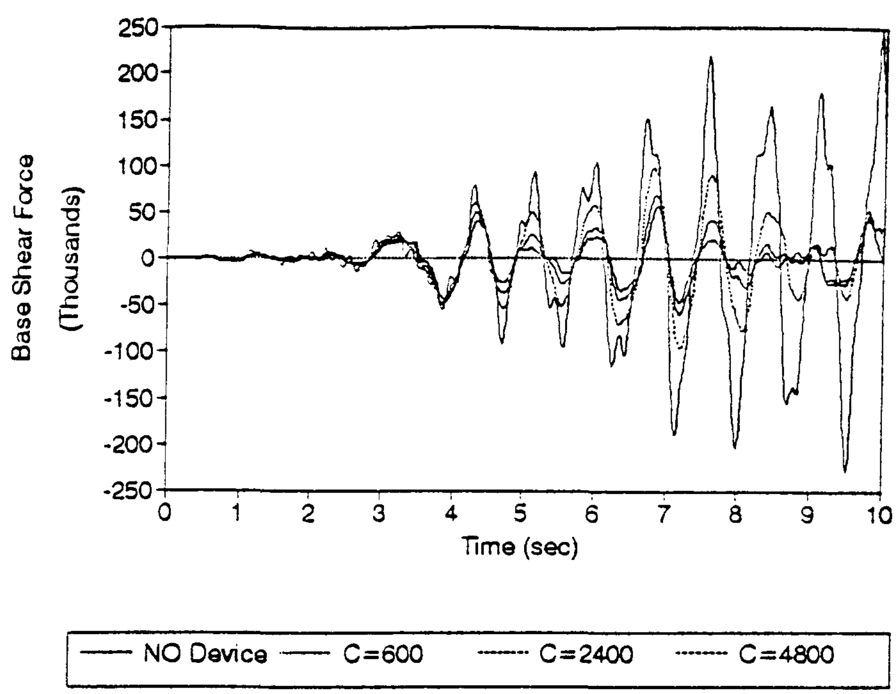

FIGURE 2-18 Comparison of Base Shear Force When the Damping Coefficients (lb-sec/in) are 600, 2400, and 4800 during Taft (ERSF=4) Ground Motion

2.4.2 Positional Effects of Fluid Dampers

The effects of the number and the position of fluid dampers were observed in Figures 2-19 and 2-20 when the structure was subjected to the El Centro ground motion. The figures show that when more dampers are mounted to the structure, smaller roof displacement and base shear force are generated. Figure 2-19 indicates that FD10 reduces about 55%, FD1 reduces about 25%, and FD5(1) reduces about 45%, of the roof displacement compared to the structure without fluid dampers. Figure 2-20 has the same consistency in terms of reducing base shear force. Furthermore, the results indicate that even though the number of dampers of 2FD5(1) and FD10 are equal, FD10 has better performance in seismic resistance. The figures also demonstrate that mounting only one damper to the first floor would reduce about 27% of base shear force and 30% of the roof displacement. Figures 2-21 and 2-22 show similar results when the structure is subjected to a stronger earthquake, the San Fernando ground motion whose peak acceleration is much stronger than that of the El Centro. Figure 2-21 indicates that FD10 reduces about 55%, FD3(1) reduces about 42%, and FD1 reduces about 35%, of the roof displacement compared to the structure without fluid dampers. Figure 2-22 has the same consistency in terms of reducing base shear force. Overall, the addition of one fluid damper to floors 1, 2, 3, 4, and 5 is an acceptable arrangement for reducing the story shear force and roof displacement for an economical design in all the cases shown in Figures 2-19-2-22.

Figures 2-23 to 2-26 show the relations between fluid damper position and the structural response (roof displacement and base shear force) when the structure is subjected to El Centro and San Fernando ground motions, respectively. Figures 2-23 and 2-25 indicate that 2FD10 has the best performance in the reduction of roof displacement. They also show that FD10 has better performance than 2FD5(1) although the number of dampers in FD10 is equal to that in 2FD5(1). Figures 2-24 and 2-26 illustrate that there is a minor difference in the reduction of base shear forces between FD5(1) and 2FD5(1), although the number of dampers in 2FD5(1) is double that in FD5(1). They also demonstrate that there is little difference between FD5(1) and FD5(2); although FD5(1) seems to have better performance.

In order to observe the effect of the number of fluid dampers, one damper placed in different locations was compared to two dampers placed in the same locations. Figures 2-27 and 2-28 show that the structure with two dampers has smaller roof displacement and base shear force than that with one damper mounted at the same location. But the difference in the reduction of roof displacement and base shear force between the structure with one damper and the structure with two dampers mounted is not great. The response (roof displacement and base shear force) of the structure without dampers and with one damper, two dampers, and three dampers mounted at each floor was compared when the El Centro and San Fernando ground motions were imposed on the structure. Figures 2-29 to 2-32 show the results of these comparisons, respectively. They show that there is little difference in the reduction of structural response among one damper, two dampers, and three dampers mounted on the structure if the damping coefficient is properly determined. It can be noted that one damper mounted on each floor has almost the same total shear force for each floor as those floors with two or three dampers mounted on them. In Figures 2-30 and 2-32, we observe that three curves of the structure equipped with fluid dampers are almost indistinguishable. This means that if a damping coefficient is selected properly, the number of fluid dampers does not have a great influence on improving seismic resistance.

The behaviors of the structure equipped with and without fluid dampers on each floor were compared for ten different earthquake peak accelerations from 100 Gal (cm/s^2) to 1000 Gal of the San Fernando ground motion. Figures 2-33 and 2-34 show that the two curves are both linear, but the curve of the structure with dampers has a smaller gradient.

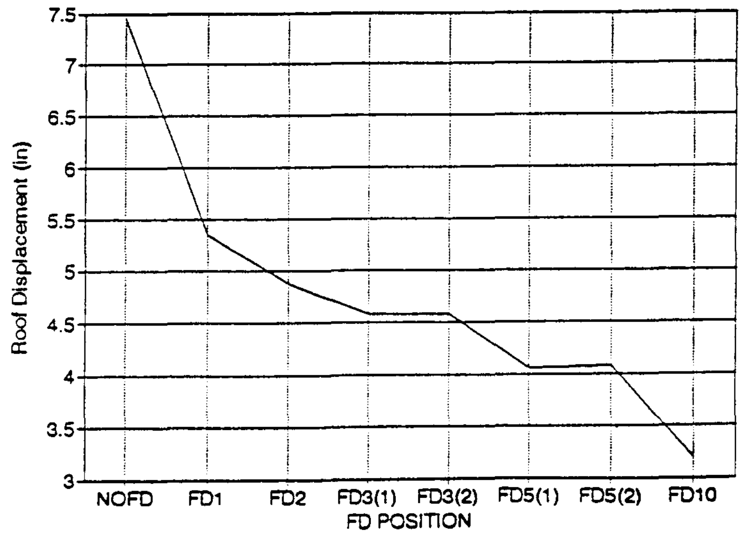

FIGURE 2-19 Relations between Fluid Damper's Position and Floor Displacement during El Centro Ground Motion

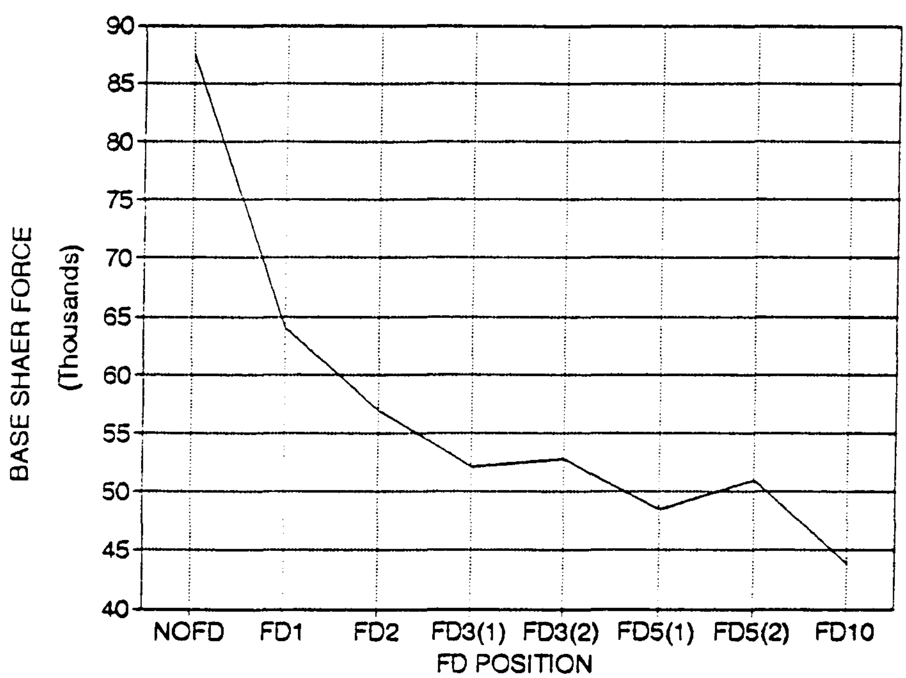

FIGURE 2-20 Relations between Fluid Damper's Position and Base Shear Force When the Structure is Subjected to El Centro Ground Motion

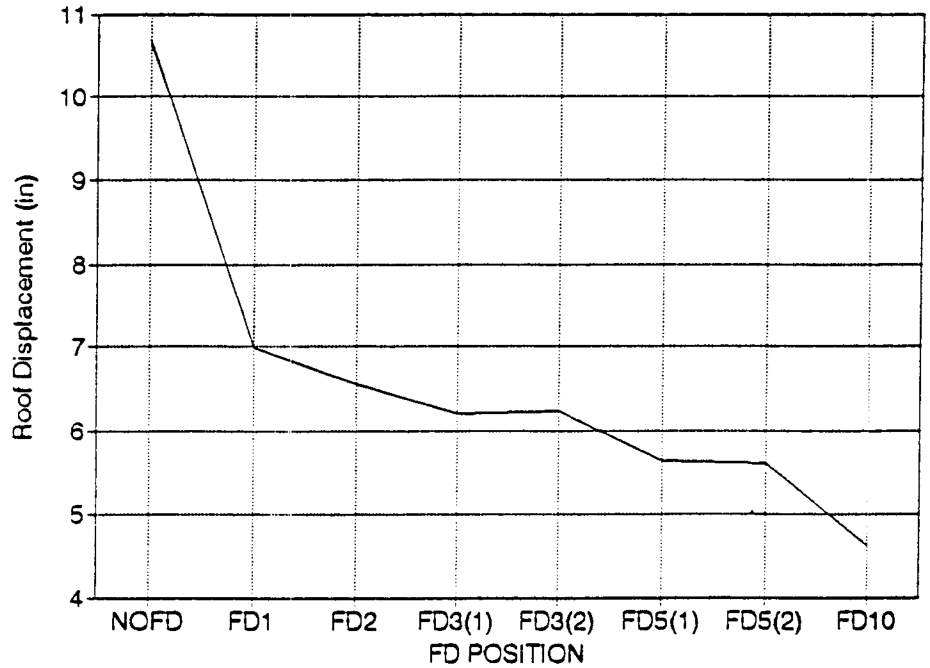

FIGURE 2-21 Relations between Fluid Damper's Position and Floor Displacement When the Structure is Subjected to San Fernando Ground Motion

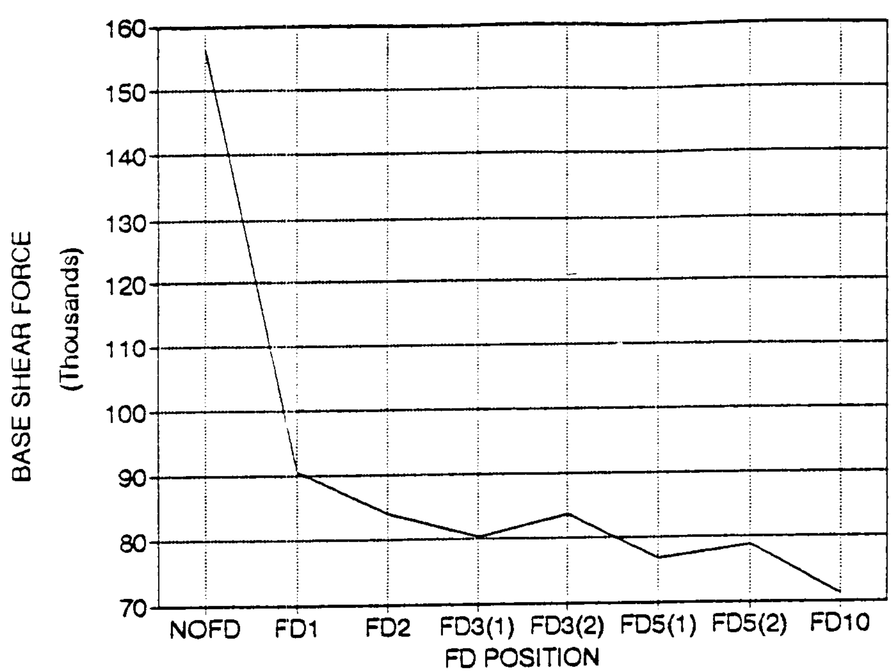

FIGURE 2-22 Relations between Fluid Damper's Position and Base Shear Force When the Structure is Subjected to San Fernando Ground Motion

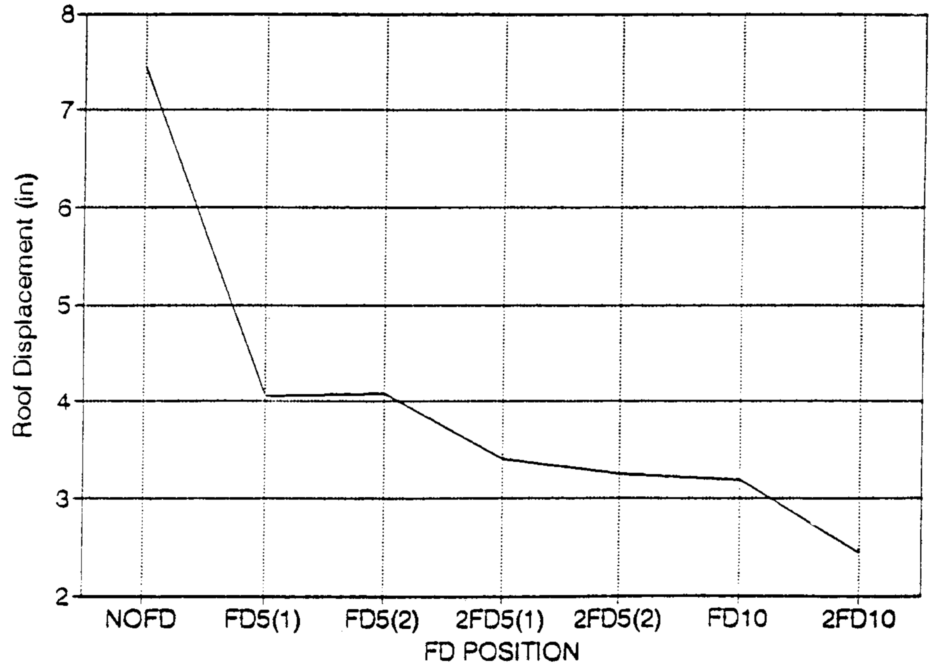

FIGURE 2-23 Relations between Fluid Damper's Position and Floor Displacement When the Structure is Subjected to Taft (ERSF=4) Ground Motion

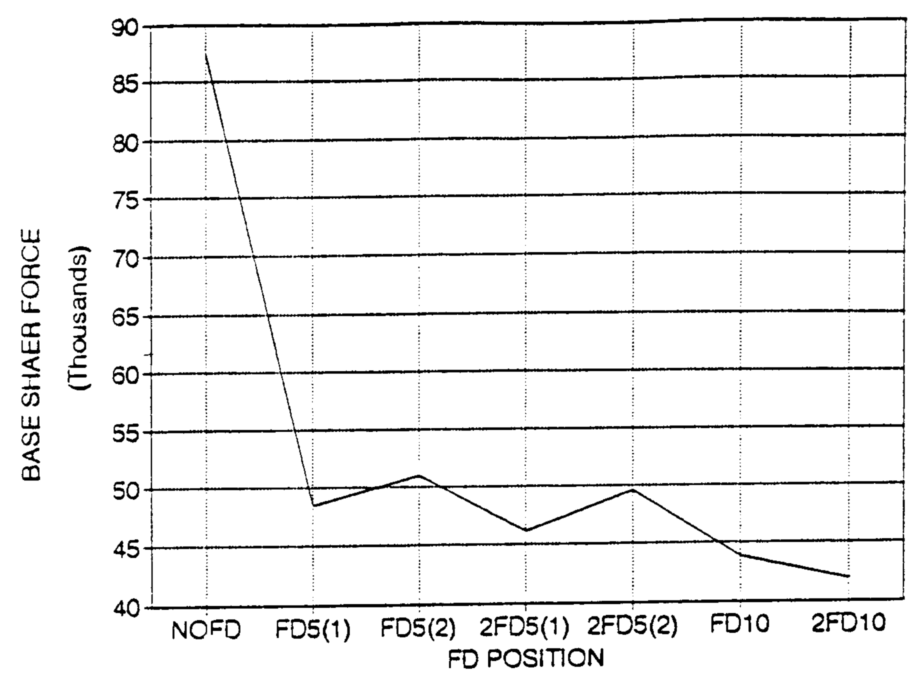

FIGURE 2-24 Relations between Fluid Damper's Position and Base Shear Force When the Structure is Subjected to Taft (ERSF=4) Ground Motion

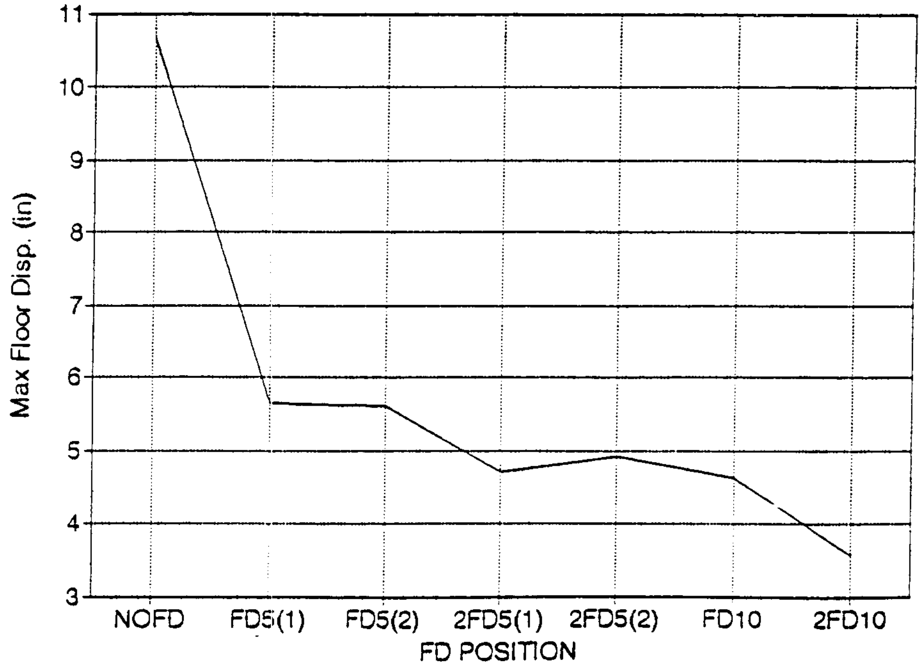

FIGURE 2-25 Relations between the Number of Fluid Dampers and Floor Displacement When the Structure is Subjected to El Centro Ground Motion

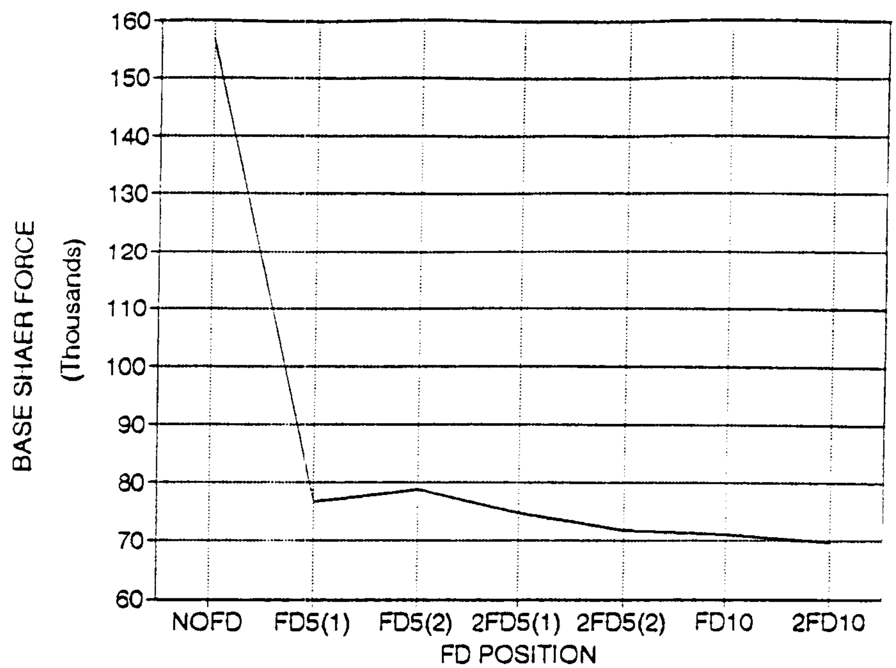

FIGURE 2-26 Relations between the Number of Fluid Dampers and Base Shear Force When the Structure is Subjected to El Centro Ground Motion

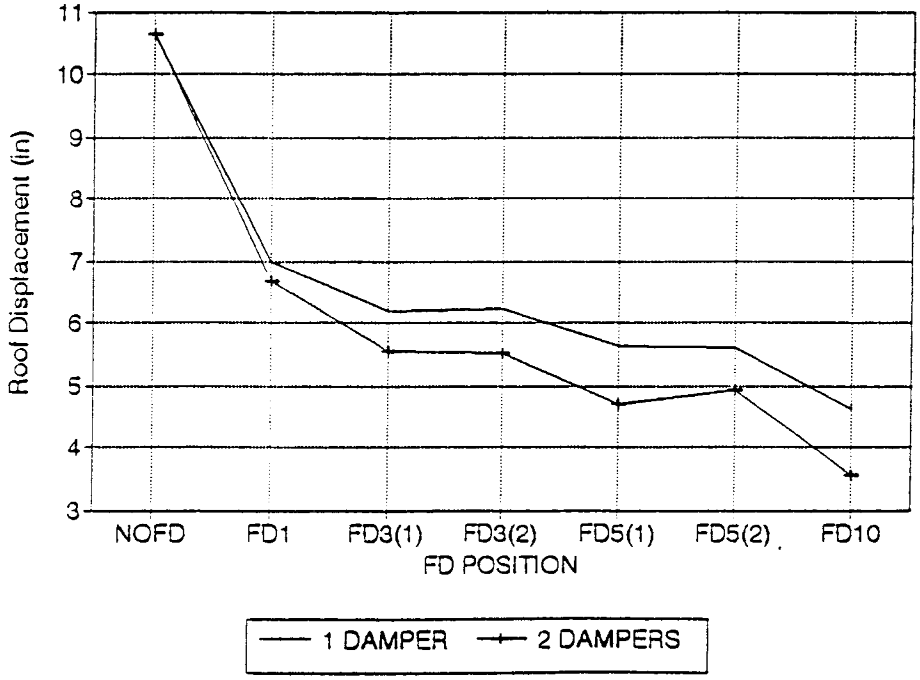

FIGURE 2-27 Relations between the Number of Fluid Dampers and Floor Displacement When the Structure is Subjected to San Fernando Ground Motion

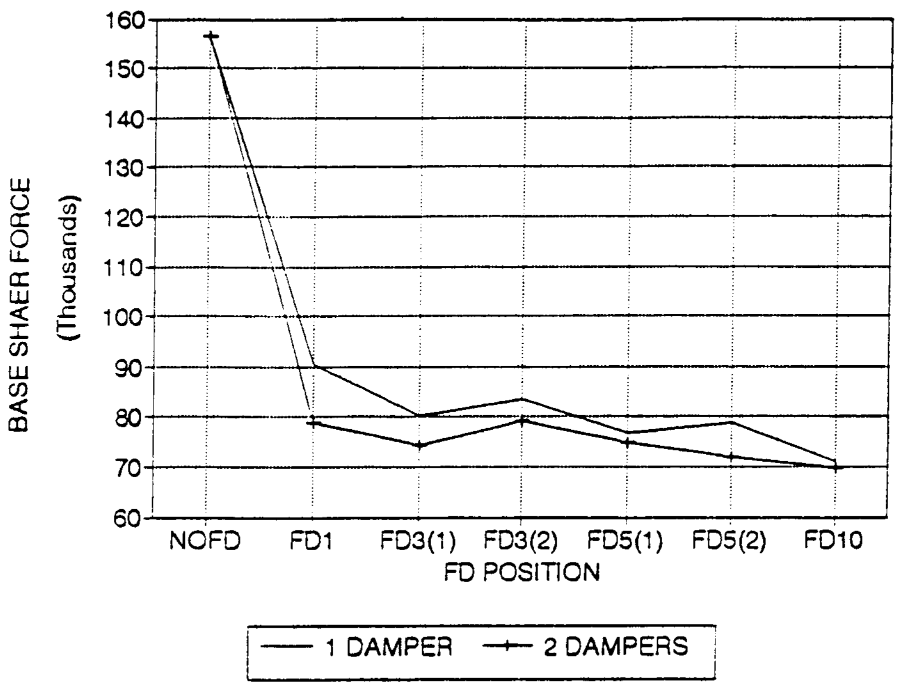

FIGURE 2-28 Relations between the Number of Fluid Dampers and Base Shear Force When the Structure is Subjected to San Fernando Ground Motion

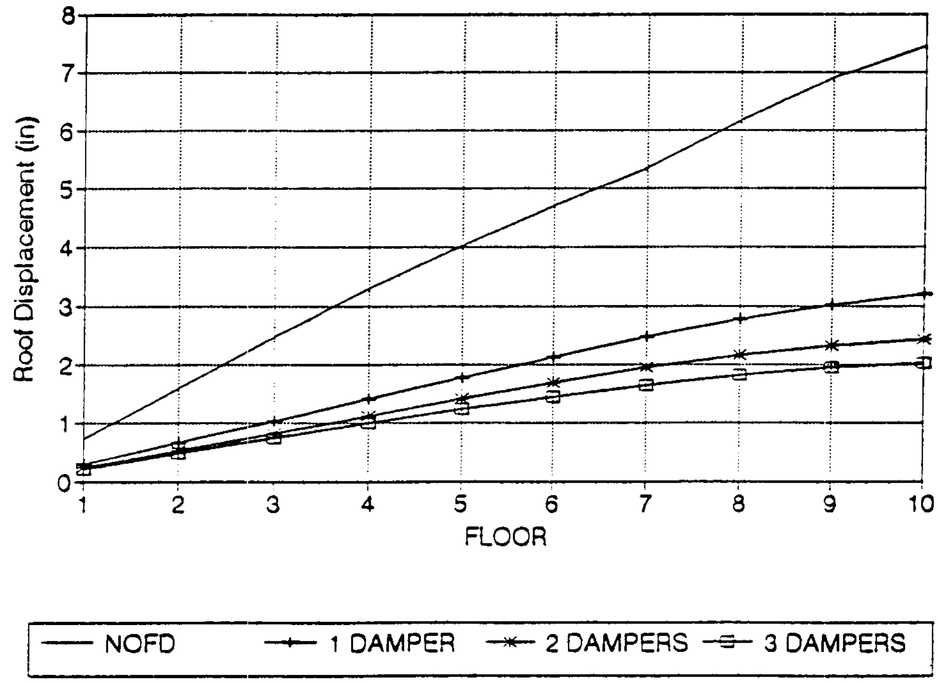

FIGURE 2-29 Relations between the Number of Fluid Dampers and Floor Displacement When the Structure is Subjected to El Centro Ground Motion

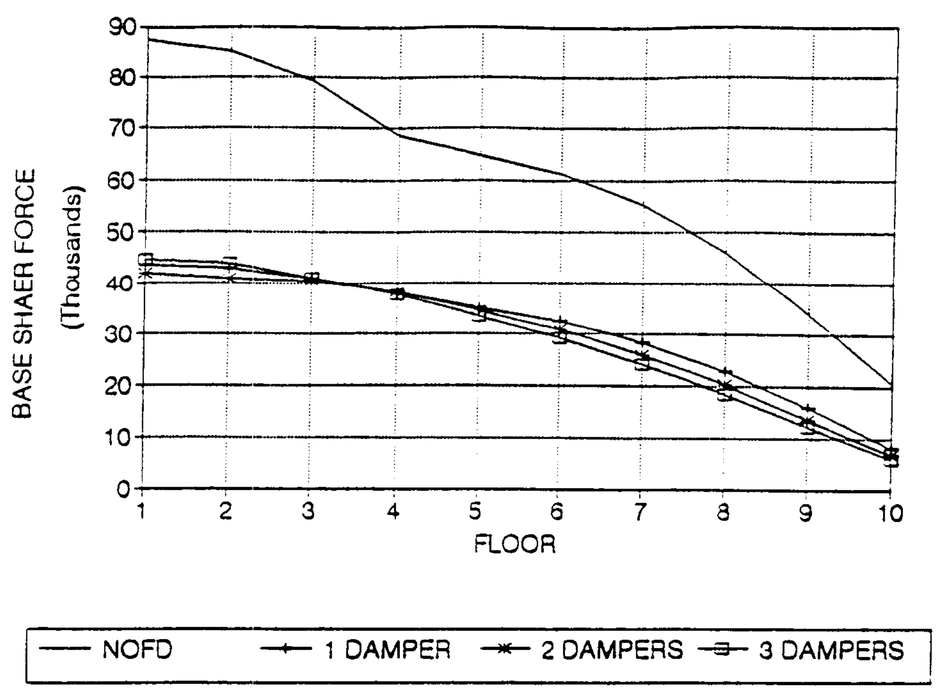

FIGURE 2-30 Relations between the Number of Fluid Dampers and Base Shear Force When the Structure is Subjected to El Centro Ground Motion

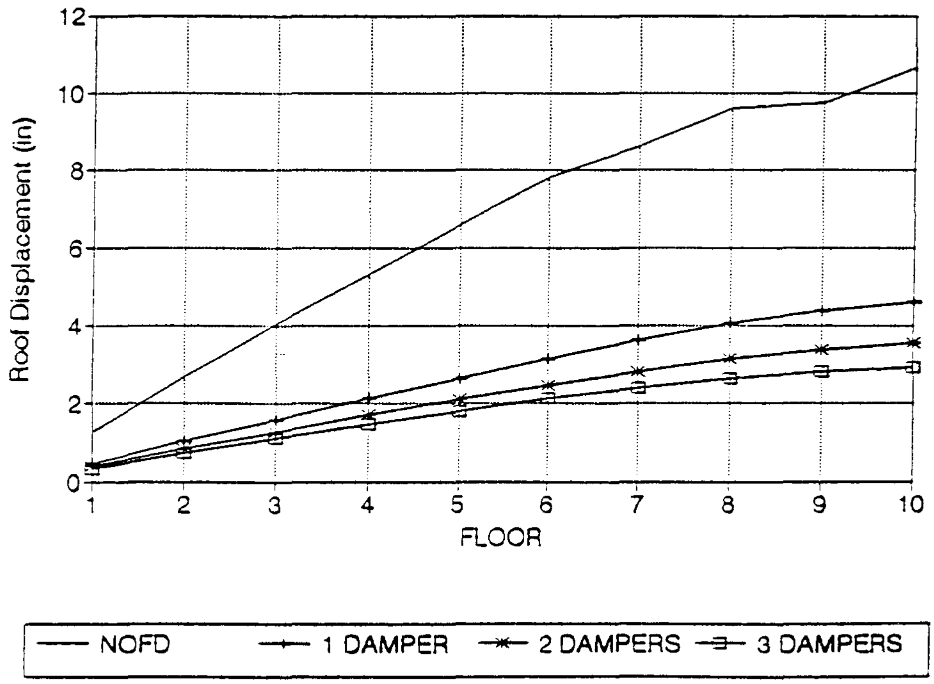

FIGURE 2-31 Relations between the Number of Fluid Dampers and Floor Displacement When the Structure is Subjected to San Fernando Ground Motion

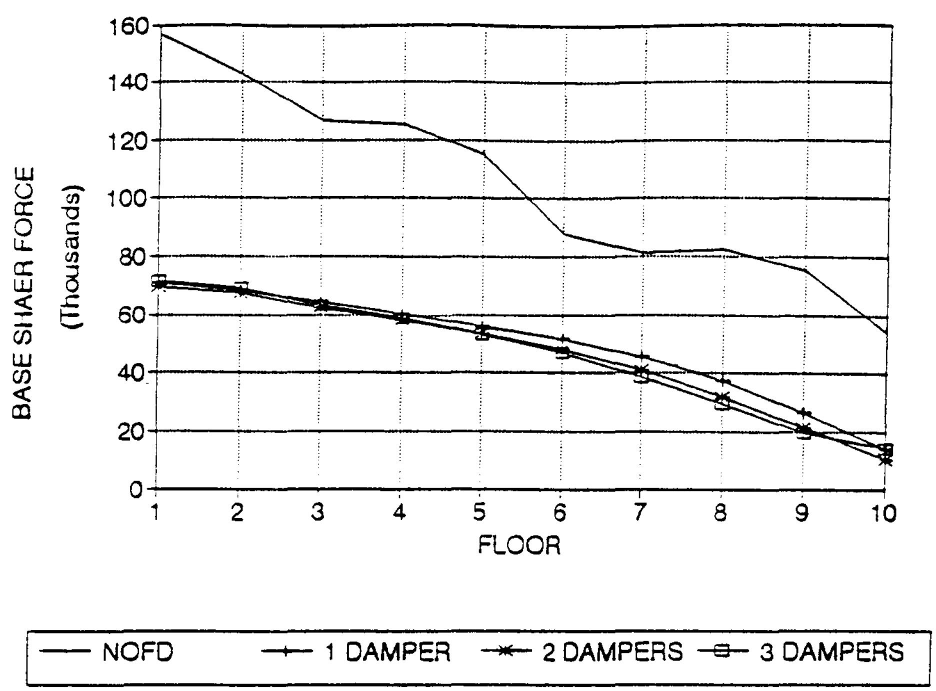

FIGURE 2-32 Relations between the Number of Fluid Dampers and Base Shear Force When the Structure is Subjected to San Fernando Ground Motion

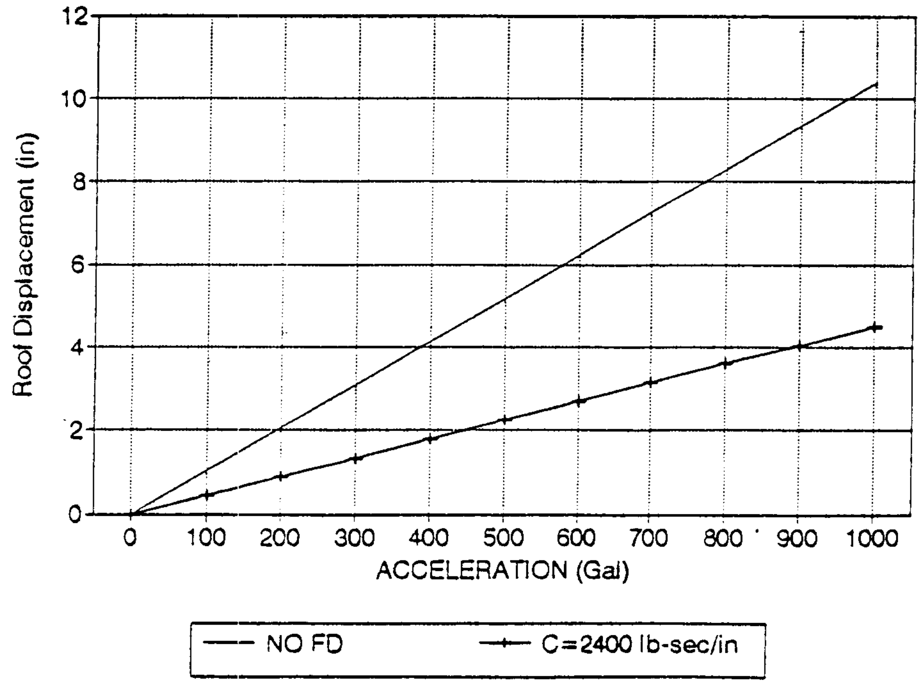

FIGURE 2-33 Comparison of Roof Displacement While the Structure is Subjected to the Peak Acceleration of 100 Gal to 1000 Gal of San Fernando Ground Motion

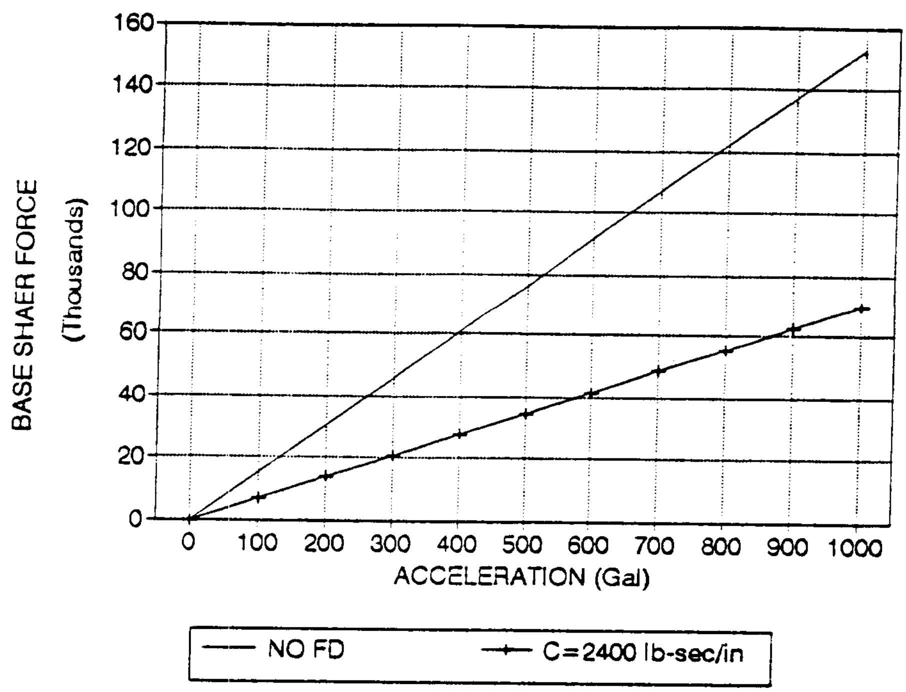

FIGURE 2-34 Comparison of Base Shear While the Structure is Subjected to the Peak Acceleration of 100 Gal to 1000 Gal of San Fernando Ground Motion

2.5 Discussion on the Fluid Dampers

The fluid viscous damper is a promising device for dissipating energy. Properly designed fluid viscous dampers can provide additional damping to the structure to reduce the amplitude of vibrations and to improve its seismic resistance. Numerical results show that the fluid damper provides very reliable mechanical behavior for seismic hazard mitigation. Unlike viscoelastic dampers, fluid dampers operate stably over a wide temperature range. The dynamic characteristics of the fluid dampers depend primarily on the damping coefficient. Because the resisting force is proportional to the damping coefficient, the floor displacement and shear force can be reduced by adopting a higher damping coefficient. But the manufacturing costs of a fluid damping device increases in order to achieve a higher damping coefficient. Therefore the selection of proper damping coefficients must be carefully considered in order to achieve the most economical design and optimal performance.

Results show that the addition of a fluid damper to the first floor effectively reduces the structural response. According to the study, the number of fluid dampers mounted on each floor is not a major parameter for increasing seismic resistance if the capacities of the fluid damper are properly chosen. The relations of force and displacement of the fluid dampers located at the 1st, and 10th floors, respectively, during the Taft (ERSF=4) ground motion are shown in Figures 2-35 to 2-36. Numerical results illustrate that fluid dampers located at the lower floors of a structure absorb more energy than those at upper floors.

Figures 2-37 to 2-39 show the comparison of response (roof displacement, column shear force at point B (see Figure 2-7), and base shear force) between the structure with and without fluid dampers. Figure 2.38 indicates that the column shear force at point B of the structure with fluid dampers takes a much smaller portion of shear force compared to that of a structure without fluid dampers. The main load-carrying structural members may be optimized for their required stiffness and load-bearing features at lower cost because the energy-absorption demands on the main structure are reduced. These results indicate that properly designed fluid dampers could be an effective device for seismic hazard mitigation.

However, the major disadvantage of using fluid dampers as energy-absorbing devices is that structural response cannot be reduced greatly in the early stage of earthquakes. This is illustrated in Figure 2-37 where the roof displacement is shown to be substantially reduced after the fourth second, while not much reduction took place from the beginning to the third second. The main reason for this phenomenon is that the resisting force of fluid dampers is dependent on velocity. Such velocity dependence in the device is generally regarded as unfavorable [56].

The dissipated energy is related to the displacement. The resisting force of the fluid dampers is proportional to the velocity. But the maximum displacement and maximum velocity do not exist at the same period. On the contrary, when the displacement reaches the maximum value, the velocity is zero. Therefore, it is impossible to reach the maximum displacement and maximum velocity simultaneously. This is why the fluid damper cannot reduce its response in time if a peak response occurs during the early stage of earthquake excitation, which is generally true in most earthquake events.

Figure 2-39 also shows that the base shear force is not substantially reduced in the early stages of seismic events; although, the maximum base shear force of the structure with fluid dampers is reduced significantly compared to that of a structure without fluid dampers. The column shear force is reduced greatly and at the same time, the goal of constraining damage to the supplemental devices is achieved.

Although the fluid device has been proven to be a promising one for seismic hazard mitigation, its failure to reduce the structural response in the early stages of earthquakes can be viewed as a shortcoming. To overcome this drawback, a combination of TPEA and fluid dampers may compensate for the shortcomings of each device. A study of a combined device is demonstrated in Section 4.

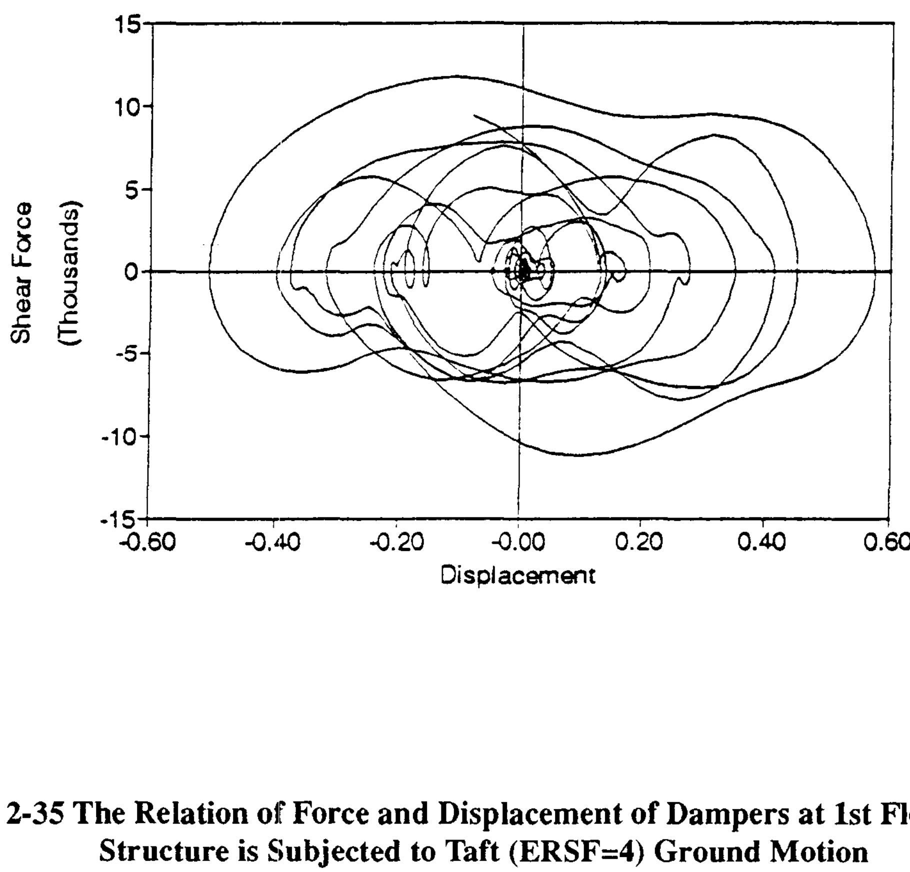

FIGURE 2-35 The Relation of Force and Displacement of Dampers at 1st Floor When the Structure is Subjected to Taft (ERSF=4) Ground Motion

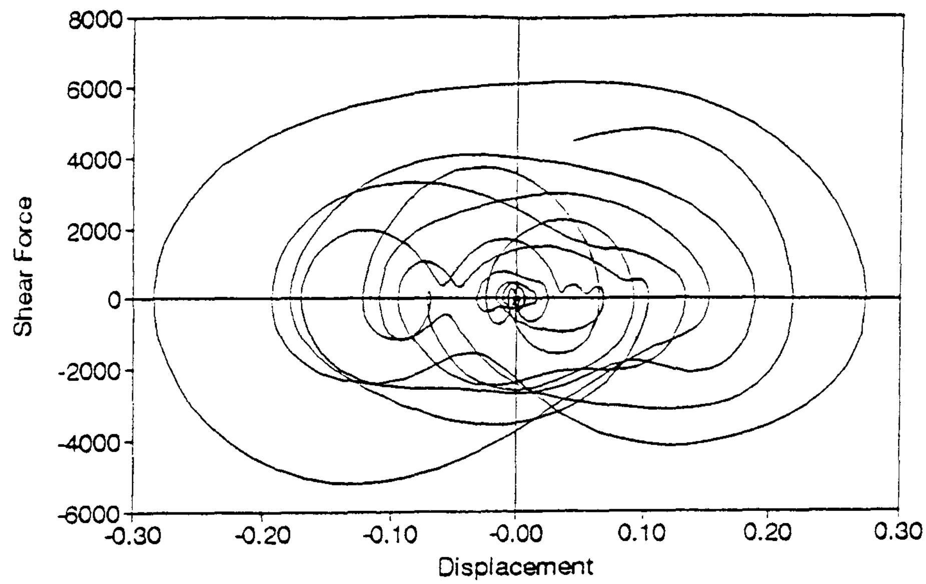

FIGURE 2-36 The Relation of Force and Displacement of Dampers at 10th Floor When the Structure is Subjected to Taft (ERSF=4) Ground Motion

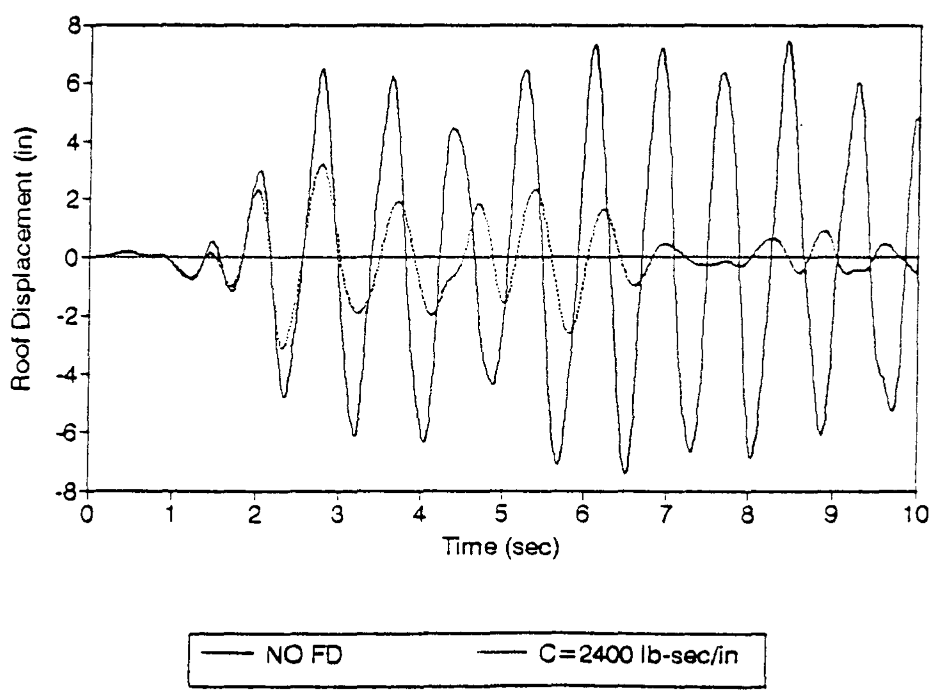

FIGURE 2-37 The Response of Floor Displacement When the Structure is Subjected to El Centro Ground Motion

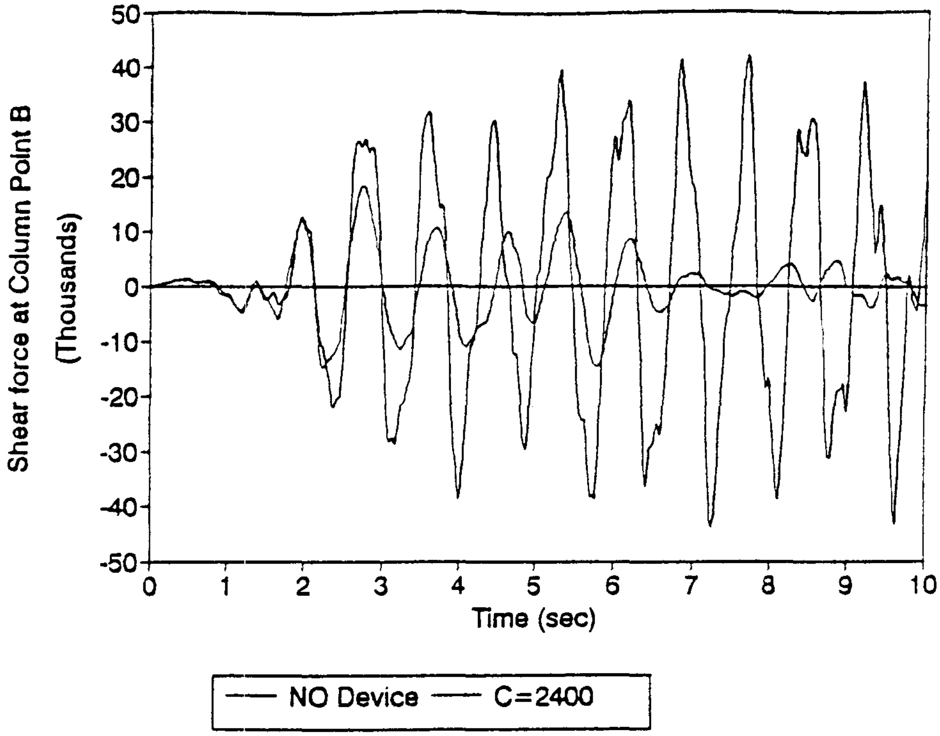

FIGURE 2-38 The Response of Column Shear Force at Point B When the Structure is Subjected to El Centro Ground Motion

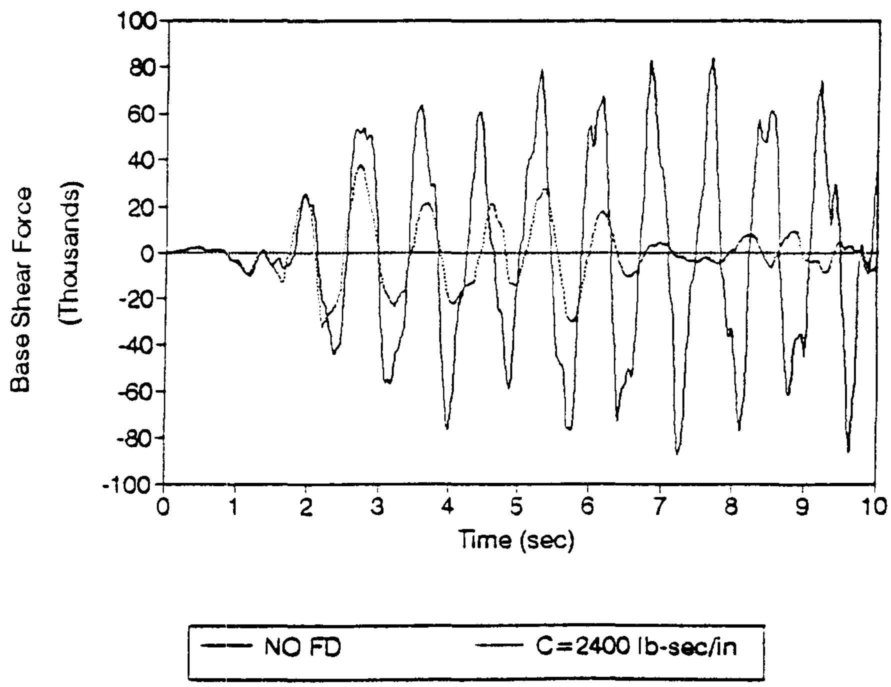

FIGURE 2-39 The Response of Base Shear Force When the Structure is Subjected to El Centro Ground Motion

2.6 Current Status of Viscoelastic Dampers Development

The feasibility of using viscoelastic dampers to mitigate earthquake-induced structural response was studied by Zhang et al. [25]. Research on seismic behavior of viscoelastically damped structure has been continuously conducted at the State University of New York at Buffalo [41,43,72]. In particular, the temperature effect has been carefully investigated. Experimental results to date show that the addition of viscoelastic dampers is effective in reducing structural response due to seismic excitation.

2.6.1 Analytical Model for Viscoelastic Dampers

An advanced analytical model is adopted for the VE damper to account for the effects of temperature and earthquake loadings [28,71]. The concept of fractional derivatives in the formulation of a stress-strain relationship for viscoelastic material is employed.

The 3-parameter function derivative model given by Bagley and Torvik [51,52] was chosen for the constitutive model. The fractional calculus model of VE behavior [52] is given by

$$\tau(t) = G_0\gamma(t) + G_1 D^{\alpha}\left[\gamma(t)\right] \tag{2.23}$$

where $\tau(t)$ is shear stress, $\gamma(t)$ is shear strain, G_0 and G_1 are constitutive model parameters, and

$$D^{\alpha}\left[\gamma(t)\right] = \frac{1}{\Gamma(1-\alpha)}\frac{d}{dt}\int_0^t \frac{\gamma(t)\,d\tau}{(t-\tau)^{\alpha}} \tag{2.24}$$

where $0 < \alpha < 1$

In general, the model parameters, G_0 and G_1, are not constant from the experimental observations. Therefore, an advanced formula is adopted for describing the material behavior of VE dampers due to arbitrary loadings and temperatures [28, 63, 67], that is

$$G_1 = G_0 = A_0\left\{1 + \mu e^{-\beta\left(\int \tau d\gamma + \theta(T - T_0)\right)}\right\} \tag{2.25}$$

where $\Gamma(\ )$ = gamma function; α, A_0, β, μ and θ are unknown coefficients which remain constant even for different arbitrary loadings and temperatures to be determined from the experimental data. T_0 and T are reference temperature and ambient temperature, respectively.

Eq.(2.25) demonstrates that the constitutive model parameters, G_0 and G_1, decay as the strain energy increases. The temperature effect is a type of initial energy stored in the material that affects the material behavior of the viscoelastic dampers. If linear interpolation of shear strain between two time steps, $(n-1)\Delta t$ and $n\Delta t$, is assumed, the strain is expressed as

$$\gamma(\tau) = \left(n - \frac{\tau}{\Delta t}\right)\gamma((n-1)\Delta t) + \left(\frac{\tau}{\Delta t} - (n-1)\right)\gamma(n\Delta t) \tag{2.26}$$

where $(n-1)\Delta t \le \tau \le n\Delta t$.

Substitution of Eq.(2.25) into Eq.(2.23) and Eq.(2.24) leads to the constitutive law for viscoelastic dampers at time step $N\Delta t$; that is

$$\tau(N\Delta t) = \left[G_0 + \frac{G_1(\Delta t)^{-\alpha}}{\Gamma(2-\alpha)}\right]\gamma(N\Delta t) + F(N\Delta t) \tag{2.27}$$

In the above equation, the previous time effect of the strain, $F(N\Delta t)$, is defined as

$$F(N\Delta t) = \frac{G_1(\Delta t)^{-\alpha}}{\Gamma(2-\alpha)}\{\{(N-1)^{1-\alpha} + (-N+1-\alpha)N^{-\alpha}\}\gamma(0)$$

$$+\sum_{n=1}^{N-1}\{(N-n-1)^{1-\alpha} - 2(N-n)^{1-\alpha} + (N-n+1)^{1-\alpha}\}\gamma(n\Delta t)\} \tag{2.28}$$

It should be noticed that the first term on the right hand side of Eq.(2.28) is equal to zero at the first step, n=1, while the fifth term is equal to zero when n=N-1. There is no singularity although the initial conditions are involved.

2.6.2 Finite Element Formulation for the Viscoelastic Dampers

A finite element formulation for the viscoelastic damper is adopted so that the damper can be easily implemented in computer programs for engineering practice [28]. Nodal points 1 and 2, shown in Figure 2-2, represent nodes at the top and the bottom of VE dampers in the thickness direction shown in Figure2-42. The global displacement at nodal points 1 and 2 shown in Figure 2-2 are $\mathbf{D}_1$(t) and $\mathbf{D}_2$(t), respectively; these are represented as

$$\mathbf{D}_1(t) = \begin{bmatrix} u_1(t) \\ u_2(t) \\ u_3(t) \end{bmatrix} \tag{2.29}$$

and

$$\mathbf{D}_2(t) = \begin{bmatrix} u_4(t) \\ u_5(t) \\ u_6(t) \end{bmatrix} \tag{2.30}$$

where u_1(t), u_2(t), and u_3(t) are global displacement at nodal point 1 in x, y, and z directions, respectively, and u_4(t), u_5(t), and u_6(t) are those at nodal point 2, respectively.

The displacement in local coordinate system. $\bar{\mathbf{D}}_1(t)$, and $\bar{\mathbf{D}}_2(t)$ are

$$\bar{\mathbf{D}}_1(t) = \mathbf{R}\mathbf{D}_1(t) \tag{2.31}$$

and

$$\bar{\mathbf{D}}_2(t) = \mathbf{R}\mathbf{D}_2(t) \tag{2.32}$$

where R is a transformation matrix related to the local and global coordinate systems. The relative displacements, $\mathbf{V}(t)$, between two nodal points 1 and 2 in local coordinate system ξ, ζ, and η, are defined as

$$\mathbf{V}(t) = \bar{\mathbf{D}}_2(t) - \bar{\mathbf{D}}_1(t) = \mathbf{RD}_2(t) - \mathbf{RD}_1(t) \tag{2.33}$$

Eq.(2.33) can be rewritten as

$$\mathbf{V}(t) = \mathbf{BU}(t) \tag{2.34}$$

where

$$\mathbf{B} = [-R,R] \tag{2.35}$$

also

$$\mathbf{U}(t) = \begin{bmatrix} \mathbf{D}_1(t) \\ \mathbf{D}_2(t) \end{bmatrix} = \begin{bmatrix} u_1(t) \\ u_2(t) \\ u_3(t) \\ u_4(t) \\ u_5(t) \\ u_6(t) \end{bmatrix} \tag{2.36}$$

and

$$\mathbf{V}(t) = \begin{bmatrix} v_\xi(t) \\ v_\zeta(t) \\ v_\eta(t) \end{bmatrix} \tag{2.37}$$

The shear strain of VE dampers in the ξ, ζ, and η directions, are

$$\begin{bmatrix} \gamma_{\xi\xi}(t) \\ \gamma_{\zeta\zeta}(t) \\ \gamma_{\eta\eta}(t) \end{bmatrix} = \begin{bmatrix} \frac{1}{h_\xi} v_\xi(t) \\ \frac{1}{h_\zeta} v_\zeta(t) \\ \frac{1}{h_\eta} v_\eta(t) \end{bmatrix} \tag{2.38}$$

where h_ξ, h_ζ and h_η are the thickness of the dampers for the ξ, ζ, and η directions, respectively. With the help of the virtual work principle, the equilibrium resisting force, **P**(t), is given by

$$\mathbf{P}(t) = \mathbf{B}^T \begin{bmatrix} \tau_{\xi\xi}(t) A_\xi \\ \tau_{\zeta\zeta}(t) A_\zeta \\ \tau_{\eta\eta}(t) A_\eta \end{bmatrix} \tag{2.39}$$

where A_ξ, A_ζ, and A_η are the areas of the damper in the ξ, ζ, and η direction, respectively.

Substitution of Eq.(2.27), Eq.(2.34), and Eq.(2.38) into Eq.(2.39) at the time step, $t=N\Delta t$, results in the following equation

$$\mathbf{P}(N\Delta t) = \mathbf{KU}(N\Delta t) + \mathbf{L}(N\Delta t) \tag{2.40}$$

where $\mathbf{P}(N\Delta t)$ is the equilibrium resisting force and the stiffness matrix $\mathbf{K}$ is

$$\mathbf{K} = \mathbf{B}^T\mathbf{E}\mathbf{B} \tag{2.41}$$

The previous time effect of equivalent nodal forces $\mathbf{L}(N\Delta t)$ is given by

$$\mathbf{L}(N\Delta t) = \mathbf{B}^T \begin{bmatrix} F_\xi (N\Delta t) A_\xi \\ F_\zeta (N\Delta t) A_\zeta \\ F_\eta (N\Delta t) A_\eta \end{bmatrix} \tag{2.42}$$

In Eq.(2.41), the Matrix $\mathbf{E}$ is expressed as

$$\mathbf{E} = \begin{bmatrix} E_{\xi\xi} & 0 & 0 \\ 0 & E_{\zeta\zeta} & 0 \\ 0 & 0 & E_{\eta\eta} \end{bmatrix} \tag{2.43}$$

where E_{ii} is

$$E_{ii} = \frac{A_i}{h_i}\left[G_0^i + \frac{G_1^i (\Delta t)^{-\alpha_i}}{\Gamma(2-\alpha_i)}\right] \tag{2.44}$$

$$i = \xi, \zeta, \eta$$

where A_ξ, A_ζ, and A_η = the total areas of the dampers in the ξ, ζ, and η directions, respectively. F_ξ, F_ζ, and F_η, defined in Eq.(2.42), are the previous time effects of strains in the ξ, ζ, and η directions, respectively. It should be noted that the $E_{\zeta\zeta}$ and $E_{\eta\eta}$ are relatively large value Largrangian multipliers, compared to $E_{\xi\xi}$, when the VE dampers are only applied in the ξ direction.

2.7 Design Parameters of Viscoelastic Dampers

As shown in Figure 2.-40, viscoelastic dampers are placed on each floor and supported by Chevron braces. Figures 2-41 to 2-42 show some details of the arrangement of VE dampers. The parameters which should be taken into careful account to properly design viscoelastic dampers for the building include: (1) area of VE dampers; (2) thickness of VE dampers; (3) position of VE dampers; and (4) ambient temperature.

The selected response parameters include: (1) the base shear force, which is the total shear shared by the viscoelastic dampers and the frame; and (2) the floor displacement. The meaning of the symbols which represent the selected conditions are represented in Tables 2-II to 2-V. For example, if the number of the viscoelastic dampers were selected as 10, 5, 3, 1, they were assigned as VE10, VE5, VE3, VE1. The total area of damper at first floor was assigned as area 1 while those for the remaining dampers were assigned as area 2. The area 2 is equal to 60% of the area 1. The unknown coefficients $A_0 = 10.26$ psi, $\beta = 0.001$, $\mu = 3.0$, $\alpha = 0.60$, $\theta = 107$, $T_o = 28^oC$ were adopted in this study.

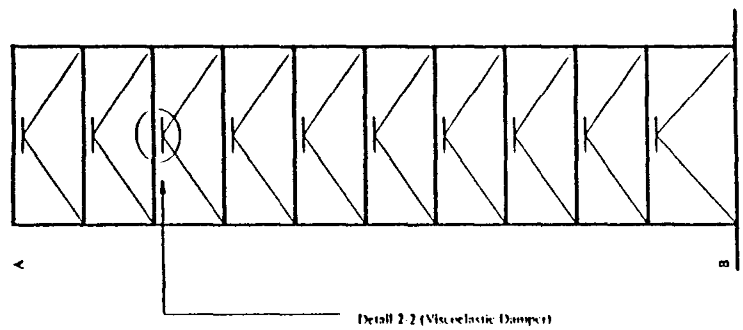

FIGURE 2-40 **Arrangement of Viscoelastic Dampers Design**

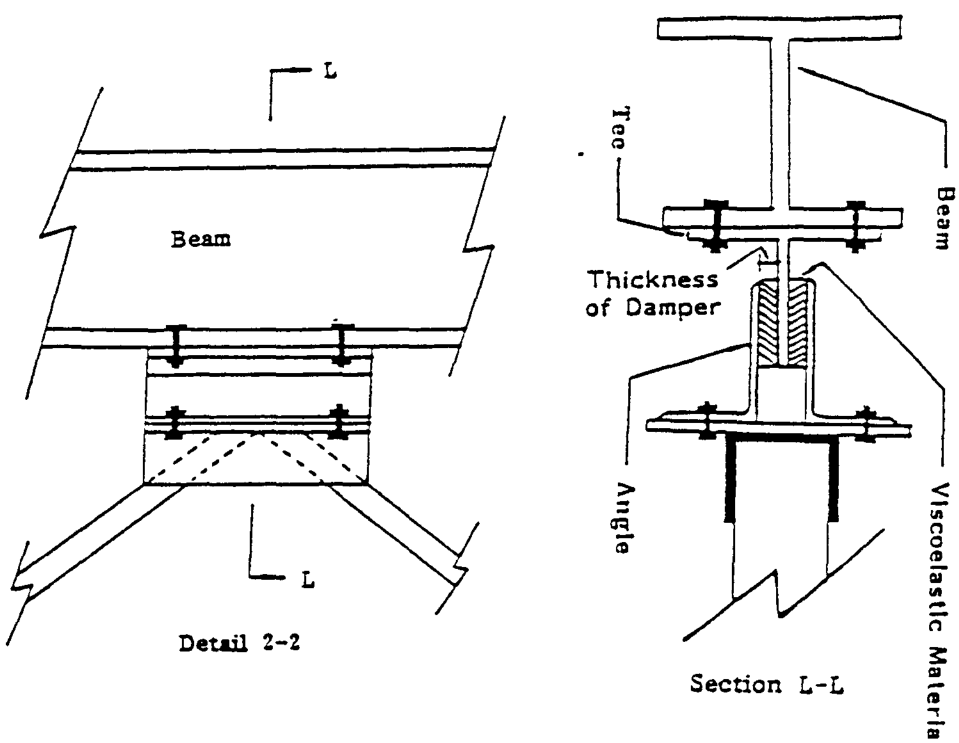

FIGURE 2-41 and 2-42 Detail of Viscoelastic Dampers

TABLE 2-II The Symbols of the Location of VE Dampers

Symbols	Explanation
VE10	Each Floor was mounted with a VE Damper
VE5	Floors 1,2,3,4,5 were mounted with a VE Damper
VE5(2)	Floors 1,3,5,7,9 were mounted with a VE Damper
VE3	Floors 1,2,3 were mounted with a VE Damper
VE3(2)	Floors 1,3,5 were mounted with a VE Damper
VE1	Floor 1 was mounted with a VE Damper

TABLE 2-III The Symbols of Area of VE Dampers

Symbol	Area 1 (in^2)	Area 2 (in^2)
a1	220	132
a2	250	150
a3	280	168
a4	310	186
a5	465	279

TABLE 2-IV The Symbols of Thickness of VE Dampers

Symbol	Thickness (in)
t1	1.30
t2	1.45
t3 -	1.60
t4	1.15
t5	1.00
t6	1.38
t7	1.34
t8	1.77

TABLE 2-V The Symbols of Temperature of VE Dampers

Symbol	Temperature (°C)
T0	0
T5	5
T10	10
T15	15
T20	20
T25	25
T30	30
T35	35
T40	40

2.7.1 Positional Effects of Viscoelastic Dampers

The effect of the number of viscoelastic dampers mounted on the structure was shown in Figures 2-43 and 2-44. Figures 2-43 indicates that when more dampers are mounted on the structure, the smaller maximum roof displacement (MRD) is produced. However, VE5(2) has a smaller MRD than VE5. This indicates that a viscoelastic damper mounted to every other floor starting from the 1st floor performs better than that mounted on the structure from floor 1 to floor 5. The results also show that the structure with VE(a3t1) has the best performance among the six cases and prove that viscoelastic dampers with greater area perform better. On the other hand, decreasing the thickness of viscoelastic dampers has resulted in better performance; however, this does not mean that the thinner the damper, the smaller the MRD responses. When the thickness of the damper is too small, the viscoelastic damper develops strain greater than its performance limit of 0.3. Therefore, the thickness of a viscoelastic damper should be carefully considered so that it will not be too small to induce large strain. At the same time, it should not be too large to increase its cost and to reduce its performance.

Figure 2-43 shows that VE3 reduces about 27% of the roof displacement, and VE10 reduces about 50%, compared to the structure without VE. Although the VE10 produces the smallest base shear force, mounting only one viscoelastic damper to the first floor could effectively reduce both base shear force and roof displacement.

The relations between the thickness of damper and its developed strain were shown in Figure 2-45. It indicates that when the thickness as are 1.0 in and 1.15 in, the strain measurements are greater than 0.3 which causes the damper to fail to perform properly.

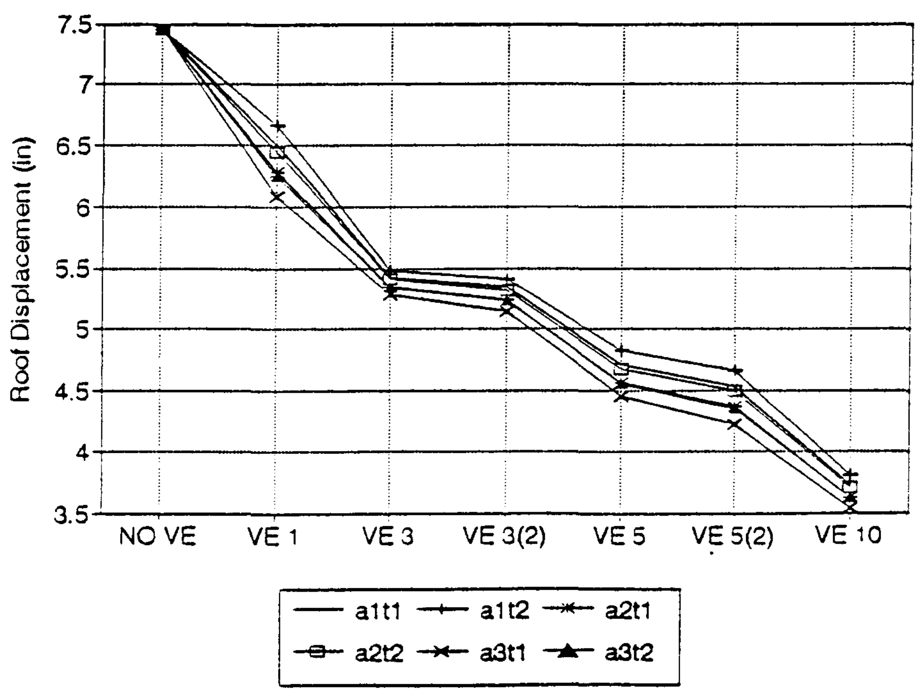

Fig.2.43 Comparison of Floor Displacement When the Structure is Subjected to El Centro Ground Motion

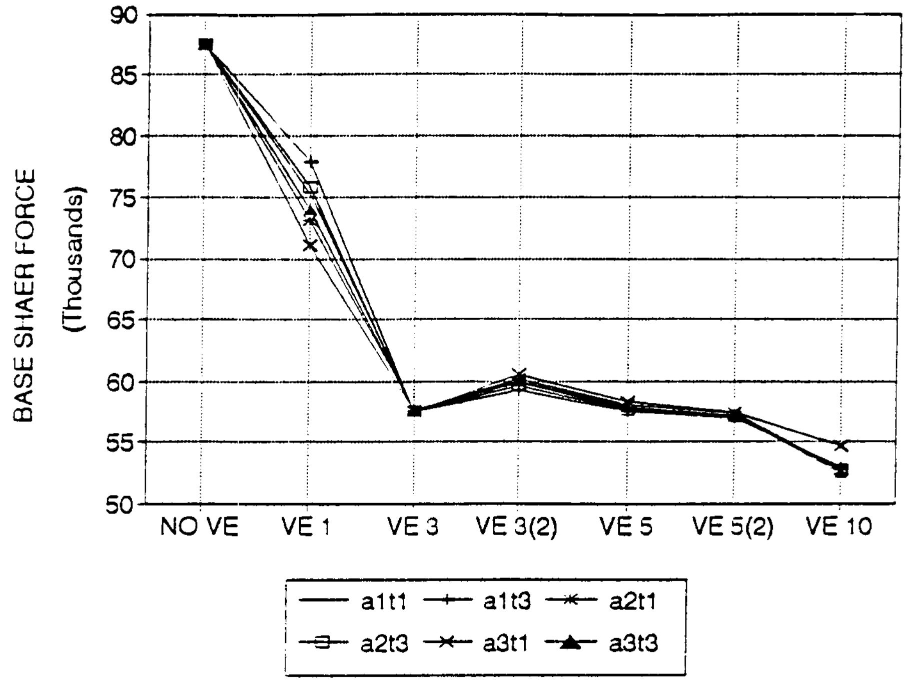

Fig.2.44 Comparison of Base Shear Force When the Structure is Subjected to El Centro Ground Motion

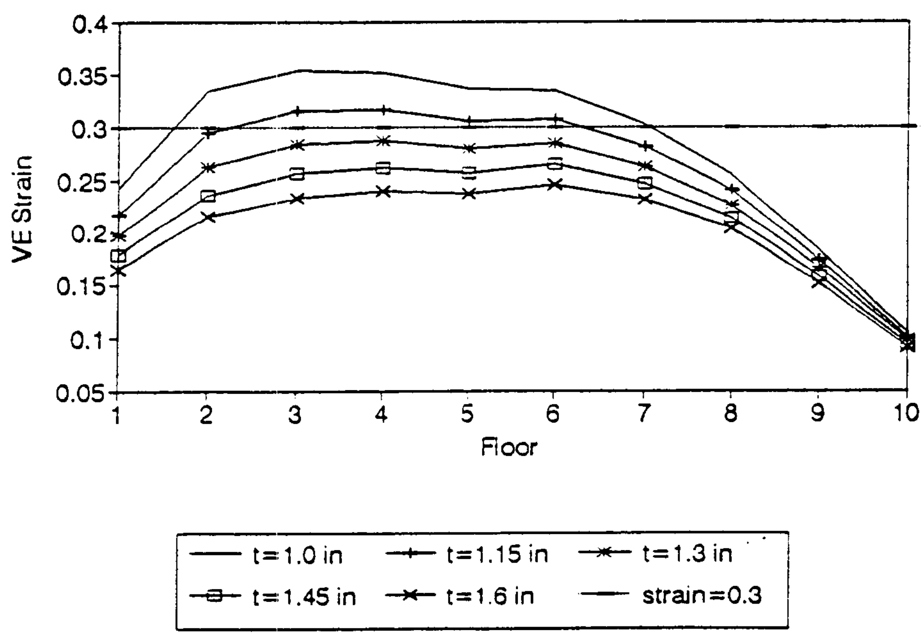

FIGURE 2-45 Comparison between the thickness and the Strain While the Structure is Subjected to El Centro Ground Motion

2.7.2 Effects of the Ambient Temperatures

The behavior of the viscoelastic damper is dependent on the ambient temperature. Since the viscoelastic dampers transfer dynamic energy into heat, their temperature rises during earthquake excitation. The temperature increase can affect the capacity of the dampers causing a severe problem. The effect of ambient temperature is, however, very complicated. Temperature increases can reduce the effective performance of the damper while temperature decreases can also increase material stiffness [43]. Both outcomes are regarded as unfavorable for the design of dampers.

The result of the temperature effects on the developed strain of the viscoelastic dampers is shown in Figure 2-46. It illustrates that the optimal selection of the viscoelastic damper at the ambient temperature 20^{o}C is not satisfactory when its temperature increases because the dampers develop strain greater than 0.3 during which the dampers fail to improve the seismic resistance. Figure 2-47 demonstrates that the thickness and the total area of the damper should be larger when the ambient temperature is higher to reduce its MRD while the thickness and the total area of the damper can be much smaller when the ambient temperature is lower in order to reach the same effects.

The maximum developed strain of the viscoelastic dampers was compared when the structure was subjected to ten different earthquake peak accelerations from 100 Gal to 1000 Gal of the San Fernando ground motion. Figure 2-48 shows that the strain of VE dampers is within its performance limit, 0.3, when the earthquake peak acceleration is less than or equal to 700 Gal of the San Fernando ground motion.

The response of the structure, with and without dampers, was compared when the structure was subjected to ten different earthquake peak acceleration from 100 Gal to 1000 Gal of the San Fernando ground motion. Figures 2-49 and 2-50 show that the curve of the structure without dampers and the curve of the structure with VE dampers are both linear when the peak acceleration is smaller than or equal to 700 Gal. The curve of the structure with VE dampers has a much smaller gradient. They also show the VE dampers fail to provide proper energy absorbing capacity when the peak acceleration is larger than 800 Gal because the strain measurement is greater than 0.3 which causes the damper to function improperly.

2.8 Comparison between Numerical Solutions and Experimental Results

In order to provide evidence of the accuracy of the numerical results, a comparison is made between numerical solutions and experimental results when a 2/5 scale steel structure, equipped to added VE dampers, is subjected to Hachinohe earthquake (1968) ground motion.

2.8.1 Test Structure

The test structure is a 2/5-scale five-story steel frame constructed under a U.S.-China cooperative research program on dynamic testing and analysis [73]. Overall dimensions of the test frame are 52.0" x 52.0" in plan and 224.0" in height, as shown in Figure 2-51 [74]. The modal member properties are listed in Table 2-VI [75].

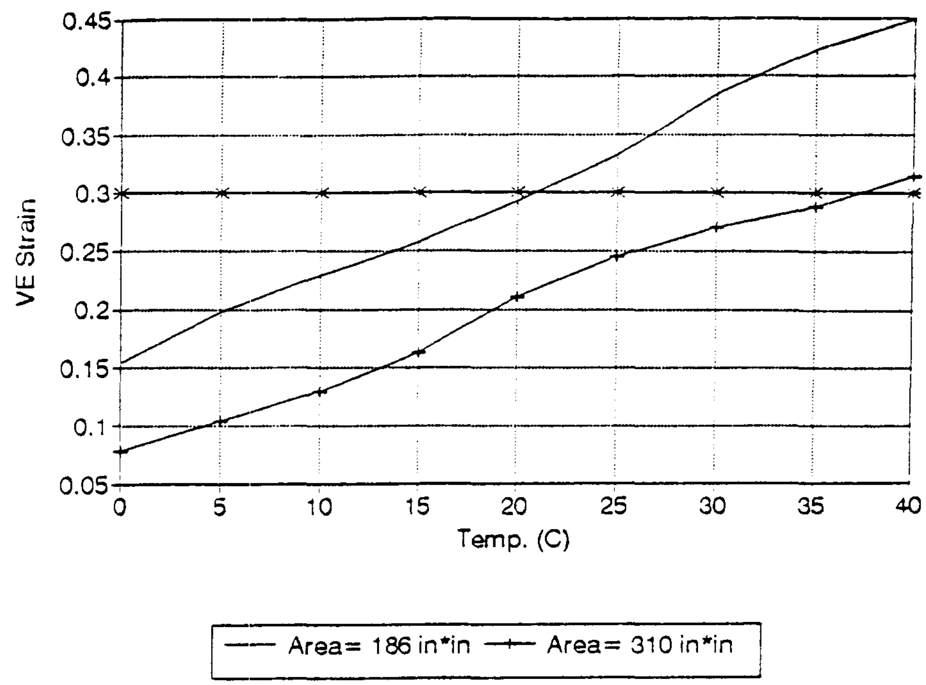

FIGURE 2-46 Comparison of Strain at different temperatures While the Structure is Subjected to El Centro Ground Motion

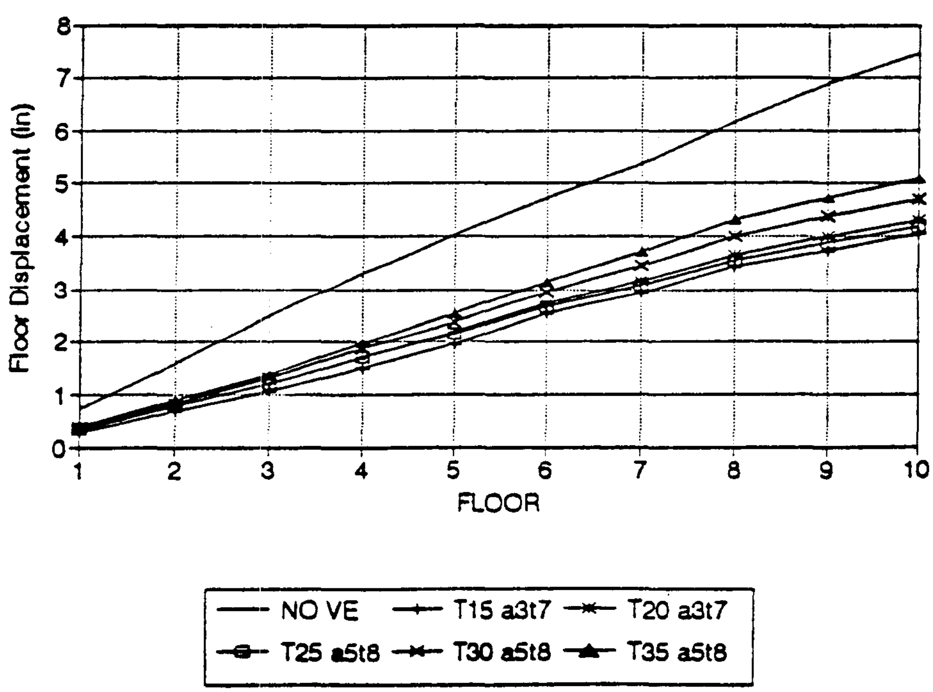

FIGURE 2-47 The Response of Floor Displacement at each Floor While the Structure is Subjected to El Centro Ground Motion

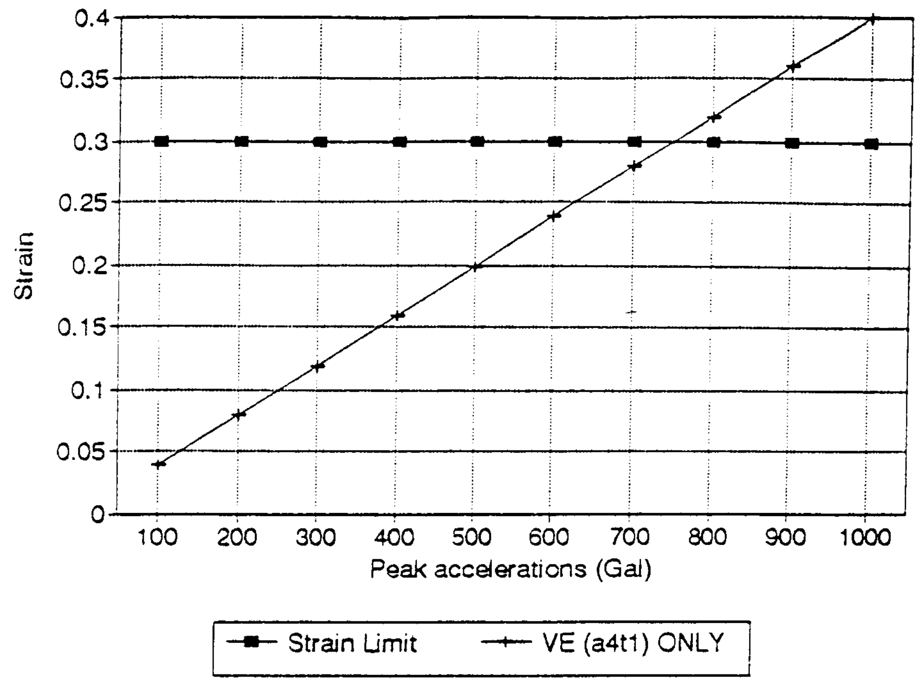

FIGURE 2-48 Comparison of Strain measurements When the Structure is Subjected to the Peak Acceleration of 100 Gal to 1000 Gal of San Fernando Ground Motion

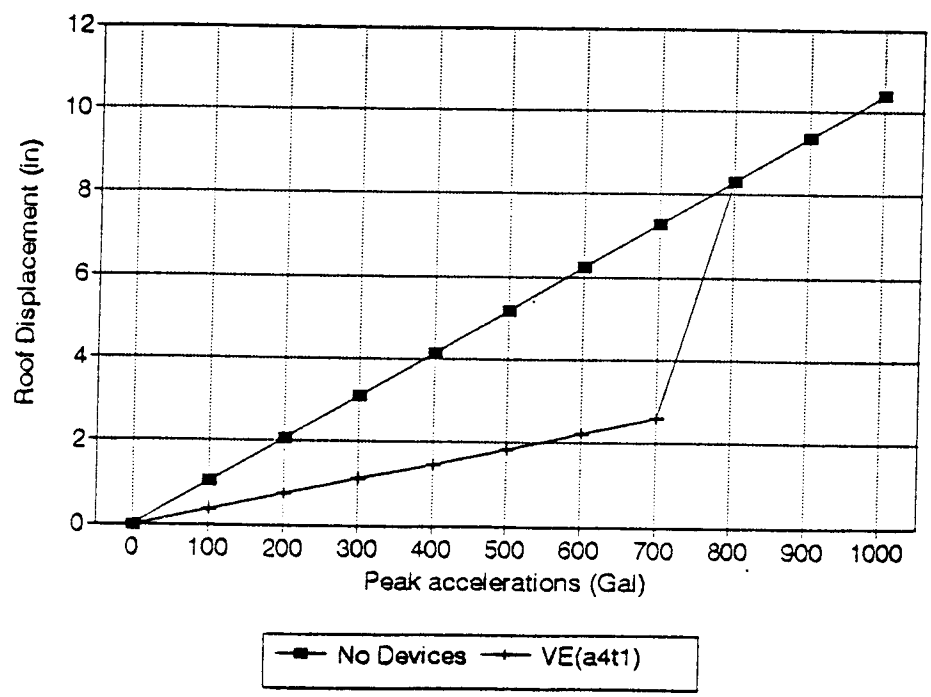

FIGURE 2-49 Comparison of Roof Displacement When the Structure is Subjected to the Peak Acceleration of 100 Gal to 1000 Gal of San Fernando Ground Motion

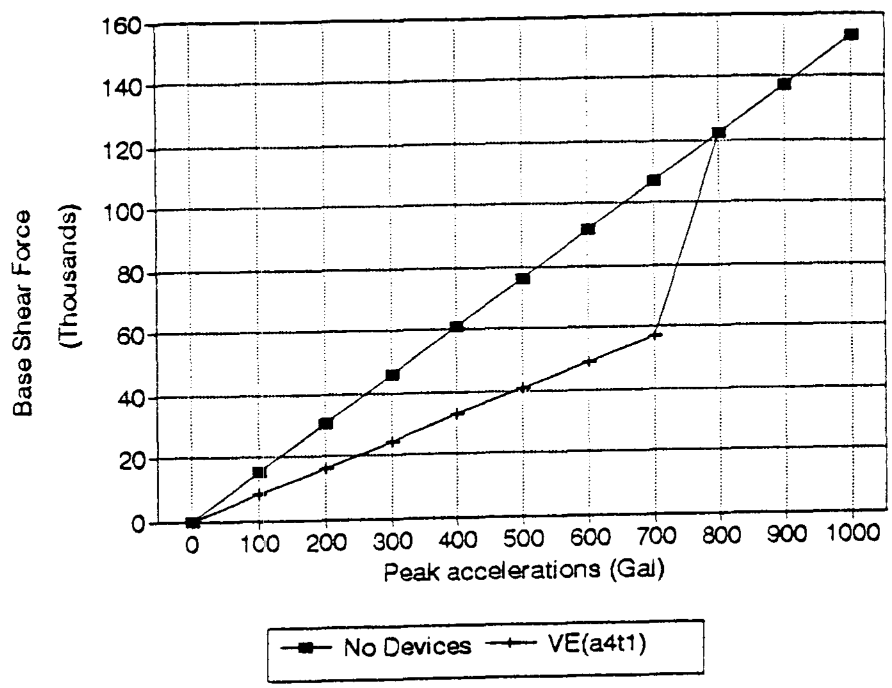

FIGURE 2-50 Comparison of Base Shear Force When the Structure is Subjected to the Peak Acceleration of 100 Gal to 1000 Gal of San Fernando Ground Motion

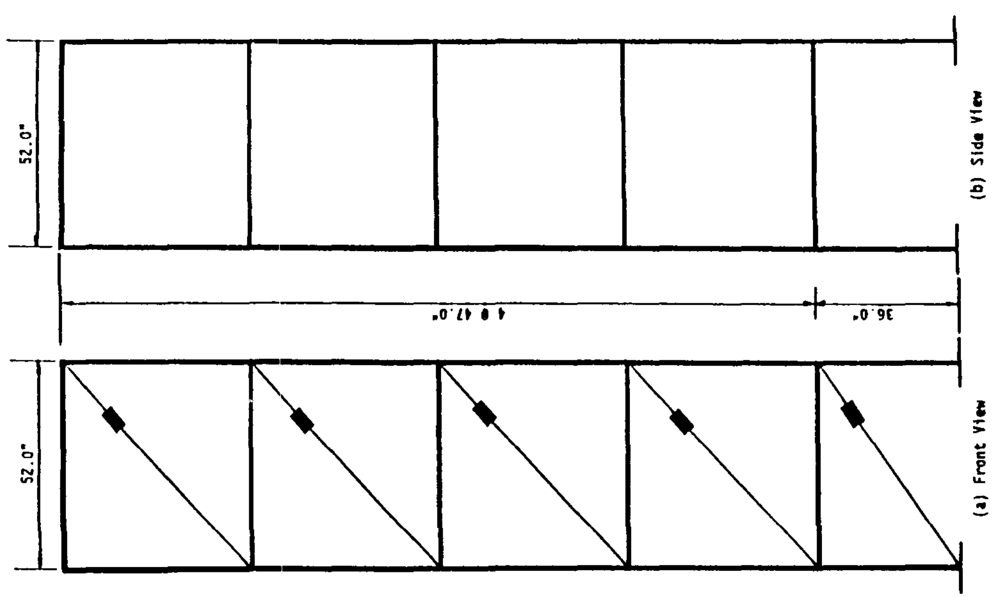

FIGURE 2-51 Five-Story Steel Frame with Added Viscoelastic Dampers [74]

TABLE 2-VI Prototype and Model Member Properties (Unit: Inches) [75]

COLUMN	PROTOTYPE	MODEL	
		THEORETICAL	ACTUAL
b_f	9.84	3.94	3.75
t_f	0.55	0.22	0.25
d_w	11.02	4.41	4.25
t_w	0.39	0.16	0.125
Area	15.19	2.43	2.41
I_x	407.5	10.43	10.30
S_x	67.2	4.3	4.34
Z_x	74.72	4.78	4.35
I_y	87.65	2.24	2.20
S_y	17.81	1.14	1.17
Z_y	27.1	1.73	1.76
$b_f/(2t_f)$	8.93	8.93	7.50
d_w/t_w	27.97	27.97	34.0

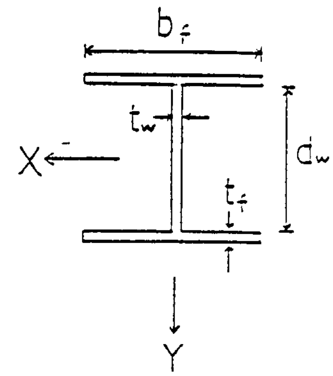

BEAM	PROTOTYPE	MODEL	
		THEORETICAL	ACTUAL
b_f	4.65	1.86	1.75
t_f	.51	0.20	0.25
d_w	8.82	3.53	3.38
t_w	0.39	0.16	0.125
Area	8.29	1.33	1.30
I_x	126.95	3.25	3.28
S_x	25.79	1.65	1.69
Z_x	30.07	1.92	1.94
$b_f/(2t_f)$	4.54	4.54	3.50
d_w/t_w	22.38	22.38	27.0

A lumped mass system simulating the dynamic properties of the prototype structure was accomplished by adding steel plates at each floor level. The weight at each floor is 1.27 kips for the first four floors and 1.31 kips for the fifth floor. All the girder-to-column joints are fully welded as rigid connections. This type of design produces a frame which behaves as a lumped mass five-degree-of-freedom system when subjected to lateral loads [74].

A total of ten viscoelastic dampers were mounted on the five-story model structure, of which one damper was installed in diagonal bracing at each panel of the model. The diagonal bracing members with added VE dampers were connected by bolts to the gusset plates welded to the girders. Each set of bracing is composed of two double angles (L 1-1/2 x 1-1/2 x 1/8) with a VE damper connected at the upper 1/3 part of the bracing [74].

2.8.2 Analytical Results and Experimental Results

The time-scaled 0.12g peak acceleration of Hachinohe earthquake ground motion record, shown in Figure 2-52, was used as the input excitation to the model structure. The thickness and area of added VE damper adopted for this study are 0.2 in and 1.5 in^2, respectively. The calculated natural frequency of the model structure without added dampers corresponding to the first mode of vibration is 3.175 Hz. The critical damping used in the analytical study is 0.6%. The experimental and analytical results of the floor displacement at different temperatures are listed in Table 2-VII. The comparisons of absolute accelerations between analytical and experimental results are listed in Table 2-VIII. The results of the response of model structure, with and without added dampers, are very satisfactory.

Figures 2-53 and 2-54 present the experimental and analytical results of the damper effectiveness on roof displacement. Figures 2-55 and 2.-56 show the analytical and experimental results of the damper effectiveness on absolute acceleration at fifth floor. The results are satisfactory according to these figures.

A comparison between experimental and analytical results on temperature effect is also made. Figure 2-57 shows the displacement at each floor of the structure with and without dampers at 25°C and at 30°C. The structure's floor displacement curves of experimental and analytical results for the structure with added viscoelastic dampers are almost indistinguishable. Figure 2-58 demonstrates the absolute acceleration at each floor of the structure with and without dampers at 25°C and at 30°C. The structure's absolute acceleration curves of experimental and analytical results for the structure with added viscoelastic dampers are almost indistinguishable. Figures 2-59 shows the response of floor displacement at the fifth floor when the dampers are exposed to different temperatures. The difference between analytical and experimental results are very barely noticeable. Overall, the correlation between numerical results and test results is illustrated in Figures 2-57, 2-58, and 2-59 where a very good agreement can be seen.

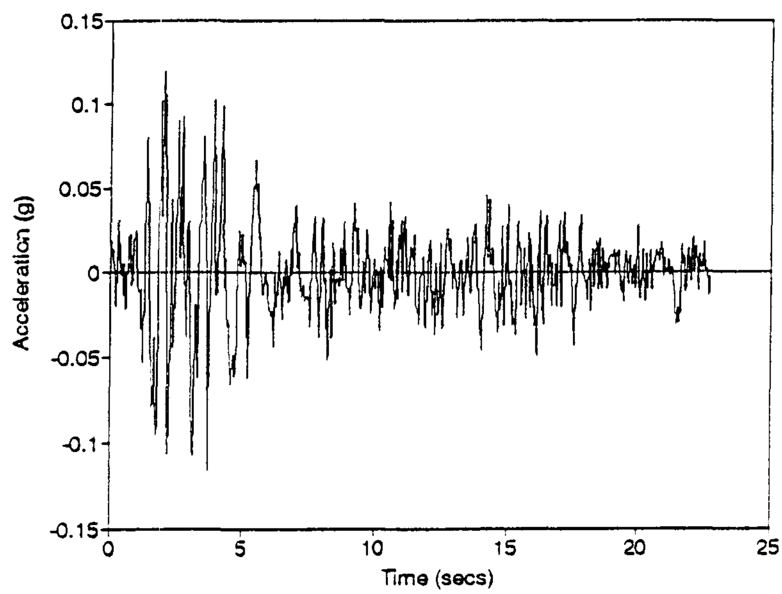

FIGURE 2-52 Time-Scaled Hachinohe Earthquake Ground Motion

TABLE 2-VII A Experimental Results (Floor Displacement: Inches)

Story Floor	No Damper	25°C	30°C	34°C	38°C	42°C
5	1.066	0.213	0.282	0.366	0.461	0.558
4	0.874	0.183	0.242	0.318	0.401	0.490
3	0.677	0.145	0.190	0.250	0.314	0.383
2	0.426	0.091	0.122	0.162	0.200	0.242
1	0.149	0.039	0.049	0.060	0.070	0.082

TABLE 2-VII B Analytical Results (Floor Displacement: Inches)

Story Floor	No Damper	25°C	30°C	34°C	38°C	42°C
5	1.063	0.211	0.285	0.336	0.485	0.549
4	0.944	0.188	0.253	0.298	0.429	0.485
3	0.734	0.148	0.198	0.233	0.333	0.375
2	0.448	0.093	0.123	0.144	0.204	0.229
1	0.131	0.030	0.038	0.044	0.061	0.068

TABLE 2-VIII A Experiment Results (Absolute Acceleration: g)

Story Floor	- No Damper	25°C	30°C	34°C	38°C	42°C
5	1.151	0.251	0.290	0.371	0.466	0.576
4	0.909	0.229	0.270	0.338	0.418	0.508
3	0.777	0.195	0.243	0.286	0.340	0.404
2	0.538	0.166	0.197	0.221	0.255	0.286
1	0.241	0.136	0.149	0.148	0.153	0.164

TABLE 2-VIII B Analytical Results (Absolute Acceleration: g)

Story Floor	No Damper	25°C	30°C	34°C	38°C	42°C
5	1.099	0.248	0.293	0.356	0.428	0.500
4	0.930	0.222	0.280	0.331	0.390	0.440
3	0.820	0.200	0.245	0.285	0.321	0.368
2	0.554	0.166	0.191	0.212	0.242	0.269
1	0.221	0.136	0.143	0.147	0.149	0.154

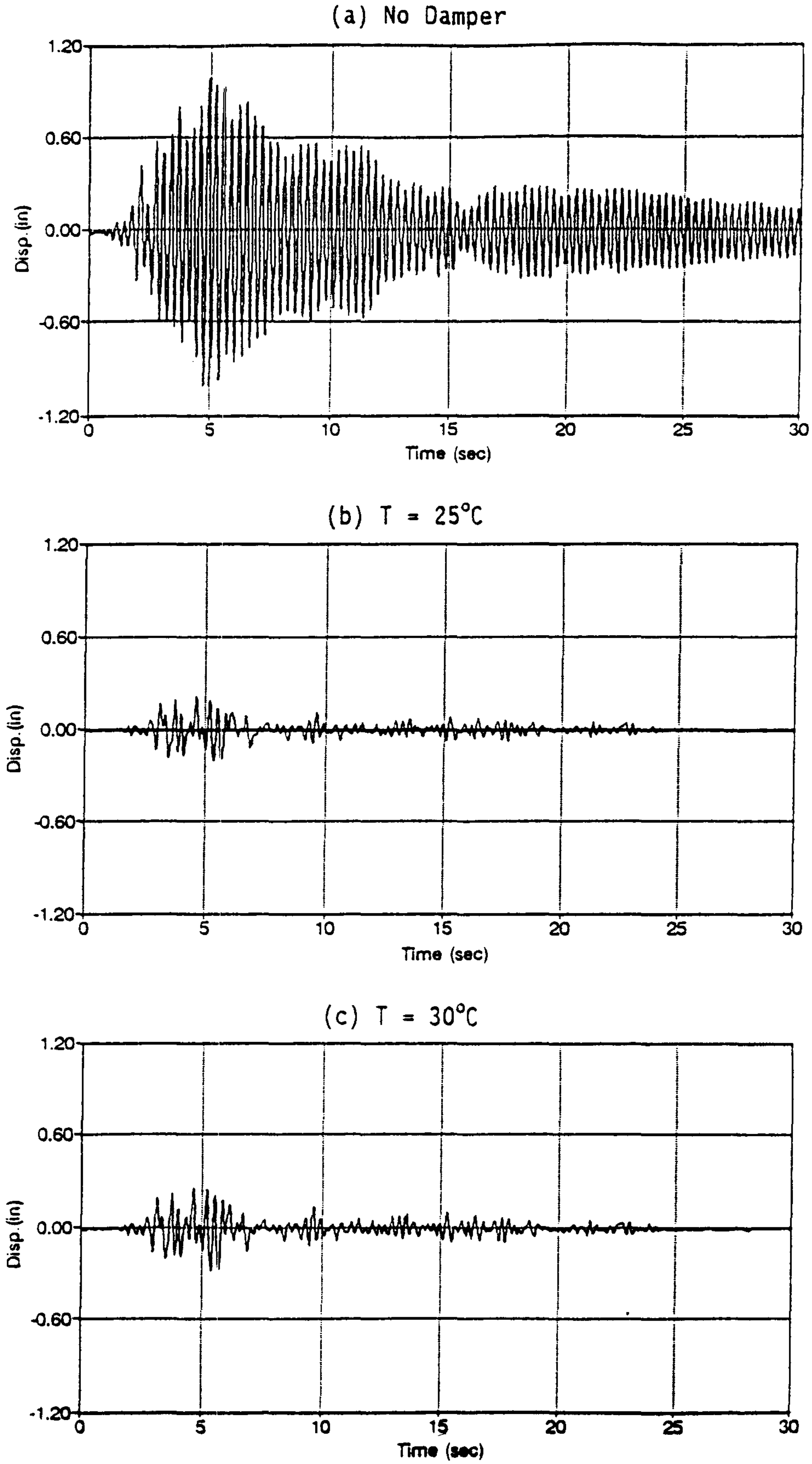

FIGURE 2-53 Damper Effectiveness on Roof Displacement (Experimental Results) [74]

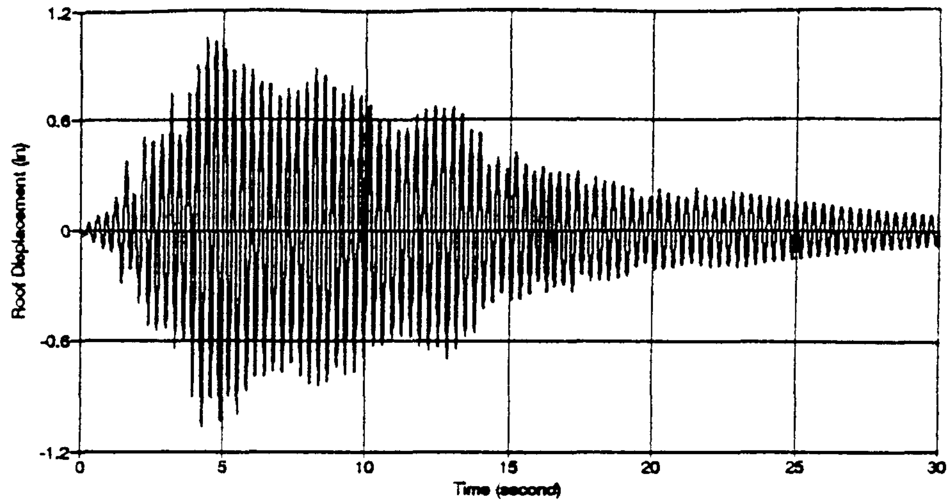

(b) T = 25°C

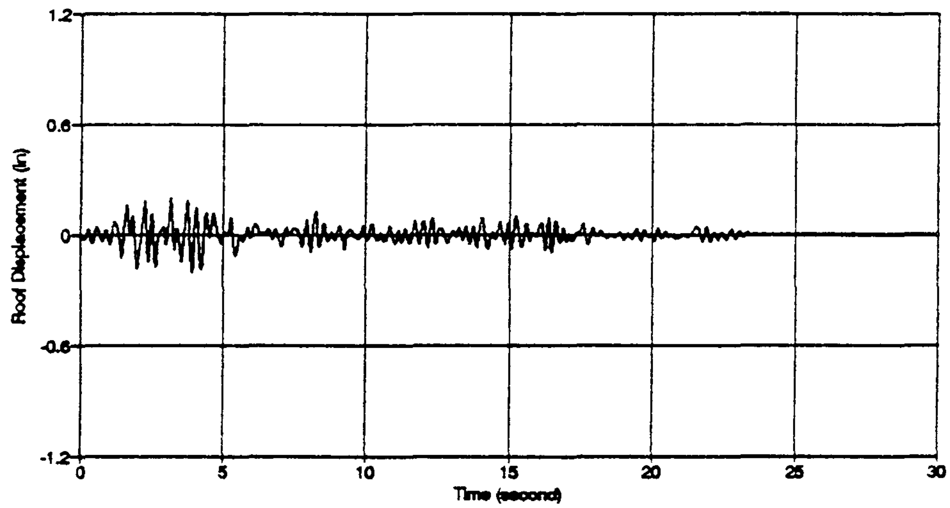

(c) T = 30°C

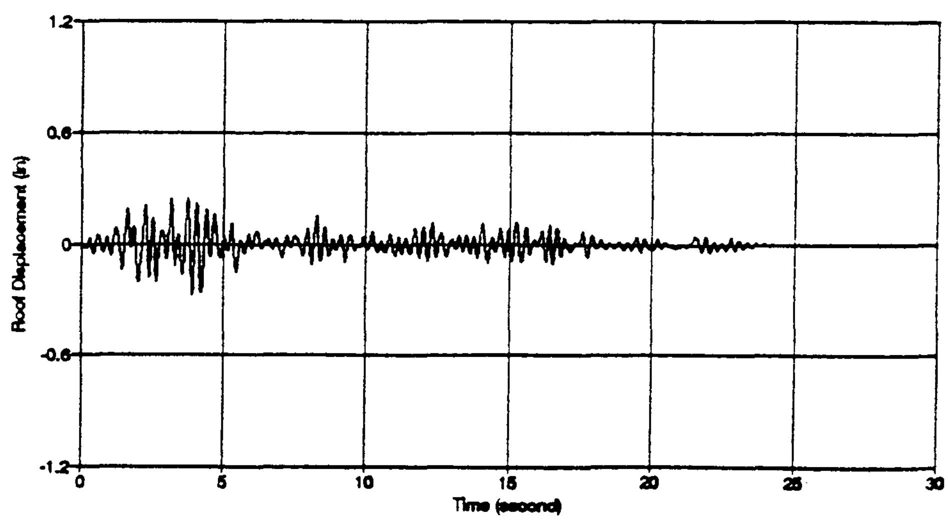

FIGURE 2-54 Damper Effectiveness on Roof Displacement (Analytical Results)

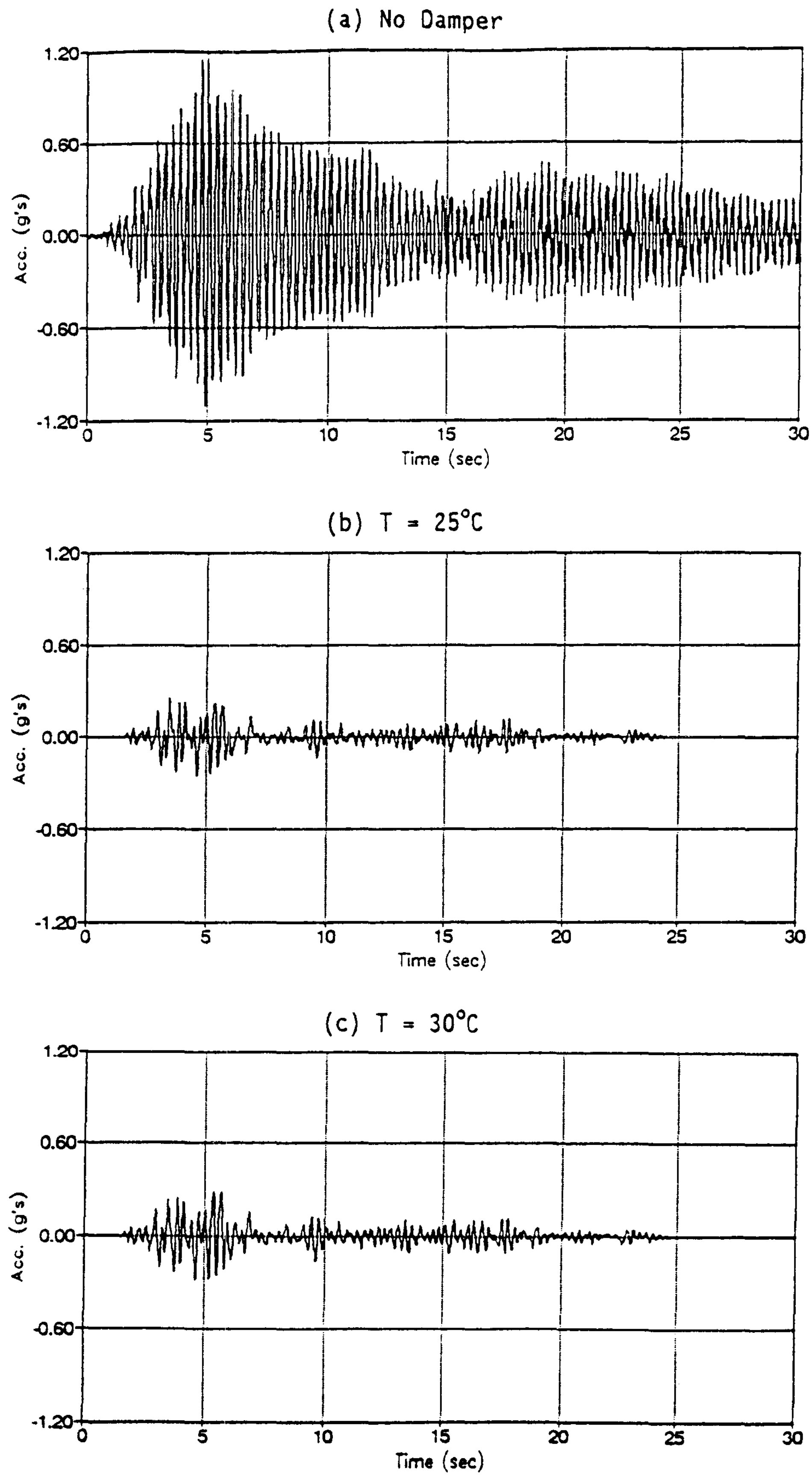

FIGURE 2-55 Damper Effectiveness on Acceleration (Experimental Results) [74]

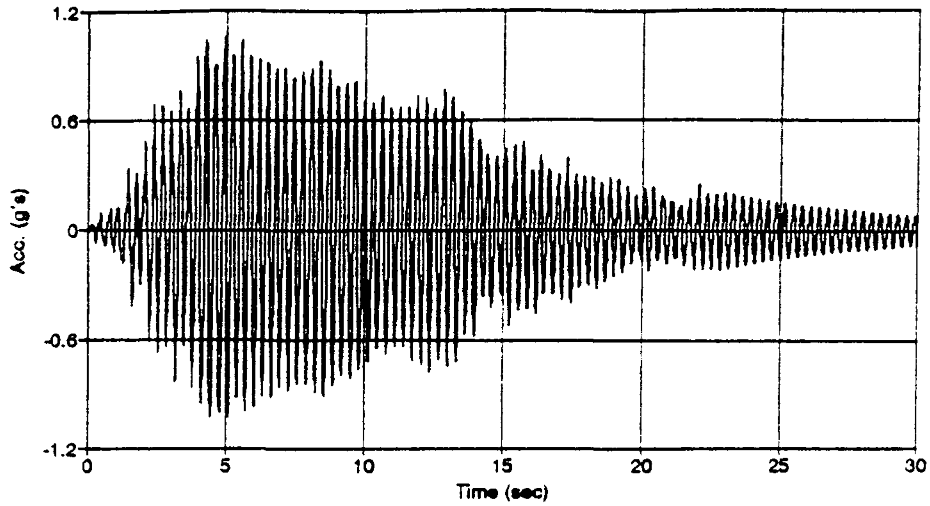

(b) T = 25°C

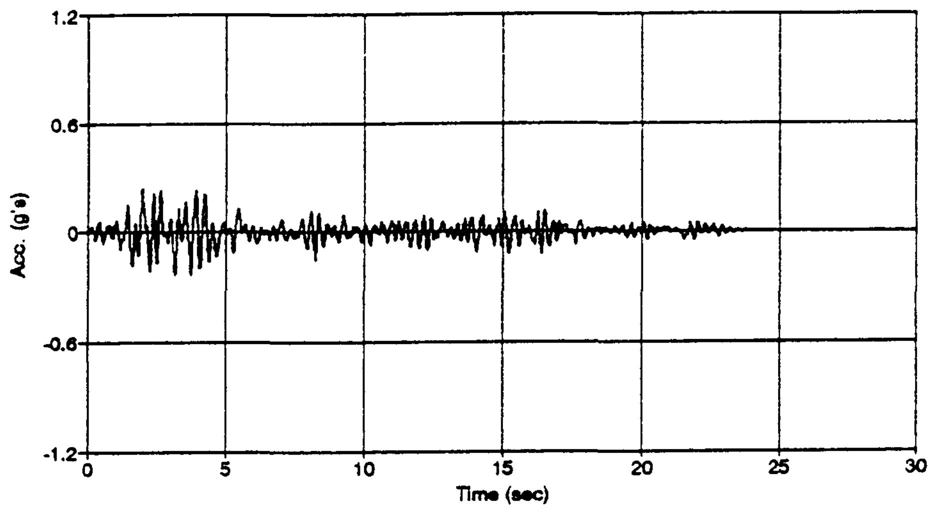

(c) T = 30°C

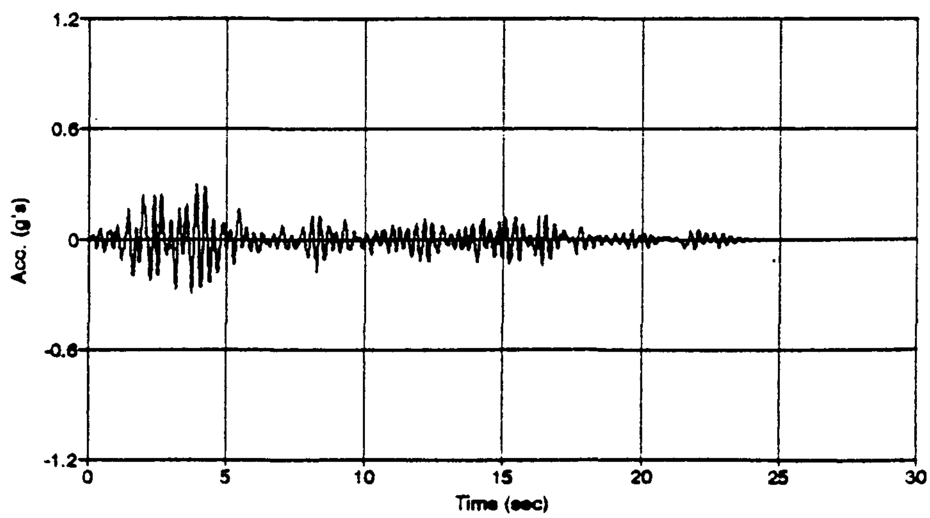

FIGURE 2-56 Damper Effectiveness on Acceleration (Analytical Results)

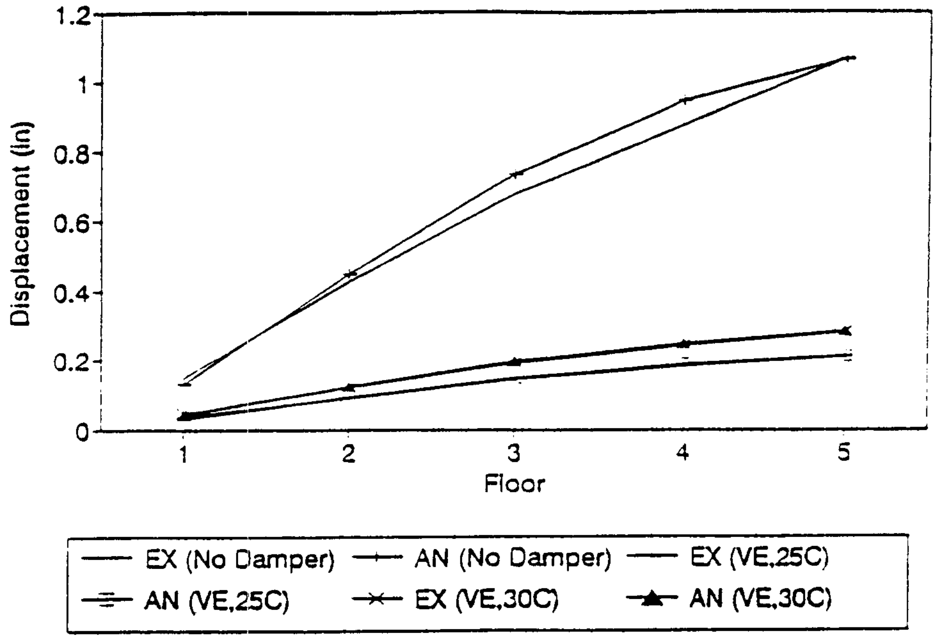

FIGURE 2-57 Comparison between Analytical and Experimental Results When the Structure is Subjected to Hachinohe Ground Motion

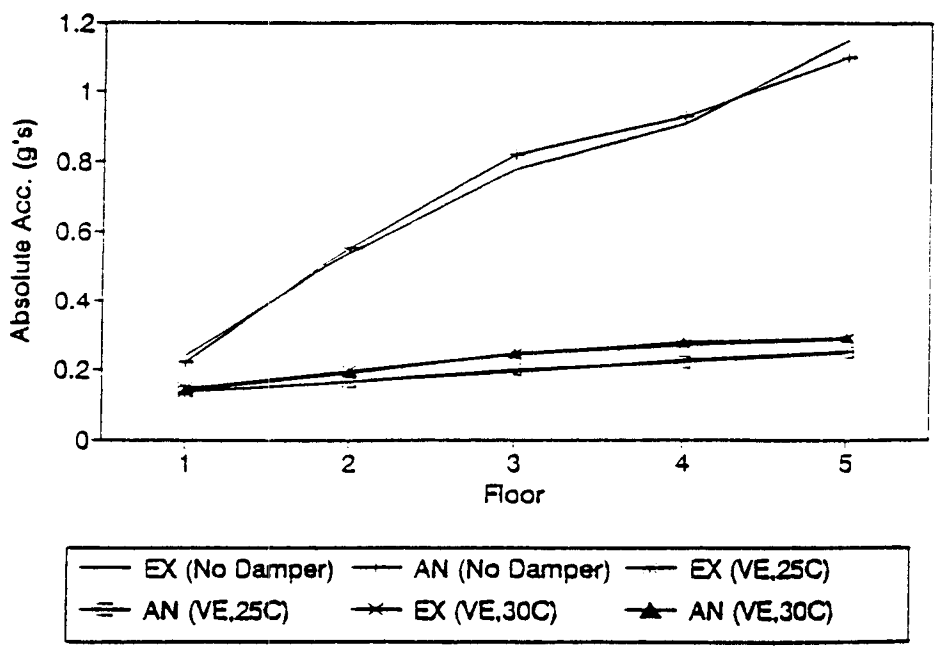

FIGURE 2-58 Comparison between Analytical and Experimental Results When the Structure is Subjected to Hachinohe Ground Motion

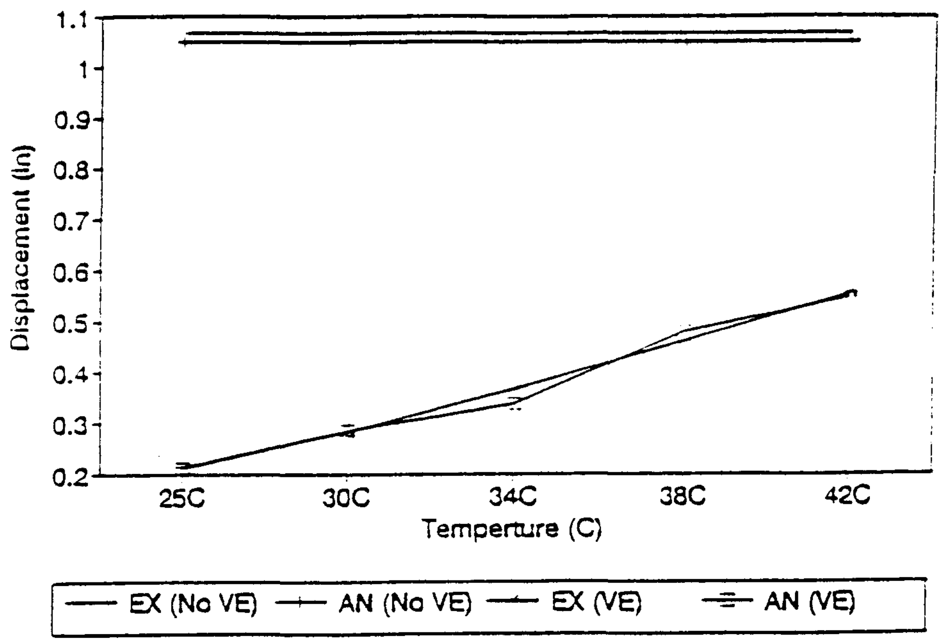

FIGURE 2-59 Comparison between Analytical and Experimental Results When the Structure is Subjected to Hachinohe Ground Motion

2.9 Discussion on the Viscoelastic Dampers

Properly designed viscoelastic dampers can increase the overall level of structural damping to improve seismic resistance of buildings. Numerical results show that the energy-absorption capacity of the viscoelastic damper decreases as ambient temperature increases. Due to temperature effects, the optimal design of viscoelastic dampers may need to be changed for different temperature environments. Therefore, the temperature effect should be considered one of the most important factors in damper design.

Results also show that the thickness of the damper plays an important role in improving the seismic resistance. During the design stage, critical decisions must be made about selecting the optimal damper thickness to maintain strain measurements under 0.3 and to ensure that the damper design is effective and economical. The total area of the viscoelastic dampers should also be determined properly to strengthen its capacity of seismic resistance without high cost. Mounting dampers to all stories of the structure is not necessarily the most economical design, but adding a viscoelastic damper to the first floor will effectively reduce the response of the structure.

Numerical results illustrate that VE dampers located at the lower floors of a structure absorb more energy than those at upper floors. Figures 2-60 to 2-65 show that relationship of stress and strain of the VE dampers located at the 1st, 5th, and 10th floors, respectively. The time-history responses (roof displacement, column shear force at point B, and base shear force) of the structure with and without VE dampers are shown in Figures 2-66 to 2-68 when the structure is subjected to El Centro ground motion. Figures 2-66 to 2-68 illustrate that not only floor displacement, but also shear stress of the structure are significantly reduced during earthquakes by adding viscoelastic dampers properly. In Figure 2.-66, the structure with VE generates 13 peaks while the structure without VE generates 12 peaks. Thus, we can say that the natural frequency is not changed significantly because adding VE dampers to the structure does not generally increase the structure's stiffness.

Figure 2-67 indicates that the columns of the structure with VE dampers take a much smaller portion of base shear force compared to those of the structure without VE dampers. The main structural components may be optimized for their required stiffness and load-bearing features at lower cost because the energy-absorption demands on the main structural members are lessened.

A drawback of adopting viscoelastic dampers as energy-absorbing devices for seismic hazard mitigation is the structural response cannot be reduced greatly in the early stages of an earthquake and cannot provide a safe-failure mechanism in the event of strong earthquakes. As shown in Figure 2-66, the roof displacement is substantially reduced after the fourth second. Meanwhile, it is not reduced from the first to third seconds. The main reason for this phenomenon is the velocity dependence in these devices is generally regarded as unfavorable, as it casts uncertainty upon the magnitude of the resisting force [56]. The viscoelastic dampers are made from a velocity proportional viscous material. Because the maximum displacement and the maximum velocity of the dampers never occur at the same time, there exists a conflict between dissipating the energy and developing resisting forces. Therefore, if a peak response occurs during early stages of earthquake excitation, which is generally true for most events, the VE dampers would be unable to reduce its response greatly in time. As a result, the structure may suffer severe damage under extreme earthquake loadings.

The selection of design parameters for the VE dampers depends on the structure's dynamic characteristics, the expected earthquake intensity, and ground motion characteristics, such as amplitude, frequency content and duration of the ground motion. According to the numerical results, determination of the design properties of viscoelastic dampers is a complex process. Multiple layers of viscoelastic dampers could be considered as an alternative design to overcome the possibility of developing large strain during earthquakes. This design, producing different strains in the viscoelastic damper, will provide reliable energy absorption capacity when subjected to different earthquakes. In addition, a combination of TPEA and VE dampers may be considered a reliable energy-absorbing system because each can compensate for the shortcomings of the other device. A combination of VE and TPEA will be discussed later.

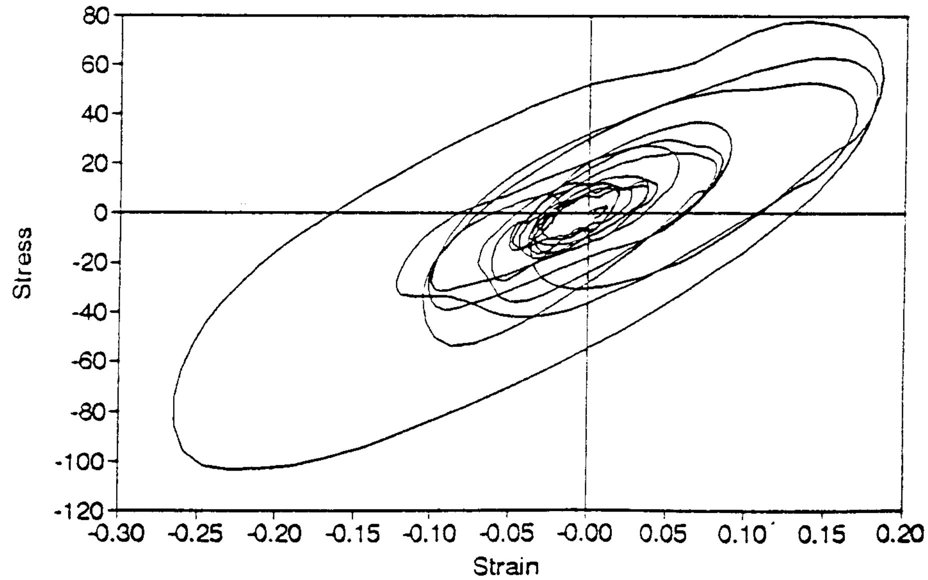

Fig.2.60 The Relation of Force and Displacement of Dampers at 1st Floor When the Structure is Subjected to El Centro Ground Motion

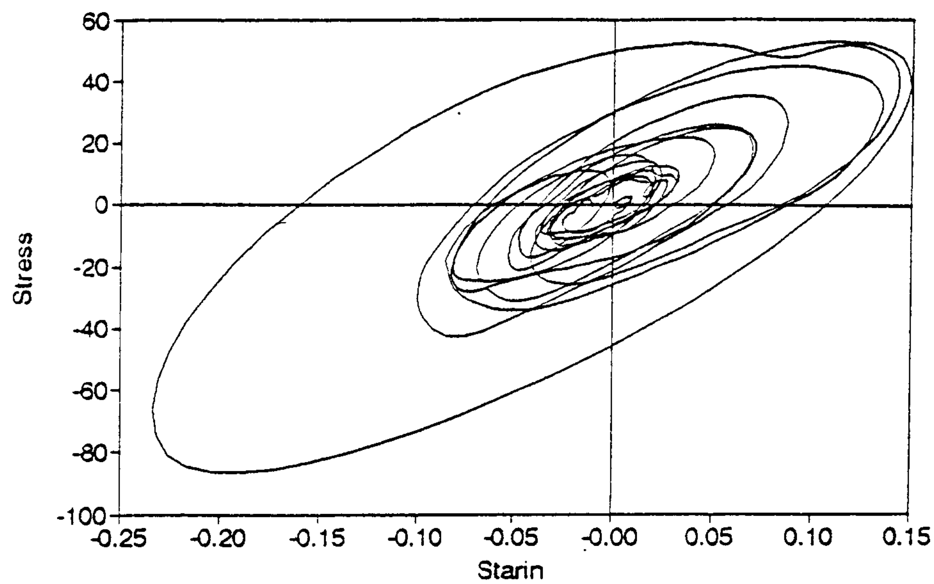

FIGURE 2-61 The Relation of Force and Displacement of Dampers at 5th Floor When the Structure is Subjected to El Centro Ground Motion

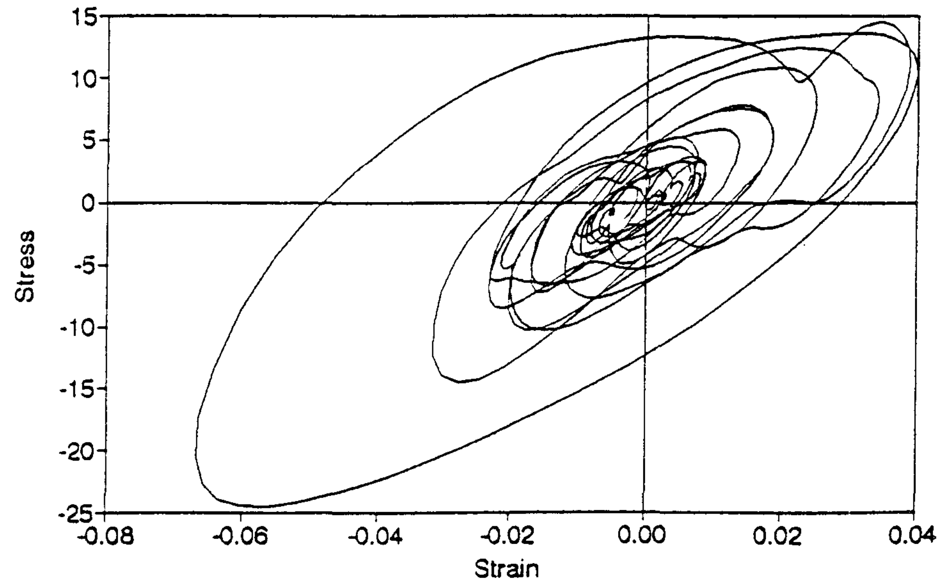

FIGURE 2-62 The Relation of Force and Displacement of Dampers at 10th Floor When the Structure is Subjected to El Centro Ground Motion

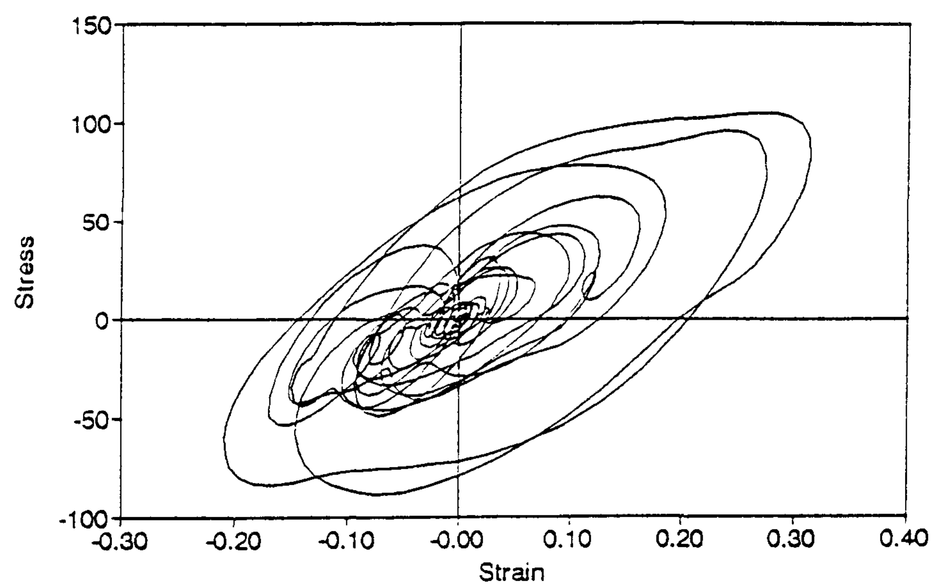

FIGURE 2-63 The Relation of Force and Displacement of Dampers at 1st Floor When the Structure is Subjected to San Fernando Ground Motion

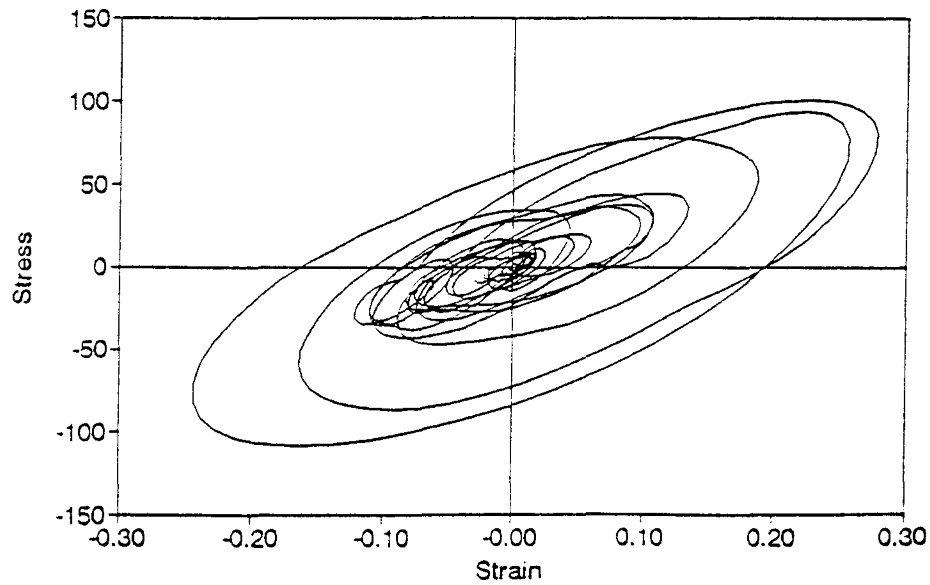

FIGURE 2-64 The Relation of Force and Displacement of Dampers at 5th Floor When the Structure is Subjected to San Fernando Ground Motion

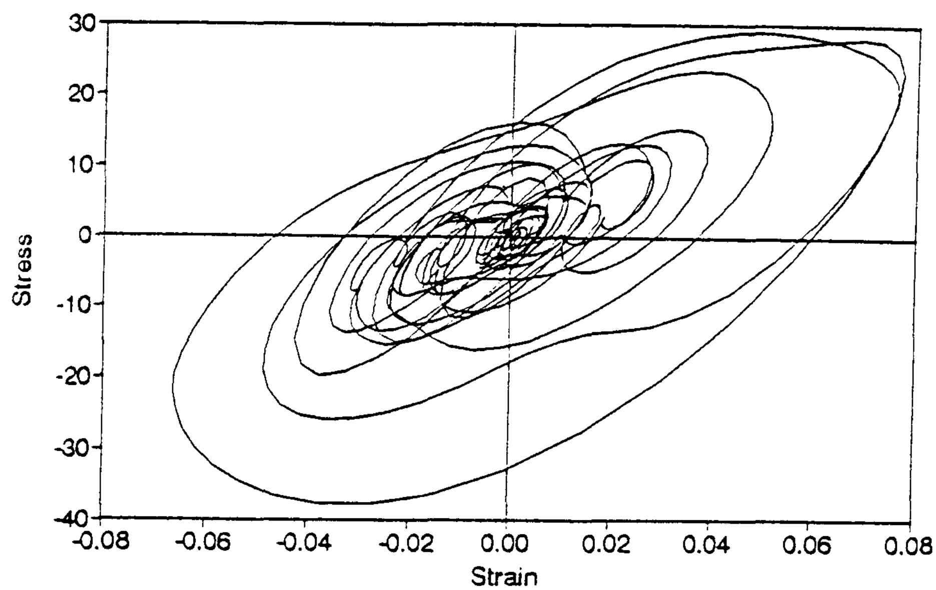

FIGURE 2-65 The Relation of Force and Displacement of Dampers at 10th Floor When the Structure is Subjected to San Fernando Ground Motion

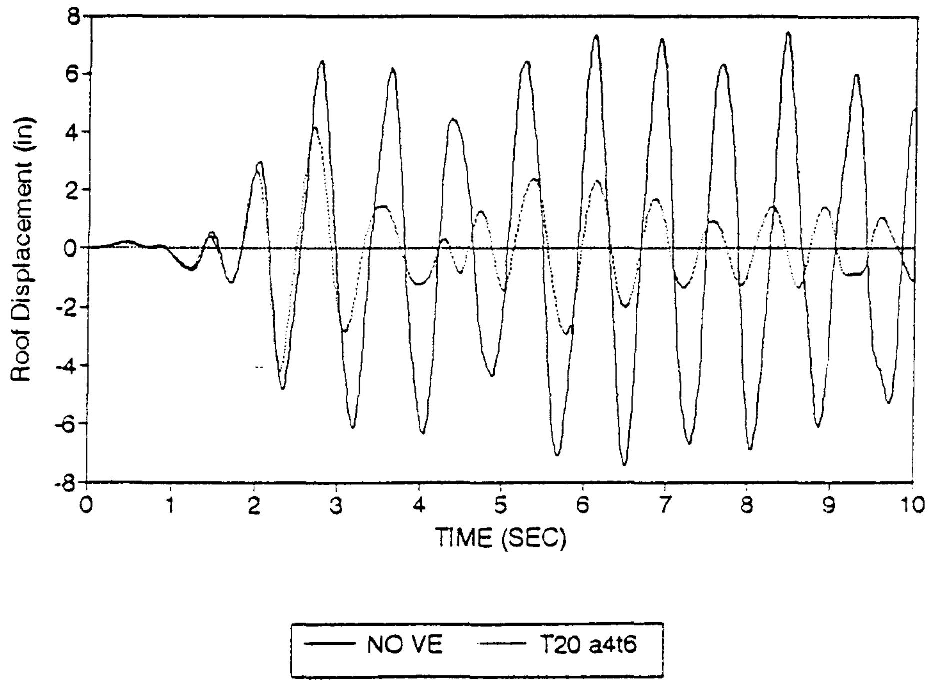

FIGURE 2-66 The Response of Floor Displacement When the Structure is Subjected to El Centro Ground Motion

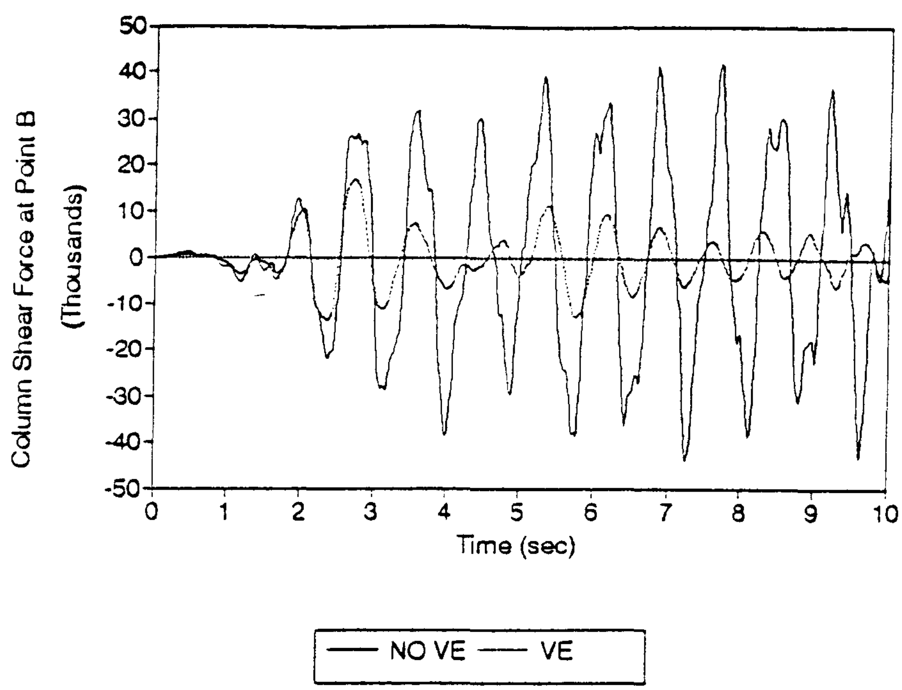

FIGURE 2-67 The Response of Column Shear Force at Point B When the Structure is Subjected to El Centro Ground Motion

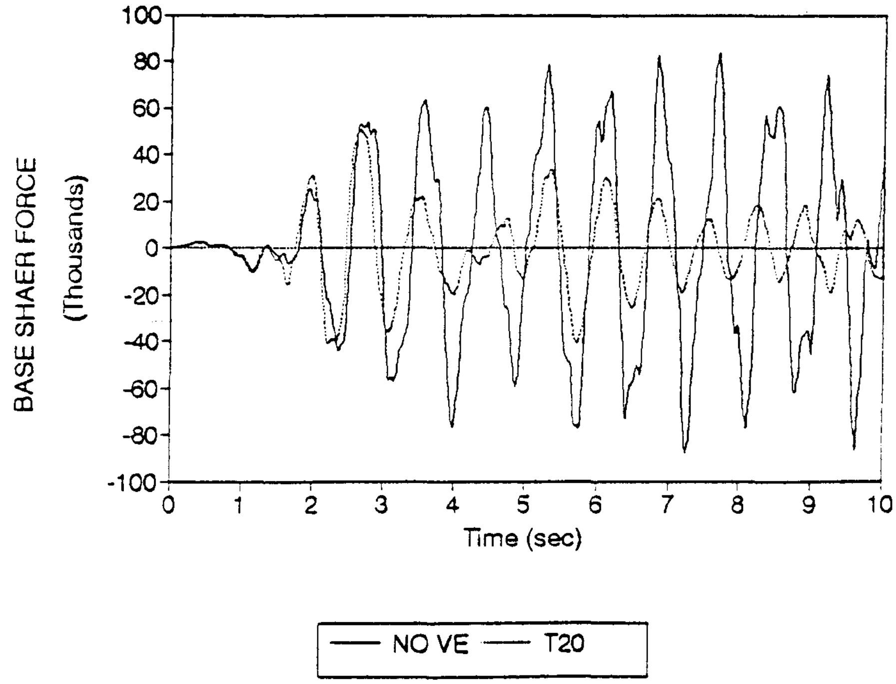

FIGURE 2-68 The Response of Base Shear Force When the Structure is Subjected to El Centro Ground Motion

SECTION 3
Seismic Study of High-Rise Buildings with TPEA

3.1 Current Status of TPEA Device Development

The use of a plate energy absorber (TPEA) is a relatively new concept. At the present time, a cooperative research project to investigate the effective of the tapered-plate energy absorber (TPEA) for earthquake-resistant structures is being carried out jointly by the National Taiwan University and State University of New York at Buffalo. From the test results [66], it is confirmed that TPEA can sustain an extremely large number of yielding reversals. Thus, such devices are a promising alternative for seismic hazard mitigation of buildings and other structures.

3.1.1 Analytical Model for TPEA Devices

A two-surface plasticity model [49, 66] is adopted so that the behavior of the TPEA devices subjected to earthquake loadings can be predicted accurately. The analytical model is verified by the experimental results described in the following section.

The derivation procedure of the adopted model is similar to that used by Chen and Powell [45] by using the Mroz Theory. The constitutional relationship formulated will be a stress resultant and deformation relationship instead of a stress resultant and displacement relationship. Figure 3-1 shows that the yield and bounding surfaces [49, 66] follow the kinematic and isotropic hardening rules, respectively. The stress resultant (force) within the yield surface will be purely elastic, and the changes in the generalized plastic modulus will be related by a shape factor while the stress resultant is located on the yield surface and moves toward the bounding surface. In the two-surface plasticity model proposed by Tseng [46, 49, 66], the shape and the size of the bounding surface will not change when the plastic strain is developed due to the movement of yield surface inside the region bounded by this bounding surface. The yield surface, which moves within or with the bounding surface, however, can expand or contract because of accumulated plastic strain and plastic energy.

The generalized stress resultants, F, for the general case are shown in Figure 3-1. In the formulation, the stress resultants include two forces only. The two forces are axial force, P, and transverse shear force, V. It should be noted that the flexural characteristics of the TPEA element are a function of the transverse shear force V. The generalized resultants may be written as:

$$\boldsymbol{F}^T = [P, V] \tag{3.1}$$

Assuming ϕ is the generalized yield function for the TPEA element, the outward normal direction to the yield surface is given by:

$$\hat{\boldsymbol{n}} = \frac{\phi_{,F}}{\left[\phi_{,F}^T, \phi_{,F}\right]^{1/2}} \tag{3.2}$$

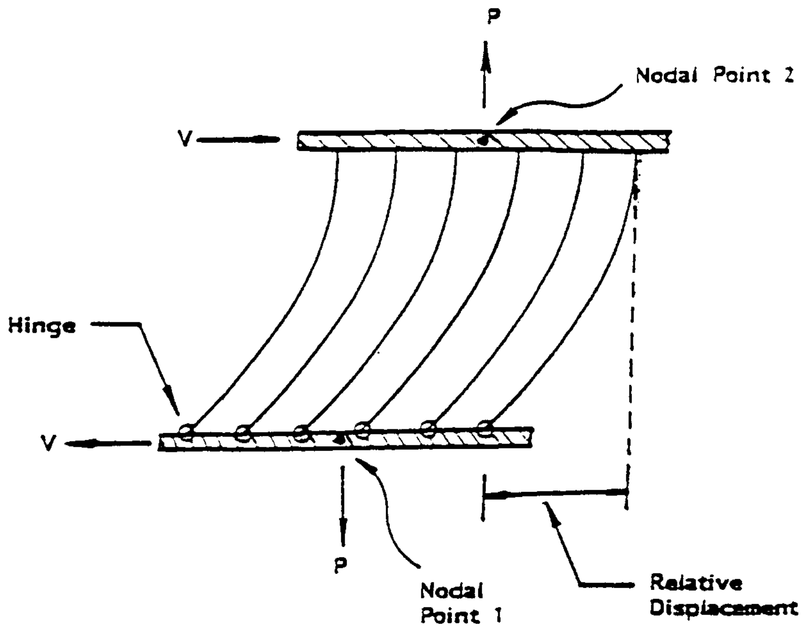

FIGURE 3-1 Mechanical Behavior of TPEA Device [66]

where

$$\phi_{,F}^{T} = \left[\frac{\partial\phi}{\partial P}, \frac{\partial\phi}{\partial V}\right] \tag{3.3}$$

and $\vec{n}$ is the unit outward normal vector to the yield surface.

The plastic deformation increment $d\vec{u}_p$ is defined as follows, according to the normality rule:

$$d\vec{u}_p = \vec{n} \cdot du_p \tag{3.4}$$

where du_p is the magnitude of the plastic deformation.

The increment of stress resultants dF in the normal direction n is defined as $d\vec{F}_n$; that is

$$d\vec{F}_n = \vec{n}\left(\vec{n}^T \cdot d\vec{F}\right) \tag{3.5}$$

Assuming the relationship between the increment of stress resultant in the normal direction, $d\vec{F}_n$, and the plastic deformation, $d\vec{u}_p$, follows the flow rule, one obtains

$$d\vec{F}_n = \boldsymbol{K}_p d\vec{u}_p \tag{3.6}$$

where $\boldsymbol{K}_p$ is a 2 x 2 diagonal matrix of generalized plastic stiffness from the individual force-deformation relationship.

Assuming K_p^a and K_p^v represent this relationship in the axial and transverse directions, respectively, then $\boldsymbol{K}_p$ can be expressed as

$$\boldsymbol{K}_p = diag\left[K_p^a, K_p^v\right] \tag{3.7}$$

because the projection of the tangent component of the stress resultant increment in the normal direction vanishes

$$\vec{n}^T \cdot d\vec{F}_n = \vec{n}^T \cdot d\vec{F} \tag{3.8}$$

Substituting Eq.(3.4) and Eq.(3.6) into Eq.(3.8) yields

$$\vec{n}^T \cdot d\vec{F} = \vec{n}^T \cdot d\vec{F}_n = \vec{n}^T \cdot \boldsymbol{K}_p d\vec{u}_p = \vec{n}^T \cdot \boldsymbol{K}_p (\vec{n} \cdot du_p) \tag{3.9}$$

From Eq.(3.9), one can obtain

$$du_p = \frac{\vec{n}^T \cdot d\vec{F}}{\vec{n}^T \boldsymbol{K}_p \vec{n}} \tag{3.10}$$

Substitution of Eq.(3.10) into Eq.(3.4) leads to

$$d\vec{u}_p = \frac{\vec{n} \cdot \vec{n}^T}{\vec{n}^T \boldsymbol{K}_p \vec{n}} d\vec{F} \tag{3.11}$$

The total deformation $d\vec{u}$ can be decomposed into the elastic part $d\vec{u}_e$, and the plastic part $d\vec{u}_p$ in the premise that the deformation decomposition principle holds in the theory of incremental plasticity. If this condition is met, one can obtain

$$d\vec{u} = d\vec{u}_e + d\vec{u}_p \tag{3.12}$$

The relationship between the increments of the elastic deformation and the force is given by

$$d\vec{F} = \boldsymbol{K}_e d\vec{u}_e \tag{3.13}$$

where $\boldsymbol{K}_e$ is a 2 x 2 diagonal matrix of elastic stiffness from the individual force deformation relationship. If K_e^a and K_e^v are elastic moduli for the axial and transverse directions, respectively, then

$\boldsymbol{K}_e$ is given by

$$\boldsymbol{K}_e = diag\left[K_e^a, K_e^v\right] \tag{3.14}$$

Substituting Eq.(3.13) and Eq.(3.11) into Eq.(3.12), one obtains

$$d\vec{u} = d\vec{u}_e + d\vec{u}_p = \left[\boldsymbol{K}_e^{-1} + \frac{\vec{n}\vec{n}^T}{\vec{n}^T\boldsymbol{K}_p\vec{n}}\right]d\vec{F} \tag{3.15}$$

Obviously, Eq.(3.15) can be rewritten as

$$d\vec{F} = \left[\boldsymbol{K}_e^{-1} + \frac{\vec{n}\cdot\vec{n}^T}{\vec{n}^T\boldsymbol{K}_p\vec{n}}\right]^{-1} d\vec{u} = \boldsymbol{K}_{ep}d\vec{u} \tag{3.16}$$

where

$$\boldsymbol{K}_{ep} = \left[\boldsymbol{K}_e^{-1} + \frac{\vec{n}\cdot\vec{n}^T}{\vec{n}\ \boldsymbol{K}_p\vec{n}}\right]^{-1} \tag{3.17}$$

It should be noted that K_{ep} is the modified stiffness of K_e due to the plastic flow and can be obtained by using the Sherman-Morrison formula [47]. The Sherman-Morrison formula [47] is given by

$$\left[A + \boldsymbol{u}\boldsymbol{u}^T\right]^{-1} = A^{-1} - \frac{A^{-1}\boldsymbol{u}\boldsymbol{u}^T A^{-1}}{\boldsymbol{u}^T A^{-1}\boldsymbol{u} + \mathbf{1}} \tag{3.18}$$

With the aide of Sherman-Morrison formula, Eq.(3.17) may be rewritten as follows:

$$\boldsymbol{K}_{ep} = \left[\boldsymbol{K}_e^{-1} + \frac{\vec{n}\vec{n}^T}{\vec{n}^T\boldsymbol{K}_p\vec{n}}\right]^{-1} = \boldsymbol{K}_e - \frac{\boldsymbol{K}_e\vec{n}\vec{n}^T\boldsymbol{K}_e}{\vec{n}^T\boldsymbol{K}_e\vec{n} + \vec{n}^T\boldsymbol{K}_p\vec{n}} \tag{3.19}$$

Assume that the yield funtion ϕ for the TPEA element is given by [45]

$$\phi = a\left(\frac{P}{P_u} - \frac{X_1}{P_u}\right)^2 + \left(\frac{V}{V_u} - \frac{X_2}{V_u}\right)^2 - k_\beta^2 = 0 \tag{3.20}$$

where P = axial force
V = shear force
P_u = the axial force to cause the TPEA element fully plasticized
V_u = the transverse shear force to cause the TPEA element fully plasticized
X_1 = current offset of the yield surface in the axial force direction
X_2 = current offset of the yield surface in the shear force direction
k_β = size of the yield surface
then $\phi_{,F}$ may be expressed as

$$\phi_{,F} = \begin{bmatrix} \phi_{,P} \\ \phi_{,V} \end{bmatrix} = \begin{bmatrix} \dfrac{2a}{P_u}\left(\dfrac{P}{P_u} - \dfrac{X_1}{P_u}\right) \\ \dfrac{2}{V_u}\left(\dfrac{V}{V_u} - \dfrac{X_2}{V_u}\right) \end{bmatrix} \tag{3.21}$$

Designate $\left(\phi_{,F}^T \cdot \phi_{,F}\right)^{1/2}$ as N, hence

$$N = \left(\phi_{,F}^T \cdot \phi_{,F}\right)^{1/2} = \left(\phi_{,P}^2 + \phi_{,V}^2\right)^{1/2} \tag{3.22}$$

The unit normal direction, n, is given as

$$n = \frac{\phi_{,F}}{\left(\phi_{,F}^T \cdot \phi_{,F}\right)^{1/2}} = \begin{bmatrix} n_1 \\ n_2 \end{bmatrix} = \frac{1}{N}\begin{bmatrix} \dfrac{2a}{P_u}\left(\dfrac{P}{P_u} - \dfrac{x_1}{P_u}\right) \\ \dfrac{2}{V_u}\left(\dfrac{V}{V_u} - \dfrac{x_2}{V_u}\right) \end{bmatrix} \tag{3.23}$$

where n_1 and n_2 are components of the normal directions, n, in stress resultant space.

From Eq.(3.19), $\mathbf{K}_{ep}$, the modified stiffness of the $\mathbf{K}_e$ due to section plasticized, is given as follows

$$\boldsymbol{K}_{ep} = \boldsymbol{K}_e - \frac{\boldsymbol{K}_e \hat{n} \hat{n}^T \boldsymbol{K}_e}{\hat{n}^T \boldsymbol{K}_e \hat{n} + \hat{n}^T \boldsymbol{K}_p \hat{n}} \tag{3.24}$$

With the aid of Eq.(3.4), Eq.(3.11), and Eq.(3.24),

$$\hat{n}^T \boldsymbol{K}_e \hat{n} = n_1^2 K_e^a + n_2^2 K_e^v \tag{3.25}$$

and

$$\hat{n}^T \boldsymbol{K}_p \hat{n} = n_1^2 K_p^a + n_2^2 K_p^v \tag{3.26}$$

Let

$$S = \hat{n}^T \boldsymbol{K}_e \hat{n} + \hat{n}^T \boldsymbol{K}_p \hat{n} = n_1^2\left(K_e^a + K_p^a\right) + n_2^2\left(K_e^v + K_p^v\right) \tag{3.27}$$

Then the K_{ep} of Eq.(3.24) can be obtained

$$\boldsymbol{K}_{ep} = \begin{bmatrix} K_e^a - \dfrac{\left(n_1 K_e^a\right)^2}{S} & \dfrac{-n_1 n_2 K_e^a K_e^v}{S} \\ \dfrac{-n_1 n_2 K_e^a K_e^v}{S} & K_e^v - \dfrac{\left(n_2 K_e^v\right)^2}{S} \end{bmatrix} \tag{3.28}$$

From the geometrical relationship, the distance between the loading point at the yield surface and the matching point at the bounding surface, δ, as shown in Figure 3-2 is given by Tseng and Lee [44]

$$\delta = \frac{(-F_i)\dot{F}_i + \sqrt{\left(F_i\dot{F}_i\right)^2 - \dot{F}_i\dot{F}_i\left(F_iF_i + F_B^2\right)}}{\sqrt{\dot{F}_i\dot{F}_i}} \tag{3.29}$$

where $F_1 = \frac{P}{P_u}$, $F_2 = \frac{V}{V_u}$, $\dot{F}_1 = \frac{dP}{P_u}$, $\dot{F}_2 = \frac{dV}{V_u}$, and F_B = current size of the bounding surface.

While the stress resultant is in yielding and falls between the yield and bounding surfaces, the generalized plastic moduli K_p^a and K_p^v can be obtained by the following equations,

$$K_p^a = \left(1 + h_1\frac{\delta}{\delta_{ini} - \delta}\right)(K_0)_p^a \tag{3.30}$$

$$h_1 = \frac{A_1}{\delta_{ini}^2} \tag{3.31}$$

$$K_p^v = \left(1 + h_2\frac{\delta}{\delta_{ini} - \delta}\right)(K_0)_p^v \tag{3.32}$$

$$h_2 = \frac{A_2}{\delta_{ini}^2} \tag{3.33}$$

where δ_{ini} = the distance between the loading and matching points when the material starts yielding; $(K_0)_p^a$ and $(K_0)_p^v$ = generalized plastic moduli associated with the bounding surface; A_1 and A_2 = unknown coefficients to be determined from the experimental results. It should be noted that the ranges of h_1 and h_2 can also be attained from the experimental data.

The motion of the yield surface is essential for the determination of δ and δ_{ini} to calculate the generalized plastic modulus. Eq.(3.34) derives the motion of the yield surface. As shown in the experimental results [48], the yield surface moves along the direction of the stress resultant increment.

As shown in Figure 3-2., the center of the yield surface moves from O_Y and $O_{Y'}$ while the stress resultant moves from the loading point to the matching point. If l_1 and l_2 are the component of the unit direction of the stress resultant increment, the component of the unit vector υ_1 and υ_2 along the direction of O_Y and $O_{Y'}$ can be readily obtained from trigonometrical consideration, that is

$$\upsilon_i = \frac{1}{L}\left(\frac{(F_B - F_Y)\,(F_i + \delta l_i)}{((F_i + \delta l_i)\,(F_i + \delta l_i))^{1/2}} - \alpha_i\right) \tag{3.34}$$

where L = the distance between the points O_Y and $O_{Y'}$; α_i = the coordinate of the center of the yield surface, and F_B and F_Y are the size of the bounding and yield surfaces, respectively.

If $d\alpha_i$ is defined as the motion of the center of the yield surface, then with the aid of the consistency condition and Eq.(3.34), the following equations result

$$|d\alpha| = \frac{A\,(dP/P_u) + B\,(dV/V_u)}{A\upsilon_1 + B\upsilon_2} \tag{3.35}$$

and

$$d\alpha_i = |d\alpha| v_i \tag{3.36}$$

where

$$A = 2a\left(\frac{P}{P_u} - \frac{X_1}{P_u}\right) \tag{3.37}$$

and

$$B = 2\left(\frac{V}{V_u} - \frac{X_2}{V_u}\right) \tag{3.38}$$

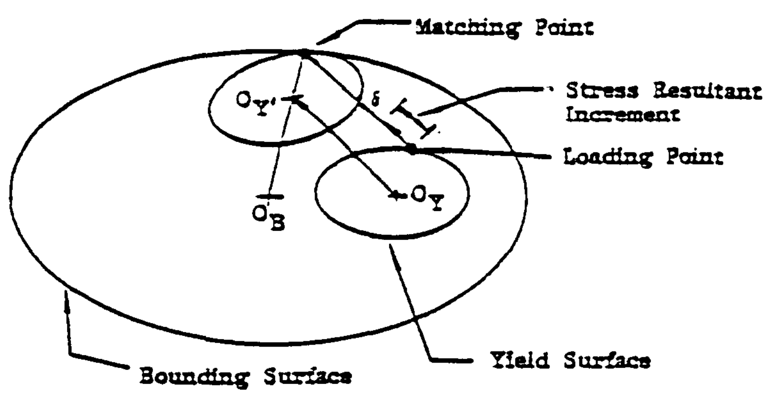

FIGURE 3-2 Motion of Yield Surface in Stress Resultant Space [44]

3.1.2 Finite Element Formulation for TPEA Devices

In this section, a finite element formulation for the TPEA element is presented. The behavior of the TPEA device is dependent on the relative displacement between the bottom and top of the steel plate or nodal points 1 and 2 as shown in Figure3.1. There are three degrees of freedom in the global coordinate system x, y and z, and three degrees of freedom in the local coordinate system ξ, ζ, and η for each node. This is illustrated in Figure 2-2.

The global displacement increments at nodal points 1, and 2 at time t are $dW_1(t)$ and $dW_2(t)$, respectively. That is

$$dW_1(t) = \begin{bmatrix} dw_1(t) \\ dw_2(t) \\ dw_3(t) \end{bmatrix} \quad (3.39)$$

and

$$dW_2(t) = \begin{bmatrix} dw_4(t) \\ dw_5(t) \\ dw_6(t) \end{bmatrix} \quad (3.40)$$

where $dw_1(t)$, $dw_2(t)$, and $dw_3(t)$ are global displacement increments at nodal point 1 in x, y, and z directions, respectively, and $dw_4(t)$, $dw_5(t)$, and $dw_6(t)$ are those at nodal point 2.

As shown in Figure 2-2, the displacement increments in the local coordinate system, $d\overline{W}_1(t)$ and $d\overline{W}_2(t)$ for nodal point 1 and point 2, respectively, are

$$d\overline{W}_1(t) = R[dW_1(t)] \quad (3.41)$$

and

$$d\overline{W}_2(t) = R[dW_2(t)] \quad (3.42)$$

in which R is a 2 x 3 transformation matrix associated with the local and global coordinate systems. The increment of relative displacement $dU(t)$, between nodal points 1 and 2, shown in Figure 3-1 and Figure 2-2, in local coordinate system ξ and ζ is defined as

$$dU(t) = d\overline{W}_2(t) - d\overline{W}_1(t) = R\left[dW_2(t) - dW_1(t)\right] \quad (3.43)$$

Eq.(3.43) can be rewritten in the following matrix form:

$$dU(t) = \boldsymbol{B}dD(t) \quad (3.44)$$

where

$$\boldsymbol{B} = \left[-R\ R\right] \quad (3.45)$$

$$dD(t) = \begin{bmatrix} dW_1(t) \\ dW_2(t) \end{bmatrix} = \begin{bmatrix} dw_1(t) \\ dw_2(t) \\ dw_3(t) \\ dw_4(t) \\ dw_5(t) \\ dw_6(t) \end{bmatrix} \tag{3.46}$$

and

$$dU(t) = \begin{bmatrix} dU_\xi(t) \\ dU_\zeta(t) \end{bmatrix} \tag{3.47}$$

in which $dU_\xi(t)$ and $dU_\zeta(t)$ are the relative displacement increments in the ξ and ζ directions, respectively.

Substituting Eq.(3.44) into Eq.(3.16) leads to

$$dF(t) = K_{ep}dU(t) = K_{ep}BdD(t) \tag{3.48}$$

Premultiplication of Eq.(3.48) by $\mathbf{B}^T$ yields the finite element formulation for the TPEA element at time t, that is

$$dP(t) = B^T dF(t) = B^T K_{ep} BdD(t) = KdD(t) \tag{3.49}$$

where the stiffness **K** is

$$K = B^T K_{ep} B \tag{3.50}$$

and the force increment $dP(t)$ in the global coordinate system is

$$dP(t) = B^T dF(t) \tag{3.51}$$

3.1.3 Verification of Analytical Model

Results obtained from the analytical model are compared with the experimental results in order to demonstrate the performance of the analytical model for the TPEA device.

Assuming the base of the tapered plate is fully restrained and neglecting the shear deformation, the theoretical elastic lateral stiffness of a TPEA device, K_e^v of Eq.(3.14) is

$$K_e^v = \frac{NEbt^3}{6h^3} \tag{3.52}$$

where E is the Young's modulus, N is the number of tapered plates, t is the thickness of the tapered plate, b is the base width of the tapered plate, and h is the height of the tapered plate.

The yield strength, V_y, and the plastic strength, V_p, of the device are [66]

$$V_y = \frac{\sigma_y N b t^2}{6h} \tag{3.53}$$

and

$$V_p = \frac{\sigma_y N b t^2}{4h} \tag{3.54}$$

where σ_y is the yield stress.

The TPEA device consists of several tapered plates welded to a common base plate (see Figure1.1). The schedule of the TPEA specimens is given in Table 3-I.

TABLE 3-I Schedule of Specimens

TPEA	No of Plates	B (in)	t (in)	h (in)	K_e^v (Kips/in)	K_{exp}^v (Kips/in)
1A2	8	5.25	0.7874	8.642	153.48	151.83
1A3	8	5.35	0.7874	12.00	58.35	59.90
1B3	8	5.51	1.3780	16.32	128.3	136.13

(K_{exp}^v is the experimental elastic lateral stiffness)

Both unknown coefficients A_1 and A_2 in Eq.(3.31) and Eq.(3.33) were taken as 20. The ranges of h_1 and h_2 of Eq.(3.31) and Eq.(3.33) were taken as follows: $10 \le h_1 \le 20$, and $20 \le h_2 \le 30$, respectively. The elastic modulus is 29000 ksi, and yield stresses for steel plates in the TPEA specimens are 42.9 ksi for specimen 1A2, 39.29 ksi for specimen 1B3, respectively.

The comparisons of the analytical and experimental results are shown in Figures 3-3 and 3-4 [66]. They demonstrate that the analytical results are in good agreement with the experimental results. It is also demonstrated in Table 3-I that the elastic stiffness is very predictable when considering flexural deformation only. It should be noted that the analytical model does not account for sudden changes of the stiffness during the last few loading cycles resulting from the contacts of the adjacent plates.

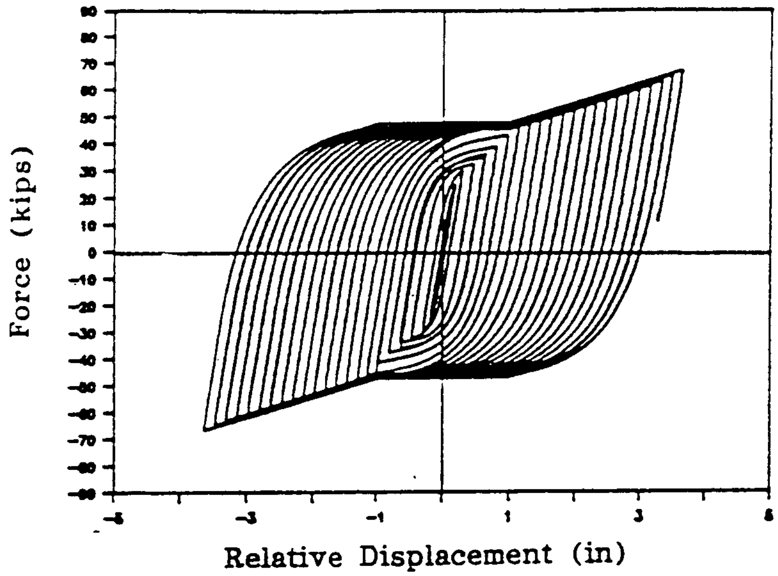

FIGURE 3-3 Analytical Results for Specimen [66]

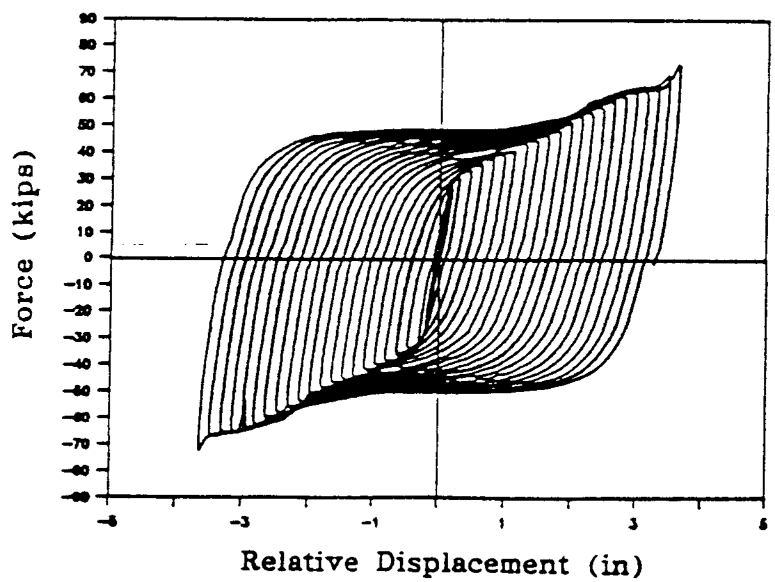

FIGURE 3-4 Experimental Results for Specimen [66]

3.2 The Parameters of TPEA Elements

A 10-story moment resistant steel frame, shown in Figure 2-3, has an elastic modulus and Poisson's ratio equal to $3x10^7$ psi and 0.3, respectively. The weight of each floor is 25.47 lbs/in. In the analysis, it was assumed that the floors were rigid in their own plan. Table 3.-II presents the properties of the column of the 10-story building. As shown in Figure 3-5, TPEA devices were mounted on each floor, and supported by Chevron bracing.

TABLE 3-II The Properties of the Column of the 10-Story Building

Floor	Area(in^2)	I(in^4)	K_s(Kips/in)
1	49.1	2020	115.6
2	40.0	1590	94.95
3	37.3	1480	84.70
4	35.0	1370	77.47
5	32.7	1270	71.06
6	24.7	928	59.37
7	22.9	851	51.40
8	20.0	724	44.26
9	17.9	641	39.12
10	17.9	641	36.37

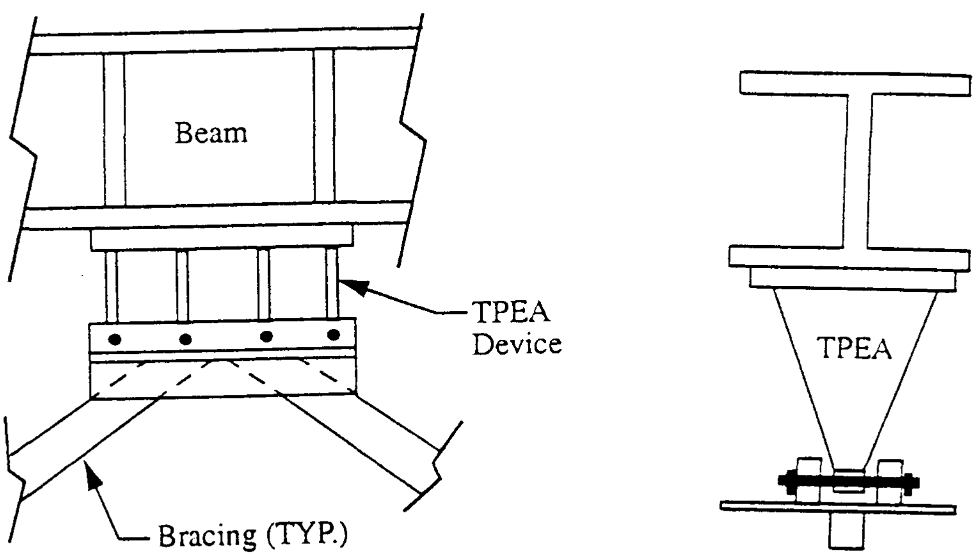

FIGURE 3-5 Frames with TPEA Devices and Bracing Members

3.2.1 Horizontal Stiffness of Bracing Members

The bracing members supporting TPEA devices must be designed strong enough to resist either yielding in tension or buckling in compression. In other words, the bracing members should remain elastic during earthquakes. The horizontal elastic stiffness of a bracing member can be written as

$$K = AE/L \tag{3.55}$$

where A is cross-sectional area of the bracing member, E is elastic modulus, and L is the length of the bracing member.

In order to satisfy equations of equilibrium, the horizontal and vertical components of the force and displacement for bracing one, and bracing two can be written as:

$$\begin{bmatrix} F_{1x} \\ F_{1y} \end{bmatrix} = K \begin{bmatrix} \cos^2\gamma & \cos\gamma\sin\gamma \\ \cos\gamma\sin\gamma & \sin^2\gamma \end{bmatrix} \begin{bmatrix} \delta_x \\ \delta_y \end{bmatrix} \tag{3.56}$$

$$\begin{bmatrix} F_{2x} \\ F_{2y} \end{bmatrix} = K \begin{bmatrix} \cos^2\eta & \cos\eta\sin\eta \\ \cos\eta\sin\eta & \sin^2\eta \end{bmatrix} \begin{bmatrix} \delta_x \\ \delta_y \end{bmatrix} \tag{3.57}$$

where γ is the angle between the bracing member and the horizontal beam, and η is $\pi - \gamma$.

Eq. (3.57) can be rewritten as

$$\begin{bmatrix} F_{2x} \\ F_{2y} \end{bmatrix} = K \begin{bmatrix} \cos^2\gamma & -\cos\gamma\sin\gamma \\ -\cos\gamma\sin\gamma & \sin^2\gamma \end{bmatrix} \begin{bmatrix} \delta_x \\ \delta_y \end{bmatrix} \tag{3.58}$$

The sum of the horizontal forces is given by

$$F_x = F_{1x} + F_{2x} = 2\delta_x \cos^2\gamma K \tag{3.59}$$

The horizontal stiffness of the two bracing members is given by

$$K_b = \frac{F_x}{\delta_x} = 2K\cos^2\gamma = \frac{2EA}{L}\cos^2\gamma \tag{3.60}$$

3.2.2 B/D and SR Ratios

The B/D ratio can be defined as the ratio of K_b to the elastic lateral stiffness of a TPEA device K_e^v. The B/D ratio can be written as:

$$B/D = \frac{K_b}{K_e^v} = \frac{12Ah^3\cos^2\gamma}{LNbt^3} \tag{3.61}$$

Because a TPEA element consists of a TPEA device and the bracing members in series, the elastic stiffness of a TPEA element, including supporting bracing member, K_T is a function of K_b and K_e^v such that

$$\frac{1}{K_T} = \frac{1}{K_b} + \frac{1}{K_e^v} \tag{3.62}$$

and

$$K_T = \frac{K_b K_e^v}{K_b + K_e^v} = \frac{K_e^v}{1 + \frac{1}{B/D}} \tag{3.63}$$

The stiffness ratio SR is defined as the ratio of the horizontal TPEA element stiffness, K_T, to the building story stiffness, K_s, without the TPEA elements in place.

$$SR = \frac{K_T}{K_s} \tag{3.64}$$

In order to examine the effect of B/D and SR ratios on the response of the 10-story building frames, three ground motions, shown in Figures 2.-4 to 2-6, are imposed in the horizontal direction to the 10-story building. Tables 3-III to 3-VIII display the property of TPEA elements at each floor while SR is changed from 1 to 6 and B/D is 2. The yield stress for steel plates in the TPEA devices is 42.86 ksi (0.2958 KN/mm^2).

TABLE 3-III The Properties of TPEA (SR=1, B/D=2)

Story Floor	No. of Plates	b (in)	t (in)	h (in)	Brace Area (in^2)
1	4	4.0	0.7874	6	2.94
2	4	3.26	0.7874	6	1.79
3	4	2.92	0.7874	6	1.60
4	4	3.4	0.7874	6.5	1.46
5	4	3.1	0.7874	6.5	1.34
6	3	3.48	0.7874	6.5	1.12
7	3	3.0	0.7874	6.5	0.97
8	2	3.9	0.7874	6.5	0.84
9	2	3.44	0.7874	6.5	0.74
10	2	3.2	0.7874	6.5	0.68

TABLE 3-IV The Properties of TPEA (SR=2, B/D=2

Story Floor	No. of Plates	b (in)	t (in)	h (in)	Brace Area (in^2)
1	5	4.9	0.7874	5.5	5.88
2	5	4.02	0.7874	5.5	3.58
3	5	3.6	0.7874	5.5	3.20
4	4	4.1	0.7874	5.5	2.93
5	4	3.77	0.7874	5.5	2.69
6	4	3.15	0.7874	5.5	2.24
7	3	4.66	0.7874	6	1.94
8	3	4.05	0.7874	6	1.67
9	3	3.6	0.7874	6	1.48
10	3	3.35	0.7874	6	1.37

TABLE 3-V The Properties of TPEA (SR=3, B/D=2)

Story Floor	No. of Plates	b (in)	t (in)	h (in)	Brace Area (in^2)
1	5	5.52	0.7874	5	8.83
2	5	4.54	0.7874	5	5.39
3	5	4.05	0.7874	5	4.81
4	4	4.62	0.7874	5	4.39
5	4	4.28	0.7874	5	4.03
6	4	3.57	0.7874	5	3.37
7	3	5.45	0.7874	5.5	2.92
8	3	4.70	0.7874	5.5	2.51
9	3	4.15	0.7874	5.5	2.22
10	3	3.86	0.7874	5.5	2.06

TABLE 3-VI The Properties of TPEA (SR=4, B/D=2)

Story Floor	No. of Plates	b (in)	t (in)	h (in)	Brace Area (in^2)
1	6	6.13	0.7874	5	11.77
2	6	5.04	0.7874	5	7.19
3	6	4.50	0.7874	5	6.41
4	5	4.93	0.7874	5	5.85
5	5	4.53	0.7874	5	5.37
6	5	3.78	0.7874	5	4.49
7	4	4.09	0.7874	5	3.89
8	4	3.52	0.7874	5	3.35
9	4	3.12	0.7874	5	2.96
10	3	3.86	0.7874	5	2.75

TABLE 3-VII The Properties of TPEA (SR=5, B/D=2

Story Floor	No. of Plates	b (in)	t (in)	h (in)	Brace Area (in^2)
1	6	5.59	0.7874	4.5	14.71
2	6	4.59	0.7874	4.5	8.95
3	6	4.09	0.7874	4.5	8.0
4	5	4.5	0.7874	4.5	7.32
5	5	4.12	0.7874	4.5	6.715
6	5	3.45	0.7874	4.5	5.61
7	4	5.12	0.7874	5	4.855
8	4	4.4	0.7874	5	4.18
9	4	3.89	0.7874	5	3.695
10	4	3.62	0.7874	5	3.435

TABLE 3-VIII The Properties of TPEA (SR=6, B/D=2)

Story Floor	No. of Plates	b (in)	t (in)	h (in)	Brace Area (in^2)
1	7	5.75	0.7874	4.5	16.56
2	7	4.72	0.7874	4.5	10.78
3	7	4.2	0.7874	4.5	8.16
4	7	3.86	0.7874	4.5	8.78
5	6	5.65	0.7874	5	8.07
6	6	4.73	0.7874	5	6.74
7	6	4.08	0.7874	5	5.86
8	5	4.23	0.7874	5	5.04
9	5	3.74	0.7874	5	4.44
10	5	3.48	0.7874	5	4.13

3.2.3 Structural Response Parameters

The unit of displacement is the inch and the unit of force is pounds in this study. The response parameters used include: (1) the floor displacements (FD), which is the displacement at a floor with respect to the ground; (2) the roof displacements (RD), which is the displacement at the top relative to the ground; (3) the base shear forces (BSF), which is the total lateral shear partially carried by the TPEA elements and partially by the frame members; (4) the column shear force (CSF), which is the shear force taken by the column; and (5) the ductility ratio. The ductility ratio is defined as

$$\mu = \frac{\Delta_{max}}{\Delta_y} = \frac{\Delta_{max}Et}{\sigma_y h^2} \tag{3.65}$$

where Δ_y is the yield displacement of TPEA device and Δ_{max} is the maximum displacement of TPEA device.

A large value of story drift indicates large deformations of structural and non-structural members at that story. Floor displacement should be controlled so that excessive deformations of structural and non-structural members and the second order $(P - \Delta)$ forces due to these deformations can be avoided.

A large TPEA stiffness could be obtained by allowing a small yield displacement with a designed device yield force. Thus, a TPEA device would yield early during earthquakes to dissipate more hysteretic energy so that the main structural members have less chance to experience inelastic response. However, a small yield displacement of the device could cause a large yield ductility ratio which may result in exceeding the selected design ductility ratio. It is important to select a proper yield displacement according to the expected earthquake intensity so that the response ductility ratio will be within the design limit.

3.3 Effect of B/D

As shown in Eq.(3.63), the stiffness of TPEA element, K_T, is a function of K_e^v and B/D ratio which is the ratio of the stiffness of the bracing members to the stiffness of TPEA. A parameter α is defined as the function of B/D.

$$\alpha = \frac{1}{1 + \frac{1}{B/D}} \tag{3.66}$$

Eq.(3.63) can be rewritten as

$$K_T = \alpha K_e^v \tag{3.67}$$

The relationship of α and B/D is shown in Figure 3-6. Note that α rapidly increases as B/D increases from zero to 5 while α slowly increases to its limit 1 when B/D increases from 5 to 100. The effect of B/D has little influence on the reduction of the structural response during ground motion. In other words, it would be ineffective to try to improve the seismic resistance by adopting larger B/D ratios. The bracing members should only be designed economically to remain elastic during earthquakes since the hysteretic energy dissipating capacity depends on the TPEA devices only and is not affected by the stiffness of the bracing members.

The effect of the B/D ratio on the reduction of the structural response was studied with different B/D ratios. Ground motion records from the El Centro earthquake, San Fernando earthquake, and Taft earthquake with the Earthquake Record Scale Factor (ERSF) being 4, were imposed on the structure to analyze the inelastic response. The influence of B/D on the maximum floor displacement (MFD), maximum base shear (MBS), and maximum ductility ratio (MDC) can be observed in Figures 3-7 to 3-15 while SR=4 is chosen when the structure was subjected to three selected ground motions. According to Figures 3-7 to 3-15, B/D has little influence on the reduction of the structural response which verifies the previous assumption. The results show that the curves of the structural response (MFD, MBS, and MDC) do not change significantly when B/D is changed from 1 to 5. As shown in Figure 3-7, displacement at each floor varies little when B/D is changed from 1 to 5. Likewise, Figure 3-8 shows the same consistency. However, Figures 3-8, 3-11, and 3-14 demonstrate that B/D=1 has the largest base shear force of all the cases.

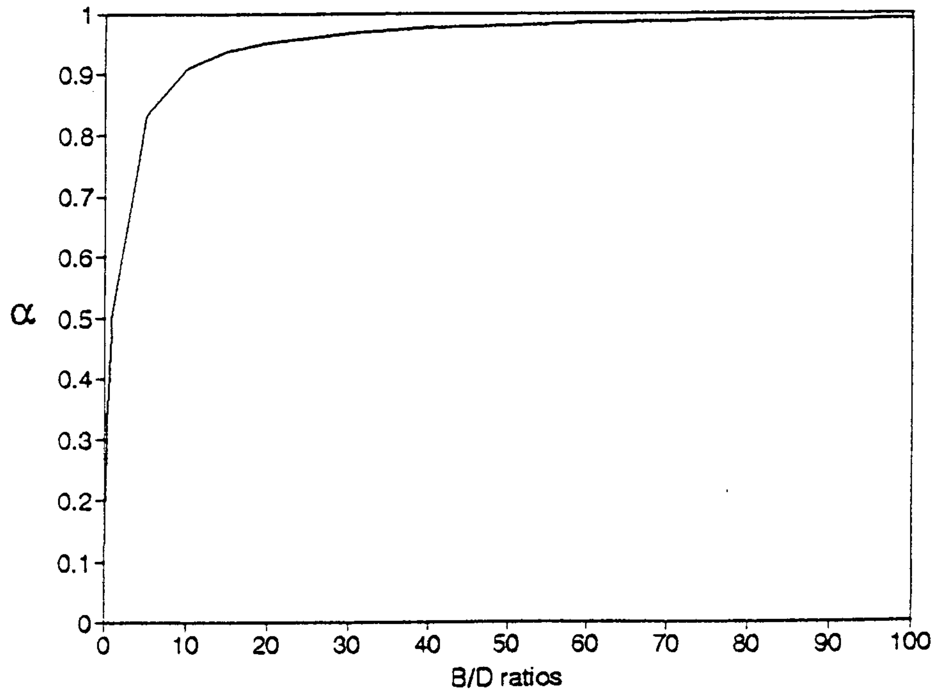

FIGURE 3-6 Relationship Between α and B/D

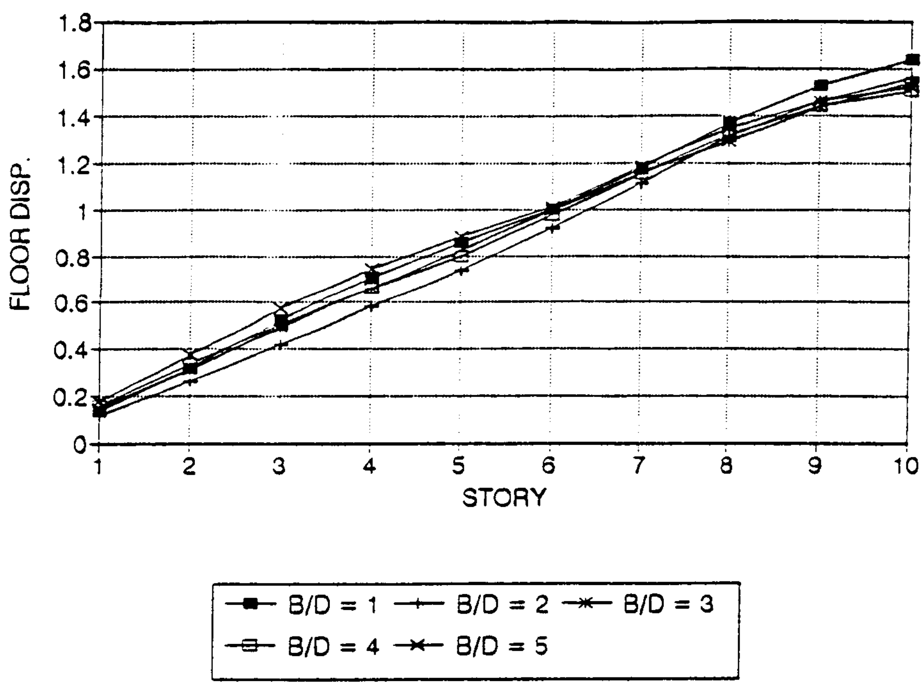

FIGURE 3-7 Relations between B/D and Floor Displacement When the Structure is Subjected to El Centro Ground Motion

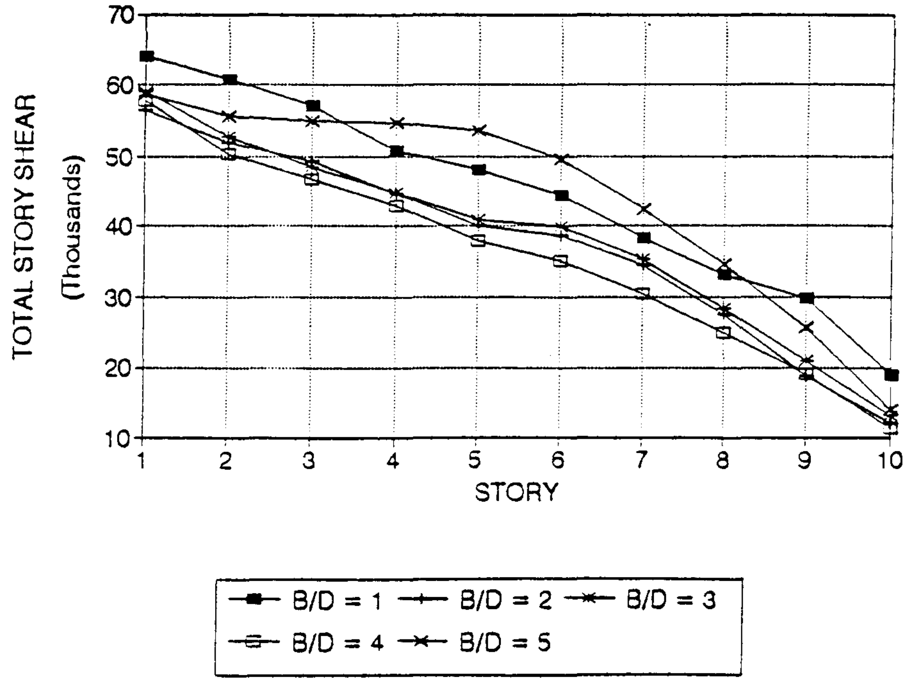

FIGURE 3-8 Relations between B/D and Base Shear Force When the Structure is Subjected to El Centro Ground Motion

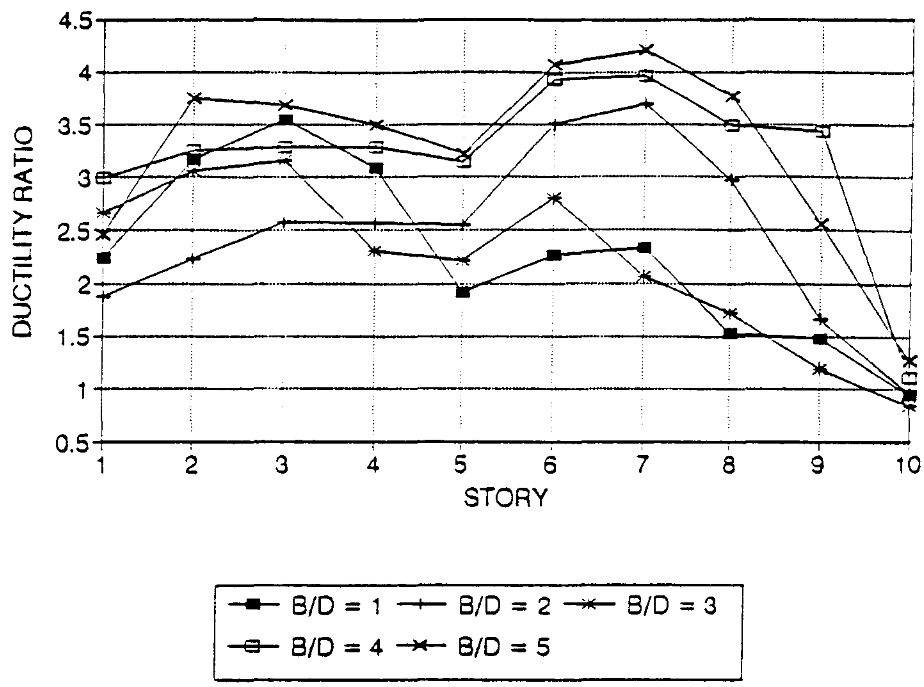

FIGURE 3-9 Relations between B/D and Ductility Ratio When the Structure is Subjected to El Centro Ground Motion

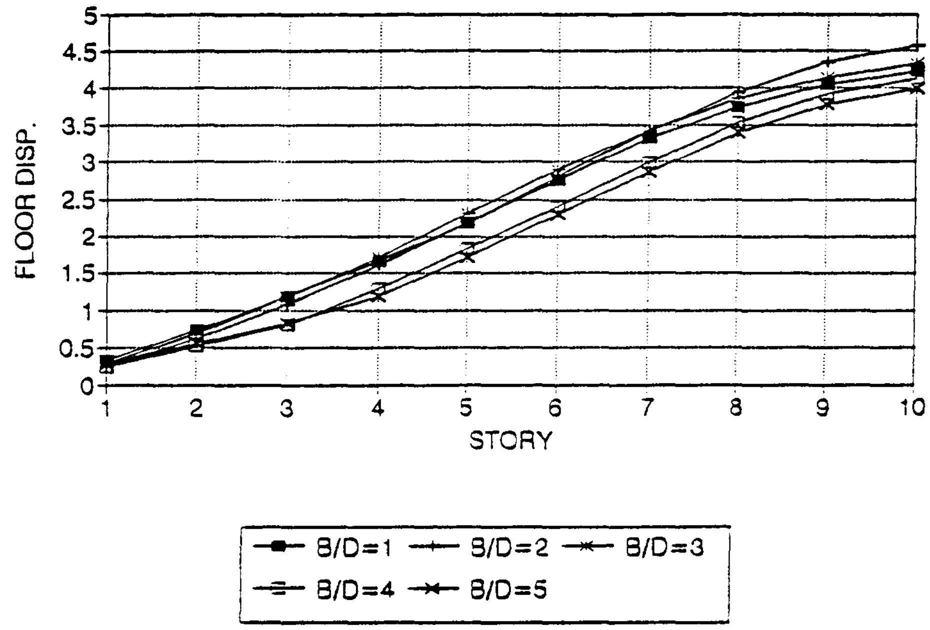

FIGURE 3-10 Relations between B/D and Floor Displacement When the Structure is Subjected to San Fernando Ground Motion

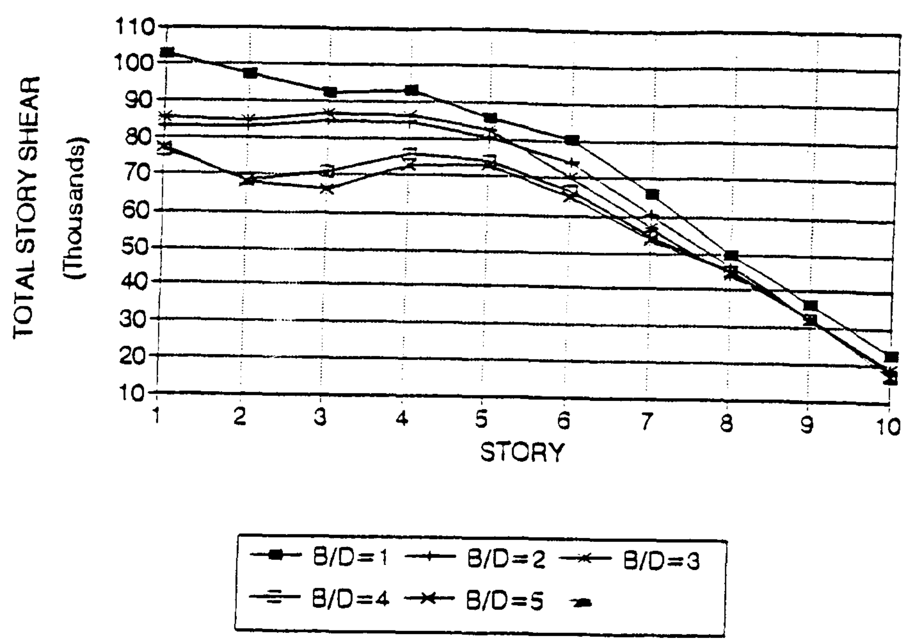

FIGURE 3-11 Relations between B/D and Base Shear Force When the Structure is Subjected to San Fernando Ground Motion

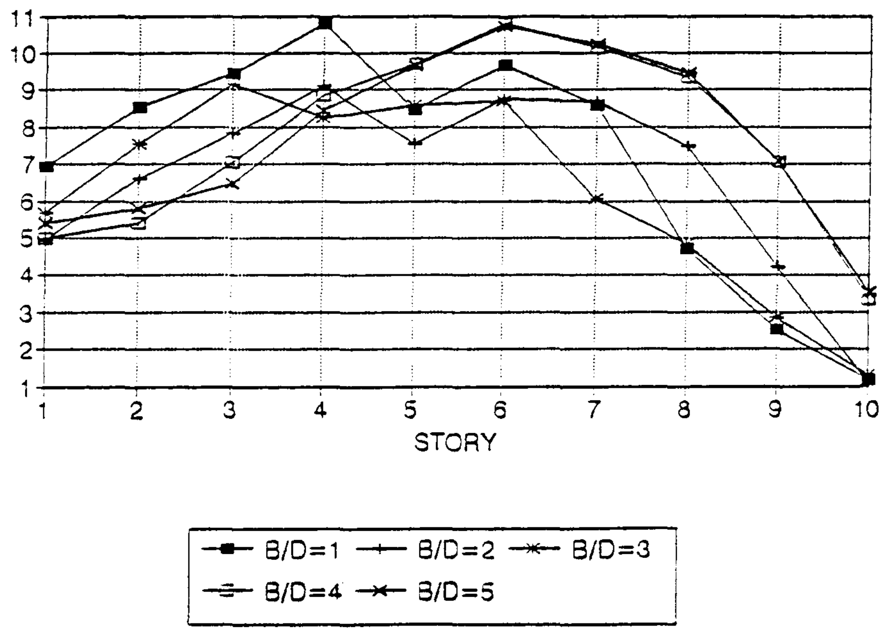

FIGURE 3-12 Relations between B/D and Ductility Ratio When the Structure is Subjected to San Fernando Ground Motion

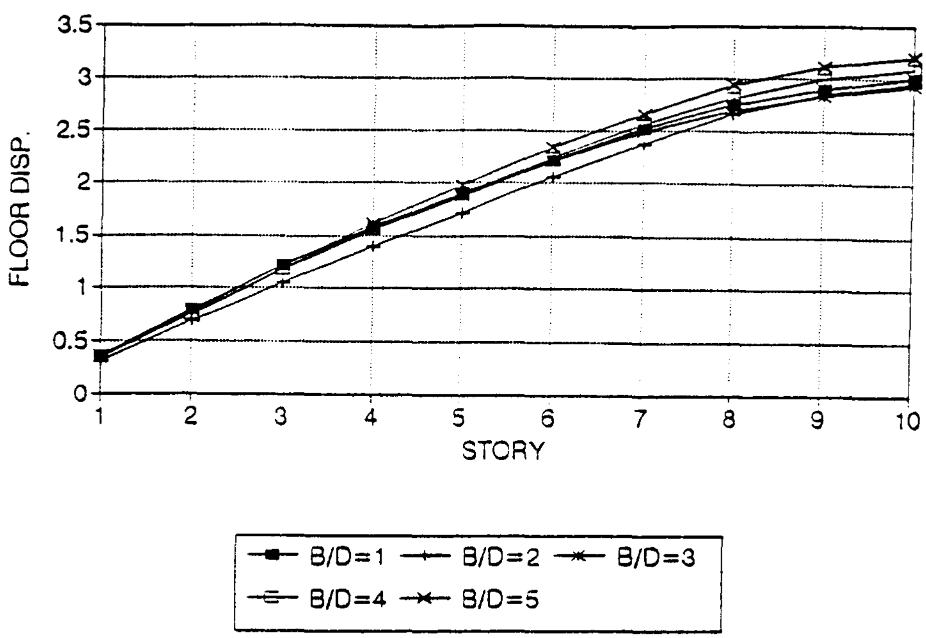

FIGURE 3-13 Relations between B/D and Floor Displacement When the Structure is Subjected to Taft (ERSF=4) Ground Motion

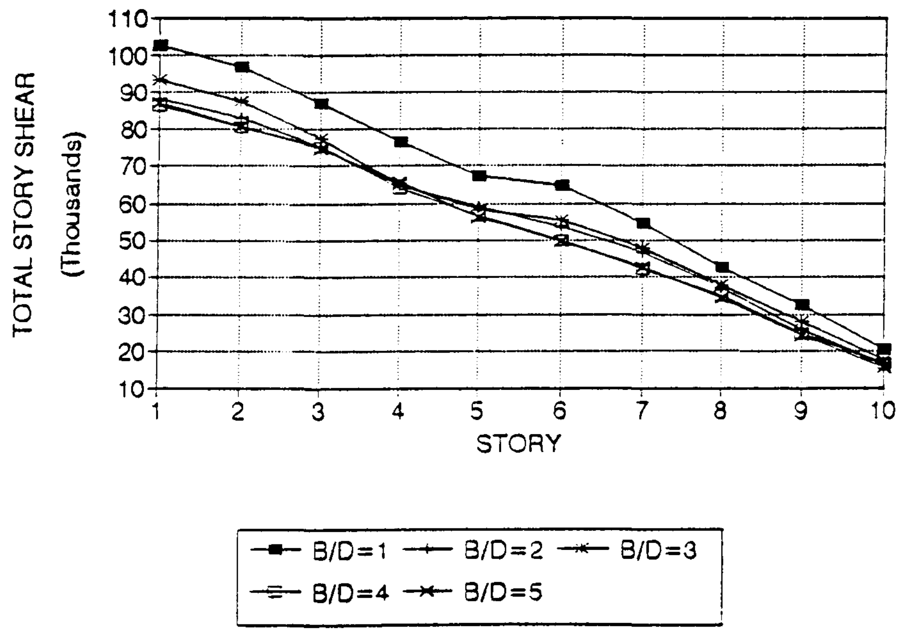

FIGURE 3-14 Relations between B/D and Base Shear Force When the Structure is Subjected to Taft (ERSF=4) Ground Motion

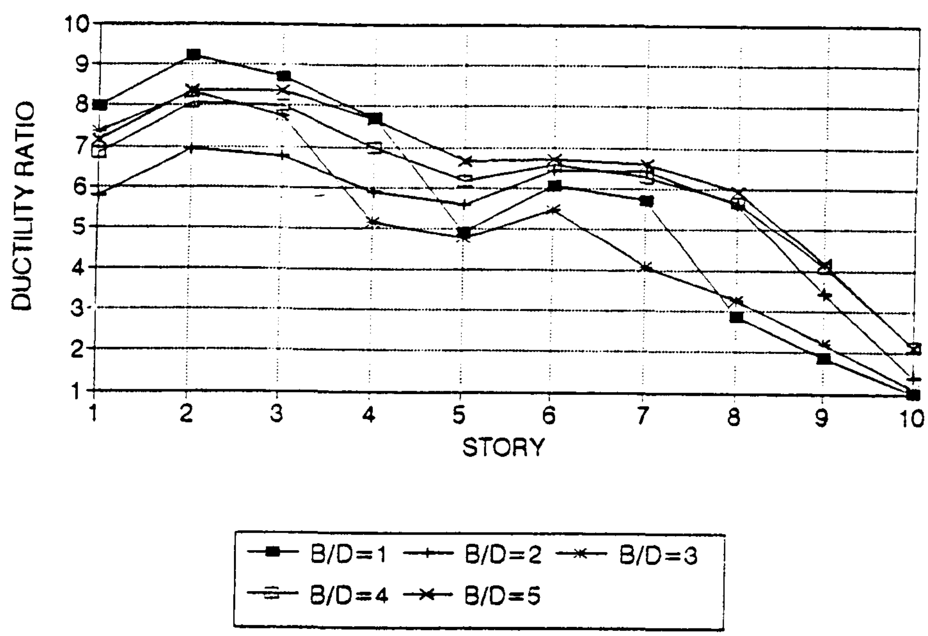

FIGURE 3-15 Relations between B/D and Ductility Ratio When the Structure is Subjected to Taft (ERSF=4) Ground Motion

The results also show that: (1) B/D=1 has the largest ductility ratio while the structure was subjected to the San Fernando and the Taft (ERSF=4) ground motions; (2) B/D=5 has the largest ductility ratio when the structure was subjected to the El Centro ground motion. The results confirm that it is not economical to try to improve seismic response by using large B/D ratios. For design purposes, a B/D ratio in the range of 2 to 3 is recommended.

Several main concerns must be addressed in the design of bracing members. First, the bracing members should be strong enough to support the TPEA device without buckling in compression or yielding in tension. Second, large B/D ratios need not be adopted to improve seismic response since the energy dissipating capacity is not affected by the stiffness of the bracing members. Last, the bracing members should remain elastic when the TPEA device yields during earthquakes.

3.4 Effect of SR

SR is the ratio of the TPEA element initial stiffness to the structural story stiffness which is a function of K_T and K_s. The structural story stiffness K_s is given in Table 3-II. The SR ratio is a very important parameter in the design of structures with TPEA because it is related to the stiffness of the structural members. Furthermore, the SR ratio could affect the structural period and the design seismic force of the structure.

The influence of SR on the maximum floor displacement, maximum shear force, and maximum ductility ratio can be observed in Figures 3-16 to 3-24. In Figure 3-16, we see that the larger the SR ratio, the smaller the displacement at each floor. However, the difference is less between SR=3 and SR=6. In Figure 3-17, the patterns are similar while SR varies from 1 to 6. However, SR=2 has the largest base shear force while SR=4 has the smallest. Figure 3-18 shows the same pattern, although, there is a greater gap at each floor.

The results show that a larger SR always performs better in terms of reducing floor displacement when the structure is subjected to the three selected earthquakes. This is because the larger SR means more stiffness is provided for greater reductions in structural displacement. The results show that: (1) SR=4 has the smallest story shear force and ductility ratio when the structural was subjected to the El Centro earthquake; (2) SR=1 has the smallest story shear force and ductility ratio while the structure was subjected to the San Fernando earthquake; and (3) SR=2 has the smallest story shear force and ductility ratio while the structure was subjected to the Taft (ERSF=4) earthquake. The selection of SR must account for the expected earthquake characteristics, ground motion intensity, and energy demands. Although the larger SR ratio may have smaller MFD, it is not necessarily true that a larger SR will be better for design because large SR ratios may lead to higher natural frequencies. This may increase the larger horizontal shear force accelerations. Increasing the SR ratio will also increase the size and the cost of the TPEA elements.

Figures 3-25 to 3-42 demonstrate the effect of B/D and SR ratios on maximum roof displacement, maximum base shear force, and maximum ductility ratio. In Figure 3-25, we see that SR=1 has the largest roof displacement and SR=2 has the second largest. The difference is less between SR=3 and SR=6. The six lines are almost level and parallel to the horizontal line. It can be said that B/D has little influence on the reducing of the roof displacement. Figure 3-26 demonstrates that B/D=2 with SR=4 has the smallest base shear force while B/D=1 with SR=2 has the largest. Figure 3-27 shows that B/D=3 with SR=4 has the smallest ductility ratio while B/D=1 with SR=1 has the largest. Figure 3-28 indicates that SR=2 reduces the roof displacement about 50% and SR=4 reduces it about 70% when compared to the structure without TPEA. The curve becomes level when SR is greater than 4. Figure 3-29 shows that SR=4 has the best performance in the reduction of the base shear force. However, SR=1 has better performance than SR=2. Again, Figure 3-30 shows that SR=4 has the smallest ductility ratio while SR=1 has the largest.

From these results it is observed that the B/D has little influence on the reduction of structural response and that adding TPEA to the structural could significantly reduce the structural response. The results also indicate that SR ratios from 2 to 4 and B/D ratios from 2 to 3 are to be recommended for design purposes.

The behaviors of the structure equipped with and without TPEA were compared while it was subjected to ten different peak accelerations from 100 Gal (cm/s^2) to 1000 Gal of the San Fernando ground motion. Figure 3-43 shows that the structure with TPEA (B/D=2, SR=4) has larger maximum base shear force than the structure without TPEA when the peak acceleration is less than 300 Gal. This is because the addition of TPEA to a structure increases the structure's stiffness and the TPEA operates in an elastic range in the lower peak accelerations of the San Fernando earthquake.The response curve of the structure with TPEA becomes smooth when the peak acceleration is between 800 Gal and 1000 Gal. When the structure is subjected to a stronger peak acceleration of ground motion, the superiority of the TPEA is more evident. Figures 3-45 and 3-46 illustrate that the structure with TPEA has a much smaller MFD than the structure without TPEA from 100 Gal to 1000 Gal. The reason for this is the addition of TPEA to the structure may lead to stronger stiffness and larger damping capacity so that the structural floor displacement would be greatly constrained.

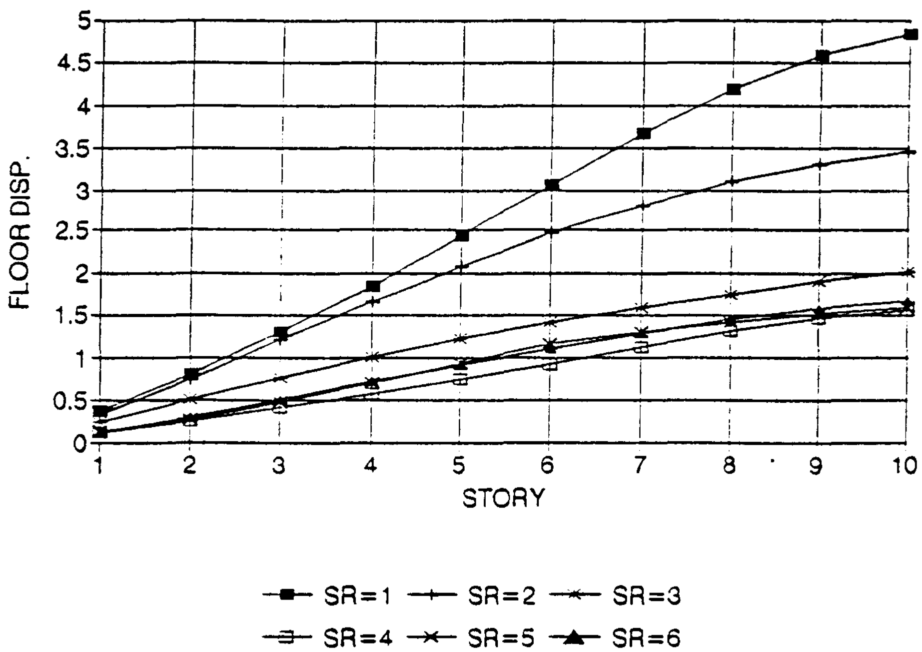

FIGURE 3-16 Relations between SR and Floor Displacement When the Structure is Subjected to El Centro Ground Motion

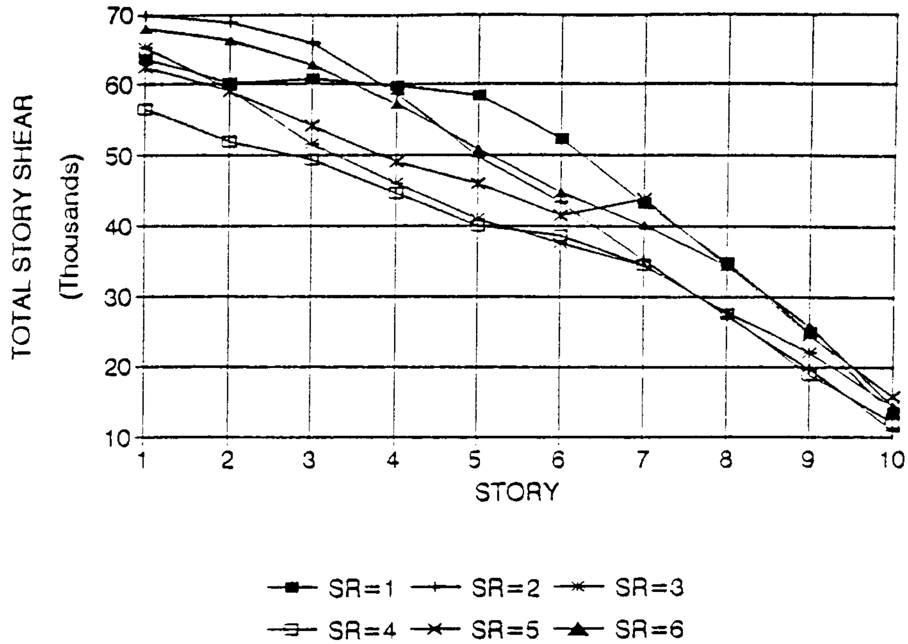

FIGURE 3-17 Relations between SR and Base Shear Force When the Structure is Subjected to El Centro Ground Motion

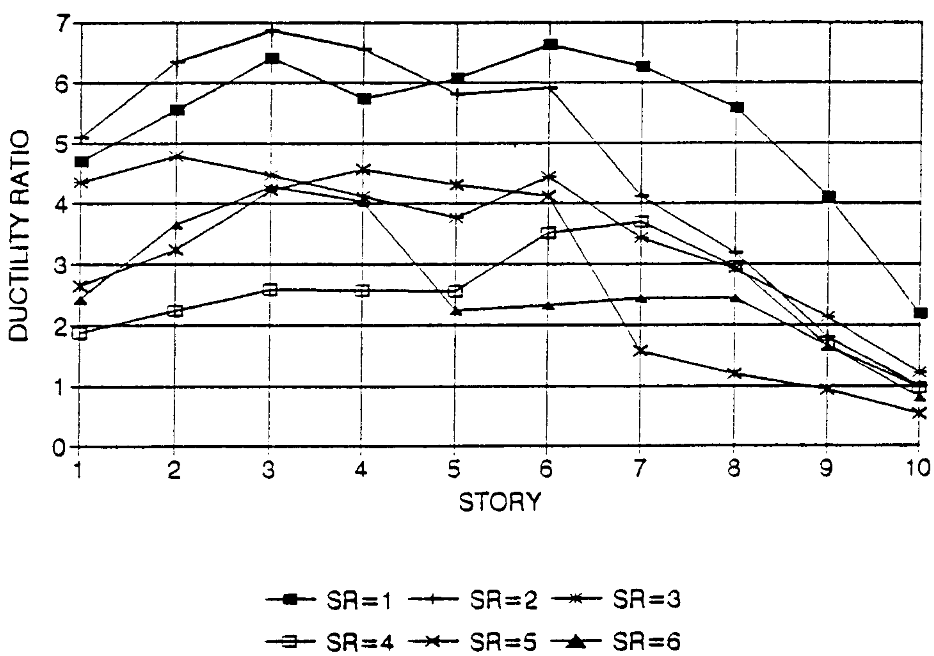

FIGURE 3-18 Relations between SR and Ductility Ratio When the Structure is Subjected to El Centro Ground Motion

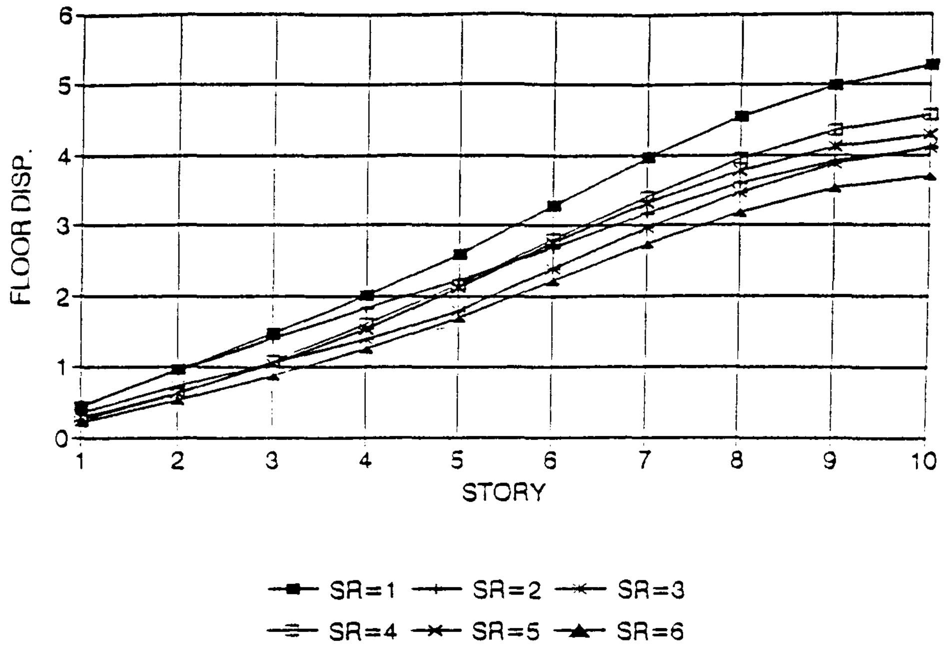

FIGURE 3-19 Relations between SR and Floor Displacement When the Structure is Subjected to San Fernando Ground Motion

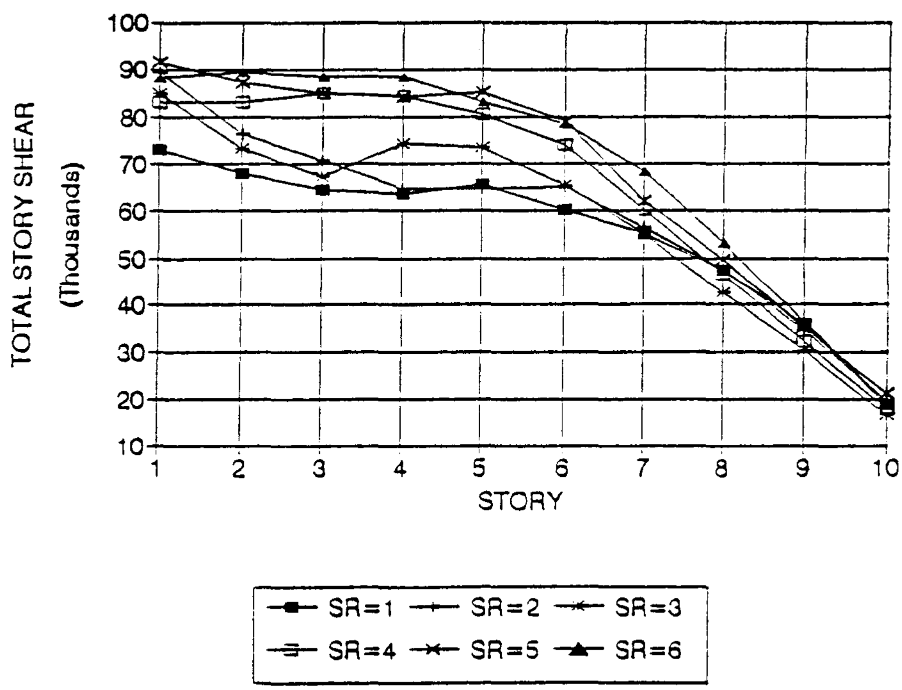

FIGURE 3-20 Relations between SR and Base Shear Force When the Structure is Subjected to San Fernando Ground Motion

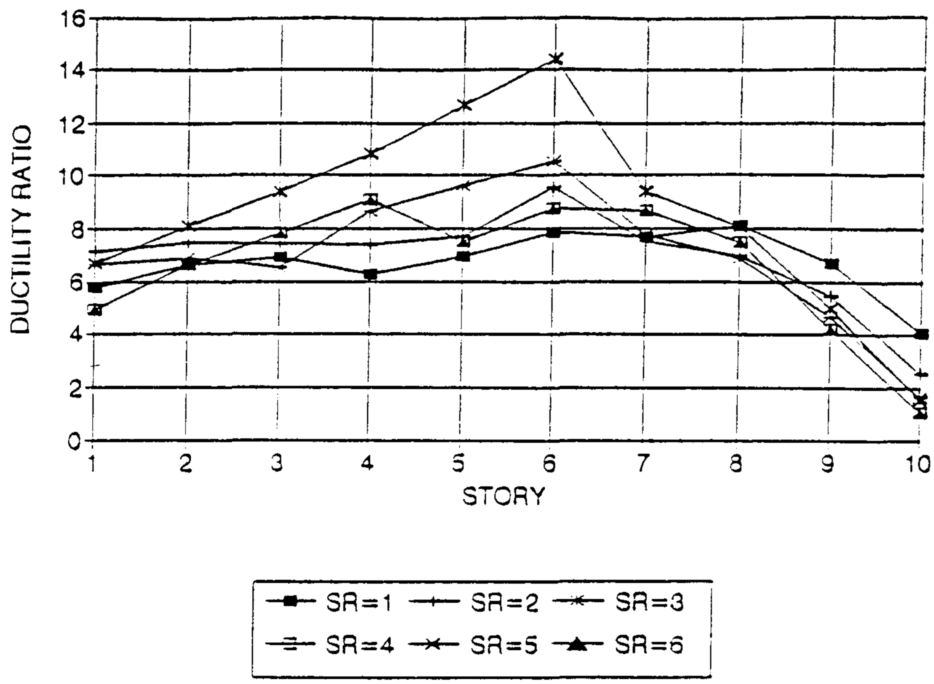

FIGURE 3-21 Relations between SR and Ductility Ratio When the Structure is Subjected to San Fernando Ground Motion

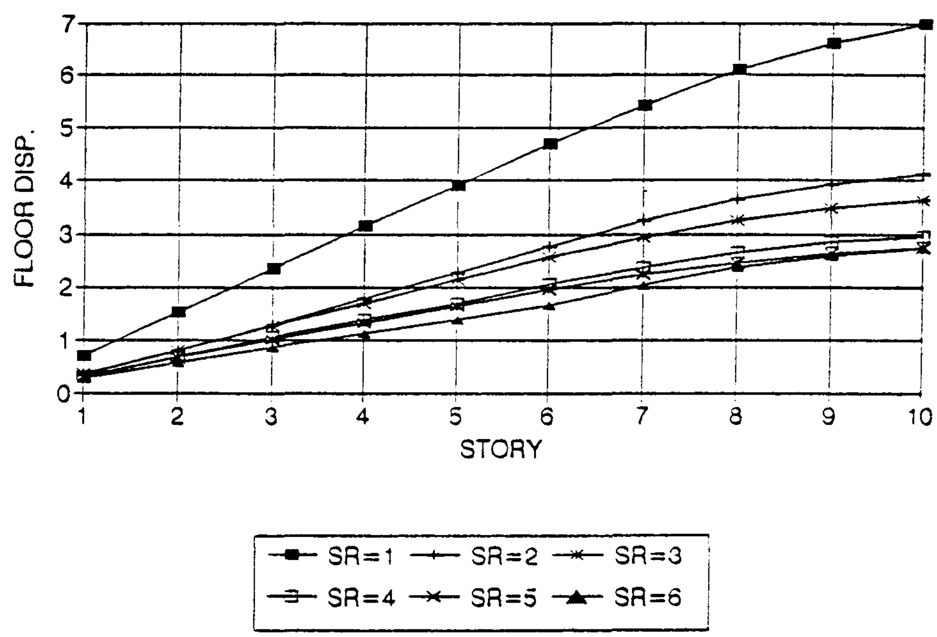

FIGURE 3-22 Relations between SR and Floor Displacement When the Structure is Subjected to Taft (ERSF=4) Ground Motion

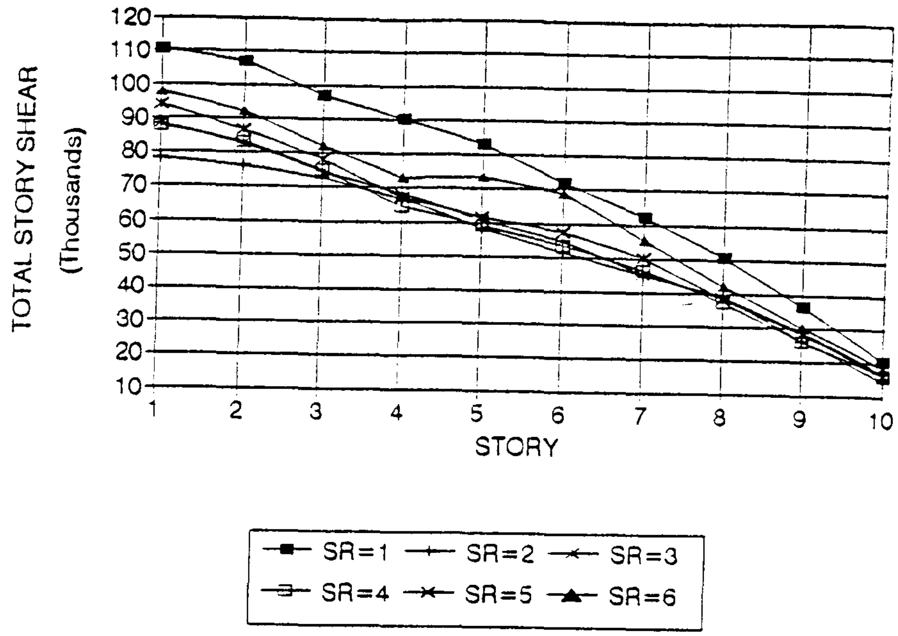

FIGURE 3-23 Relations between SR and Base Shear Force When the Structure is Subjected to Taft (ERSF=4) Ground Motion

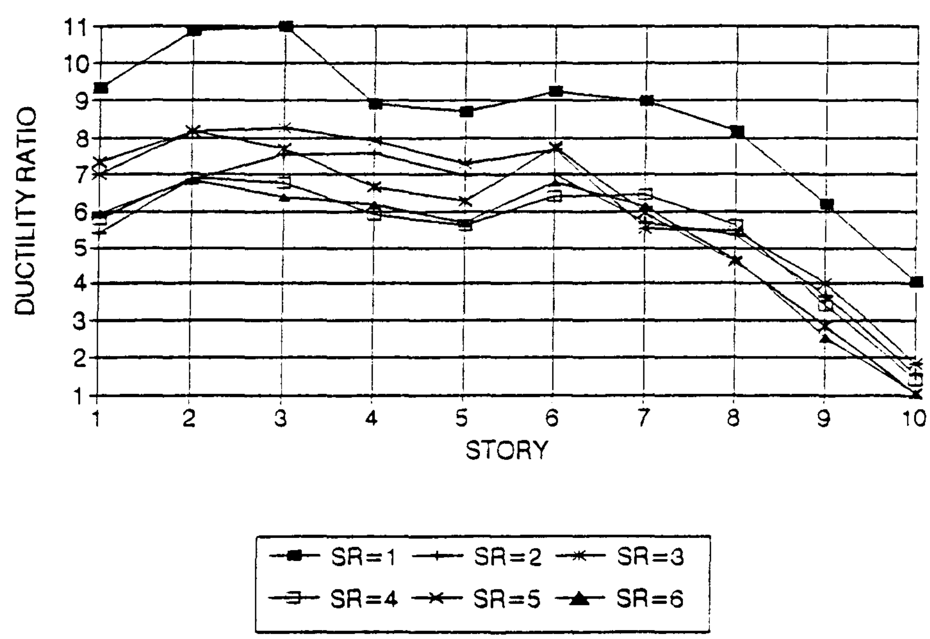

FIGURE 3-24 Relations between SR and Ductility Ratio When the Structure is Subjected to Taft (ERSF=4) Ground Motion

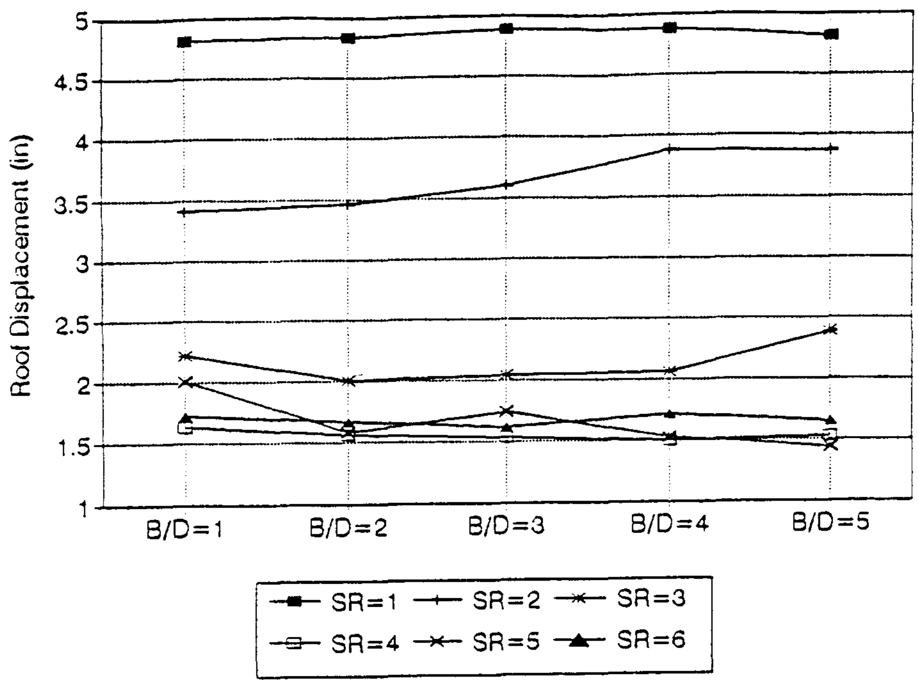

FIGURE 3-25 Comparison of B/D and SR with Floor Displacement When the Structure is Subjected to El Centro Ground Motion

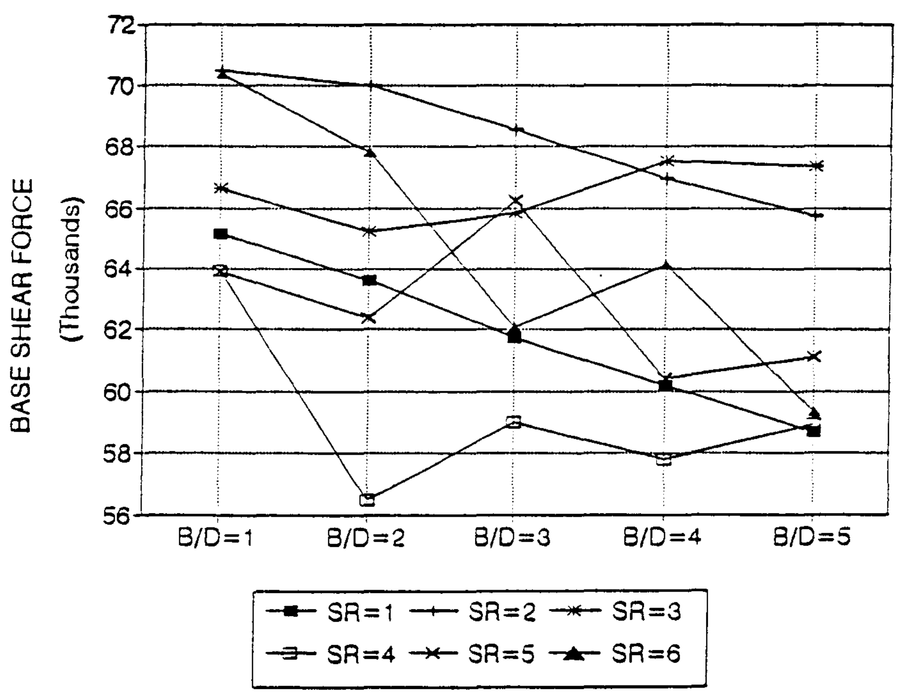

FIGURE 3-26 Comparison of B/D and SR with Shear Force When the Structure is Subjected to El Centro Ground Motion

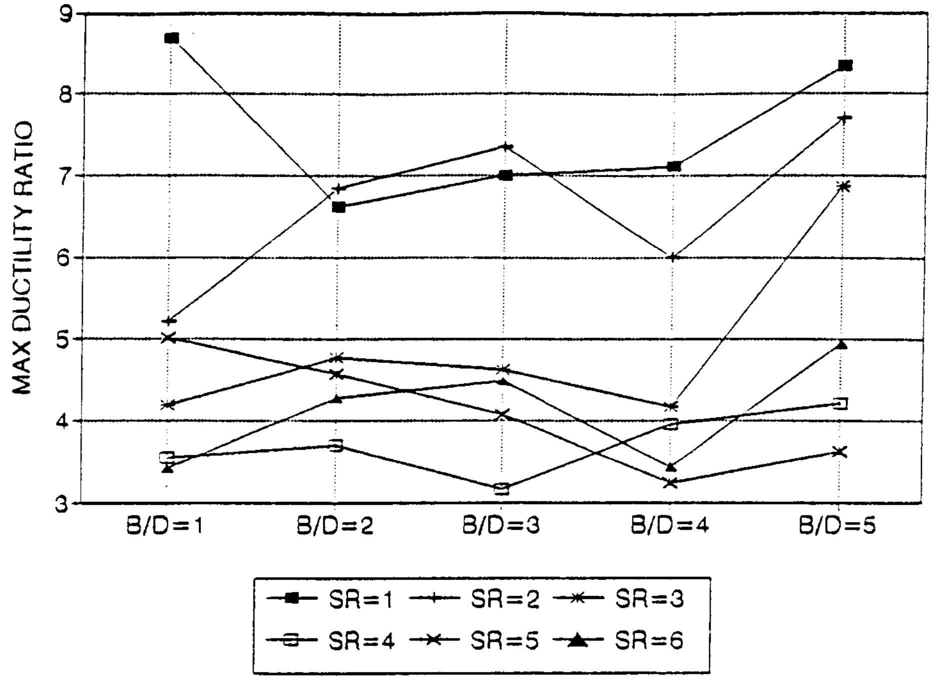

FIGURE 3-27 Comparison of B/D and SR with Ductility Ratio When the Structure is Subjected to El Centro Ground Motion

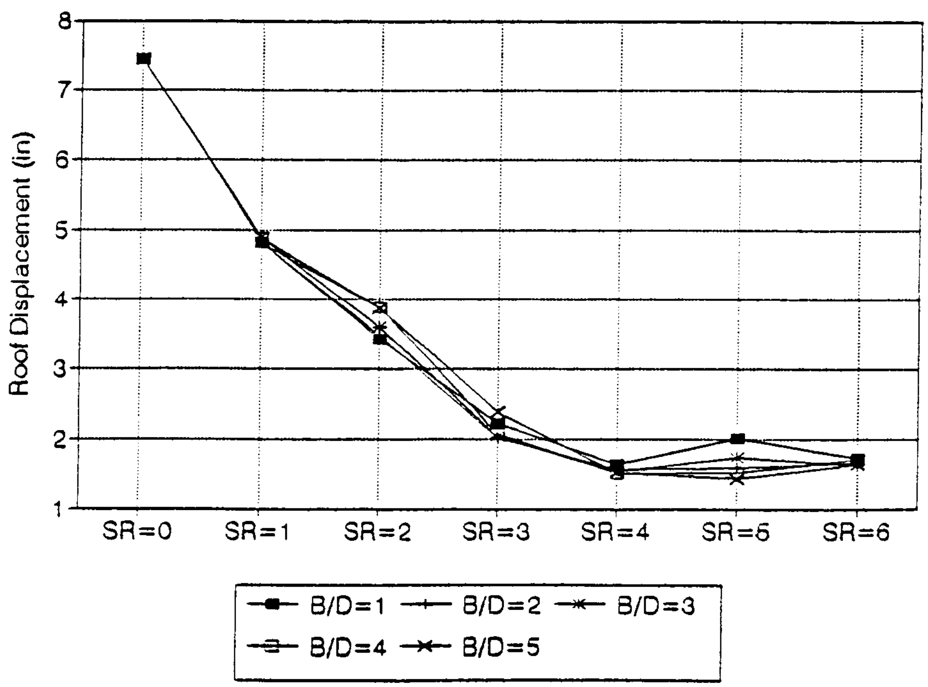

FIGURE 3-28 Comparison of SR and B/D with Floor Displacement When the Structure is Subjected to El Centro Ground Motion

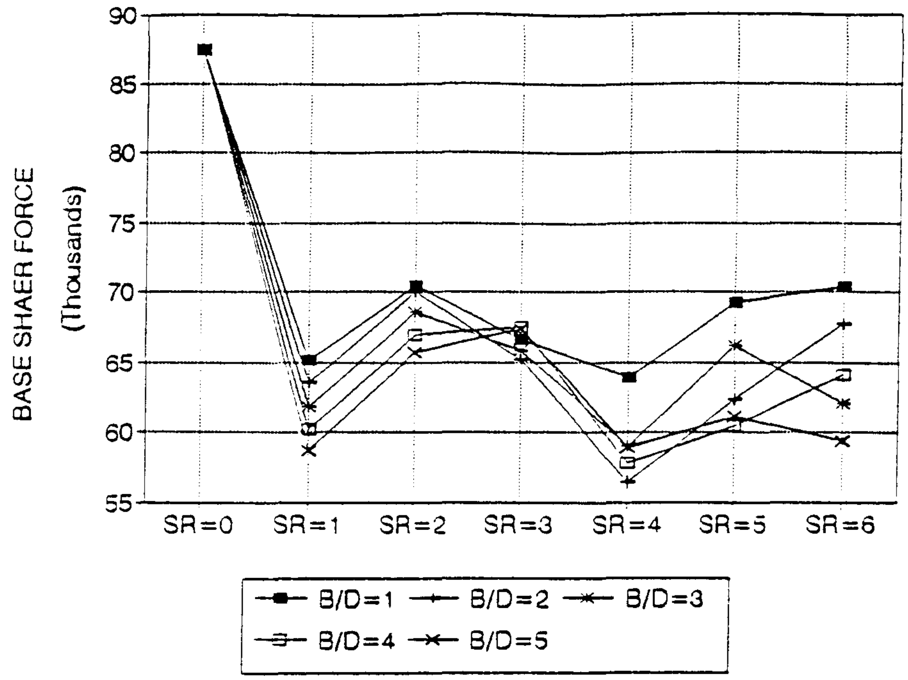

FIGURE 3-29 Comparison of SR and B/D with Base Shear Force When the Structure is Subjected to El Centro Ground Motion

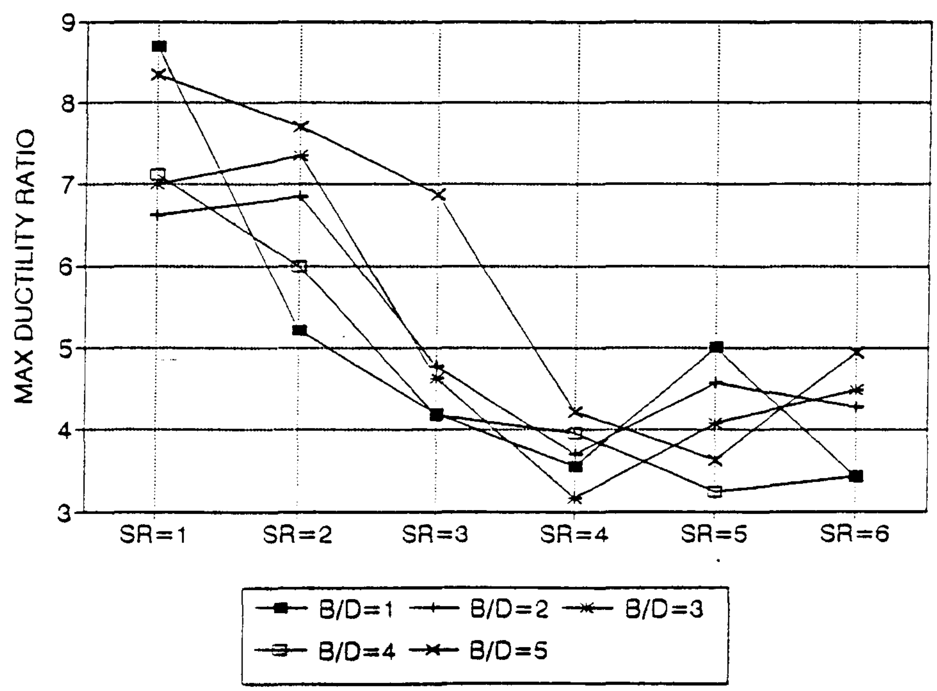

FIGURE 3-30 Comparison of SR and B/D with Ductility Ratio When the Structure is Subjected to El Centro Ground Motion

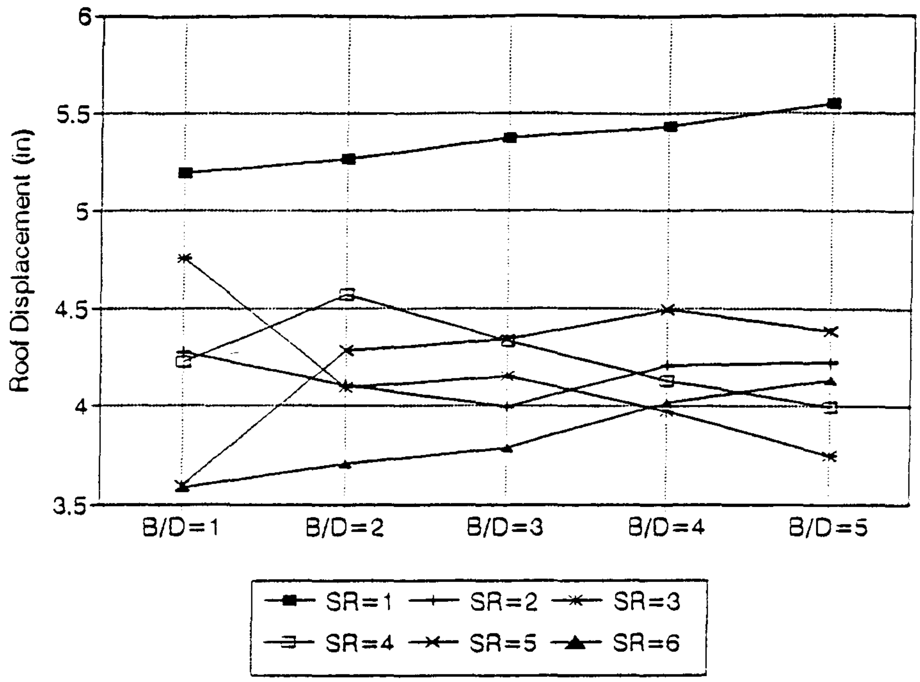

FIGURE 3-31 Comparison of B/D and SR with Floor Displacement When the Structure is Subjected to San Fernando Ground Motion

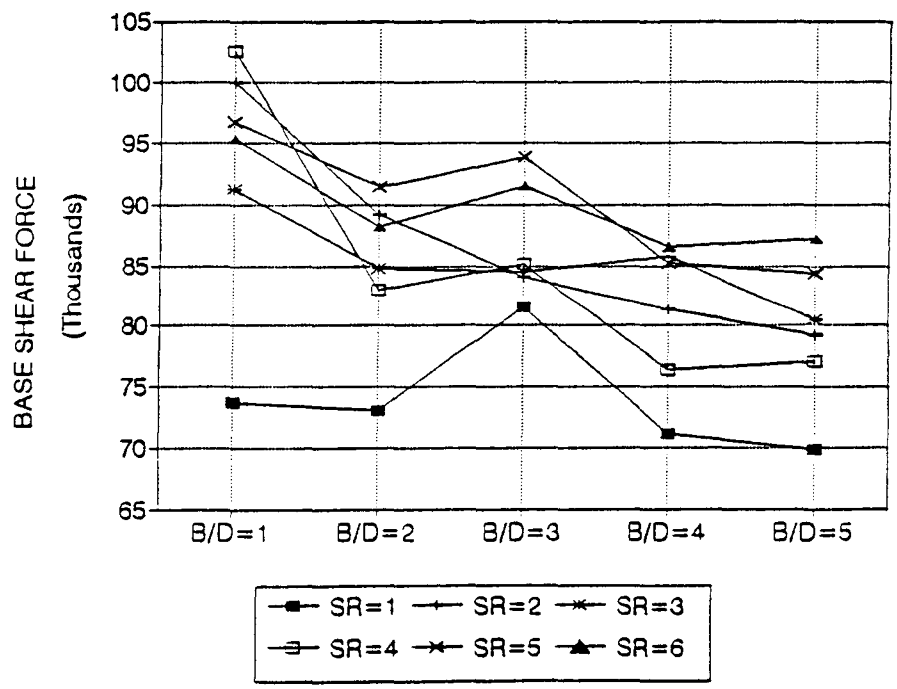

FIGURE 3-32 Comparison of B/D and SR with Base Shear Force When the Structure is Subjected to San Fernando Ground Motion

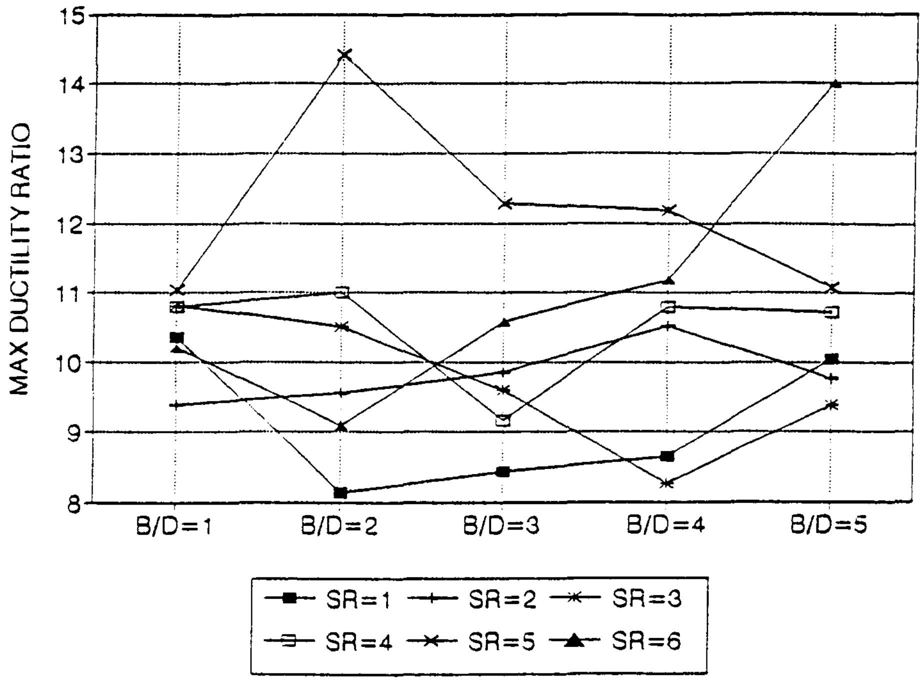

FIGURE 3-33 Comparison of B/D and SR with Ductility Ratio When the Structure is Subjected to San Fernando Ground Motion

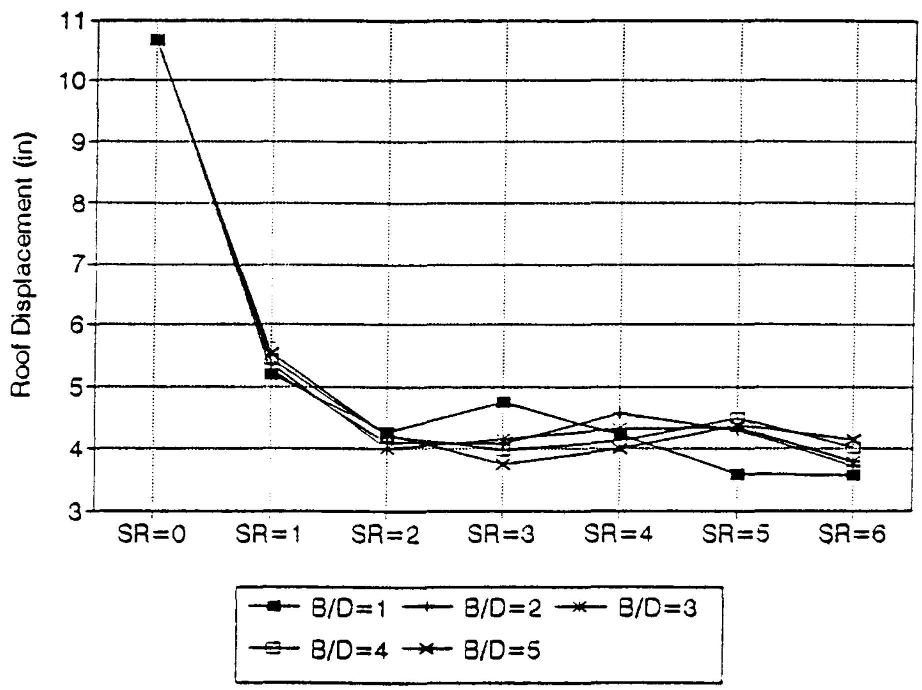

FIGURE 3-34 Comparison of SR and B/D with Floor Displacement When the Structure is Subjected to San Fernando Ground Motion

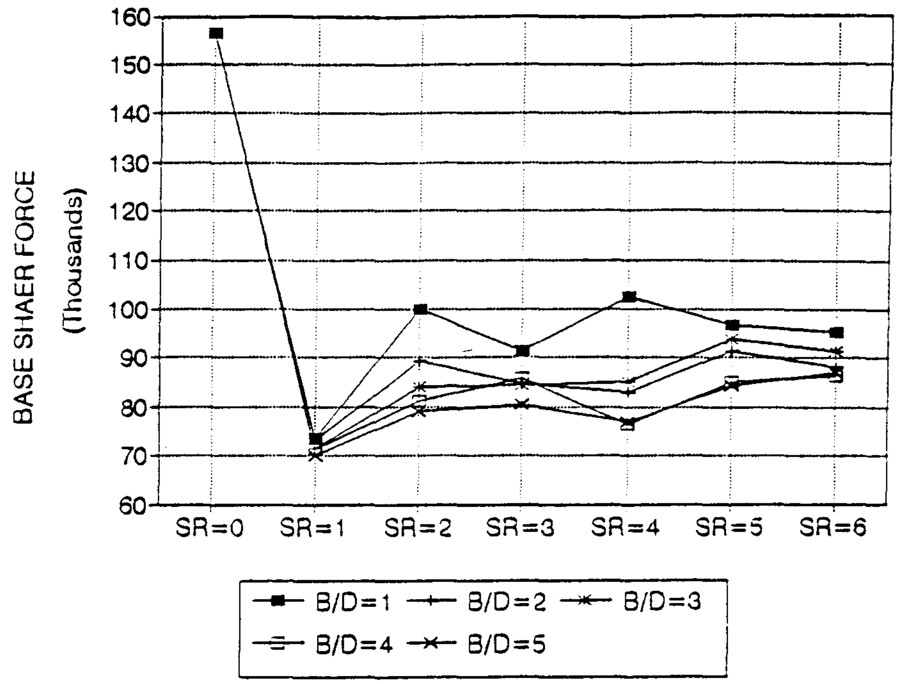

FIGURE 3-35 Comparison of SR and B/D with Base Shear Force When the Structure is Subjected to San Fernando Ground Motion

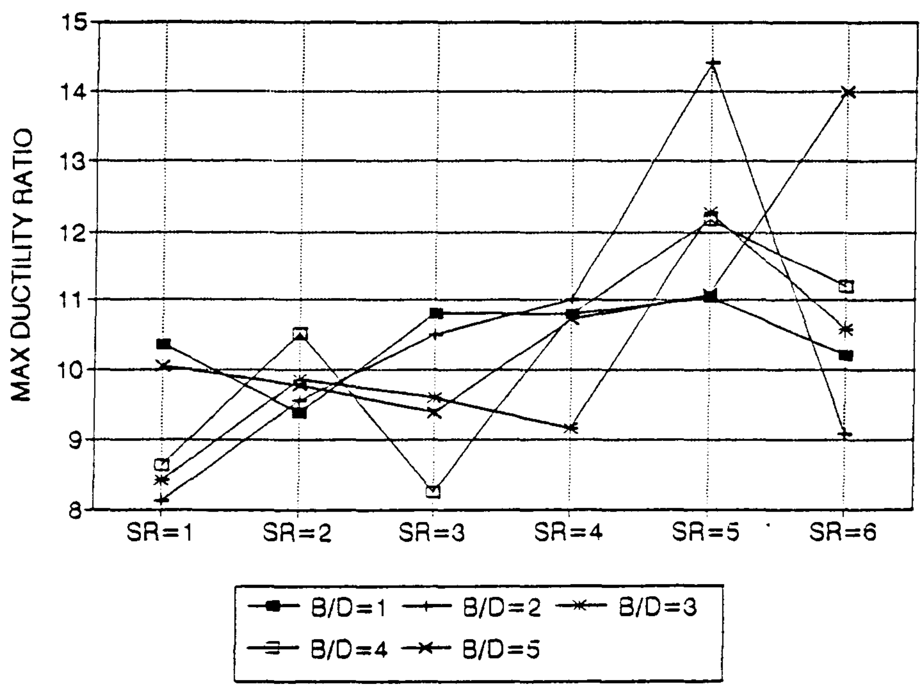

FIGURE 3-36 Comparison of SR and B/D with Ductility Ratio When the Structure is Subjected to San Fernando Ground Motion

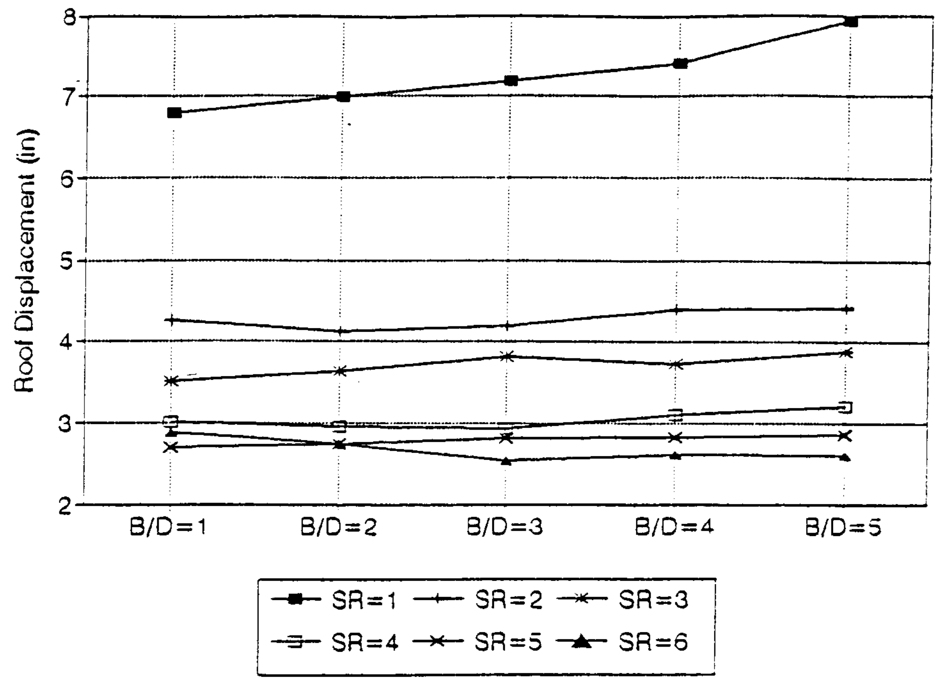

FIGURE 3-37 Comparison of B/D and SR with Floor Displacement When the Structure is Subjected to Taft (ERSF=4) Ground Motion

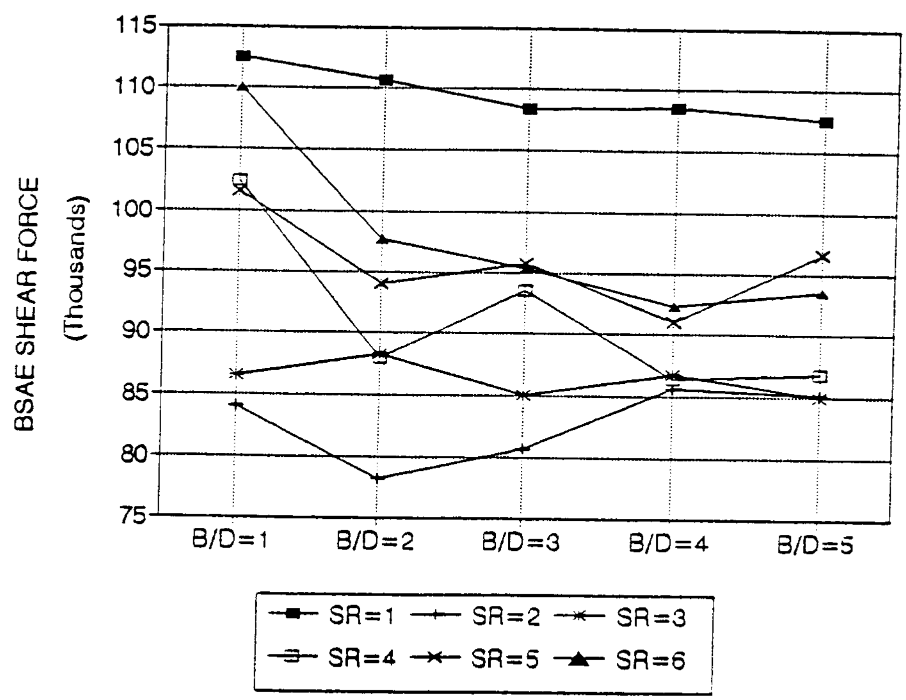

FIGURE 3-38 Comparison of B/D and SR with Base Shear Force When the Structure is Subjected to Taft (ERSF=4) Ground Motion

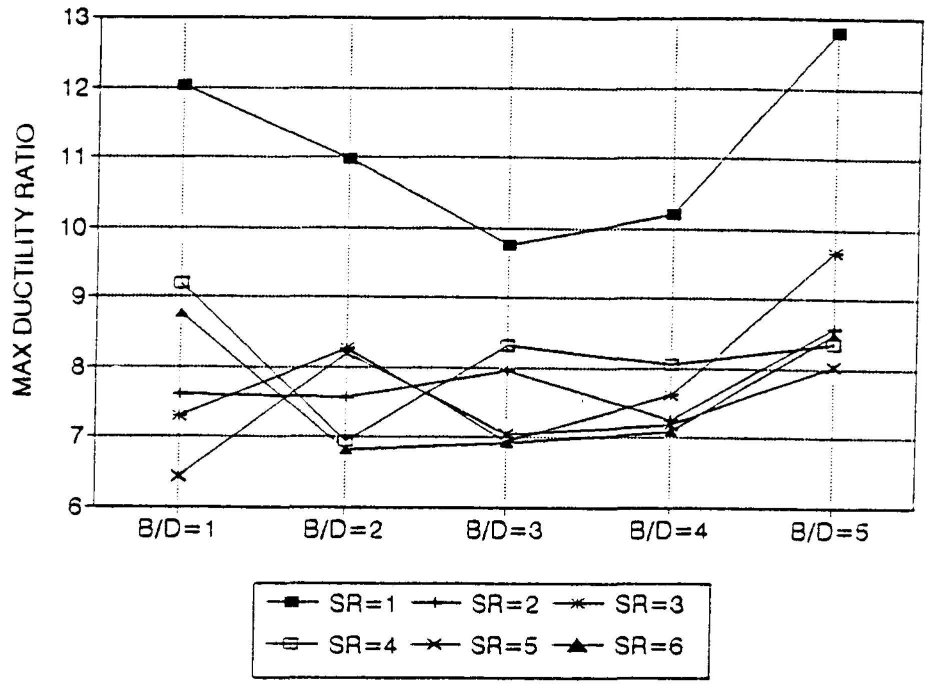

FIGURE 3-39 Comparison of B/D and SR with Ductility Ratio When the Structure is Subjected to Taft (ERSF=4) Ground Motion

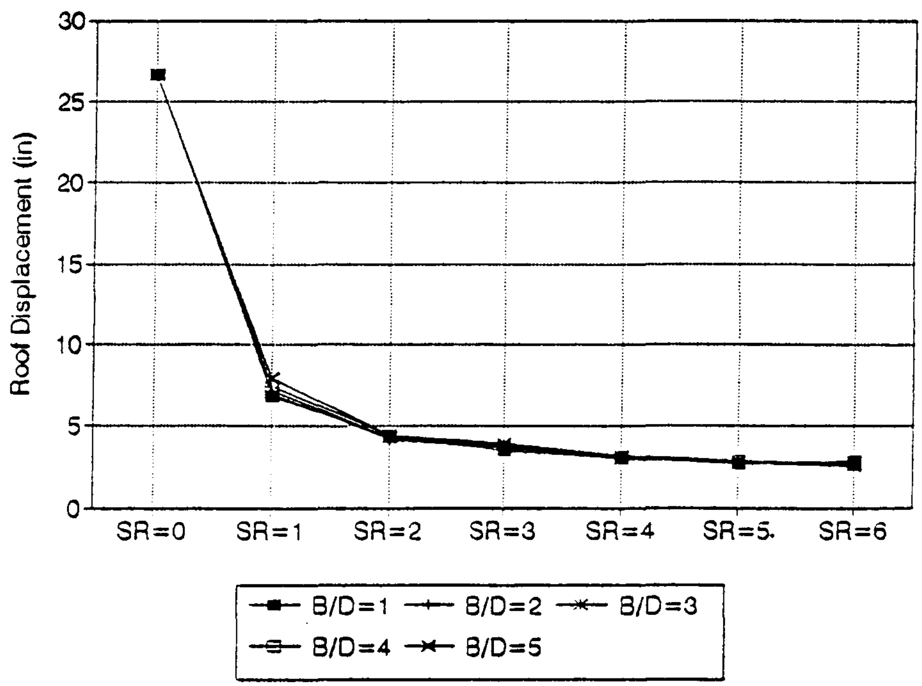

FIGURE 3-40 Comparison of SR and B/D with Floor Displacement When the Structure is Subjected to Taft (ERSF=4) Ground Motion

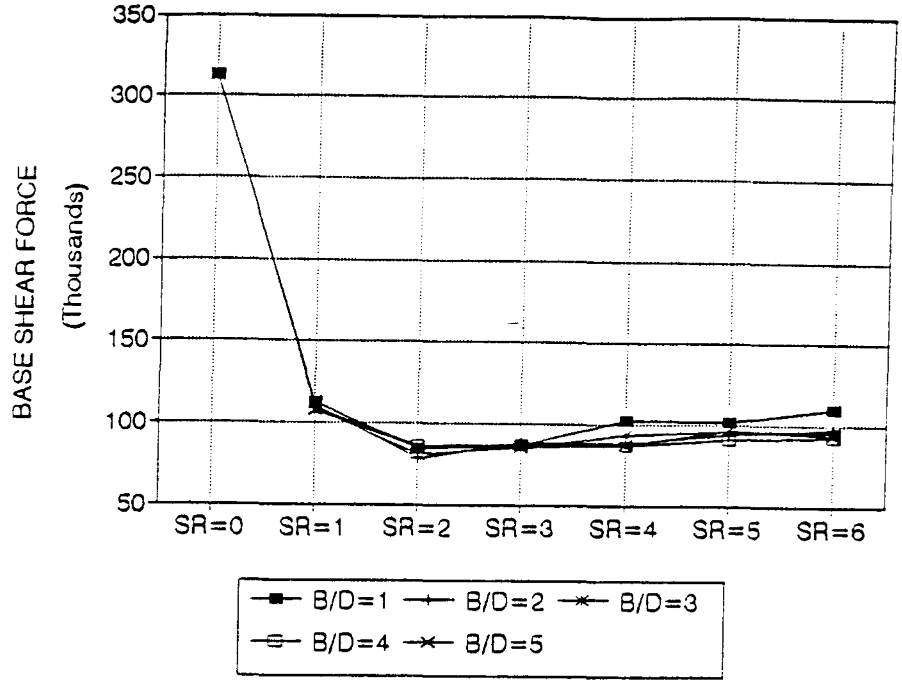

FIGURE 3-41 Comparison of SR and B/D with Base Shear Force When the Structure is Subjected to Taft (ERSF=4) Ground Motion

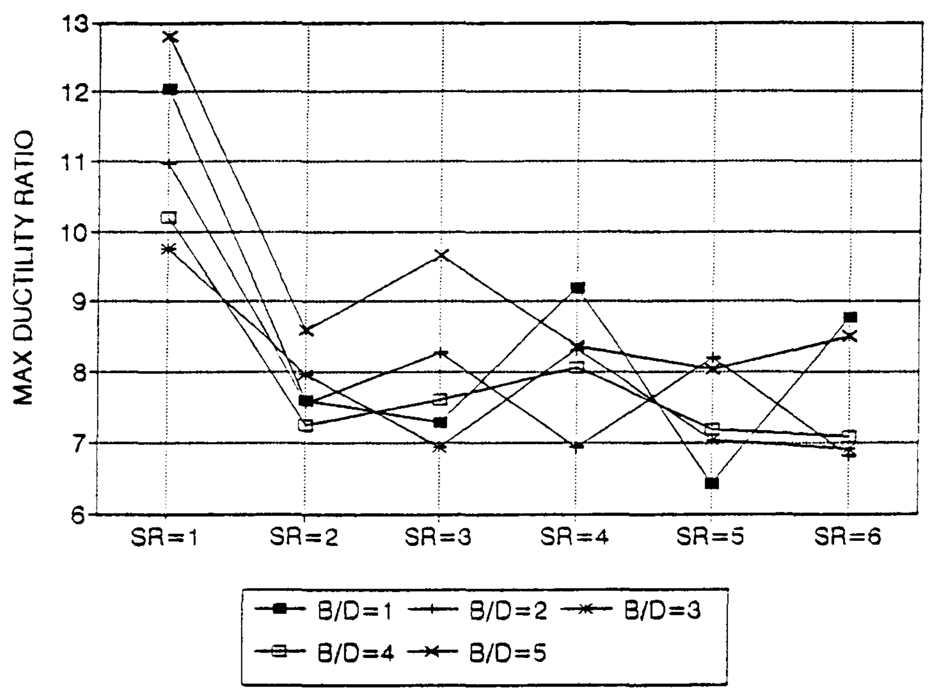

FIGURE 3-42 Comparison of SR and B/D with Ductility Ratio When the Structure is Subjected to Taft (ERSF=4) Ground Motion

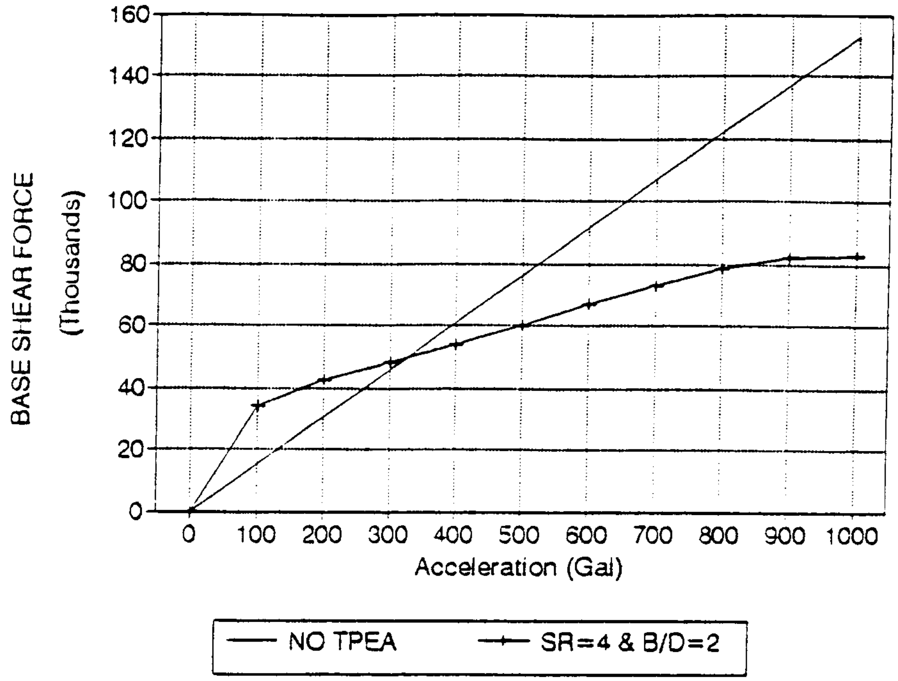

FIGURE 3-43 Comparison of Base Shear Force While the Structure is Subjected to the Peak Acceleration of 100 Gal to 1000 Gal of San Fernando Ground Motion

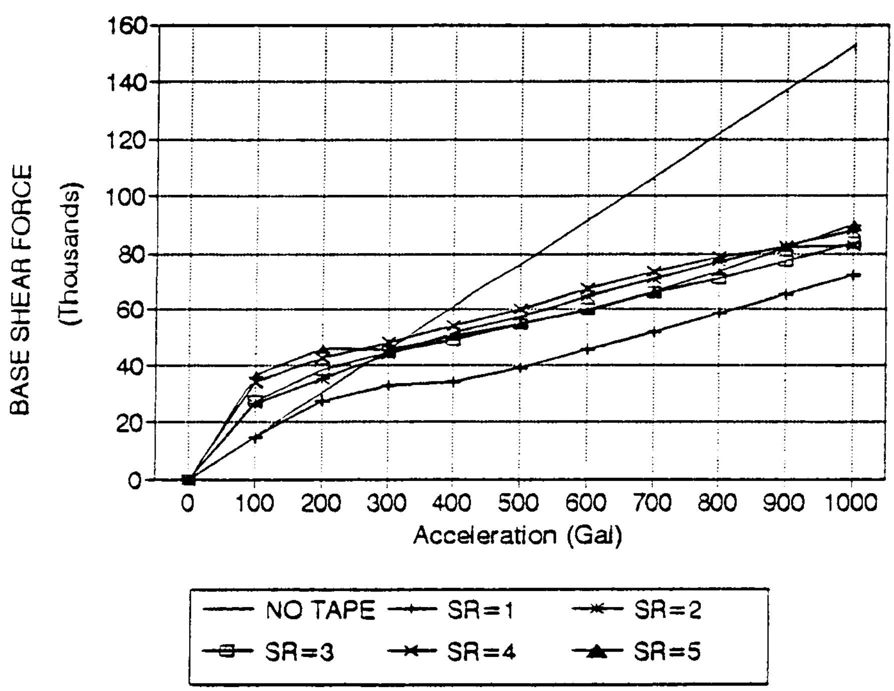

FIGURE 3-44 Comparison of Base Shear Force While the Structure is Subjected to the Peak Acceleration of 100 Gal to 1000 Gal of San Fernando Ground Motion

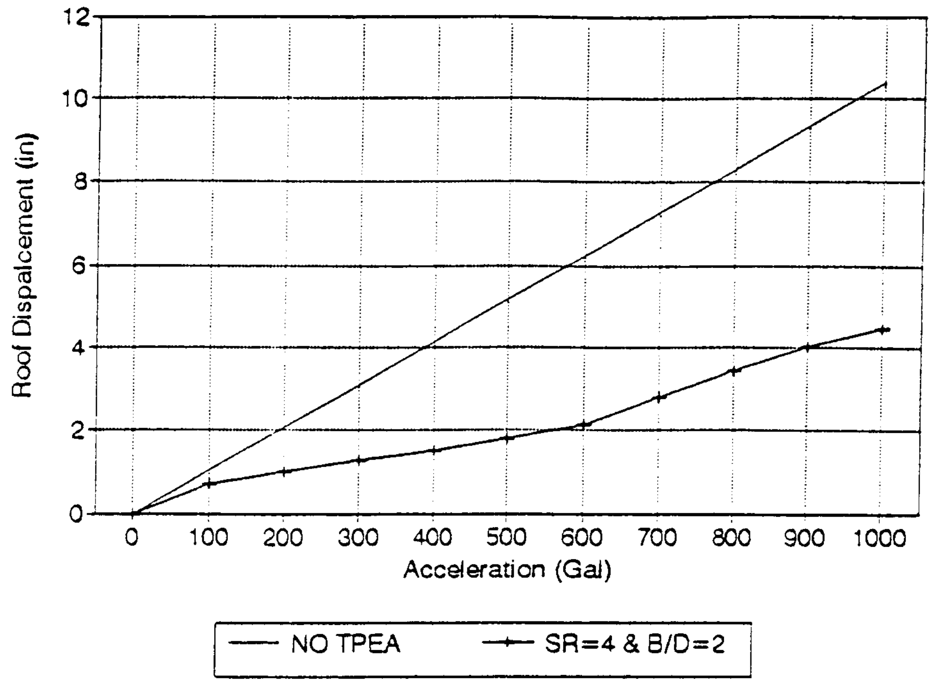

FIGURE 3-45 Comparison of Roof Displacement While the Structure is Subjected to the Peak Acceleration of 100 Gal to 1000 Gal of San Fernando Ground Motion

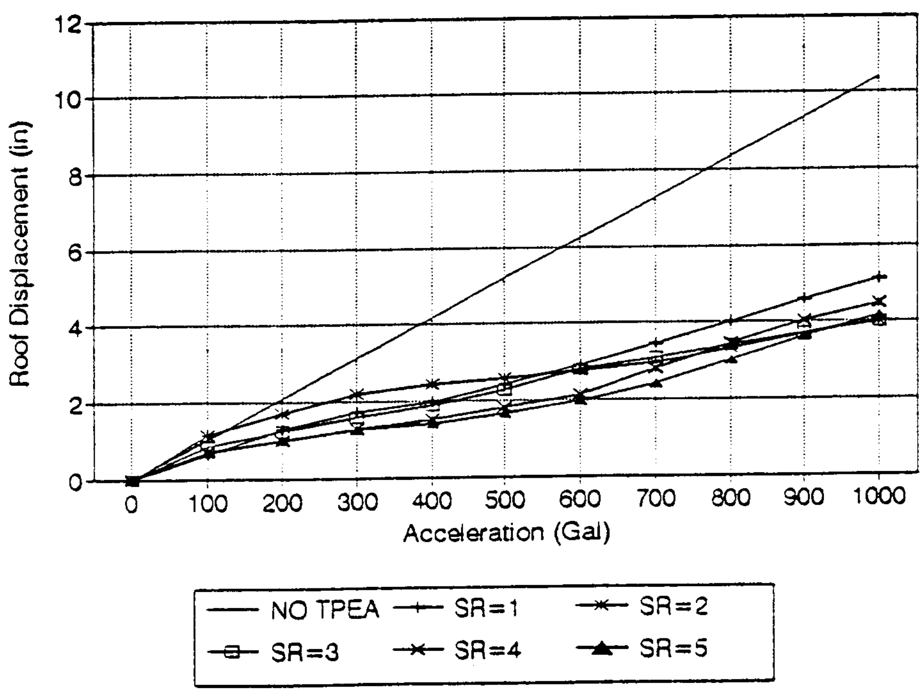

FIGURE 3-46 Comparison of Roof Displacement While the Structure is Subjected to the Peak Acceleration of 100 Gal to 1000 Gal of San Fernando Ground Motion

3.5 Comparison between a Frame with TPEA and a Frame with Simple Bracing Whose Stiffness Is the Same as That of the TPEA

In order to provide further evidence of the superiority of the TPEA, a comparison is made between a frame with TPEA (B/D=2, SR=4) and a frame with a simple bracing whose stiffness is the same as that of the TPEA. Figures 3-47 to 3-57 present the numerical results. In Figures3-48, 3-49, and 3-50, we see that a frame with TPEA performs better than a frame with a simple bracing. The properly designed TPEA devices have smaller yield displacements so that plastic deformations during an earthquake can be made to occur at the location of the devices and they can be replaced easily if damaged. However, a frame with a simple bracing does not provide such a situation. The energy dissipation capacity is increased by allowing the connection between bracing and beam through large inelastic deformation. As a result, the structure's integrity may be degraded once the connection is damaged during an earthquake and replacing the damaged connection would not be as easy as replacing a TPEA device. Furthermore, a frame with a simple bracing would induce much stronger horizontal shear forces because of the added stiffness. Consequently, such strong horizontal shear forces may jeopardize the structure. Figure 3-57 shows that the response curve of the structure with a simple bracing is linear and much larger while the response curve of the structure with TPEA becomes smooth when the peak acceleration is between 800 Gal and 1000 Gal. This provides evidence that TPEA is superior when a severe earthquake is imposed on the structure.

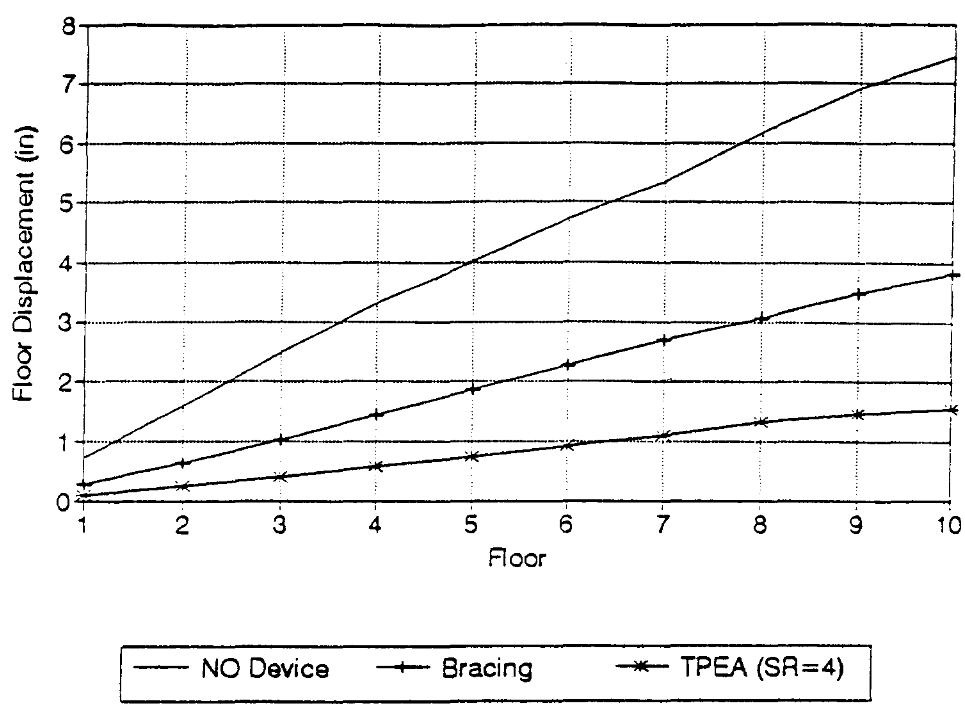

FIGURE 3-47 Comparison of Floor Displacement between a Frame with TPEA and with a Bracing When the Structure is Subjected to El Centro Ground Motion

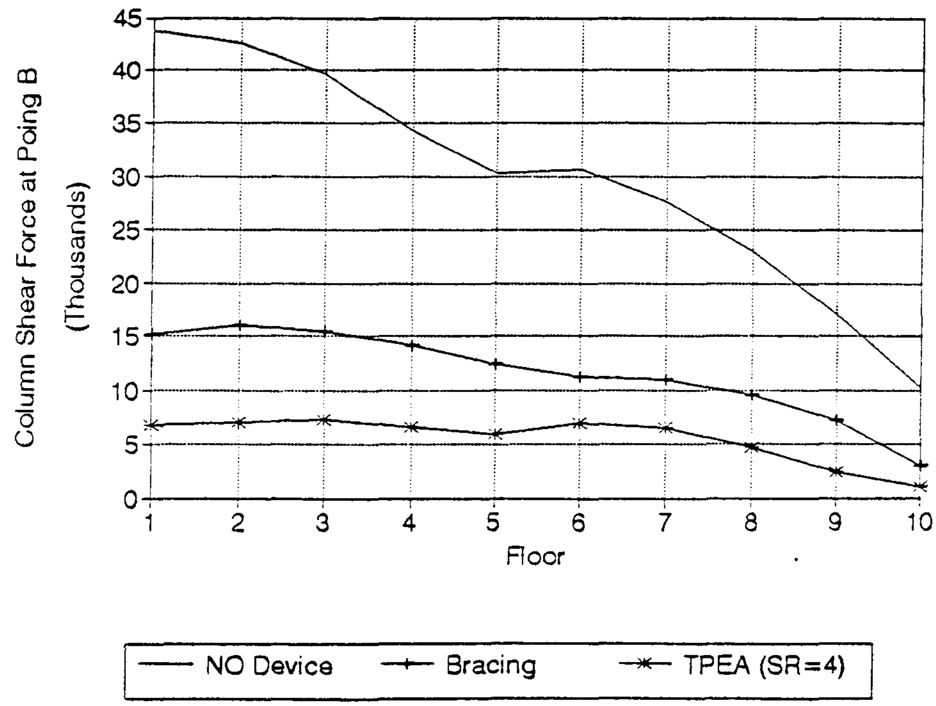

FIGURE 3-48 Comparison of Column Shear at Point B between a Frame with TPEA and a Frame with a Bracing When the Structure is Subjected to El Centro Ground Motion

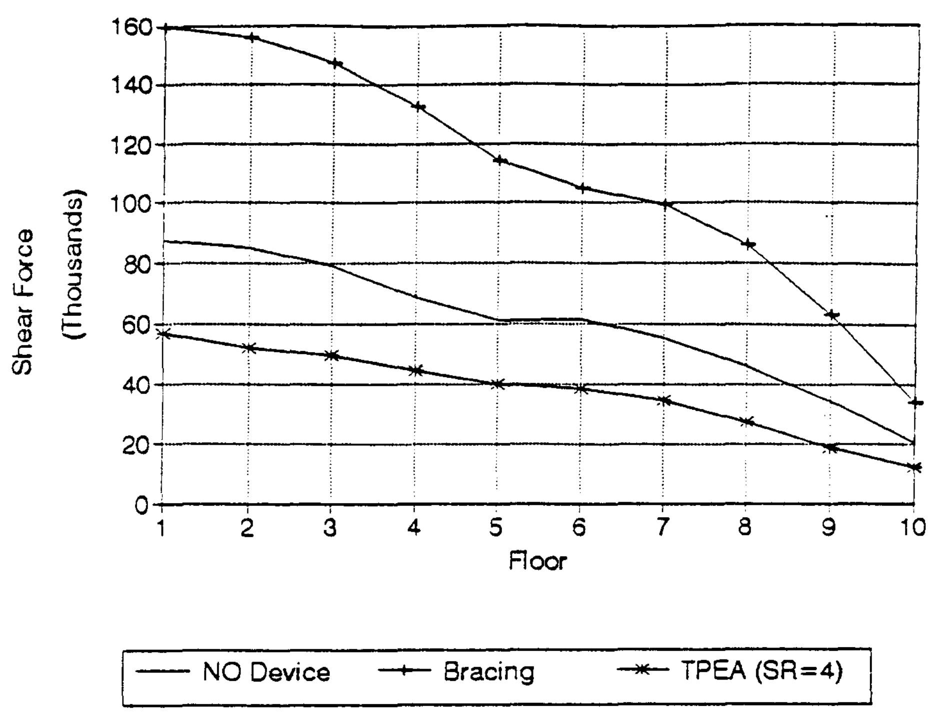

FIGURE 3-49 Comparison of Base Shear Force between a Frame with TPEA and with a Bracing When the Structure is Subjected to El Centro Ground Motion

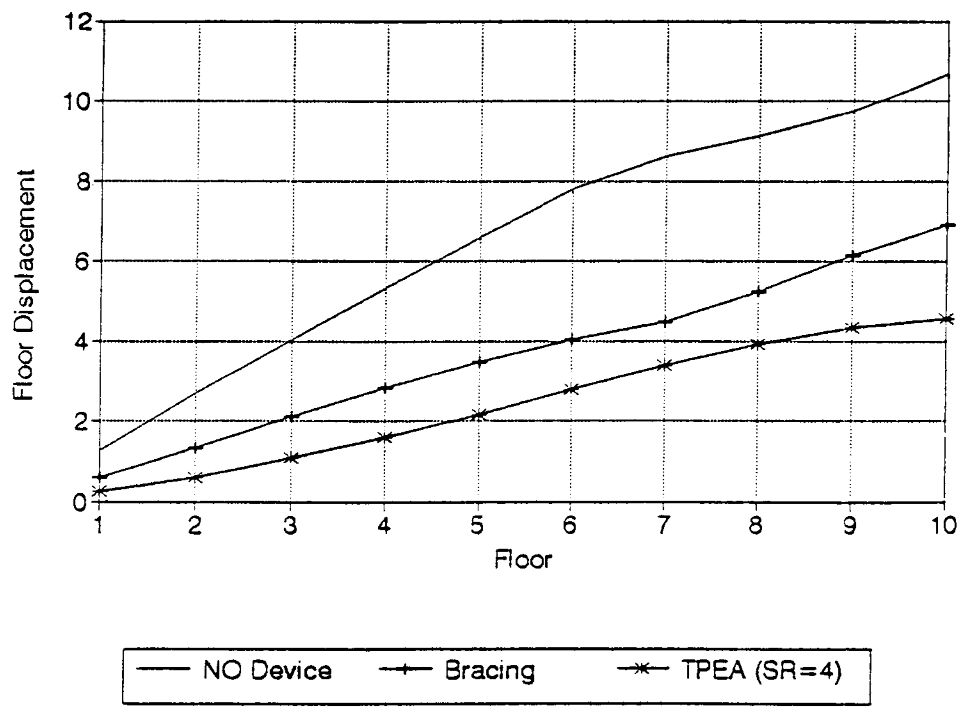

FIGURE 3-50 Comparison of Floor Displacement between a Frame with TPEA and with a Bracing When the Structure is Subjected to San Fernando Ground Motion

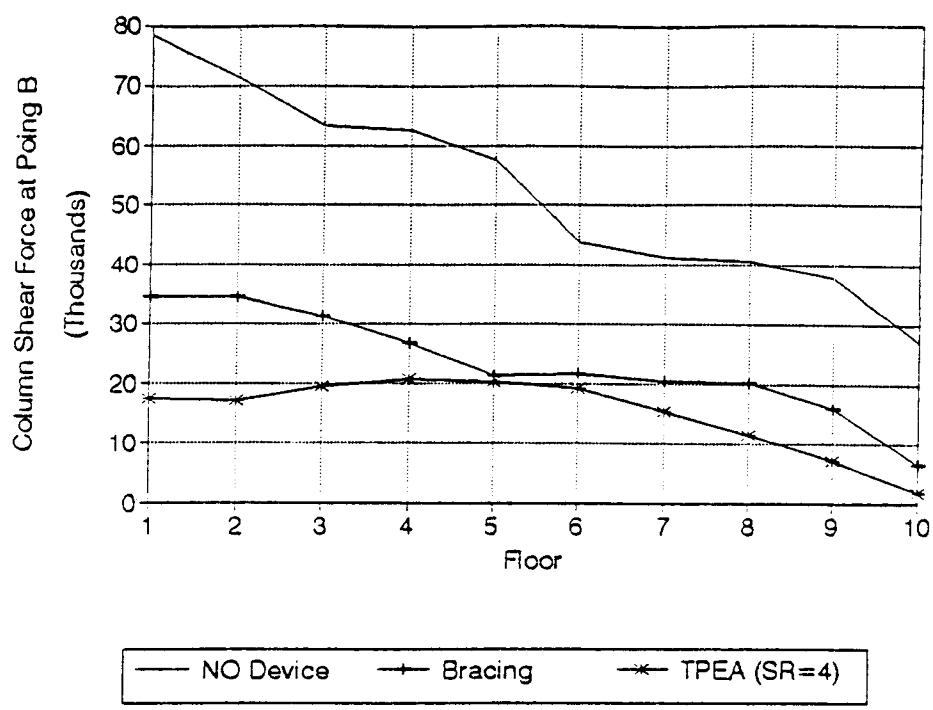

FIGURE 3-51 Comparison of Column Shear at Point B between a Frame with TPEA and a Frame with a Bracing When the Structure is Subjected to San Fernando Ground Motion

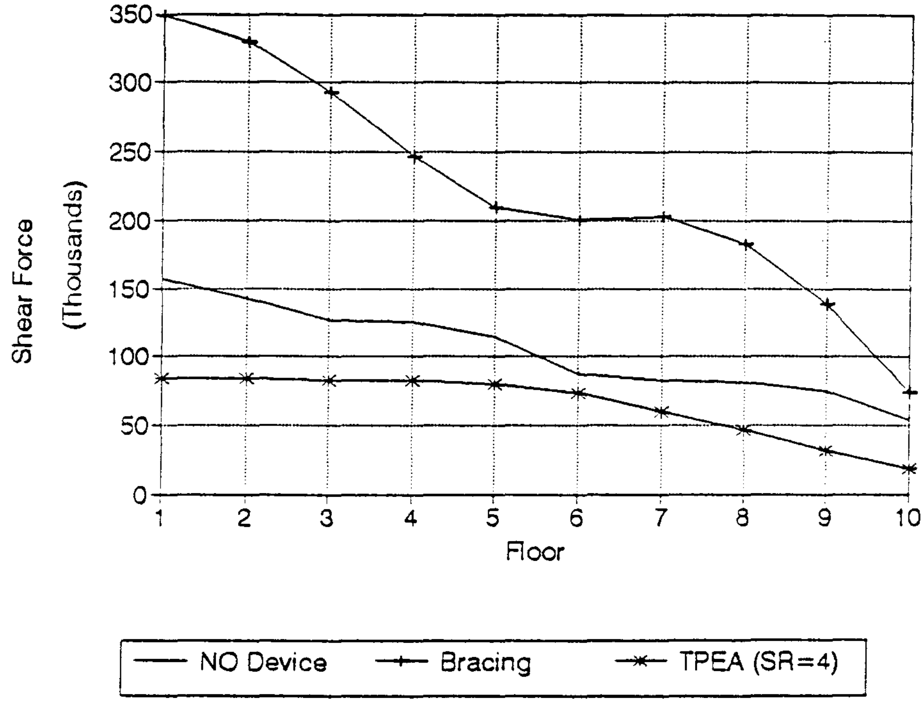

FIGURE 3-52 Comparison of Base Shear Force between a Frame with TPEA and with a Bracing When the Structure is Subjected to San Fernando Ground Motion

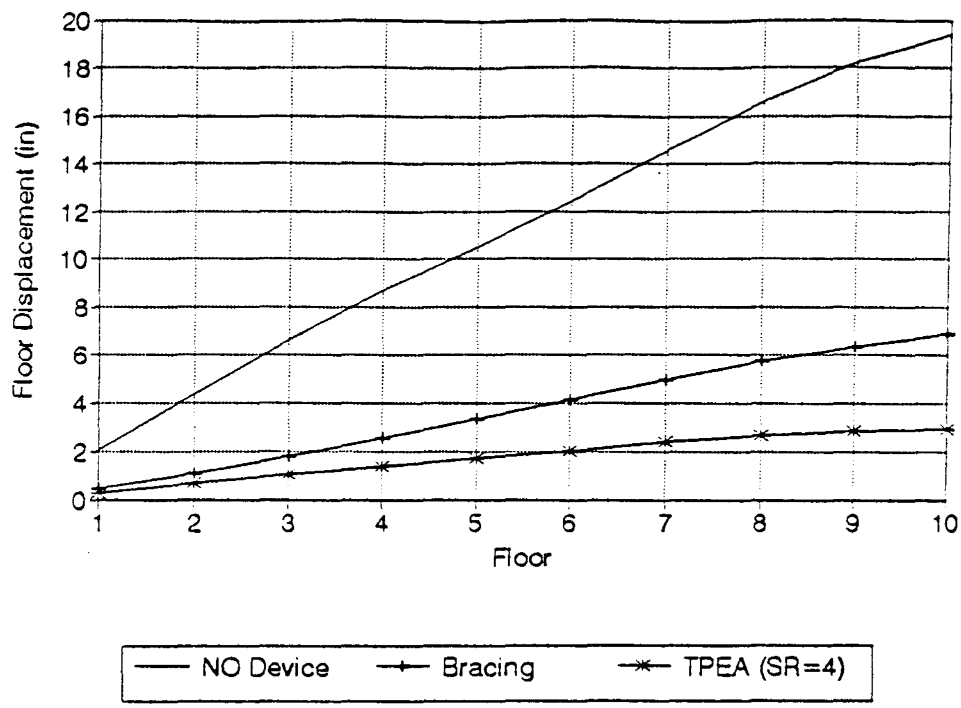

FIGURE 3-53 Comparison of Floor Displacement between a Frame with TPEA and with a Bracing When the Structure is Subjected to Taft (ERSF=4) Ground Motion

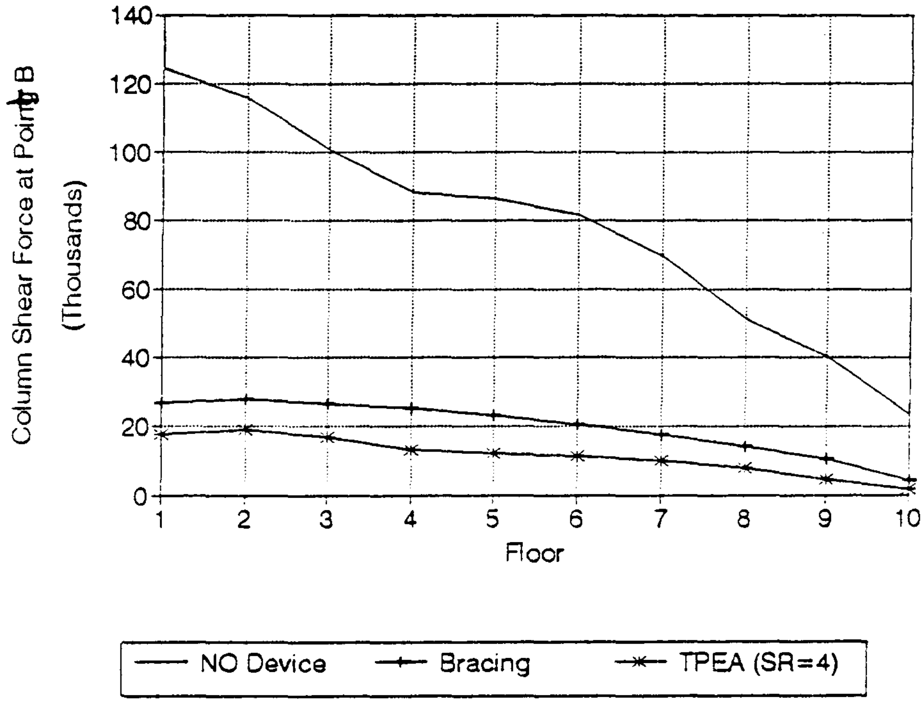

FIGURE 3-54 Comparison of Column Shear at Point B between a Frame with TPEA and a Frame with a Bracing When the Structure is Subjected to Taft (ERSF=4) Ground Motion

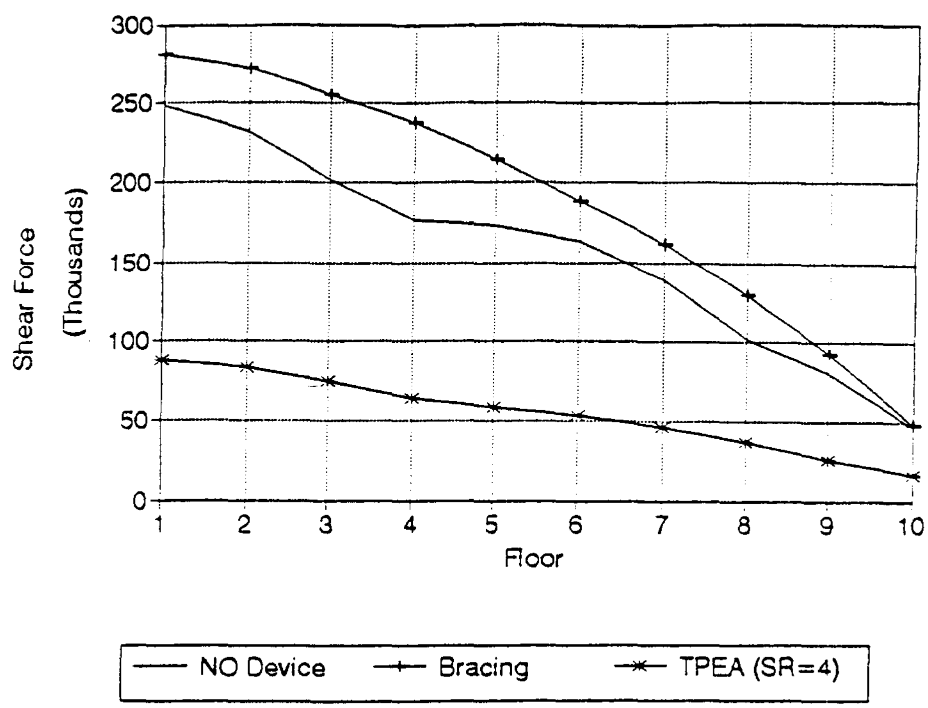

FIGURE 3-55 Comparison of Base Shear Force between a Frame with TPEA and with a Bracing When the Structure is Subjected to Taft (ERSF=4) Ground Motion

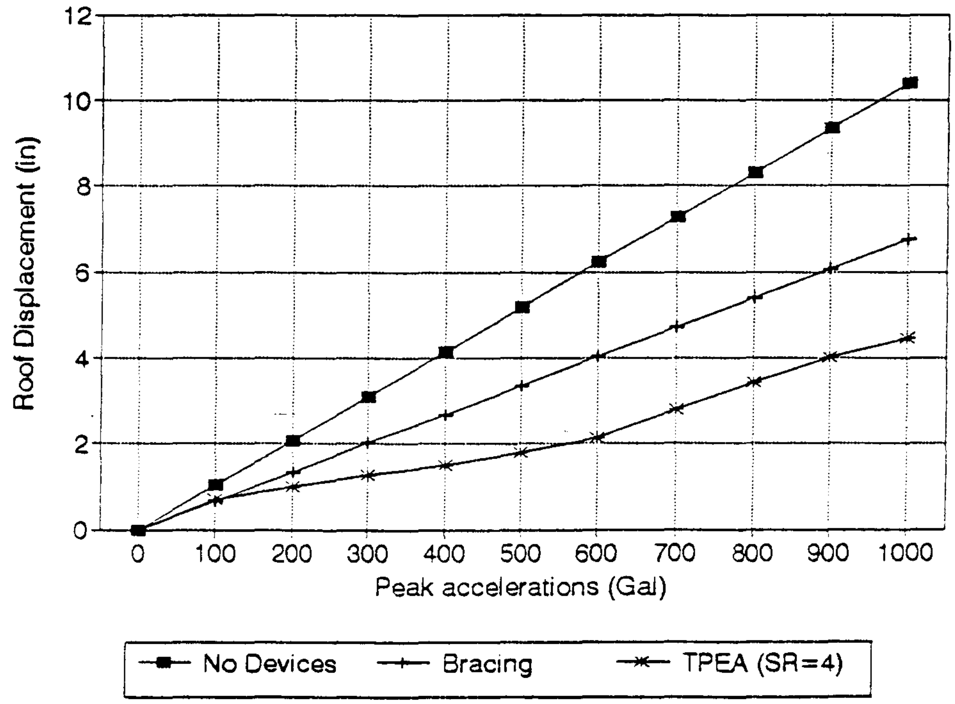

FIGURE 3-56 Comparison of Roof Displacement between a Frame with TPEA and a Frame with a Bracing When the Structure is Subjected to the Peak Acceleration of 100 Gal to 1000 Gal. of San Fernando Ground Motion

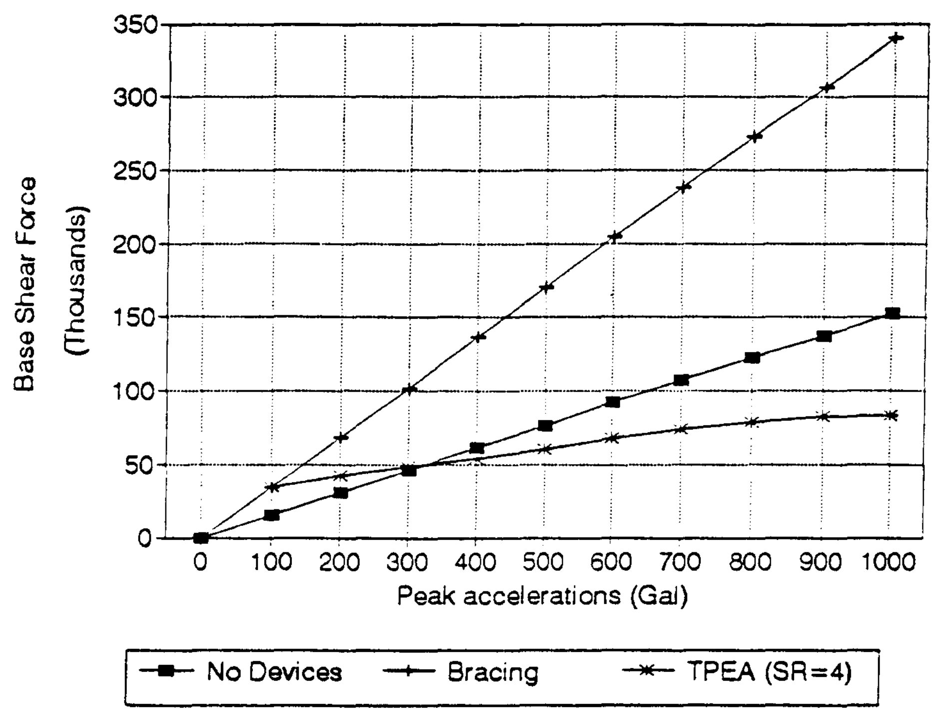

FIGURE 3-57 Comparison of Base Shear Force between a Frame with TPEA and a Frame with a Bracing When the Structure is Subjected to the Peak Acceleration of 100 Gal to 1000 Gal. of San Fernando Ground Motion

3.6 Discussion

The time-history responses (roof displacement, column shear force at point B, and base shear force) of the structure with and without TPEA are shown in Figures 3-58 to 3-60 when the structure was subjected to San Fernando ground motion. Figure 3-58 indicates that the roof displacement of the structure subjected to the San Fernando ground motions was significantly reduced when the TPEA devices were added to the structure. In Figure 3-58, the structure with TPEA (SR=4 and B/D=2) generates 21 peaks within 10 seconds while the structure without TPEA generates 11 peaks in the same amount of time. Because the natural frequency is proportional to the square root of the stiffness, SR=4 may generate two times the natural frequency compared to the structure without TPEA. Figure 3-59 also shows that the column shear force at point B was significantly reduced when the structure was equipped with TPEA devices. Figure 3-60 illustrates that overall, the maximum base shear forces were reduced greatly. However, the base shear forces were not reduced compared to the structure without devices in the very beginning of earthquake excitation. This phenomenon was caused by the TPEA devices and their supporting bracing which changed the structure's natural frequencies. In the early stage of excitation, the TPEA may not yield. As a result, the total base shear forces of the structure with TPEA induced by ground motions may be larger than that of the structure without TPEA devices in the early stage of earthquakes. But, the maximum base shear force was eventually reduced compared to the structure without TPEA devices. It should be noted that although a larger SR will lead to smaller roof displacement, a larger SR may lead to higher natural frequencies which could result in stronger horizontal shear forces accelerations. In addition, the main load-carrying frames take a much smaller portion of the shear force when TPEA devices were added to the structure.

Since most of the plastic deformations during an earthquake can be made to occur in the TPEA devices, energy demands on the other structural members can be substantially reduced. Consequently, the main structural members will experience less damage. The TPEA devices located at the lower floors contribute more to energy absorption than those in upper floors. Figures 3-61-3-63 show the relationship of force and displacement during the San Fernando ground motion for the TPEA devices (SR=4, and B/D=2) located at the 1st, 5th, and 10th floors. The TPEA devices located at the 1st floor absorb more energy while the TPEA device located at 10th floor is still within the elastic range.

The TPEA provides a strong safe failure mechanism. In other words, it would not jeopardize the structure if the TPEA device failed to protect the structure properly. Furthermore, the TPEA device is not a strain-rate-dependent, so the response of the structure can be reduced once the earthquake occurs and the material behavior of the device is temperature independent. The results demonstrate that the TPEA device is a promising alternative for the mitigation of seismic effects on buildings.

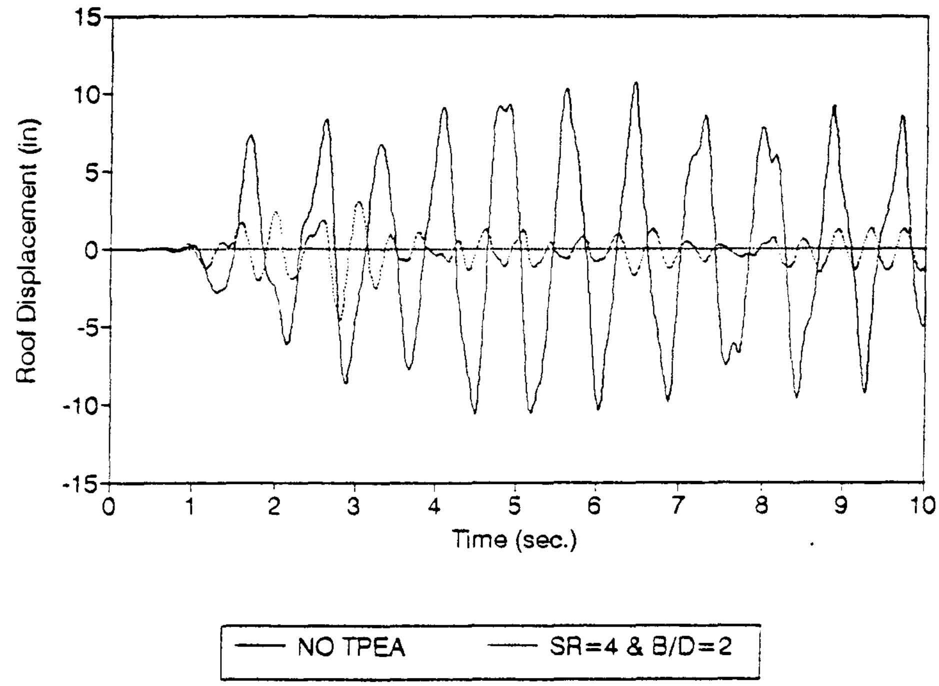

FIGURE 3-58 The response of Floor Displacement When the Structure is Subjected to San Fernando Ground Motion

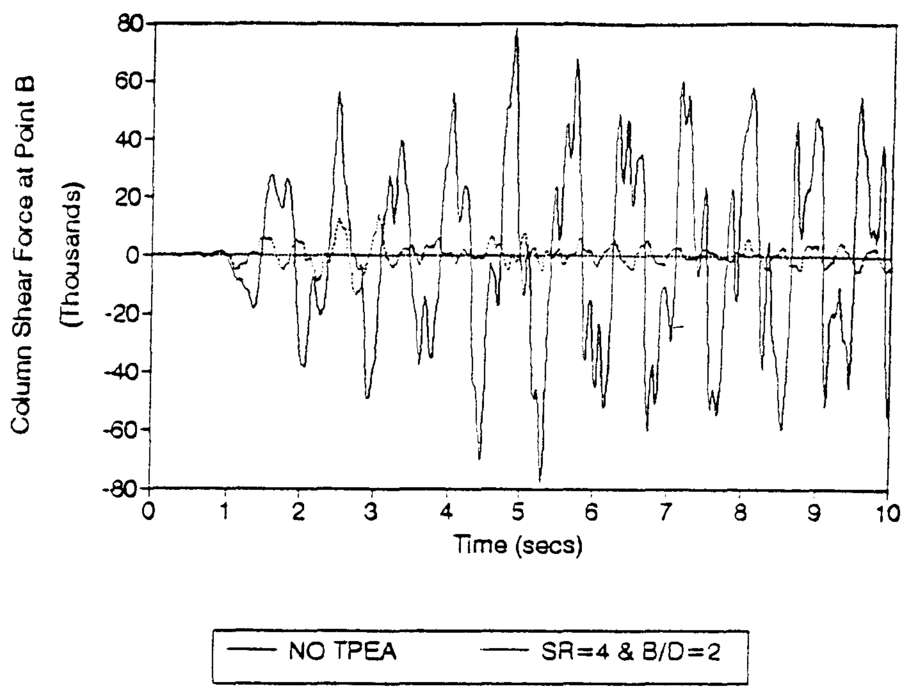

FIGURE 3-59 The response of Column Shear Force at Point B When the Structure is Subjected to San Fernando Ground Motion

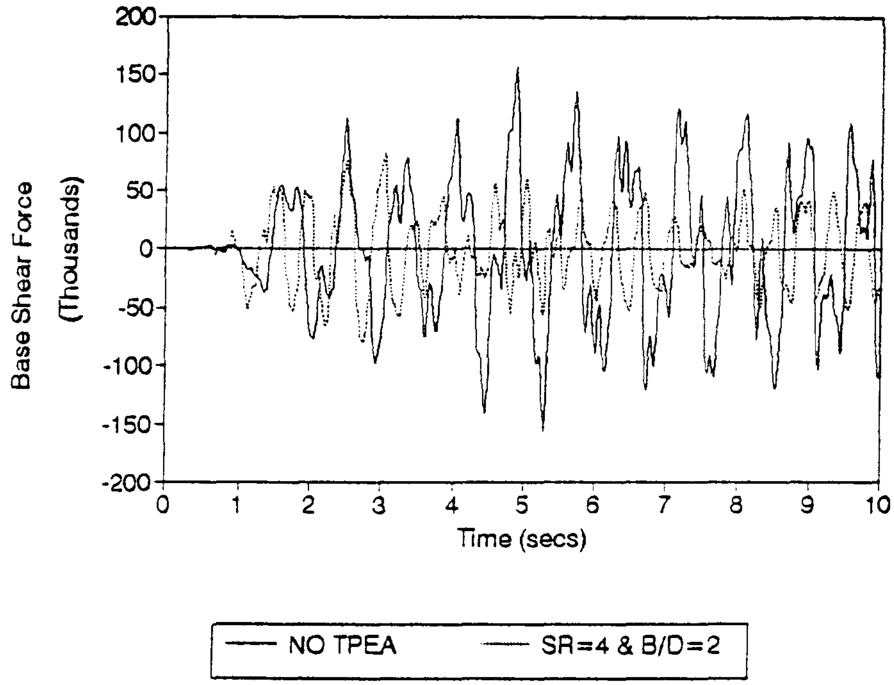

FIGURE 3-60 The response of Base Shear Force When the Structure is Subjected to San Fernando Ground Motion

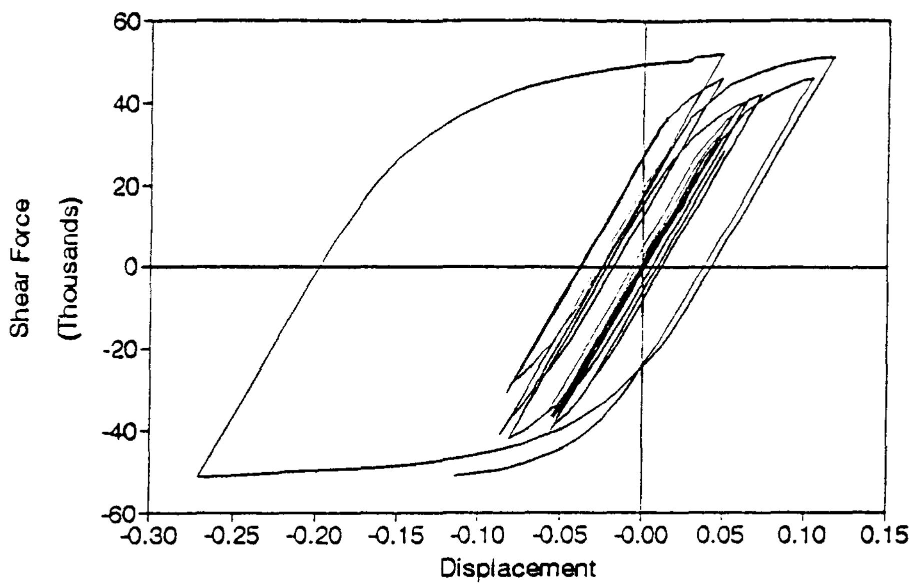

FIGURE 3-61 The Relation of Force and Displacement of TPEA at 1st Floor When the Structure is Subjected to Taft (ERSF=4) Ground Motion

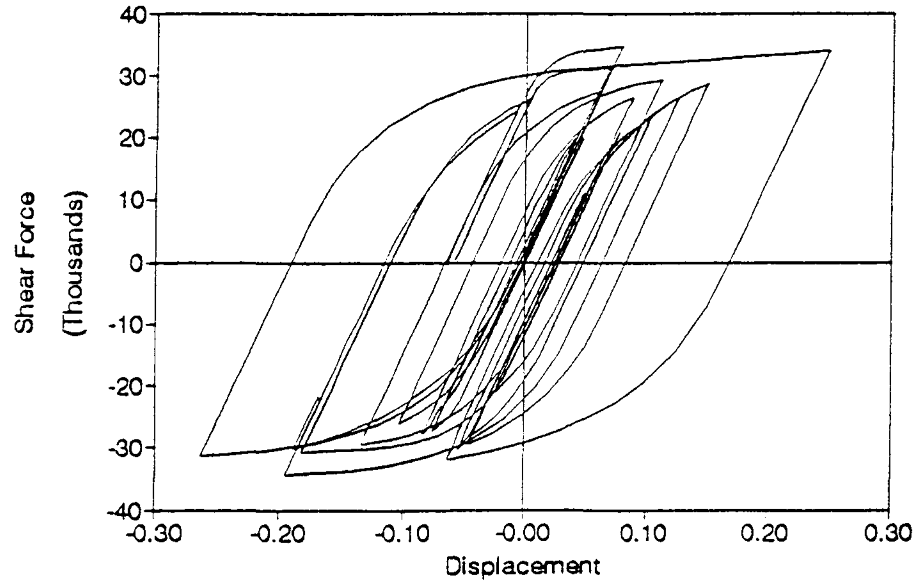

FIGURE 3-62 The Relation of Force and Displacement of TPEA at 5th Floor When the Structure is Subjected to Taft (ERSF=4) Ground Motion

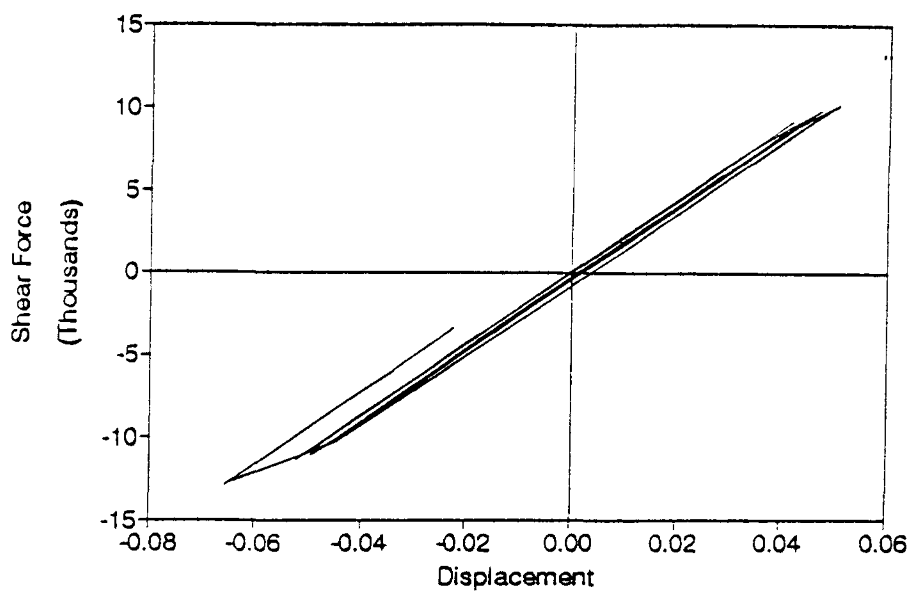

FIGURE 3-63 The Relation of Force and Displacement of TPEA at 10th Floor When the Structure is Subjected to Taft (ERSF=4) Ground Motion

SECTION 4
A Combination of Two Energy-Absorbing Devices

4.1 Introduction

Properly designed TPEA devices mounted on a building can be used to effectively control the inelastic response of the building frame. Test results [49,66] have shown that TPEA devices can sustain an extremely large number of yielding reversals and accumulate a large amount of plastic deformations without any sign of degradation. Furthermore, the TPEA, unlike viscoelastic dampers and fluid viscous dampers which are velocity dependent devices, can reduce the structural response significantly once earthquakes occur. However, the major disadvantage of the TPEA is that this device, unlike viscoelastic dampers which have found numerous applications in control wind vibration, has little effect on structural acceleration induced by wind loads. Also, under minor earthquakes, TPEA devices behave more as stiffeners rather than as dampers. Therefore, TPEA may not necessarily be useful for minor earthquakes. On the other hand, viscoelastic dampers dissipate energy even under very small arbitrary loading.

Properly designed viscoelastic dampers and fluid viscous dampers both can be used as supplemental damping devices to reduce the amplitude of vibration for controlling the response of buildings during earthquakes. However, a drawback for adopting these devices as energy-absorbing devices for seismic hazard mitigation is that the structural response cannot be significantly reduced during the early stages of earthquakes and the safe-failure mechanism cannot be provided by the devices. A combination of TPEA and viscoelastic dampers and a combination of TPEA and fluid viscous dampers may be viewed as two new alternative designs to overcome the shortcomings of each device and to improve the performance of the energy-absorbing devices for reducing the effects of both earthquake and wind loads. Such combined devices will not only provide a strong safe-failure mechanism, but also can sustain a wide range of arbitrary loading from minor earthquakes to severe ground motions and/or wind loads.

Although there are obvious commonalities between wind and earthquake forces in that both introduce lateral forces over the whole building and its components, there are still some important differences [55]. The main design concern for seismic hazard mitigation is safety while the main design concern for wind loads is comfort. Therefore, controlling displacement is more important in earthquake-resistant design while controlling acceleration is more important in wind-resistant design. Wind forces are not as random in their effects upon buildings as are earthquakes. The wind forces act primary on building surfaces. They are applied normal to the surfaces while earthquakes generate both horizontal and vertical forces, but those applied horizontally are the principal concern in most cases. Earthquake forces are inertial, essentially the product of the building mass multiplied by acceleration. Thus, seismic forces are developed in each component of a building. The total shear force (base shear) is the accumulation of these individual forces. As a result, the applied seismic forces and the forces to be resisted increase with the weight of the building. Thus, weight is a detriment in seismic design [55].

On the contrary, weight is a favorable factor against wind loads. A heavy roof, properly connected to the rest of the structure, is beneficial against wind, but will be a liability for earthquakes [55]. Because of the nature of earthquake forces, a heavy building is particularly vulnerable. To overcome the conflicts involved in designs for both wind load and earthquakes, a combination of viscoelastic dampers and TPEA on a building and a combination of fluid dampers and TPEA are studied. According to the numerical results, these new alternative devices are able to compensate for each other's shortcomings and seem to be promising energy-absorbing devices to mitigate the hazard of earthquakes and windloads. As shown in Figures 4-1 and 4-2, the combined devices of TPEA and viscoelastic dampers and the combined devices of TPEA and fluid dampers are mounted on each floor and supported by Chevron braces.

4.2 Numerical Study of a Combination of TPEA and Viscoelastic Dampers on the High-Rise Building

Tables. 4-I, 4-II, and 4-III show the symbols for the locations of viscoelastic dampers in this study. According to a previous study, the B/D ratio has little influence on the reduction of structural response during earthquakes. Therefore, B/D is selected as 2, and SR ratios from 1 to 6 are selected in this study. The relationships between the properties (the thickness and the area) of viscoelastic dampers and their developed strain are shown in Figures 4-3 to 4-5 when the structure is subjected to three selected ground motions. They show that the combined devices of the TPEA and viscoelastic dampers have the best performance in all cases. They also indicate that combining the TPEA and viscoelastic dampers will prevent the viscoelastic dampers from developing strains over their performance limit, 0.3. It can be seen that some properties of the viscoelastic damper, such as the thickness and the area, can be reduced significantly due to the addition of the TPEA to the structure. Originally, the cases of VE-only (a5t3) and VE-only (a2t1) developed strain measurement of more than 0.3 which makes the viscoelastic dampers fail to properly reduce the structural response. Adding the TPEA to the structure with viscoelastic dampers prevents the dampers from developing strain over 0.3. This outcome is particularly obvious when stronger ground motions, such as the San Fernando earthquake and the Taft earthquake (ERSF=4), are imposed on the structure.

The behavior of the structure equipped with TPEA (SR=4, B/D=2) and viscoelastic dampers is compared to the structure without any energy-absorbing device while it was subjected to ten different earthquake peak accelerations from 100 Gal to 1000 Gal of the San Fernando ground motion. Figures 4-6 to 4-11 illustrate that the TPEA is still in the elastic range while the viscoelastic dampers absorb energy when the structure is subjected to the peak accelerations of 100 Gal, 200 Gal, and 300 Gal of the San Fernando ground motion. This means that the viscoelastic dampers would provide damping to the structure to absorb energy while the TPEA operates elastically during the smaller magnitudes of earthquake ground motion. Similarly, when the structure is subjected to wind loads, the viscoelastic dampers would be able to reduce the wind sway since the TPEA has little capacity to properly resist wind loads. By combining the viscoelastic dampers and TPEA, both earthquake and wind loads can be resisted. When the structure is subjected to the peak accelerations of 800 Gal and 1000 Gal of the San fernando ground motion, both TPEA and viscoelastic dampers can dissipate seismically induced energy, but the TPEA is more effective. Figures 4-12 to 4-15 show that TPEA absorb more energy than viscoelastic dampers when both devices are jointly used as energy-absorbing devices.

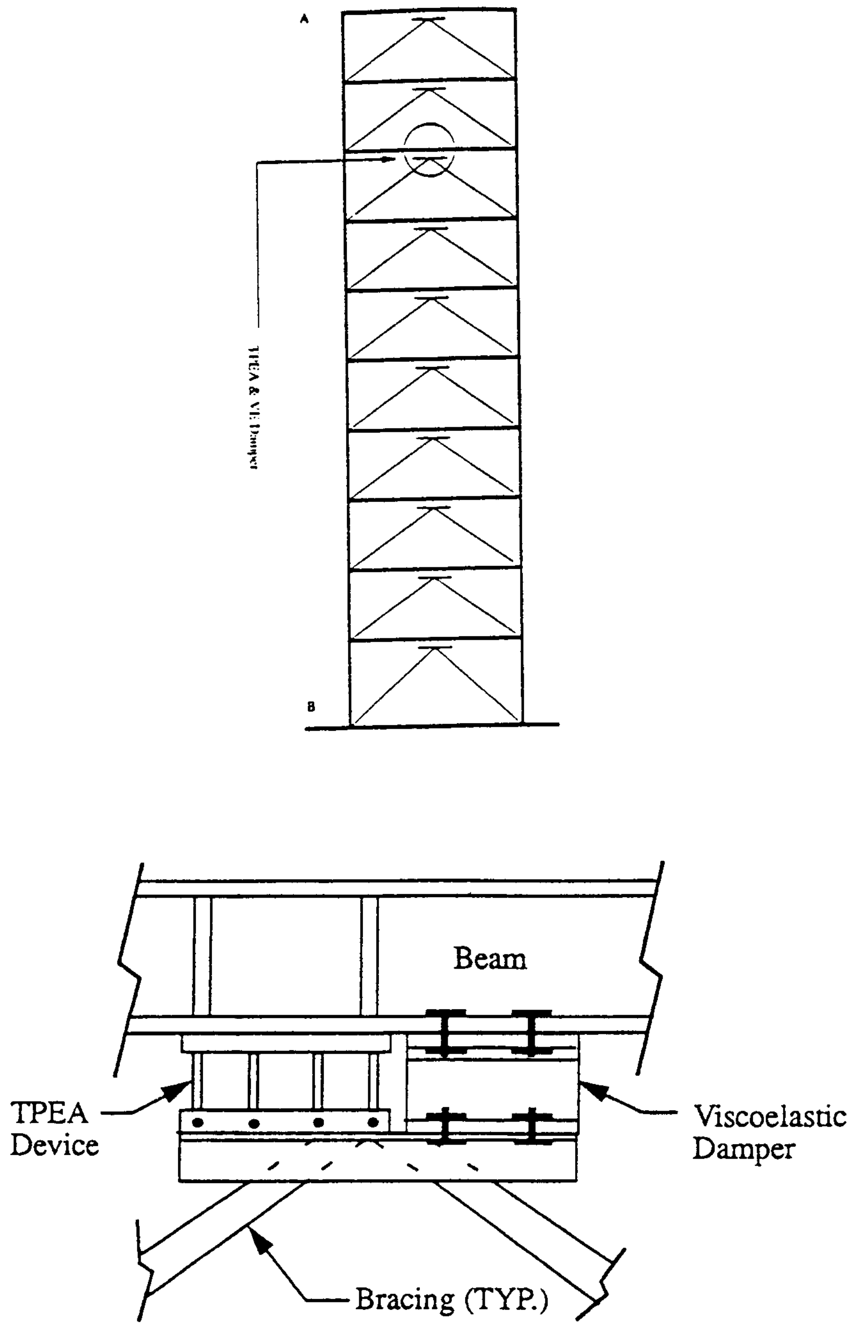

FIGURE 4-1 A Story Building Equipped with TPEA and Viscoelastic Dampers

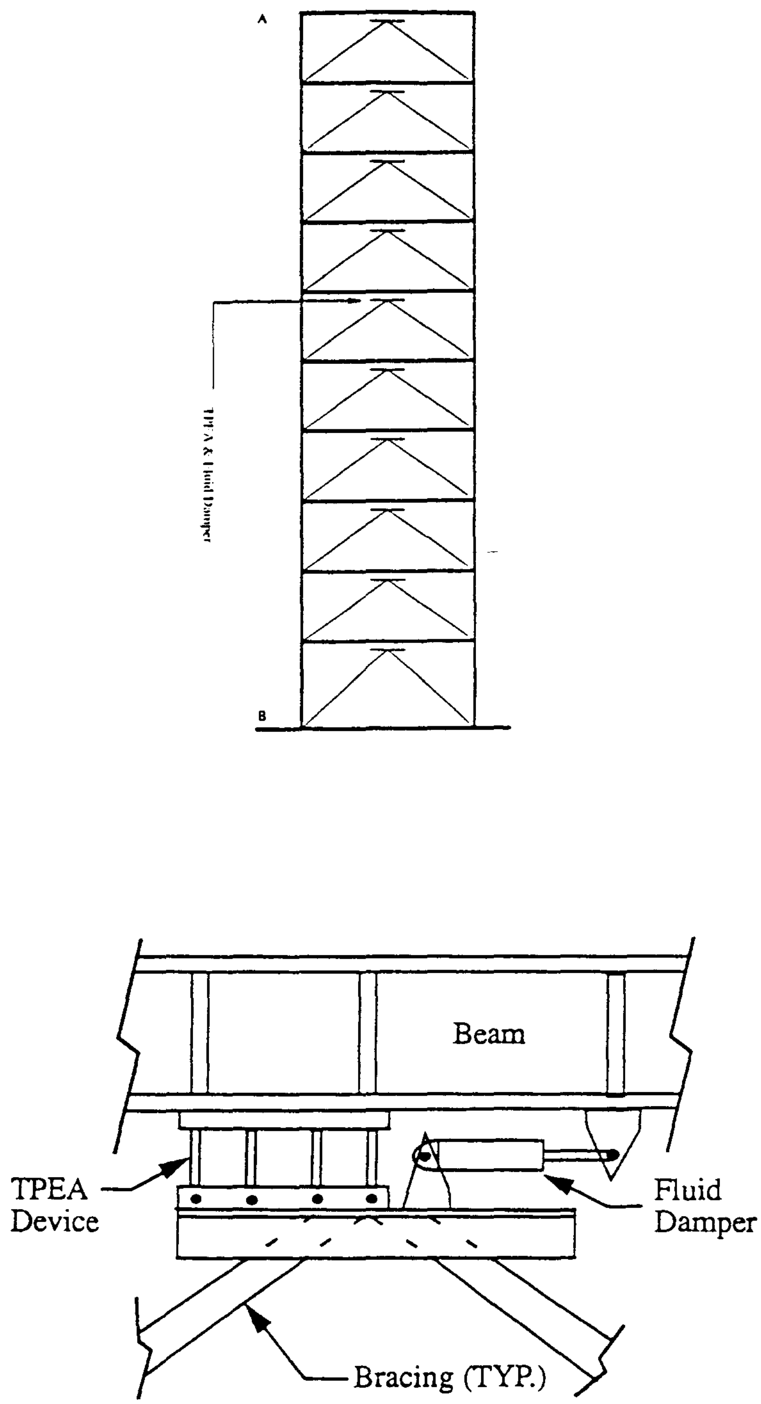

FIGURE 4-2 A 10-Story Building Equipped with TPEA and Fluid Viscous Dampers

TABLE 4-I The Symbols of the Location of VE Dampers

Symbols	Explanations
VE10	Each floor was mounted with a VE damper
2VE5(1)	Floors 1,2,3,4,5 were mounted with two VE dampers
2VE5(2)	Floors 1,3,5,7,9 were mounted with two VE dampers
VE1	Floor 1 was mounted with a VE damper

TABLE 4-II The Symbols of Area of VE Dampers

Symbols	Area 1(in^2)	Area 2(in^2)
a1	120	72
a2	150	90
a3	180	108
a4	210	126
a5	280	168
a6	310	186

TABLE 4-III The Symbols of Thickness of VE Dampers

Symbols	Thickness (in)
t1	1.00
t2	1.75
t3	1.30
t4	1.38

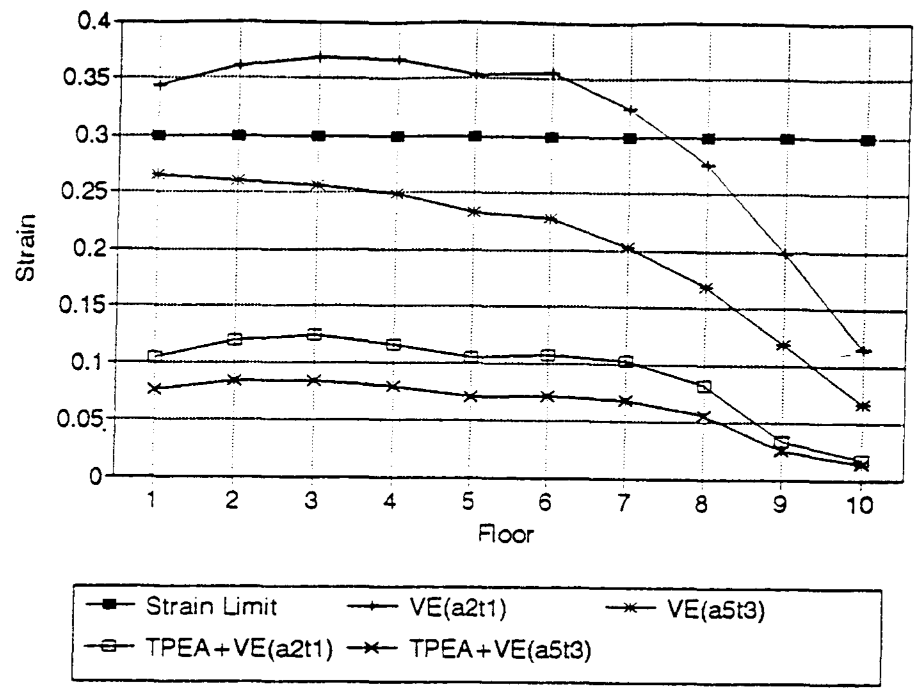

FIGURE 4-3 Comparison of Strain at Each Floor While the Structure is Subjected to El Centro Ground Motion

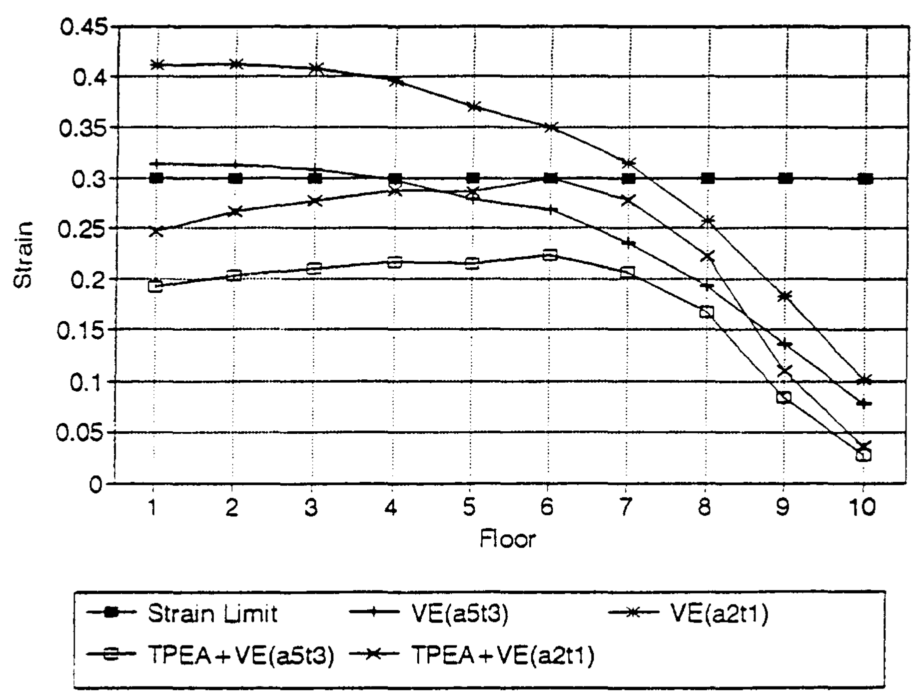

FIGURE 4-4 Comparison of Strain at Each Floor While the Structure is Subjected to San Fernando Ground Motion

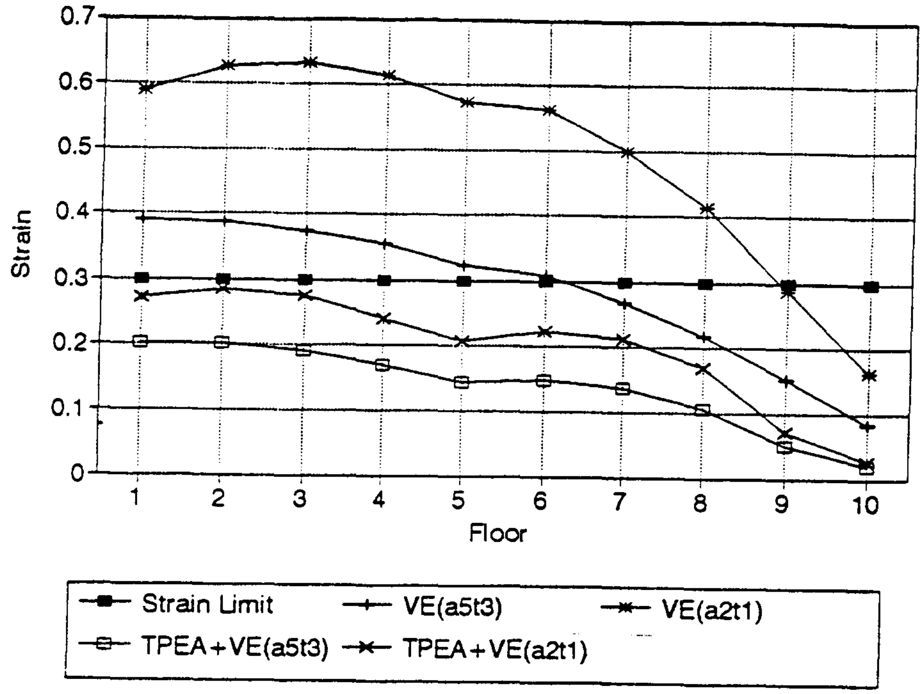

FIGURE 4-5 Comparison of Strain at Each Floor While the Structure is Subjected to Taft (ERSF=4) Ground Motion

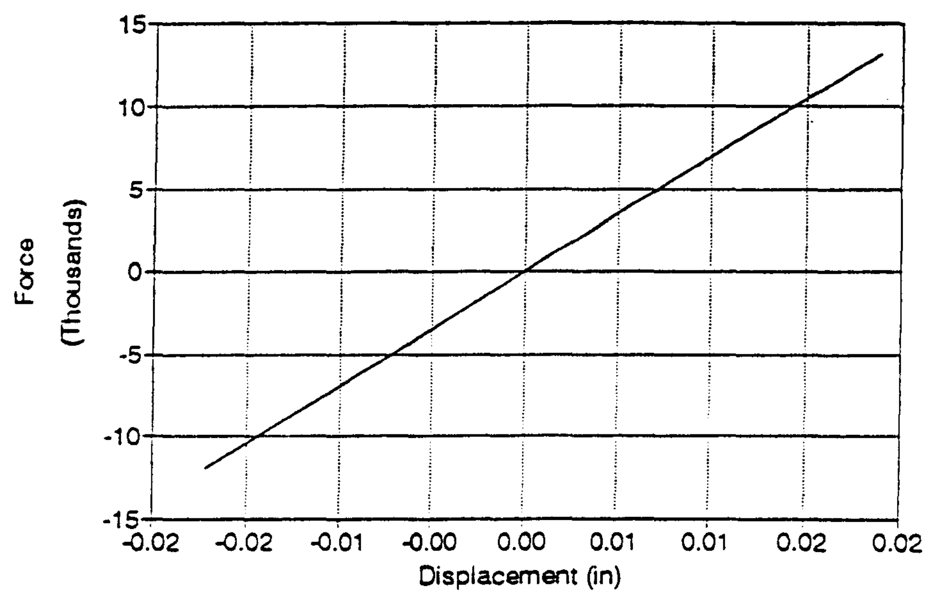

FIGURE 4-6 The Force-Displacement Relation of TPEA While the Structure is Subject to 100 Gal of San Fernando Ground Motion

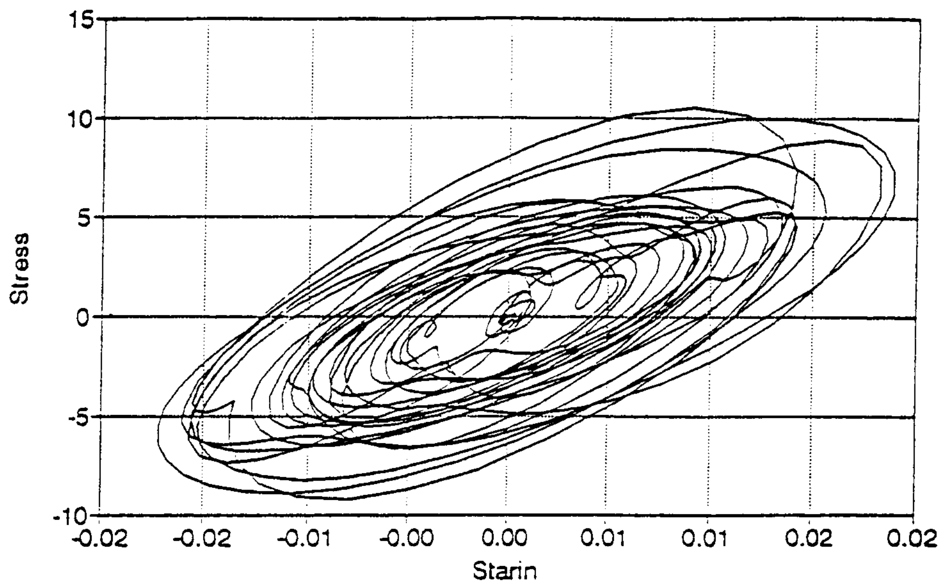

FIGURE 4-7 The Force-Displacement Relation of VE Dampers While the Structure is Subjected to 100 Gal of San Fernando Ground Motion

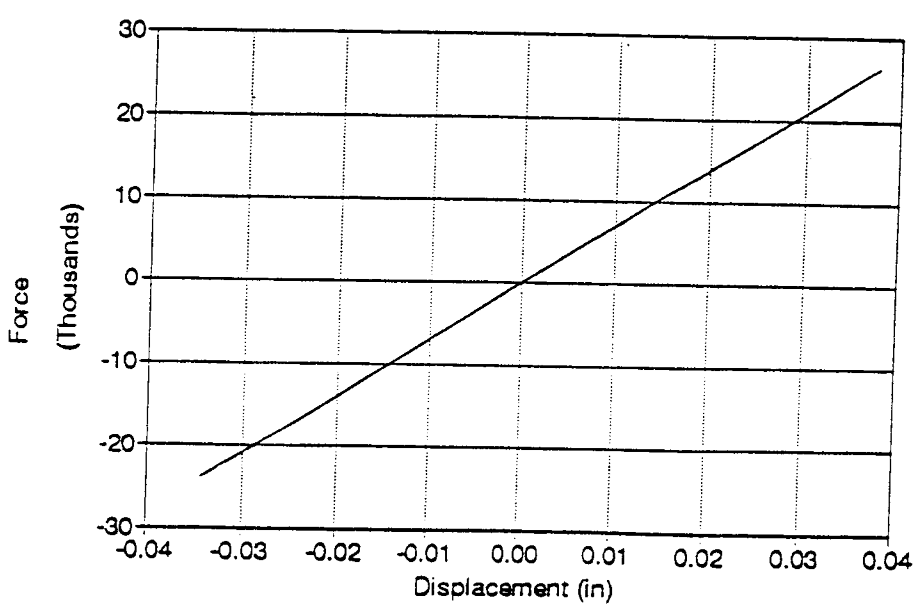

FIGURE 4-8 The Force-Displacement Relation of TPEA While the Structure is Subjected to 200 Gal of San Fernando Ground Motion

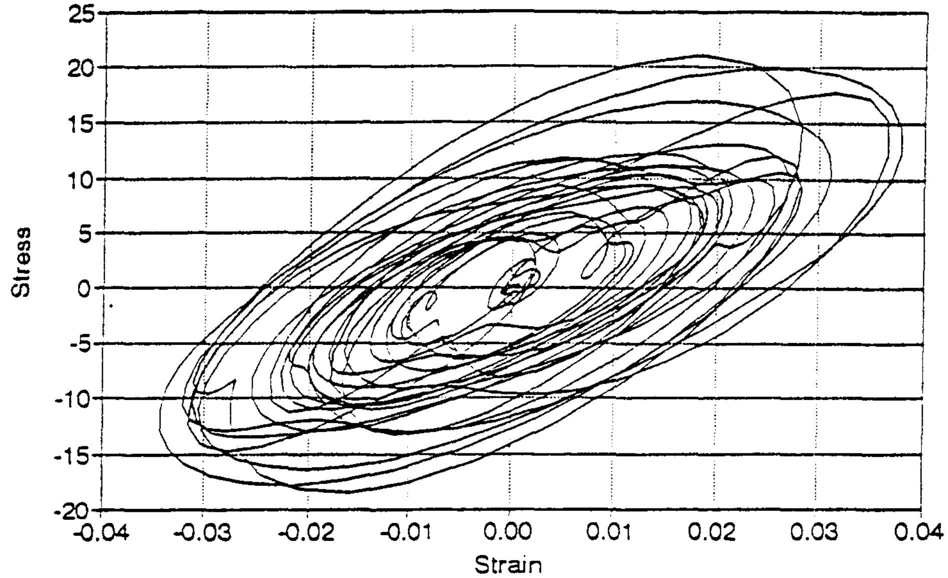

FIGURE 4-9 The Force-Displacement Relation of VE Dampers While the Structure is Subjected to 200 Gal of San Fernando Ground Motion

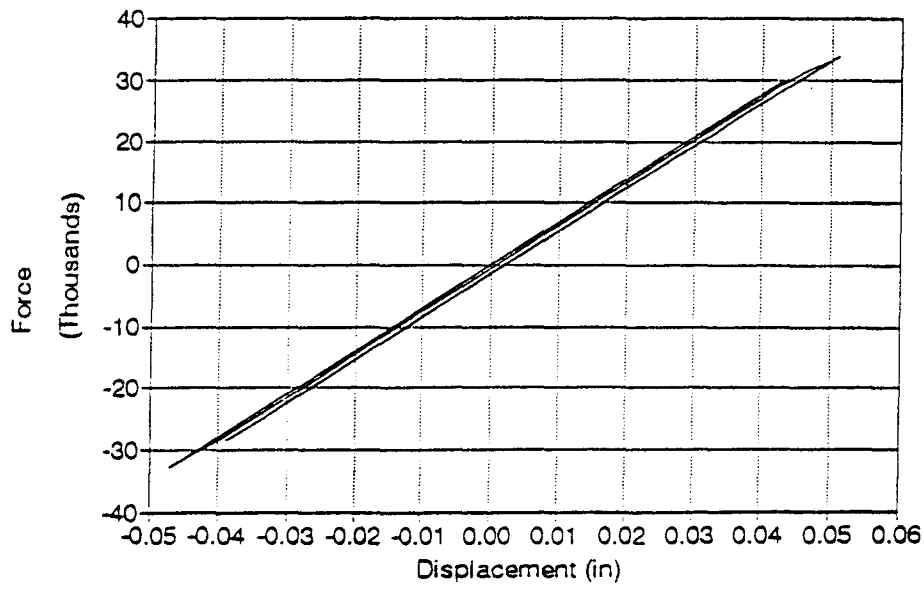

FIGURE 4-10 The Force-Displacement Relation of TPEA While the Structure is Subjected to 300 Gal of San Fernando Ground Motion

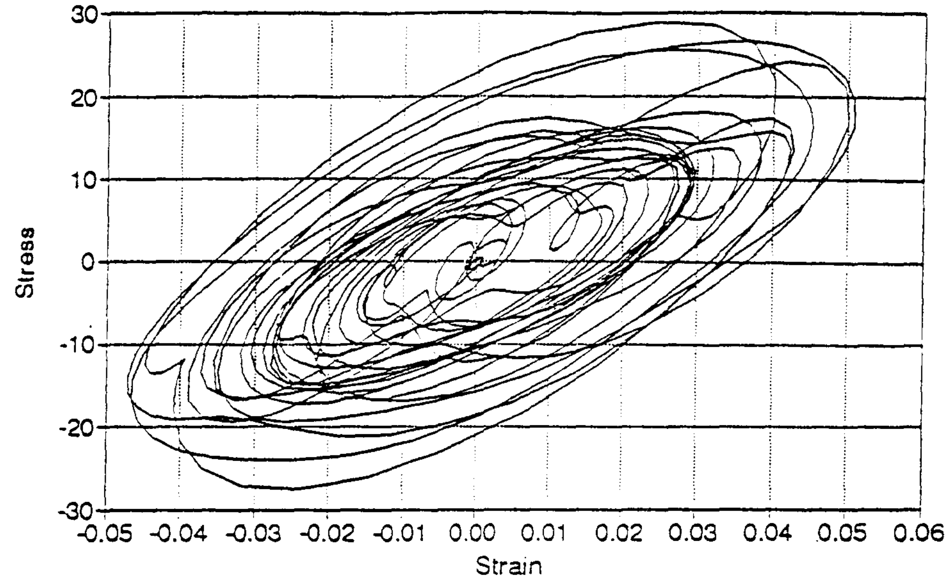

FIGURE 4-11 The Force-Displacement Relation of VE Dampers While the Structure is Subjected to 300 Gal of San Fernando Ground Motion

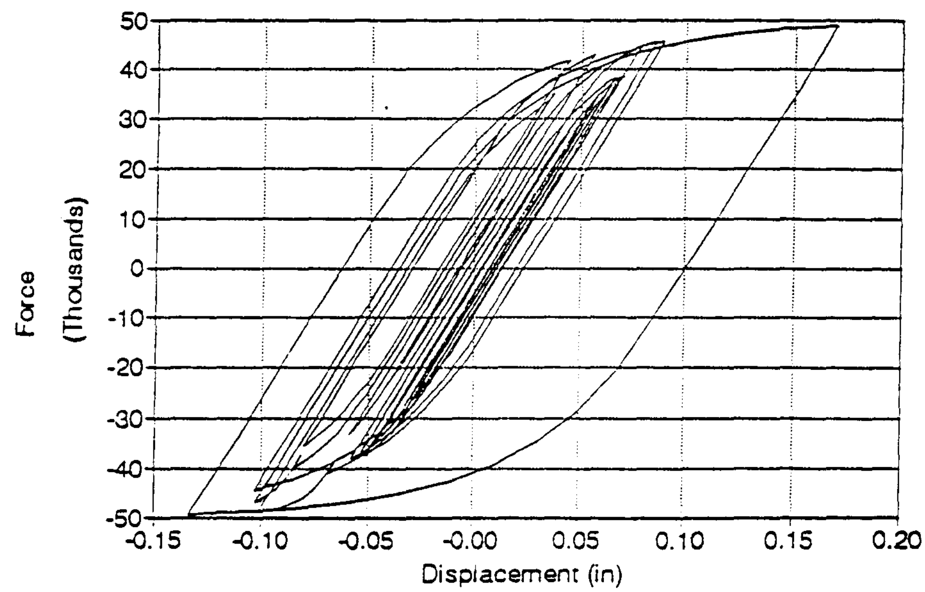

FIGURE 4-12 The Force-Displacement Relation of TPEA While the Structure is Subjected to 800 Gal of San Fernando Ground Motion

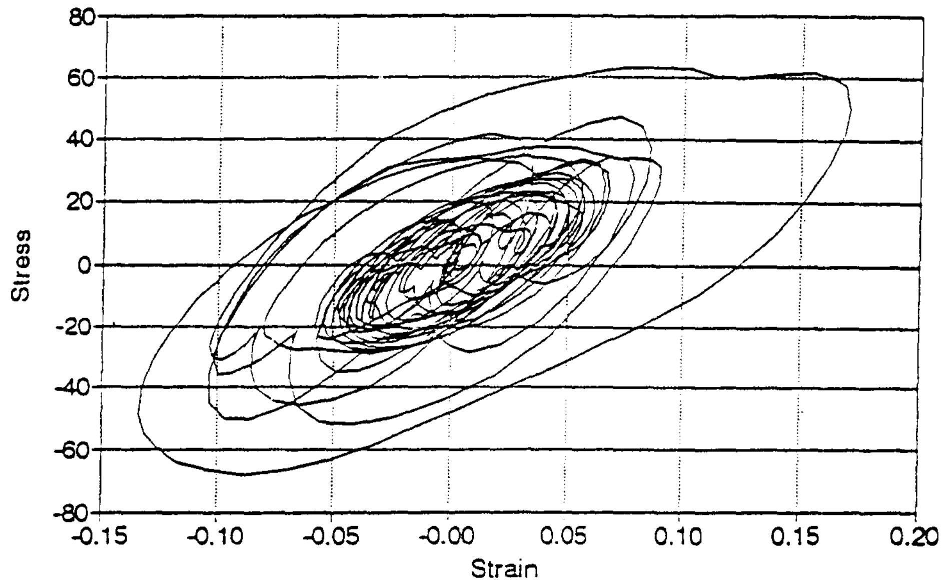

FIGURE 4-13 The Force-Displacement Relation of VE Dampers While the Structure is Subjected to 800 Gal of San Fernando Ground Motion

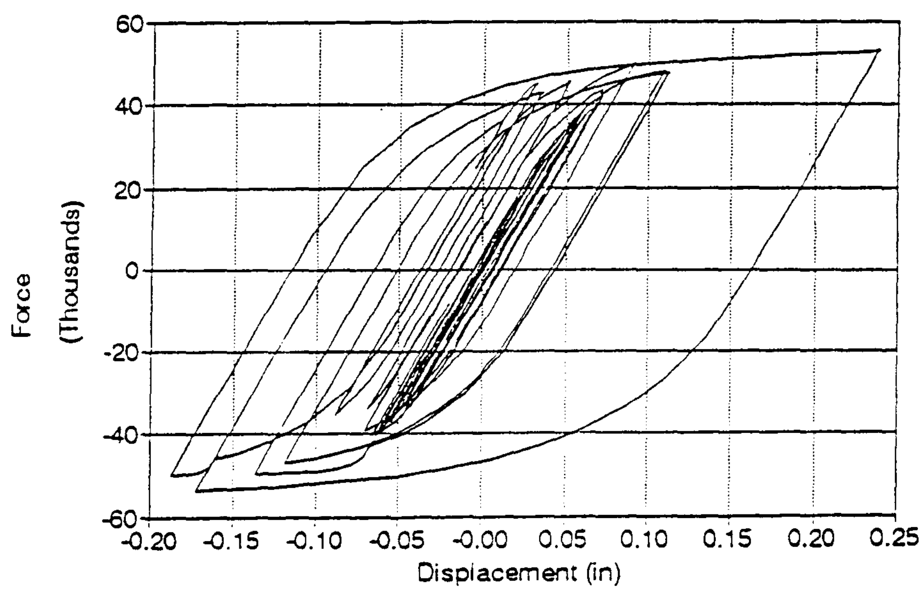

FIGURE 4-14 The Force-Displacement Relation of TPEA While the Structure is Subjected to 1000 Gal of San Fernando Ground Motion

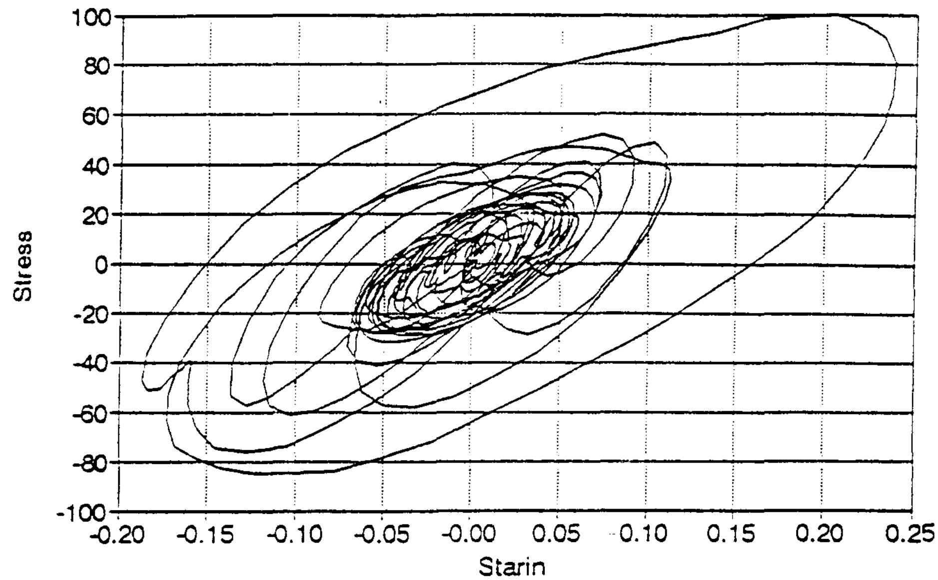

FIGURE 4-15 The Force-Displacement Relation of VE Dampers While the Structure is Subjected to 1000 Gal of San Fernando Ground Motion

The developed strain measurements of the VE dampers were compared when the structure was subjected to ten different earthquake acceleration from 100 Gal to 1000 Gal of the San Fernando ground motion. Figure 4-16 shows the strain of VE-only is over its performance limit, 0.3, when the earthquake peak acceleration is larger than 700 Gal of the San Fernando ground motion. However, it can be observed in Figure 4-16 that viscoelastic dampers can be designed to prevent the development of strain over 0.3 with a combination of TPEA and viscoelastic dampers on the structure when the peak acceleration is from 800 Gal to 1000 Gal of the San Fernando earthquake. Figure 4-17 shows that the combined devices have the smallest roof displacement, the TPEA-only ranks second, and the VE-only ranks third. The structure with viscoelastic dampers only functions properly to reduce roof displacement from 100 Gal to 700 Gal, but it fails to reduce roof displacement when the peak acceleration is greater than 800 Gal because the dampers develop a strain measurement of more than 0.3. The structure with a combination of viscoelastic dampers and TPEA, however, has the best performance in reducing roof displacement.

Figure 4-18 shows similar results except that the structure with TPEA-only and the structure with combined devices have larger base shear forces than the structure without any energy-absorbing devices when the peak acceleration is less than 300 Gal. The reason is for this the addition of TPEA to a structure increases the structure's stiffness and the TPEA operates in an elastic range at the lower peak accelerations of the San Fernando earthquake. On the other hand, the addition of viscoelastic dampers to a structure does not generally increase the structure's stiffness.

The temperature effect on the damper's developed strain is shown in Figure 4-19. It demonstrates that for the structure with VE-only, the dampers develop a strain measurement more

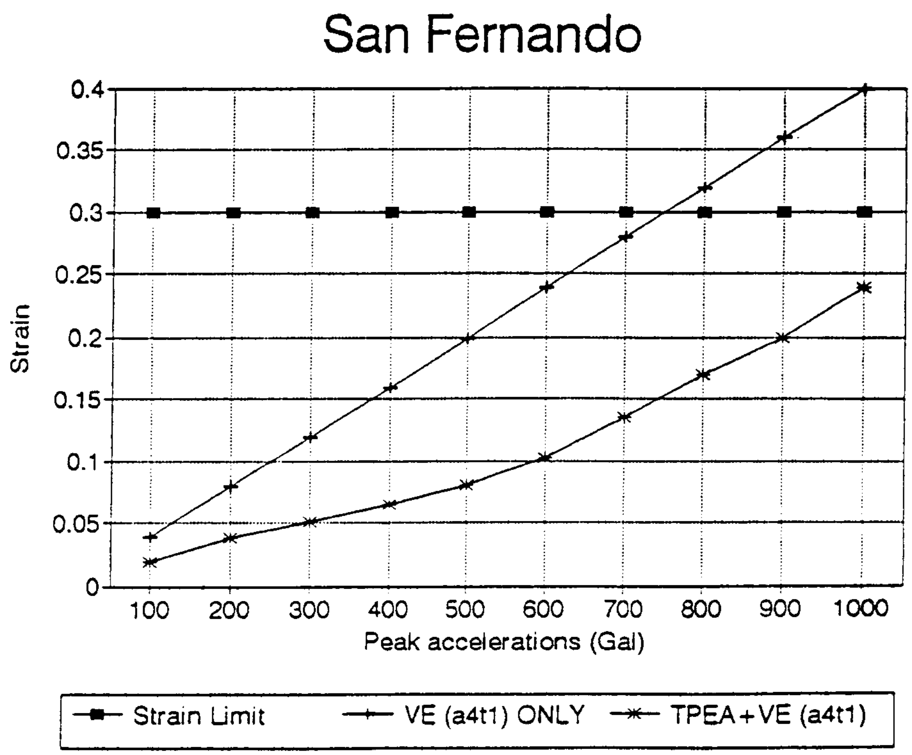

FIGURE 4-16 Comparison of Strain While the Structure is Subjected to San Fernando Ground Motion

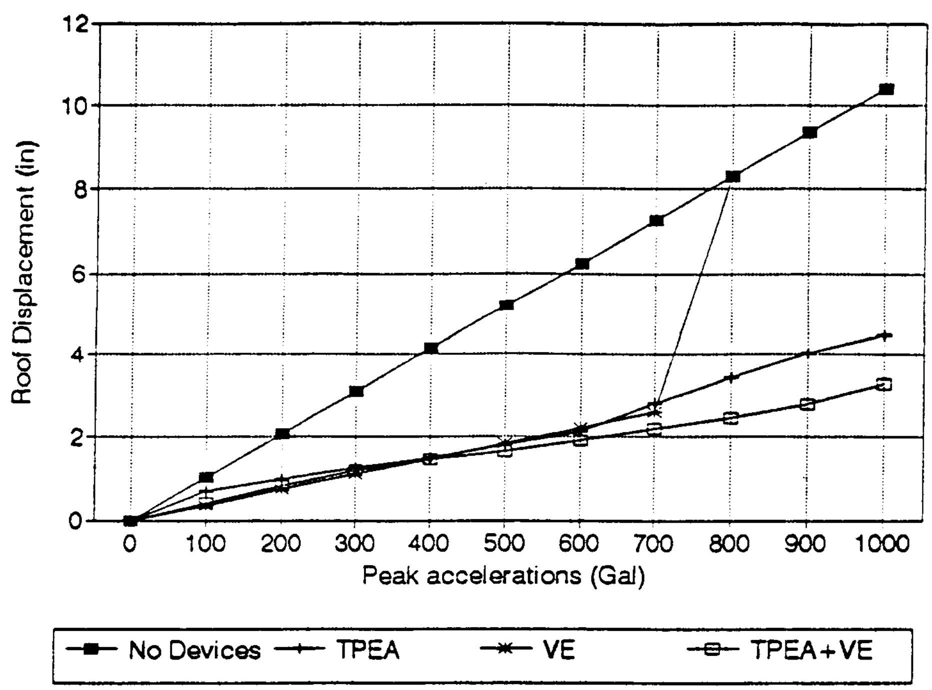

FIGURE 4-17 Comparison of roof displacement While the Structure is Subjected to San Fernando Ground Motion

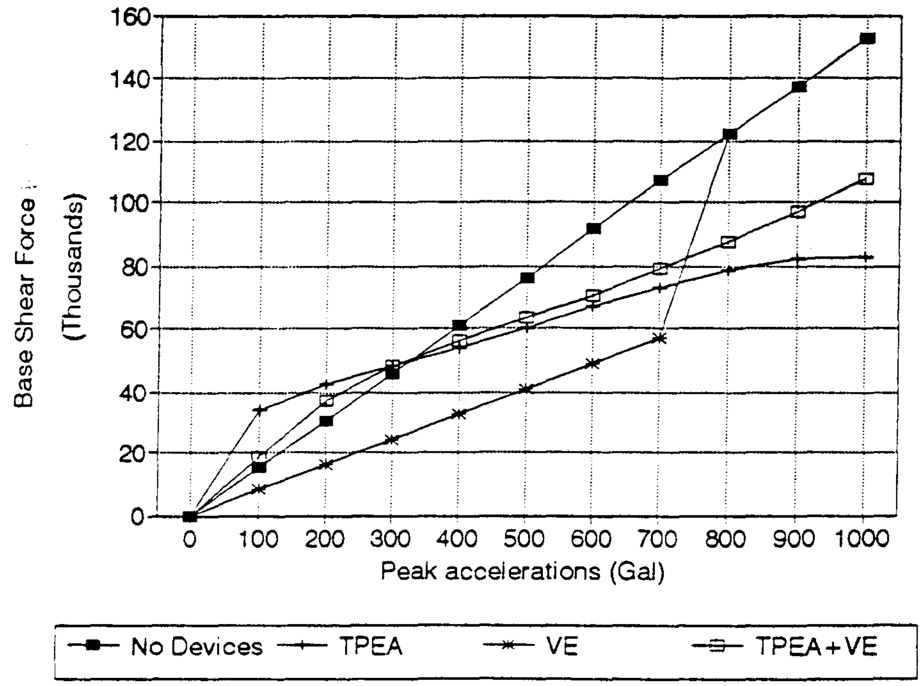

FIGURE 4-18 Comparison of Base Shear Force While the Structure is Subjected to San Fernando Ground Motion

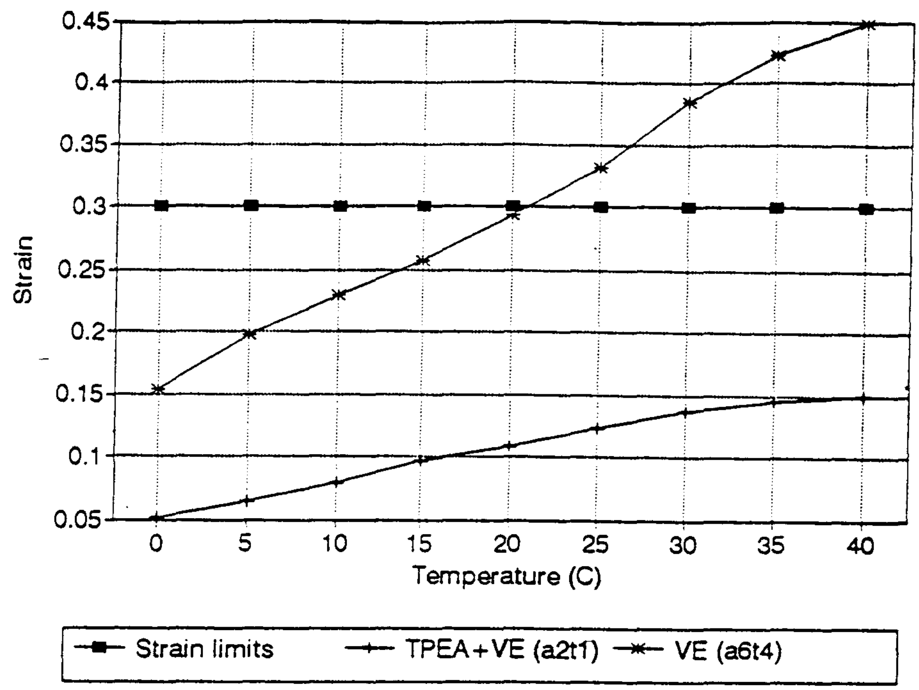

FIGURE 4-19 The Relations of Strain and Temperature While the Structure is Subjected to San Fernando Ground Motion

than their performance limit, 0.3, when the ambient temperature is greater than 20 ^{o}C while the viscoelastic dampers on the structure with combined devices still perform properly from 0^{o}C to 40^{o}C. The temperature effect on the roof displacement is also observed when the structure was equipped with TPEA and VE dampers together. Figure 4-20 shows that the roof displacement has been reduced significantly; although, viscoelastic dampers perform better at lower temperatures. The influence of the temperature becomes very insignificant when TPEA and viscoelastic dampers are mounted on the structure together.

The comparison of the response (roof displacement and base shear force) of the structure, with TPEA-only, with VE-only, with combined devices of TPEA+VE, and without dampers, on each floor were made when the structure was subjected to the three selected ground motions. Figures 4-21 to 4-26 show the outstanding performance of the combination of TPEA and viscoelastic dampers mounted on each floor of a structure. The structure with viscoelastic dampers has a satisfactory performance, but is the worst among the four selected cases. The combined devices perform best of all. Figure 4-21 illustrates that the three curves of the structure with TPEA-only, TPEA+VE (a5t3), and TPEA+VE (a2t1), are almost indistinguishable. It can be said that TPEA is the governing device when TPEA and VE dampers are jointly used. In Figure 4-22, we see that the structure with TPEA-only has the smallest base shear force; the structure without any devices has the largest; while the structure with VE-only has the second largest base shear. Figures 4-23 to 4-26 show similar results when the structure was subjected the stronger earthquake ground motions.

The SR effects on the roof displacement and base shear force are observed when the structure without dampers with TPEA-only, and with TPEA+VE is subjected to selected ground motions. As shown in Figures 4-27 to 4-30, the structure with the combination of TPEA and viscoelastic dampers has the best results. The optimal selection of SR ratio is 4 in all cases. As shown in Figures 4-27 and 4-29, all the curves have a similar pattern in reducing floor displacement. Therefore, it may be assumed that the TPEA is the governing device when used jointly with viscoelastic dampers. Figure 4-29 shows that SR=1 reduces more than 50% of the roof displacement compared to the structure without any devices. The curves begin to decay slowly when SR is greater than 2. Figure 4-30 has the same consistency except SR=2 has the smallest base shear force. Then the curves begin to move upward slowly. As shown in Figures 4-28 and 4-30, the structure with combined devices induced stronger base shear forces than the structure with TPEA-only.

The time-history responses (roof displacement, column shear force at column B, and base shear force) of the structure equipped with jointly devices and without devices are shown in Figs 4-31 to 4-39 when the structure was subjected to selected ground motions. Figures 4-31, 4-34, and 4-37 show that the roof displacement is reduced greatly overall and also is reduced once the earthquake occurs. In Figure 4-31, the structure with the combined devices generates 22 peaks of cycles within 10 seconds while the structure without any devices generates 12 peaks. The structure's natural frequency is changed due to the added TPEA and VE devices. Figures 4-32, 4-35, and 4-38 illustrate that the column takes only a very small portion of the base shear force which prevents the main load-carrying members from being damaged and lessens the energy dissipation demands on those members. Figures 4-33, 4-36, and 4-39 indicate that the base shear force is reduced overall, although the base shear force is not significantly reduced in the early stage of the

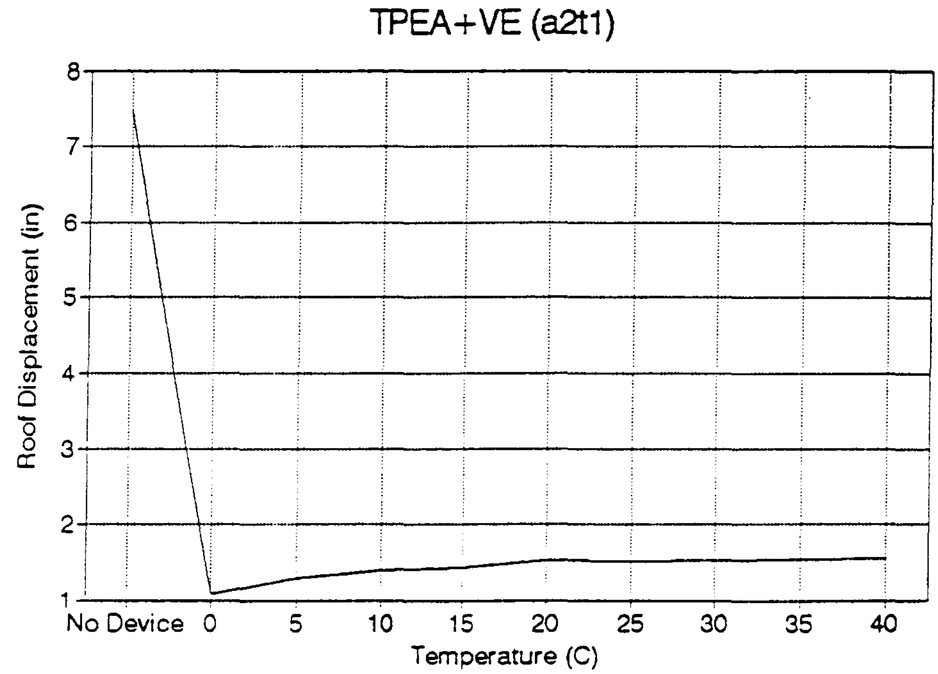

FIGURE 4-20 The Relations of Roof Displacement and Temperature While the Structure is Subjected to San Fernando Ground Motion

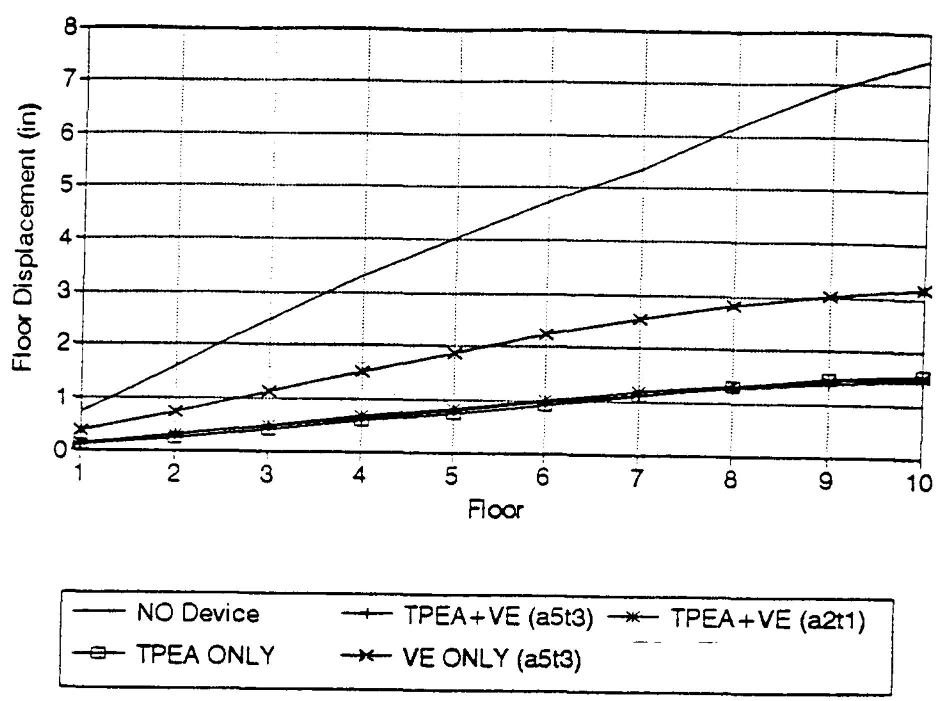

FIGURE 4-21 The Roof Displacement at Each Floor While the Structure is Subjected to El Centro Ground Motion

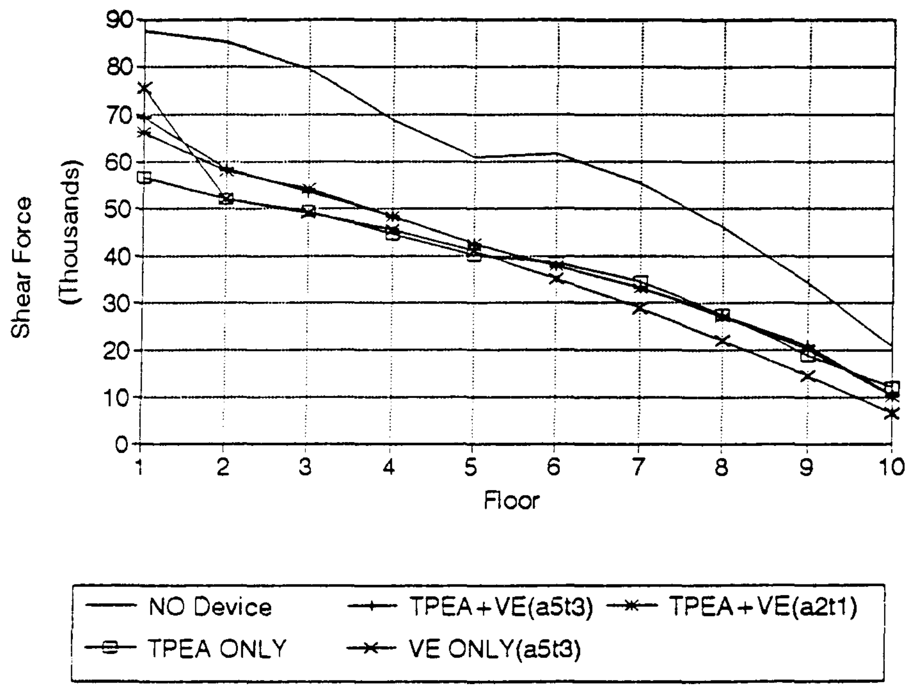

FIGURE 4-22 The Base Shear Force Base Shear Force at each floor While the Structure is Subjected to El Centro Ground Motion

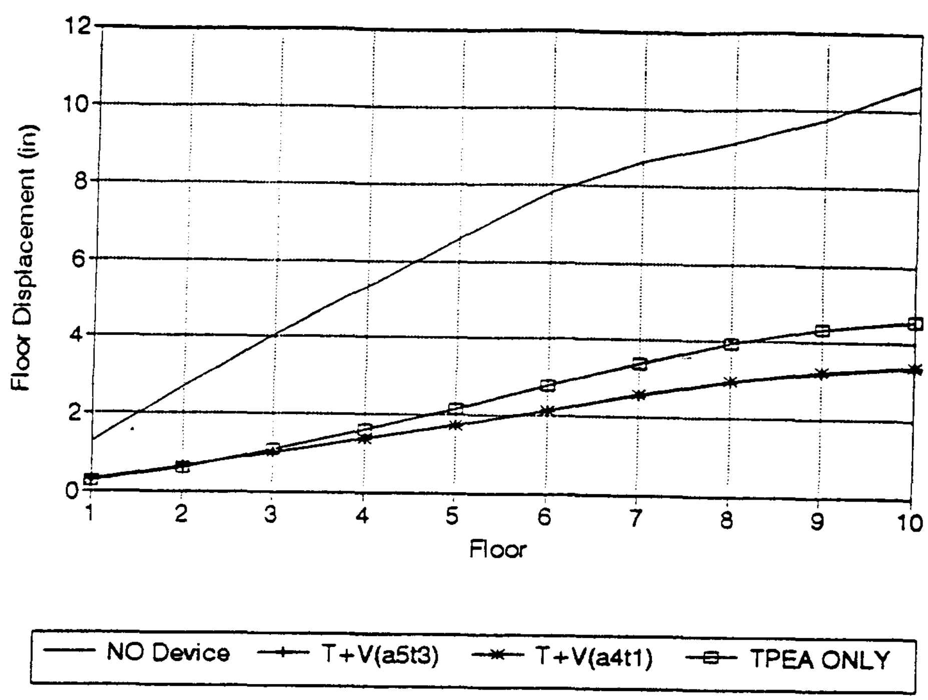

FIGURE 4-23 The Roof Displacement at Each Floor While the Structure is Subjected to San Fernando ground Ground Motion

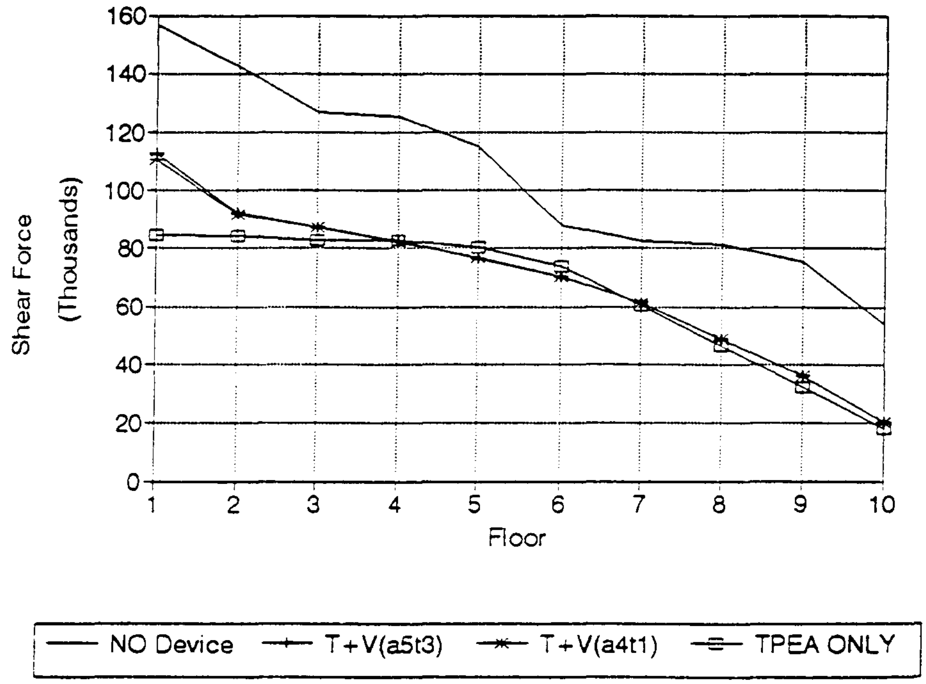

FIGURE 4-24 The Base Shear Force at Each Floor While the Structure is Subjected to San Fernando Ground Motion

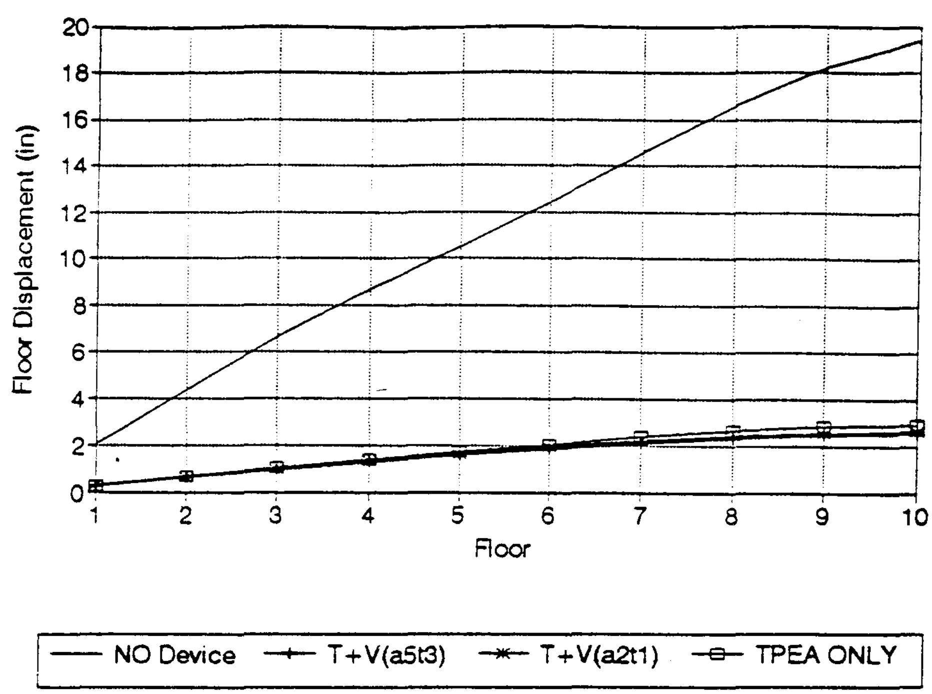

FIGURE 4-25 The roof displacement at Each Floor While the Structure is Subjected to Taft (ERSF=4) Ground Motion

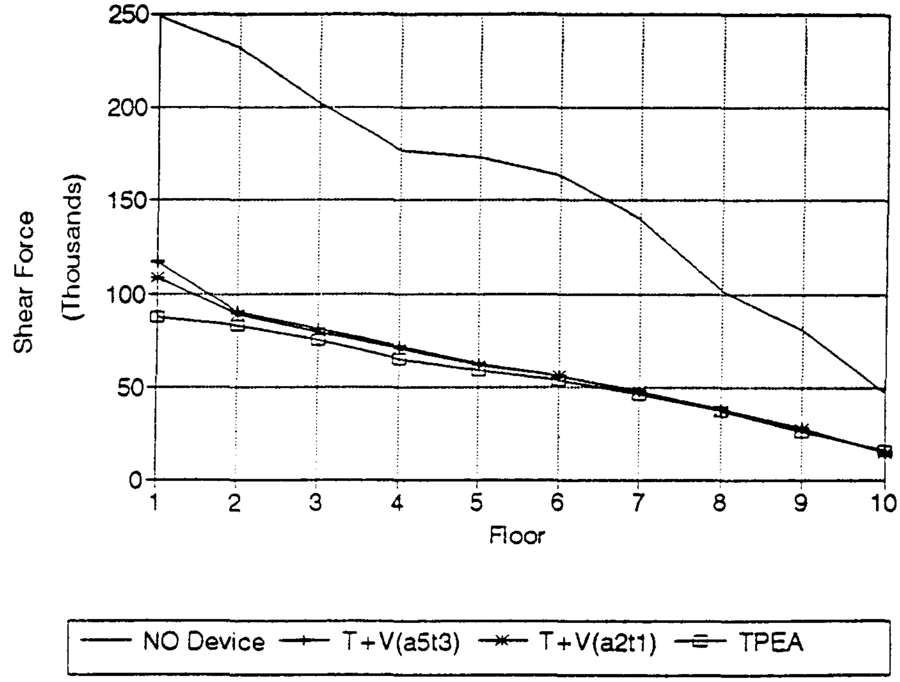

FIGURE 4-26 The Base Shear Force at Each Floor While the Structure is Subjected to Taft (ERSF=4) Ground Motion

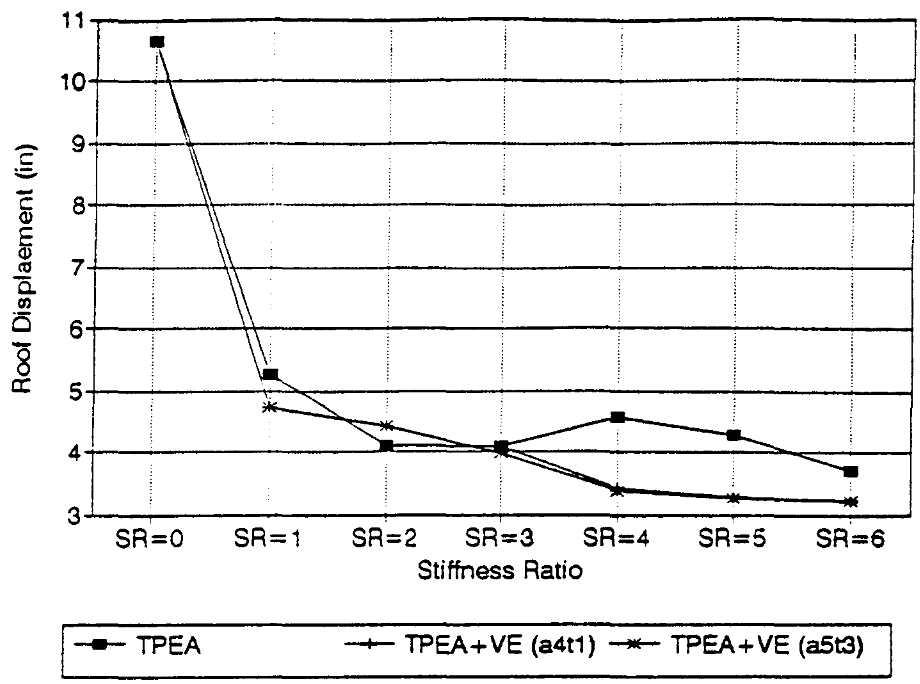

FIGURE 4-27 Comparison of SR and Roof Displacement While the Structure is Subjected to San Fernando Ground Motion

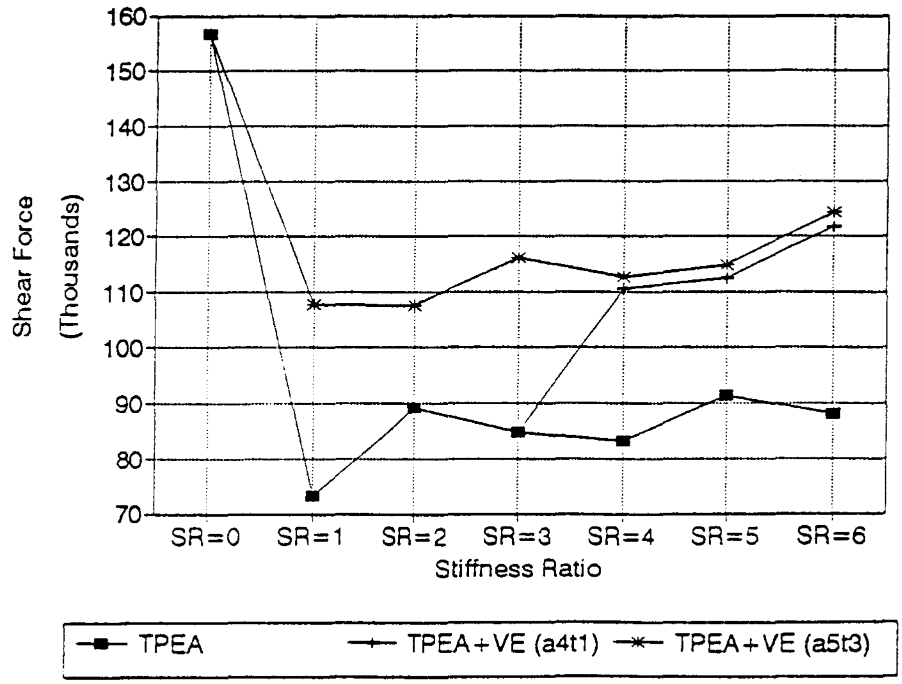

FIGURE 4-28 Comparison of SR and Base Shear Force While the Structure is Subjected to San Fernando Ground Motion

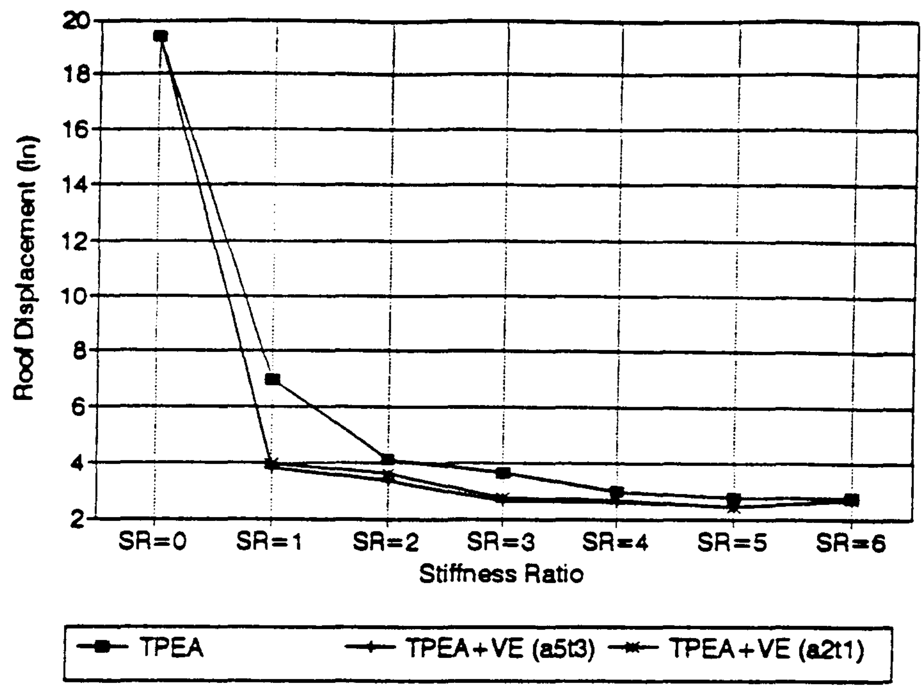

FIGURE 4-29 Comparison of SR and Roof Displacement While the Structure is Subjected to Taft (ERSF=4) Ground Motion

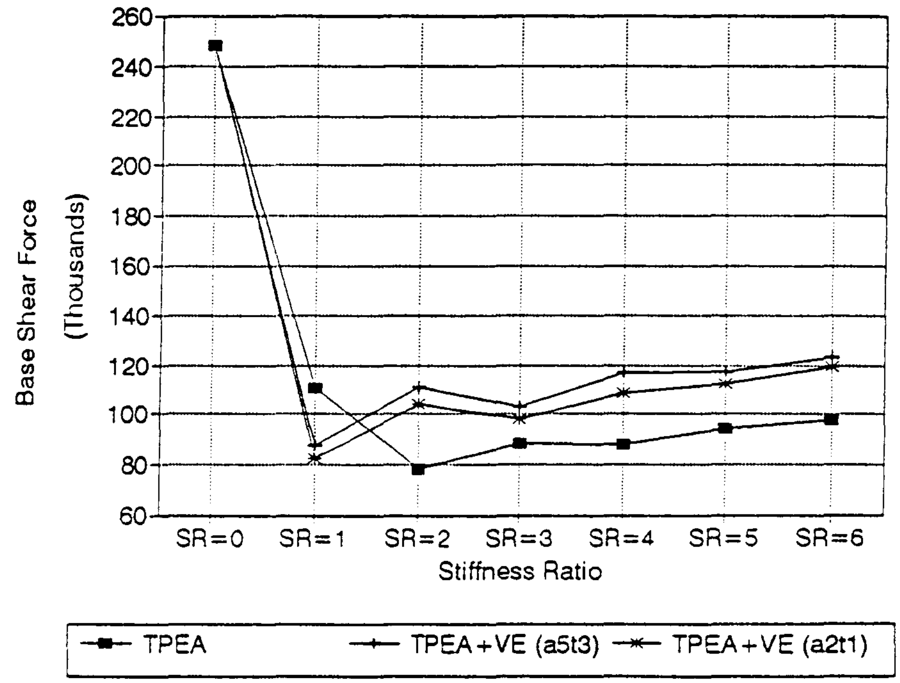

FIGURE 4-30 Comparison of SR and Base Shear Force While the Structure is Subjected to Taft (ERSF=4) Ground Motion

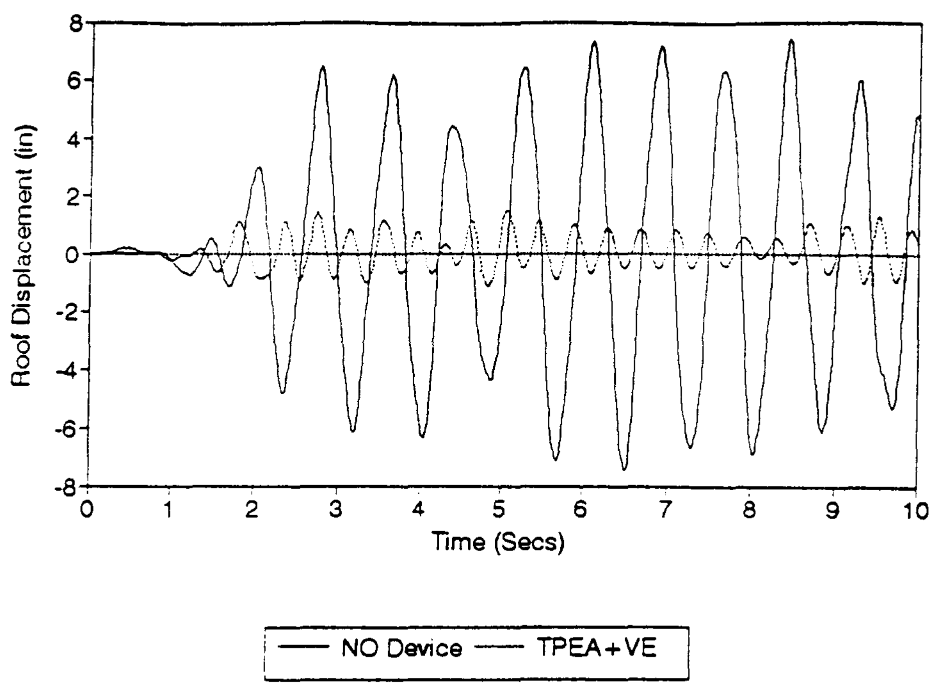

FIGURE 4-31 The Response of Roof Displacement of the structure with TPEA and VE While the Structure is Subjected to El Centro Ground Motion

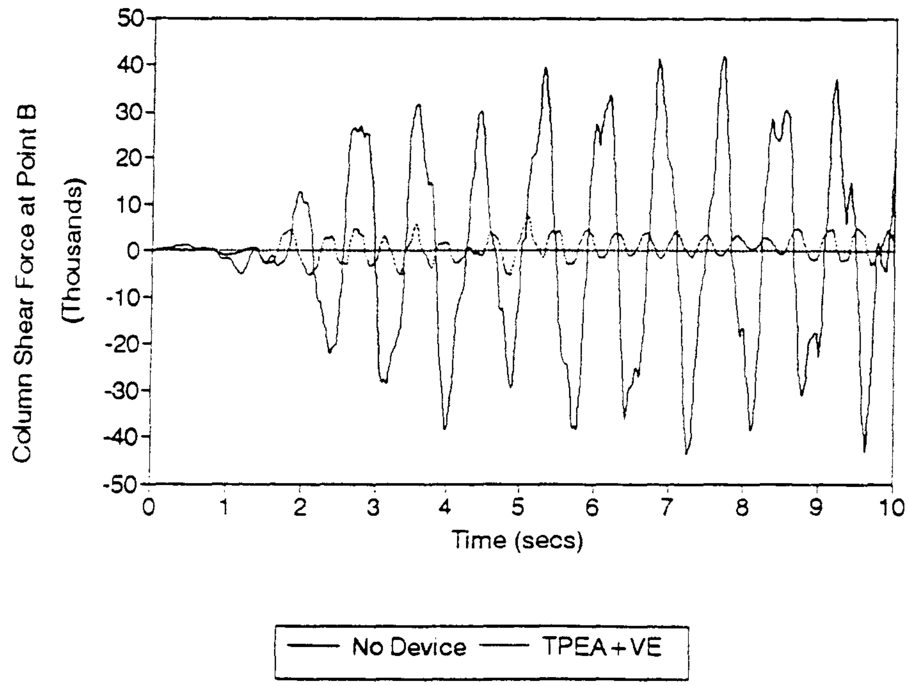

FIGURE 4-32 The Response of Column Shear Force at Point B of the structure with TPEA and VE While the Structure is Subjected to El Centro Ground Motion

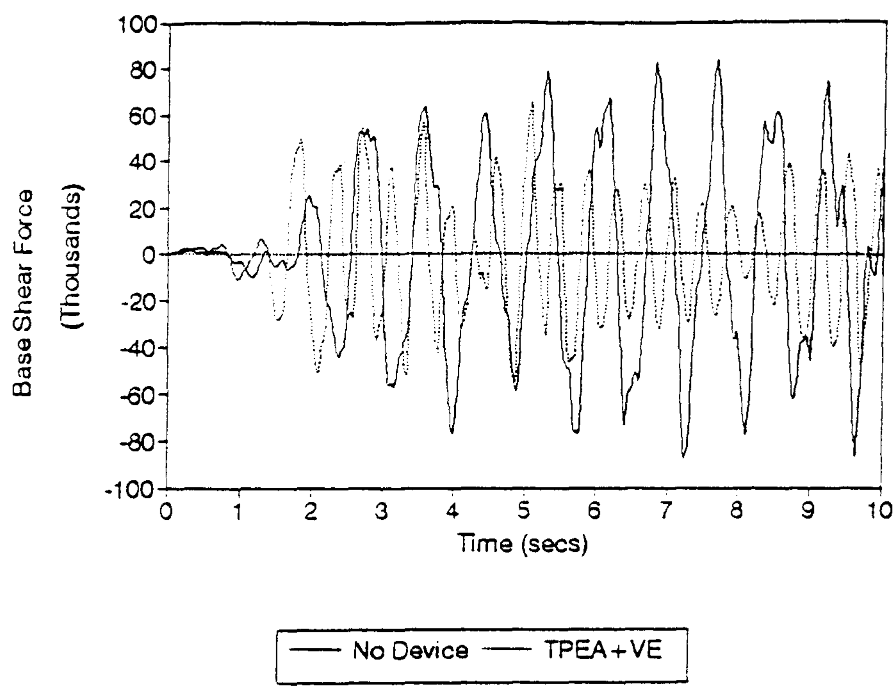

FIGURE 4-33 The Response of Base Shear Force of the structure with TPEA and VE While the Structure is Subjected to El Centro Ground Motion

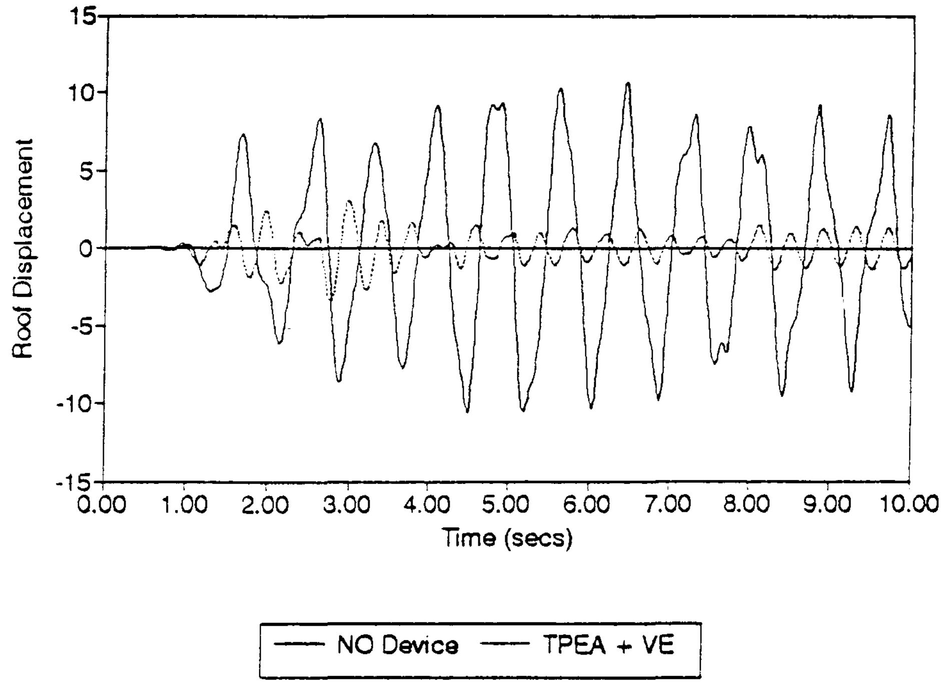

FIGURE 4-34 The Response of Roof Displacement of the structure with TPEA and VE While the Structure is Subjected to San Fernando Ground Motion

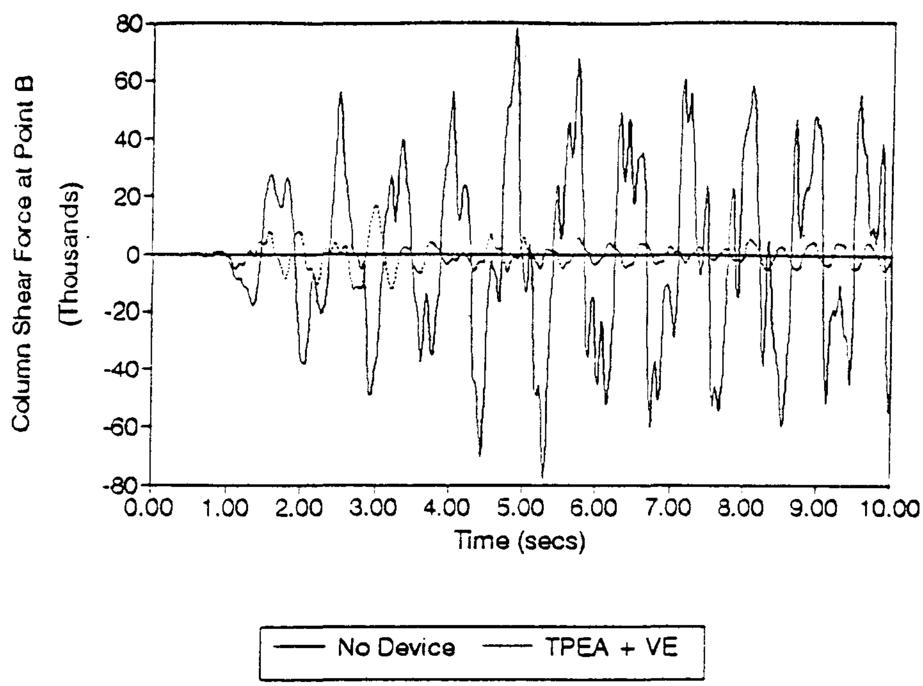

FIGURE 4-35 The Response of Column Shear Force at Point B of the structure with TPEA and VE While the Structure is Subjected to San Fernando Ground Motion

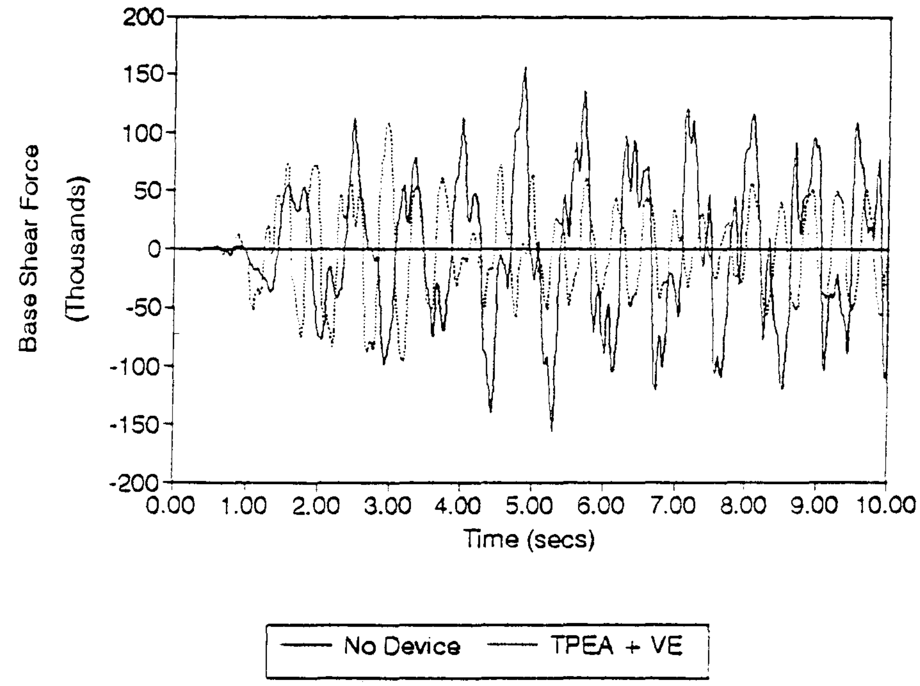

FIGURE 4-36 The response of Base Shear Force of the Structure with TPEA and VE While the Structure is Subjected to San Fernando Ground Motion

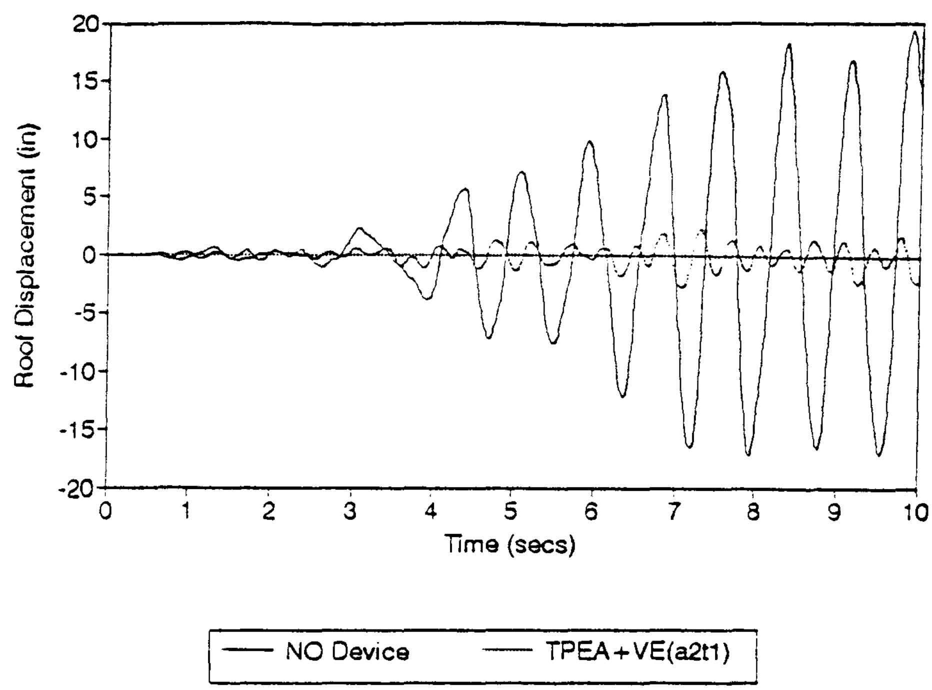

FIGURE 4-37 The Response of Roof Displacement of the Structure with TPEA and VE While the Structure is Subjected to Taft (ERSF=4) Ground Motion

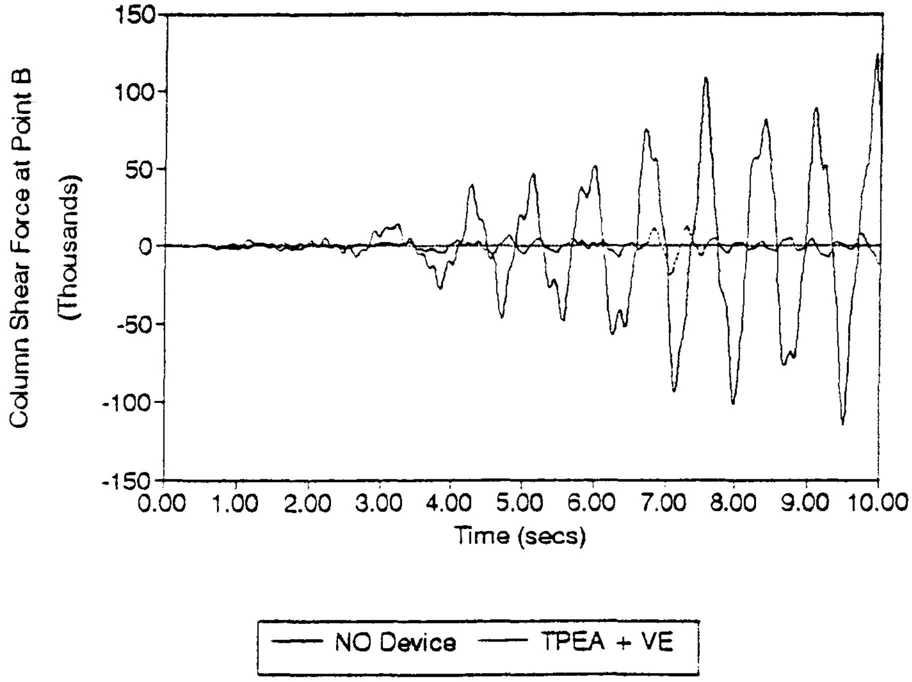

FIGURE 4-38 The Response of Column Shear Force at Point B of the structure with TPEA and VE While the Structure is Subjected to Taft (ERSF=4) Ground Motion

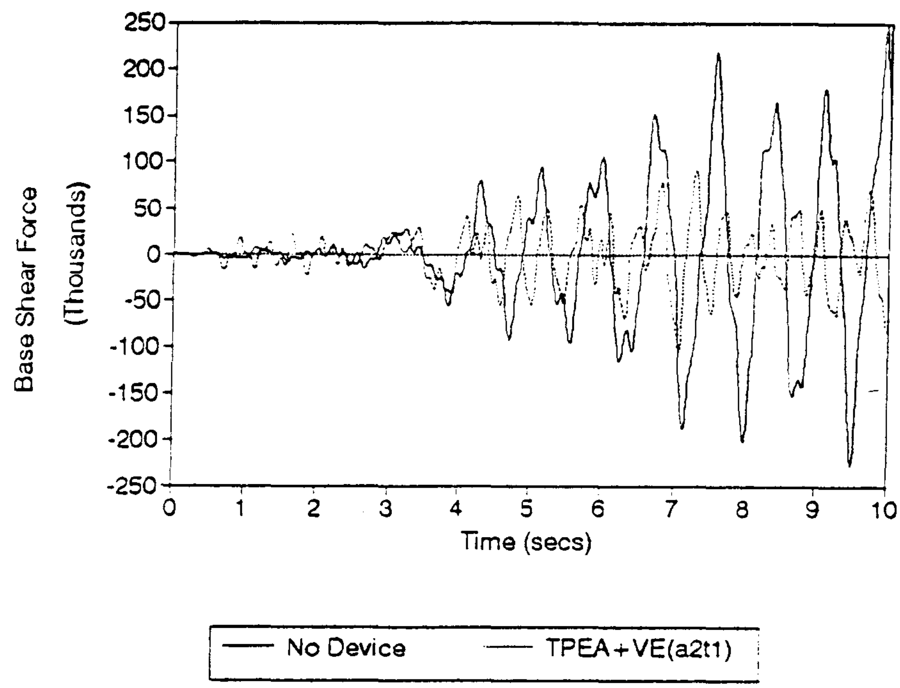

FIGURE 4-39 The Response of Base Shear Force of the Structure with TPEA and VE While the Structure is Subjected to Taft (ERSF=4) Ground Motion

excitation. The reason is the combination of TPEA and viscoelastic dampers mounted on the structure increases the structure's stiffness to change its natural frequencies. This may lead to an increase of the horizontal shear force accelerations. In particular, the TPEA may still operate in the elastic range in the early stage of an earthquake, therefore, the base shear force is not reduced greatly during that period. The combined devices provide not only additional stiffness but also hysteretic damping to a structure.

The relationships of displacement and force of TPEA and viscoelastic dampers are shown in Figures 4-40 to 4-57 when the structure is subjected to three selected ground motion. The results indicate that the combined device located at the lower floors of a building contribute more to energy absorption than those on upper floors. They demonstrate that TPEA absorbs substantial amounts of energy at the first floor while the TPEA still operates in the elastic range at the 10th floor. They also illustrate that viscoelastic dampers absorb more energy at the first floor than those at the tenth floor.

Finally, it can be concluded that the combination of TPEA and viscoelastic dampers on a structure can be a very effective and promising energy-absorbing device because they compensate for each other's shortcomings to resist both earthquake and wind loads. Adding such devices to a structure may increase cost, but it will increase the safety of the structure against earthquakes and wind loads. Moreover, adding energy-absorbing devices to the main load-carrying structural members could reduce the members' load carrying requirement and simplify the beam-column connections to offset the additional cost of the devices.

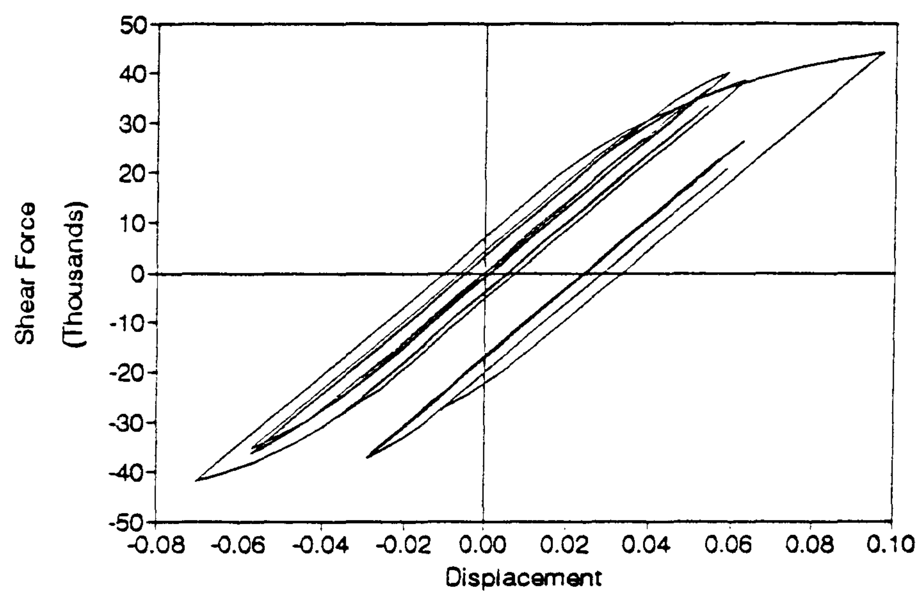

FIGURE 4-40 The Force-Displacement Relation of TPEA at 1st floor While the Structure is Subjected to El Centro Ground Motion

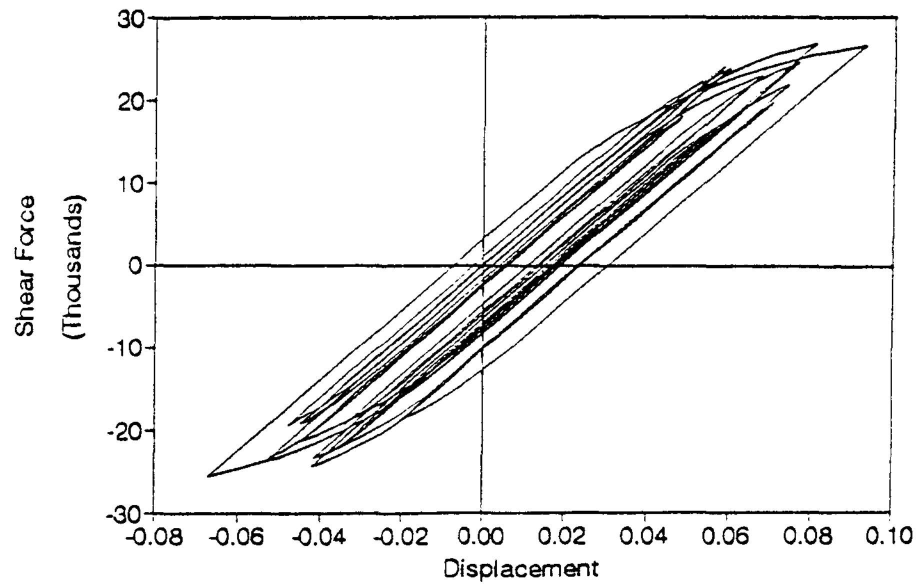

FIGURE 4-41 The Force-Displacement Relation of TPEA at 5th floor While the Structure is Subjected to El Centro Ground Motion

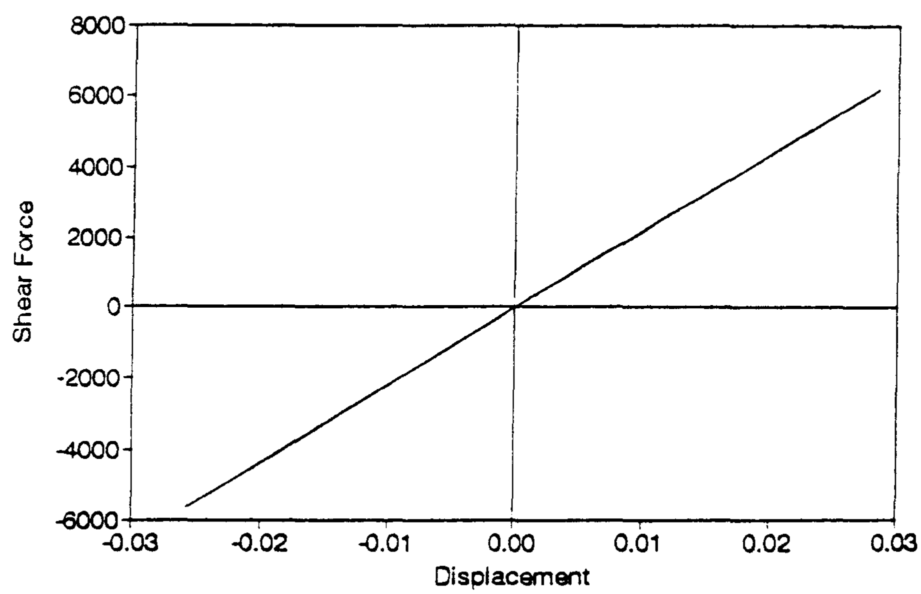

FIGURE 4-42 The Force-Displacement Relation of TPEA at 10th floor While the Structure is Subjected to El Centro Ground Motion

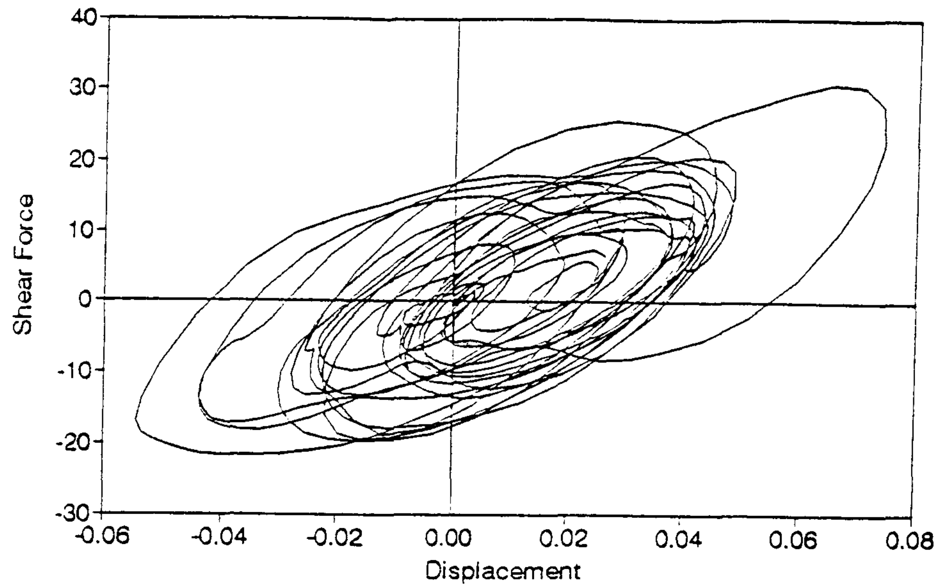

FIGURE 4-43 The Force-Displacement Relation of VE at 1st Floor While the Structure is Subjected to El Centro Ground Motion

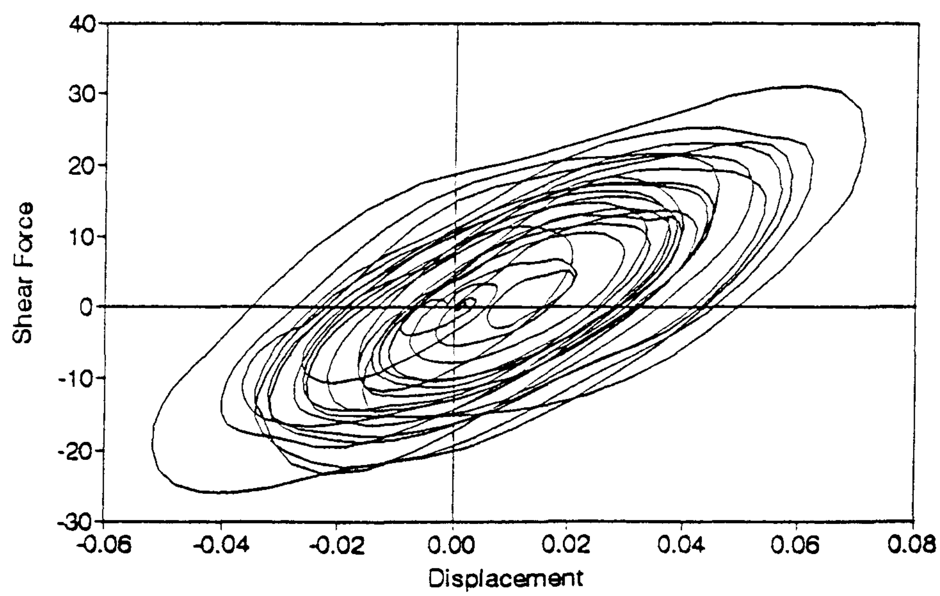

FIGURE 4-44 The Force-Displacement Relation of VE at 5th Floor While the Structure is Subjected to El Centro Ground Motion

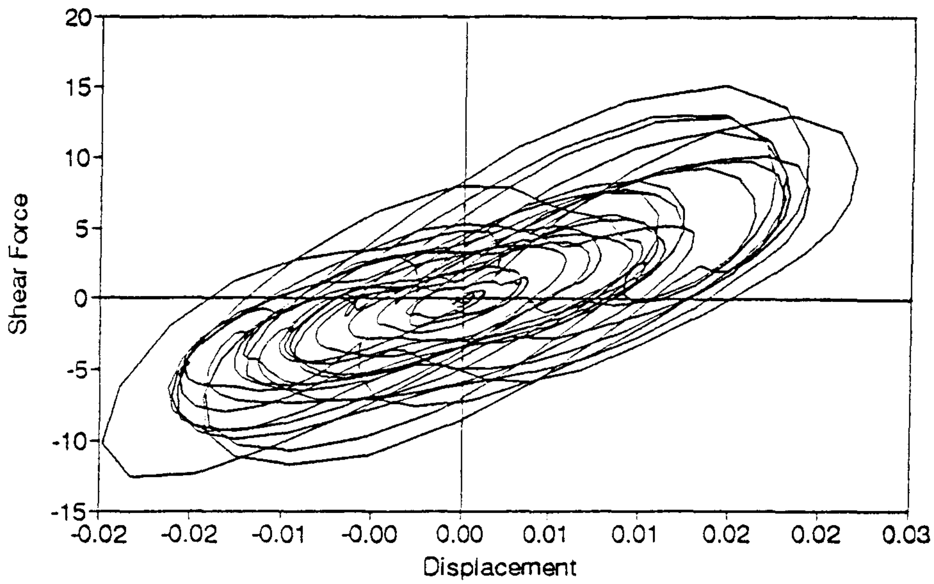

FIGURE 4-45 The Force-Displacement Relation of VE at 10th Floor While the Structure is Subjected to El Centro Ground Motion

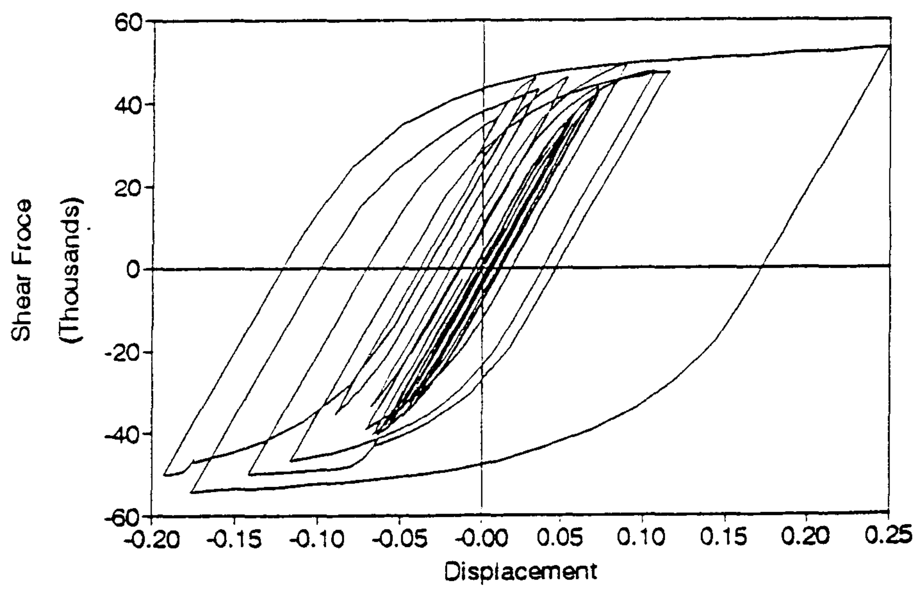

FIGURE 4-46 The Force-Displacement Relation of TPEA at 1st Floor While the Structure is Subjected to San Fernando Ground Motion

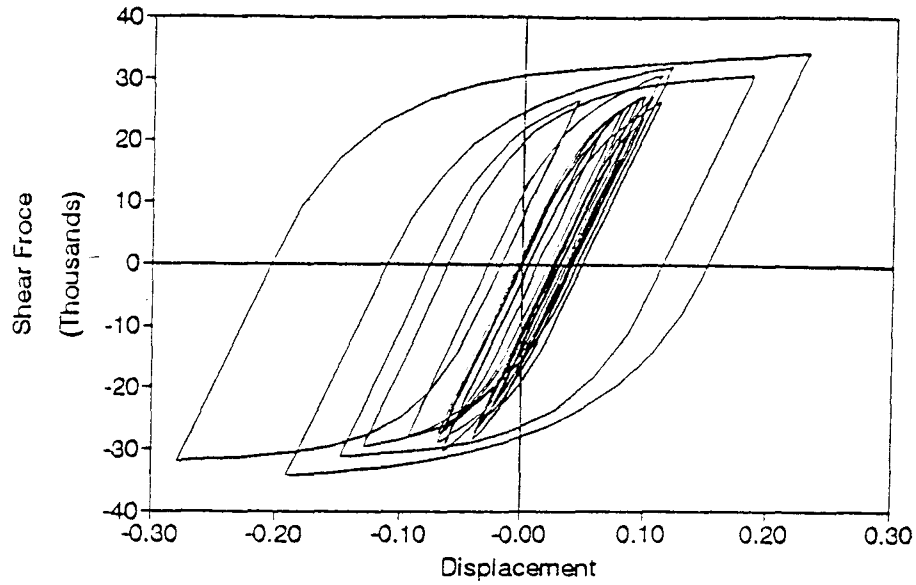

FIGURE 4-47 The Force-Displacement Relation of TPEA at 5th Floor While the Structure is Subjected to San Fernando Ground Motion

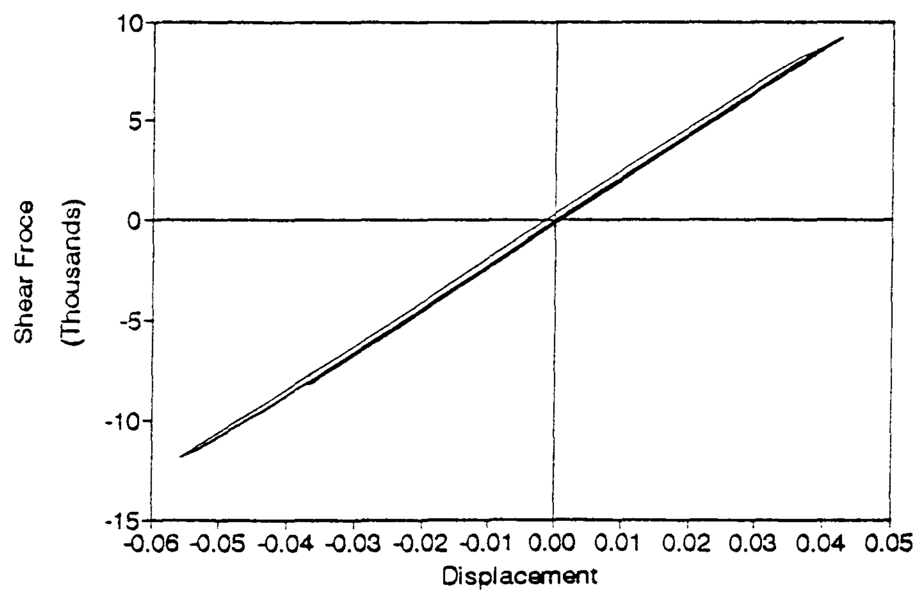

FIGURE 4-48 The Force-Displacement Relation of TPEA at 10th Floor While the Structure is Subjected to San Fernando Ground Motion

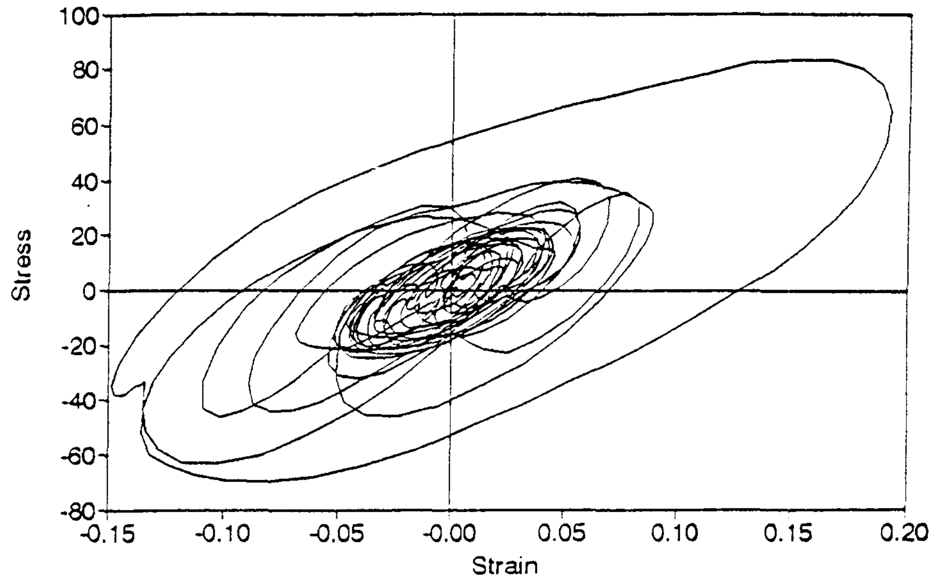

FIGURE 4-49 The Force-Displacement Relation of VE at 1st Floor While the Structure is Subjected to San Fernando Ground Motion

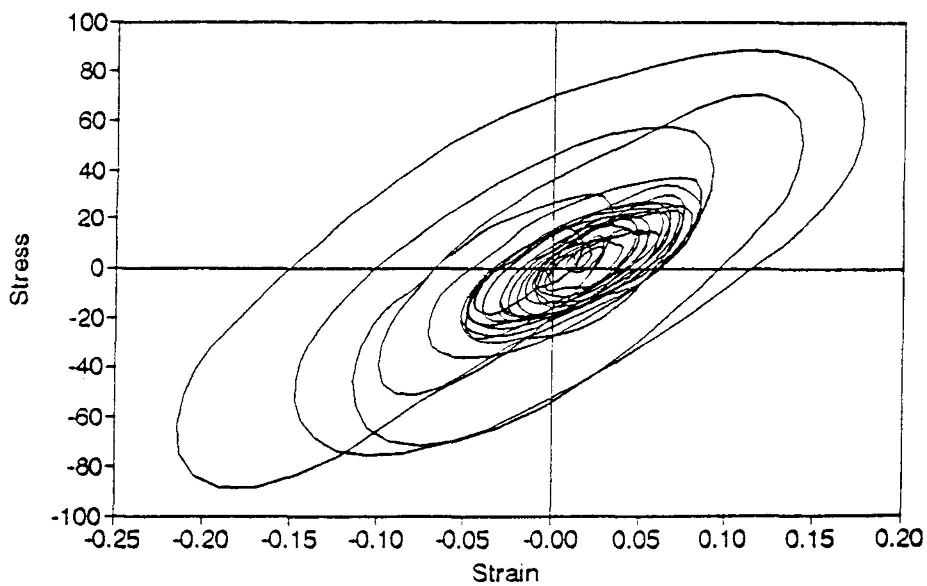

FIGURE 4-50 The Force-Displacement Relation of VE at 5th Floor While the Structure is Subjected to San Fernando Ground Motion

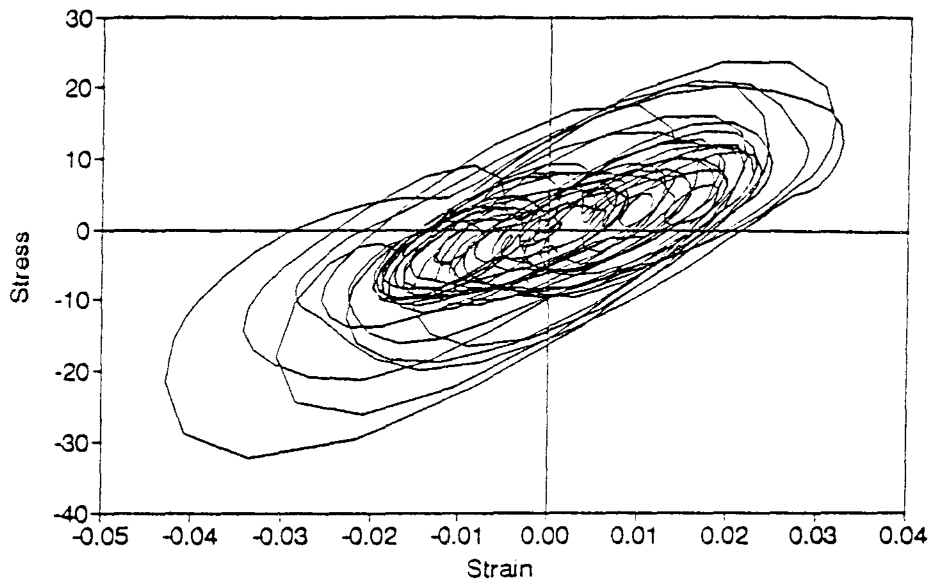

FIGURE 4-51 The Force-Displacement Relation of VE at 10th Floor While the Structure is Subjected to San Fernando Ground Motion

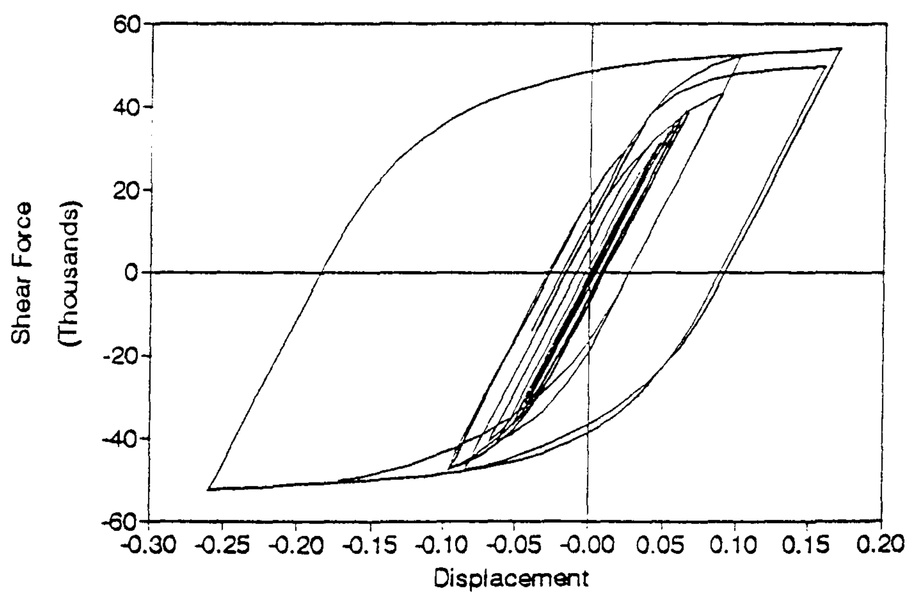

FIGURE 4-52 The Force-Displacement Relation of TPEA at 1st Floor While the Structure is Subjected to Taft (ERSF=4) Ground Motion

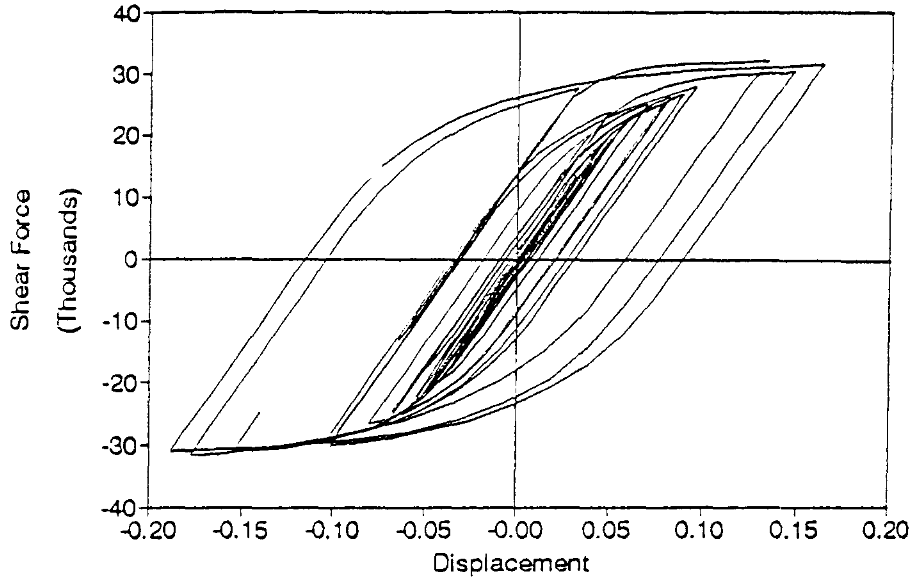

FIGURE 4-53 The Force-Displacement Relation of TPEA at 5th Floor While the Structure is Subjected to Taft (ERSF=4) Ground Motion

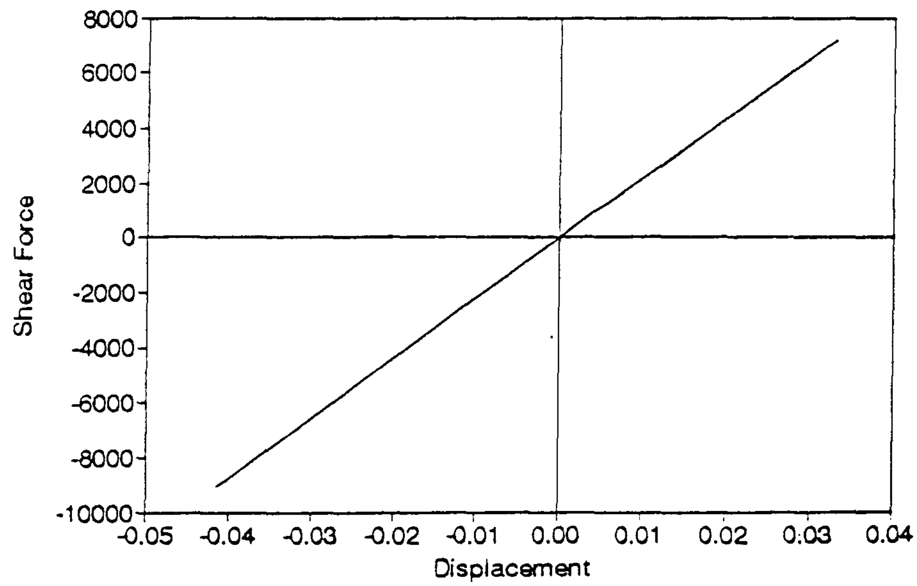

FIGURE 4-54 The Force-Displacement Relation of TPEA at 10th Floor While the Structure is Subjected to Taft (ERSF=4) Ground Motion

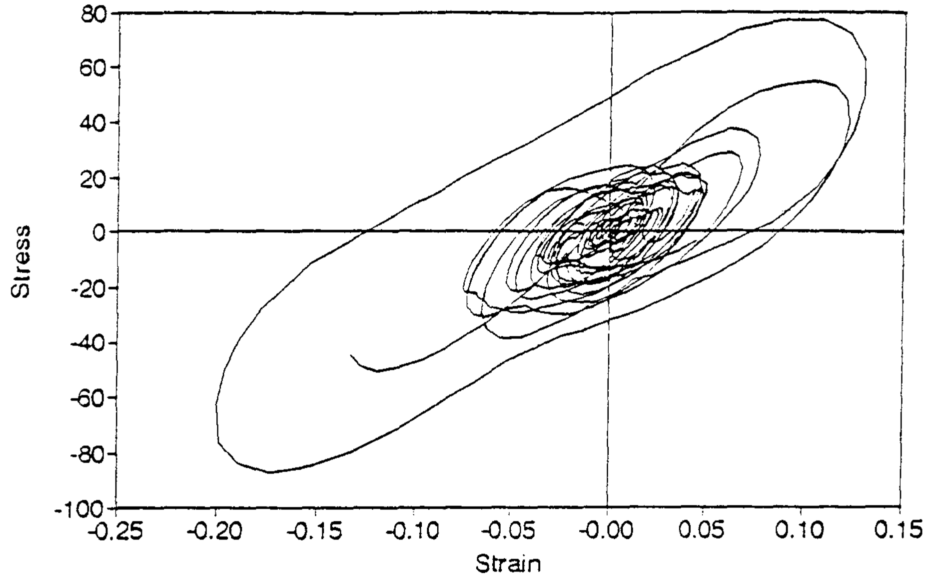

FIGURE 4-55 The Force-Displacement Relation of VE at 1st Floor While the Structure is Subjected to Taft (ERSF=4) Ground Motion

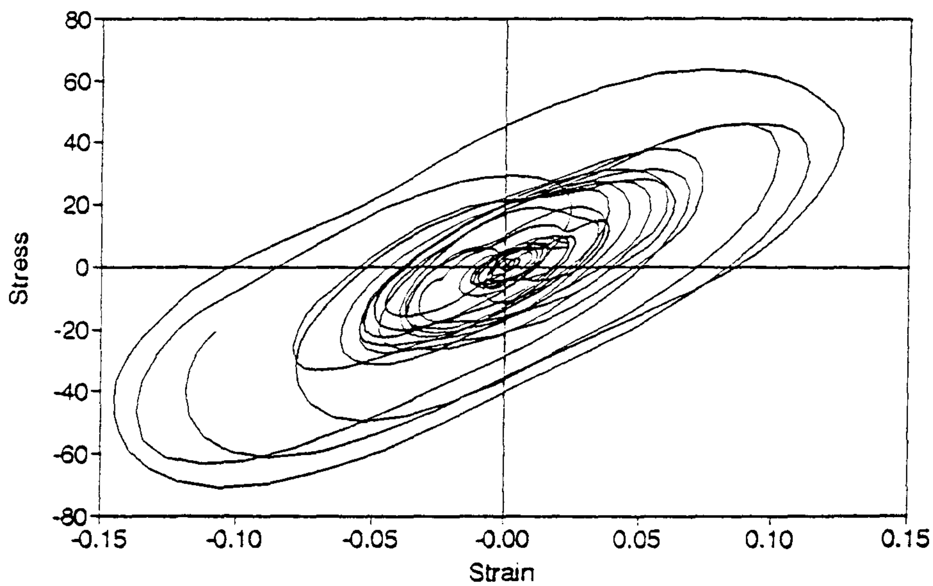

FIGURE 4-56 The Force-Displacement Relation of VE at 5th Floor While the Structure is Subjected to Taft (ERSF=4) Ground Motion

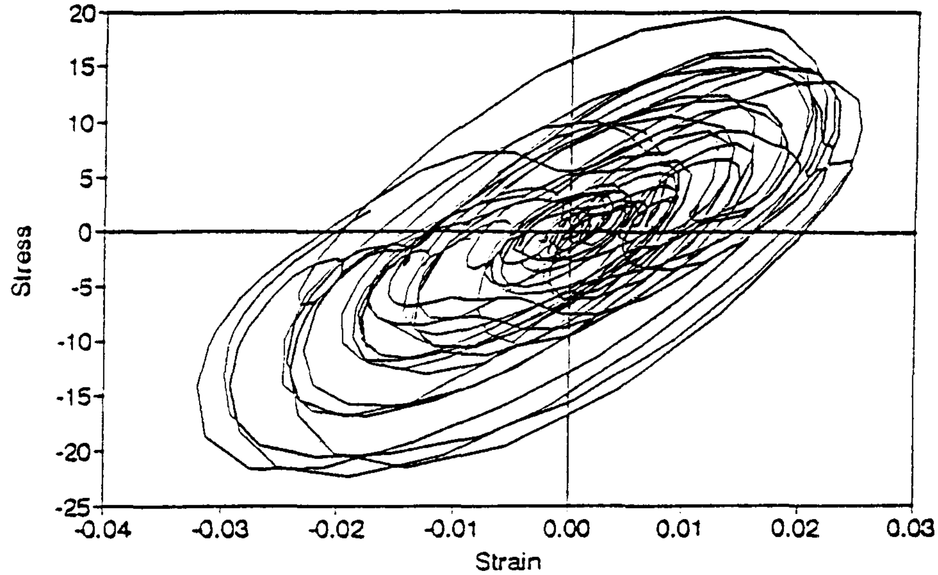

FIGURE 4-57 The Force-Displacement Relation of VE at 10th Floor While the Structure is Subjected to Taft (ERSF=4) Ground Motion

4.3 Numerical Study of a Combination of TPEA and Fluid Viscous Dampers on the High-rise Building

According to a previous study, the B/D ratio has little influence on the reduction of structural response during earthquakes. In this study, B/D is selected as 2, and SR ratios from 1 to 6 are selected. The behavior of the structure equipped with TPEA (SR=4, B/D=2) and fluid viscous dampers is compared to the structure without any energy-absorbing device while the structure was subjected to ten different earthquake peak accelerations from 100 Gal to 1000 Gal of San Fernando ground motion. Figures4-58 to 4-62 illustrate that the TPEA is still in the elastic range while the fluid dampers absorb energy when the structure is subjected to the peak accelerations of 100 Gal, 200 Gal, and 300 Gal of the San Fernando ground motion. This means that the fluid dampers would provide damping to the structure in order to absorb energy while the TPEA operates elastically during the smaller magnitudes of seismic ground motion. Similarly, when the structure is subjected to wind loads, the fluid dampers are able to reduce the wind sway since the TPEA has little capacity to resist properly wind loads. Figures 4-63 to 4-77 illustrate that the TPEA starts to dissipate energy when the peak acceleration is greater than 300 Gal of the San Fernando ground motion. They also show that TPEA and fluid dampers can dissipate seismically induced energy but the TPEA is more effective when the stronger peak acceleration ground motion was imposed to the structure. By combining the fluid dampers and TPEA on a structure, both earthquake and wind loads can be resisted greatly.

The behaviors of the structure without dampers and with fluid-damper-only, with TPEA-only, and with combined devices of TPEA and fluid dampers, were compared when the structure was subjected to ten different earthquake peak acceleration from 100 Gal to 1000 Gal of the San fernando ground motion. As shown in Figure 4-78, it is observed that the combined devices on a structure have the best performance in reducing roof displacement, the TPEA ranks second, and the fluid dampers rank third. Figure 4-79 shows similar results except that the structure with TPEA and the structure with combined devices have larger base shear force than the structure without any energy-absorbing devices when the peak acceleration is less than 300 Gal. These results actually confirm the phenomenon in Figures 4-58 to 4-77. The added TPEA operates in an elastic range at the lower peak accelerations of the San Fernando earthquake.

The curves of the structure with fluid dampers and the structure without any devices are both linear, but the curve of the structure with fluid dampers has a much smaller gradient. In Figure 4-79, we also see that the two curves of TPEA-only and TPEA with fluid dampers have a similar pattern. It may be assumed that the TPEA is the governing device when used jointly with fluid dampers.

The effects of the damping coefficient on the roof displacement and base shear force were observed when the structure, with and without combined devices of TPEA and fluid dampers, was subjected to ten different peak acceleration from 100 Gal to 1000 Gal of the San Fernando ground motion. Figure 4-80 shows that the curves of TPEA with fluid dampers are almost indistinguishable. This indicates that the value of the damping coefficient becomes less important in reducing structural response when TPEA and fluid dampers are combined on the structure. Figure 4-81 shows the same relationships. The structure with combined devices has larger base shear forces than the structure without devices when the peak acceleration is less than 300 Gal. The reason is

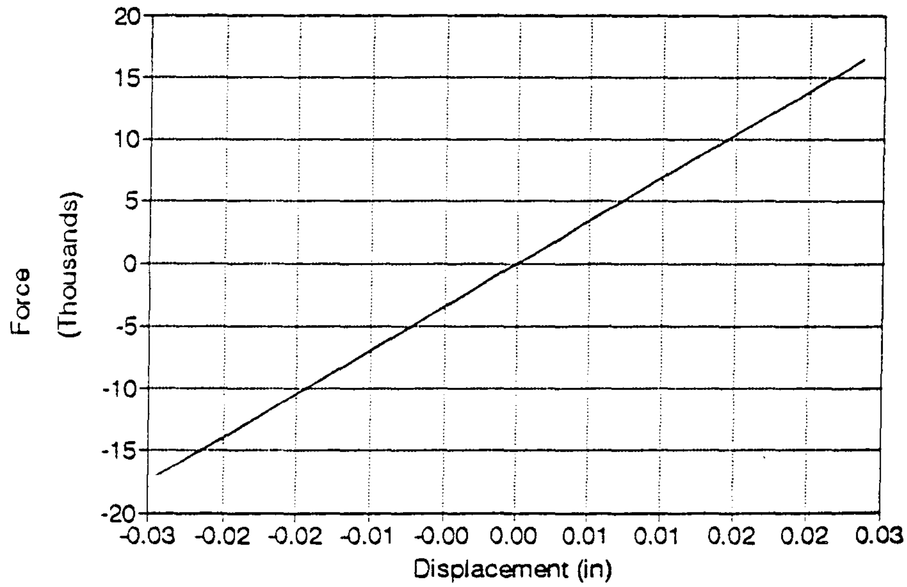

FIGURE 4-58 The Force-Displacement Relation of TPEA While the Structure is Subjected to the Peak AcceleRation of 100 Gal of San Fernando Ground Motion

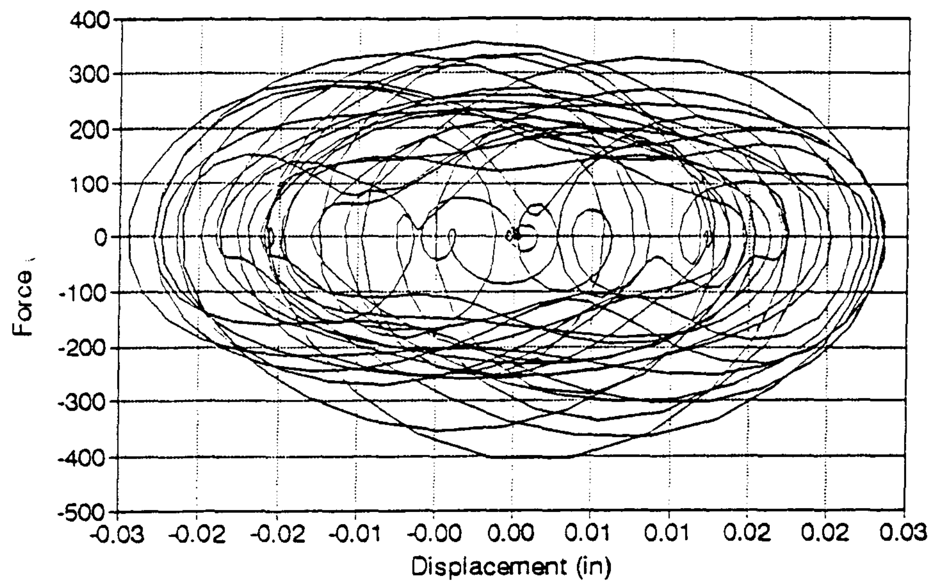

FIGURE 4-59 The Force-Displacement Relation of FD While the Structure is Subjected to the Peak AcceleRation of 100 Gal of San Fernando Ground Motion

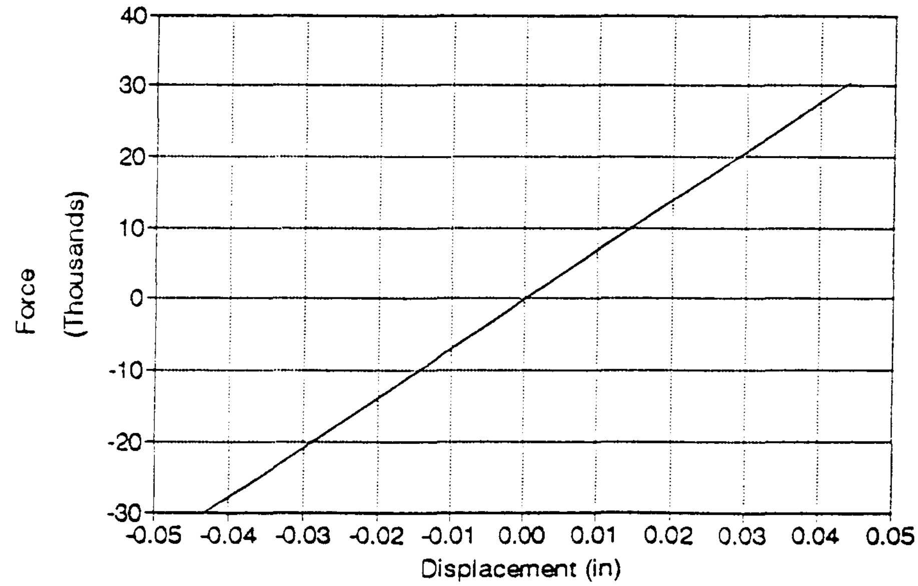

FIGURE 4-60 The Force-Displacement Relation of TPEA While the Structure is Subjected to the Peak AcceleRation of 200 Gal of San Fernando Ground Motion

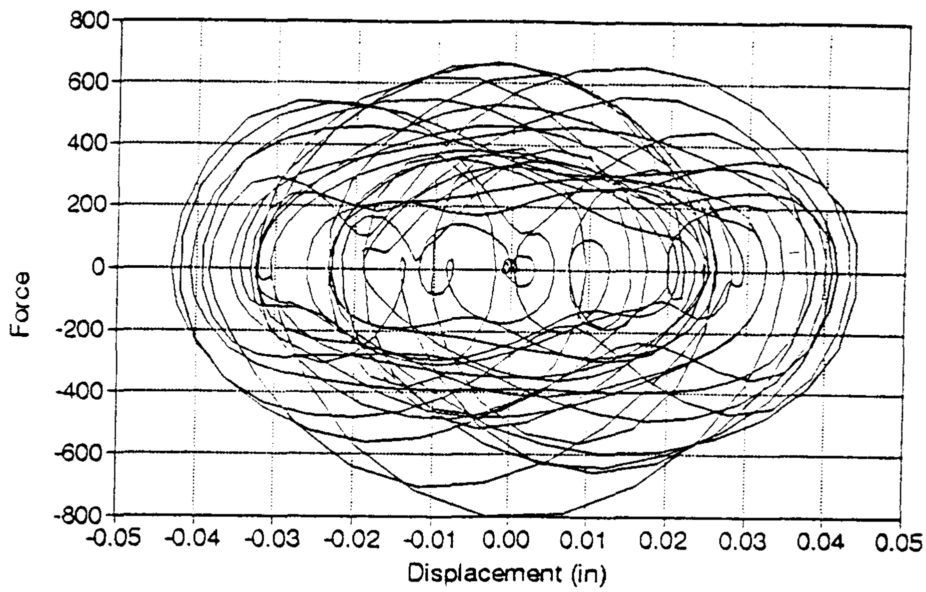

FIGURE 4-61 The Force-Displacement Relation of FD While the Structure is Subjected to the Peak AcceleRation of 200 Gal of San Fernando Ground Motion

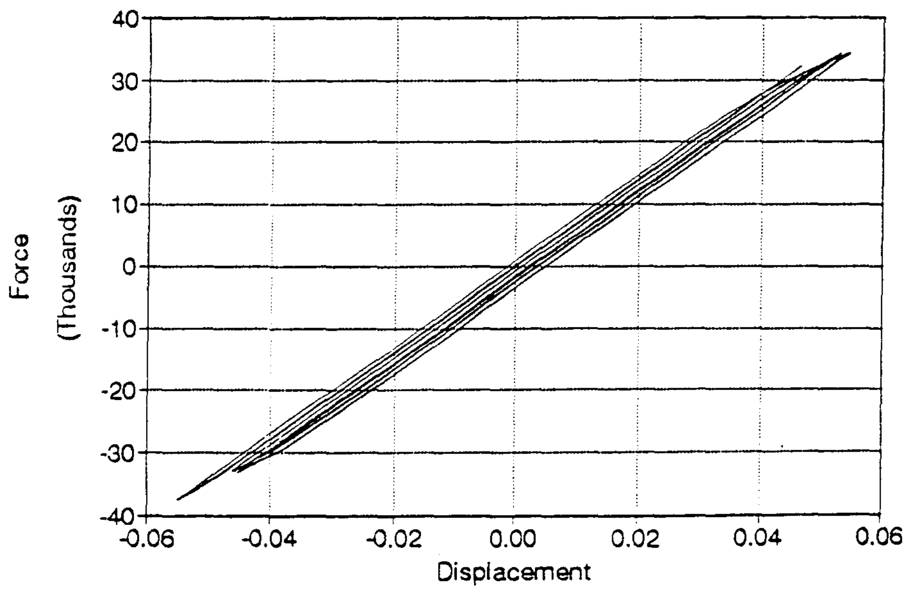

FIGURE 4-62 The Force-Displacement Relation of TPEA While the Structure is Subjected to the Peak AcceleRation of 300 Gal of San Fernando Ground Motion

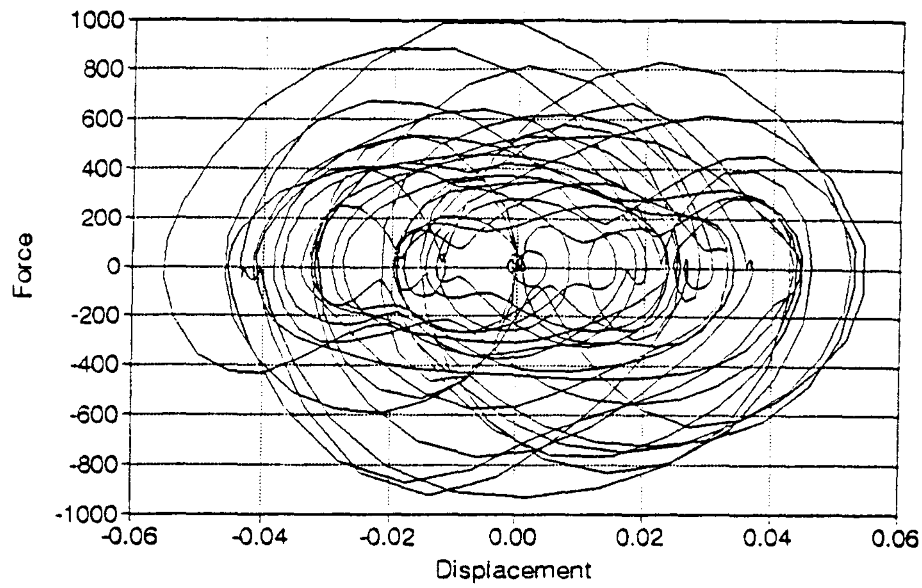

FIGURE 4-63 The Force-Displacement Relation of FD While the Structure is Subjected to the Peak AcceleRation of 300 Gal of San Fernando Ground Motion

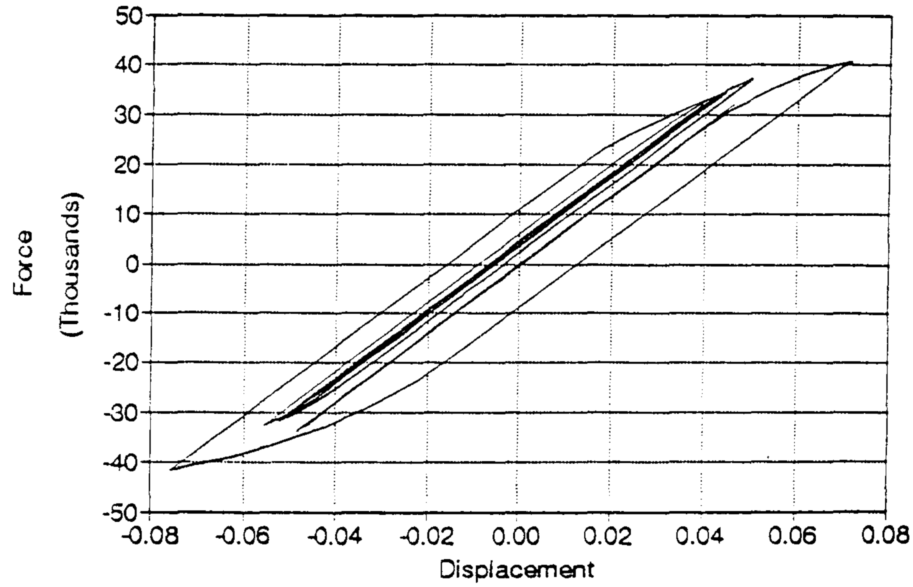

FIGURE 4-64 The Force-Displacement Relation of TPEA While the Structure is Subjected to the Peak AcceleRation of 400 Gal of San Fernando Ground Motion

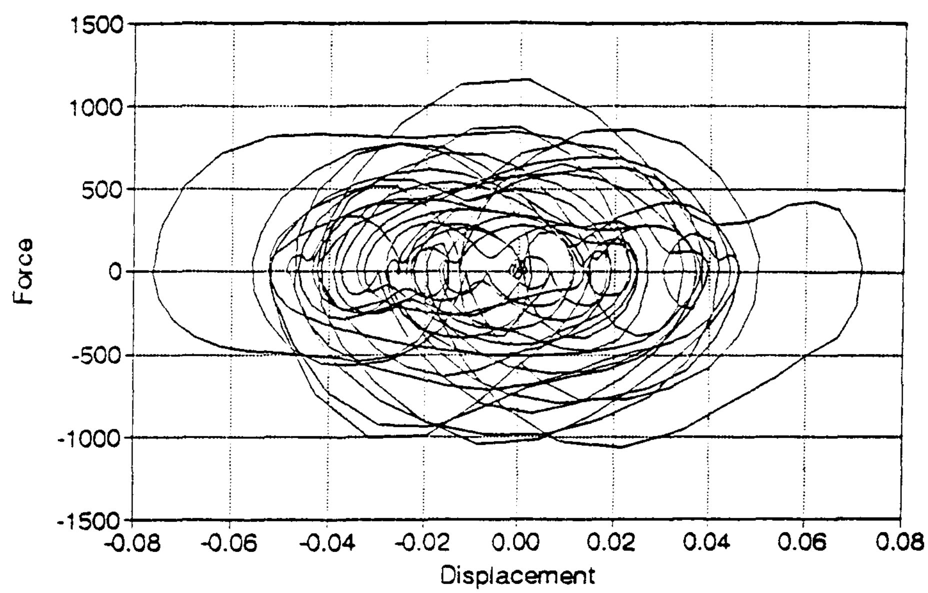

FIGURE 4-65 The Force-Displacement Relation of FD While the Structure is Subjected to the Peak AcceleRation of 400 Gal of San Fernand Ground Motion

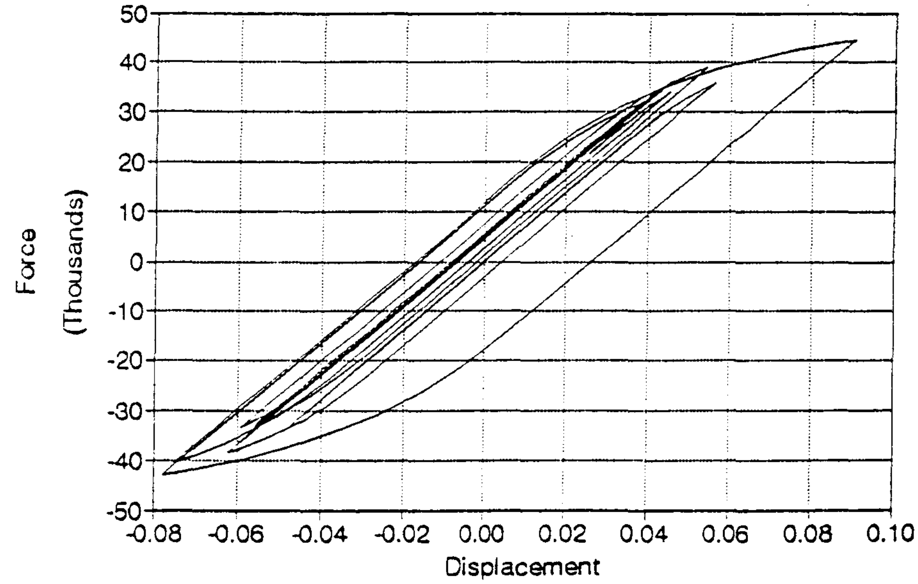

FIGURE 4-66 The Force-Displacement Relation of TPEA While the Structure is Subjected to the Peak AcceleRation of 500 Gal of San Fernando Ground Motion

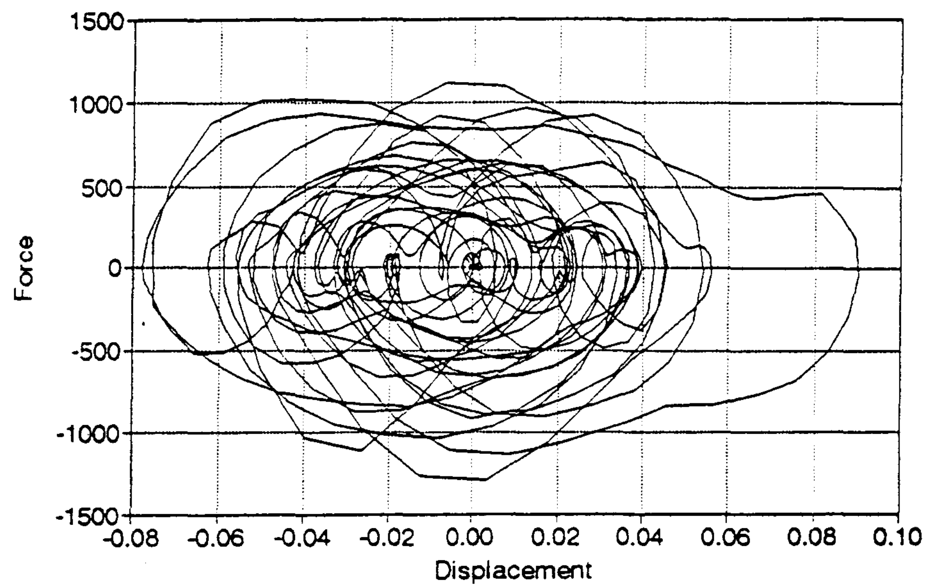

FIGURE 4-67 The Force-Displacement Relation of FD While the Structure is Subjected to the Peak AcceleRation of 500 Gal of San Fernando Ground Motion

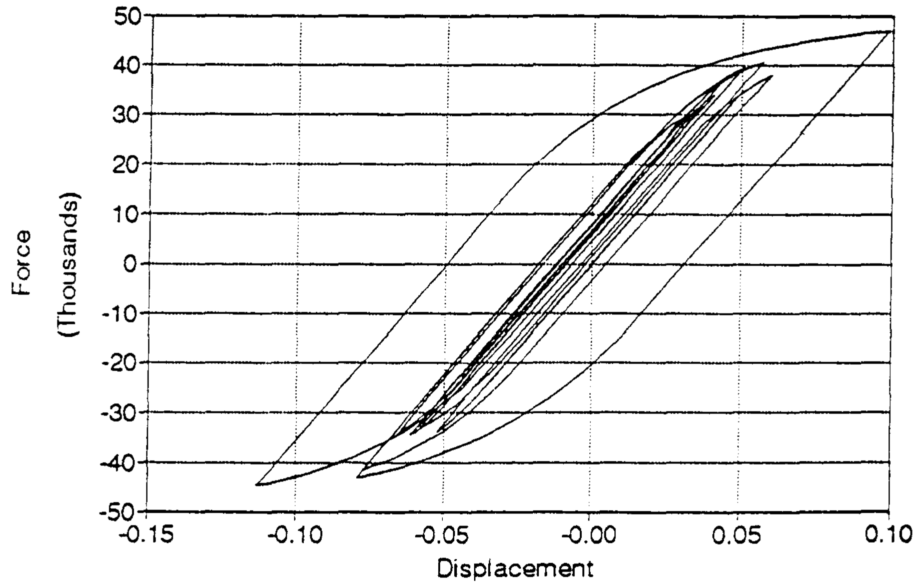

FIGURE 4-68 The Force-Displacement Relation of TPEA While the Structure is Subjected to the Peak AcceleRation of 600 Gal of San Fernando Ground Motion

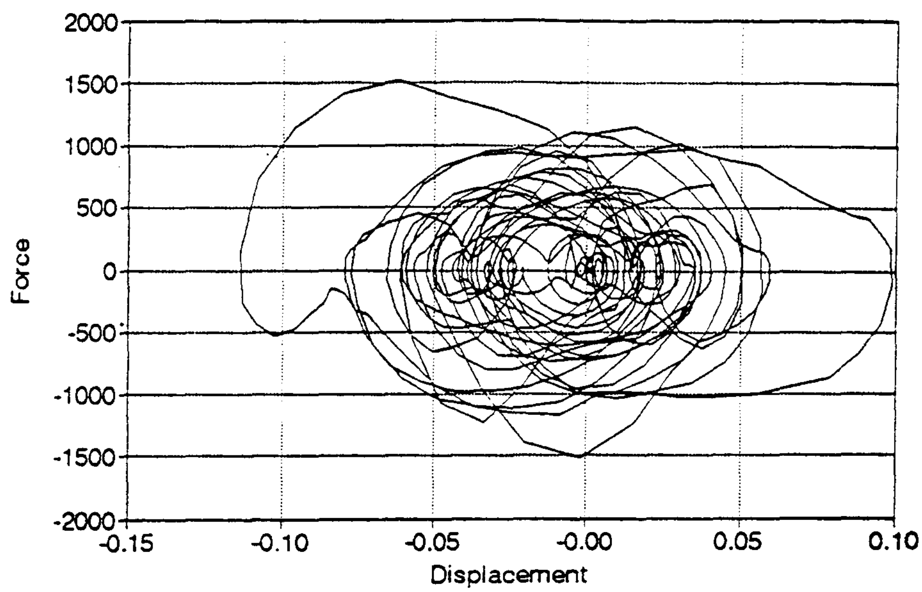

FIGURE 4-69 The Force-Displacement Relation of FD While the Structure is Subjected to the Peak AcceleRation of 600 Gal of San Fernando Ground Motion

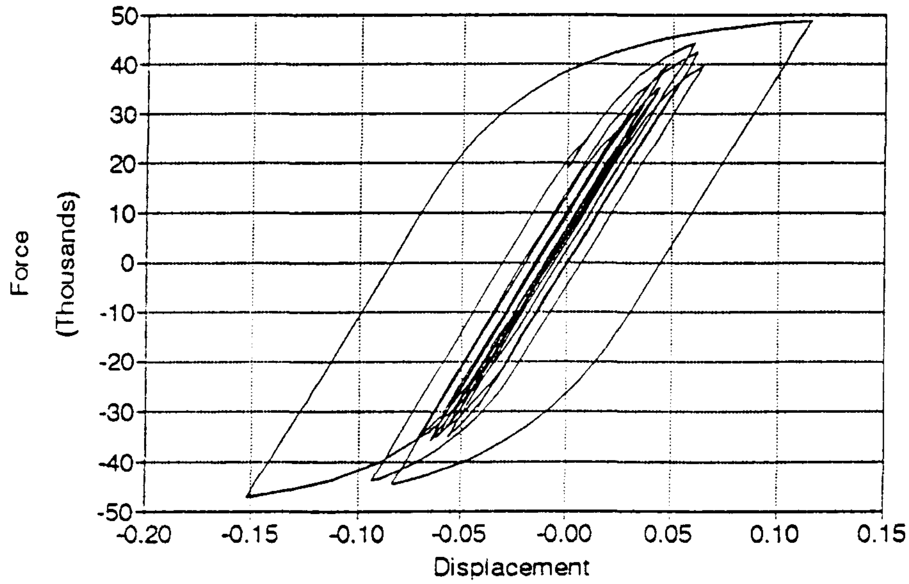

FIGURE 4-70 The Force-Displacement Relation of TPEA While the Structure is Subjected to the Peak AcceleRation of 700 Gal of San Fernando Ground Motion

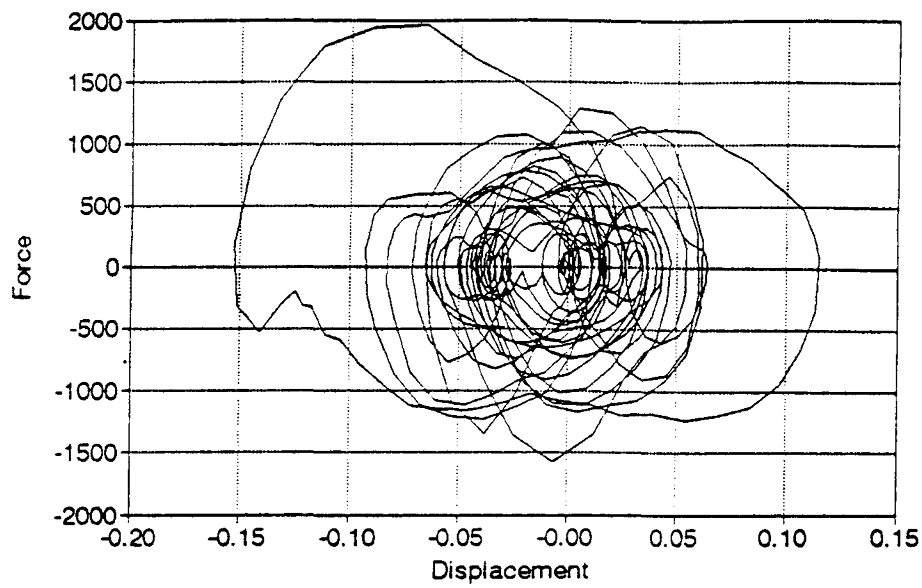

FIGURE 4-71 The Force-Displacement Relation of FD While the Structure is Subjected to the Peak AcceleRation of 700 Gal of San Fernando Ground Motion

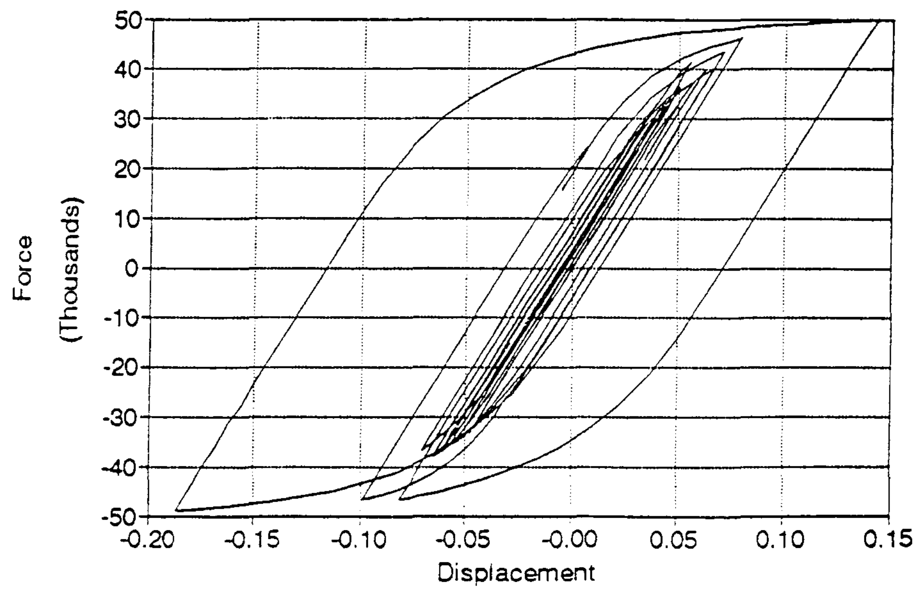

FIGURE 4-72 The Force-Displacement Relation of TPEA While the Structure is Subjected to the Peak AcceleRation of 800 Gal of San Fernando Ground Motion

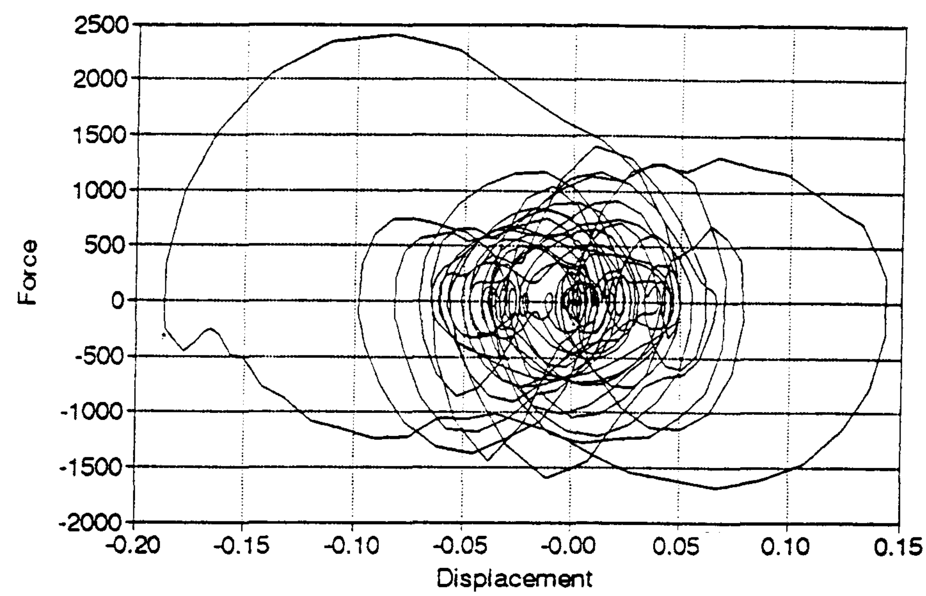

FIGURE 4-73 The Force-Displacement Relation of FD While the Structure is Subjected to the Peak AcceleRation of 800 Gal of San Fernando Ground Motion

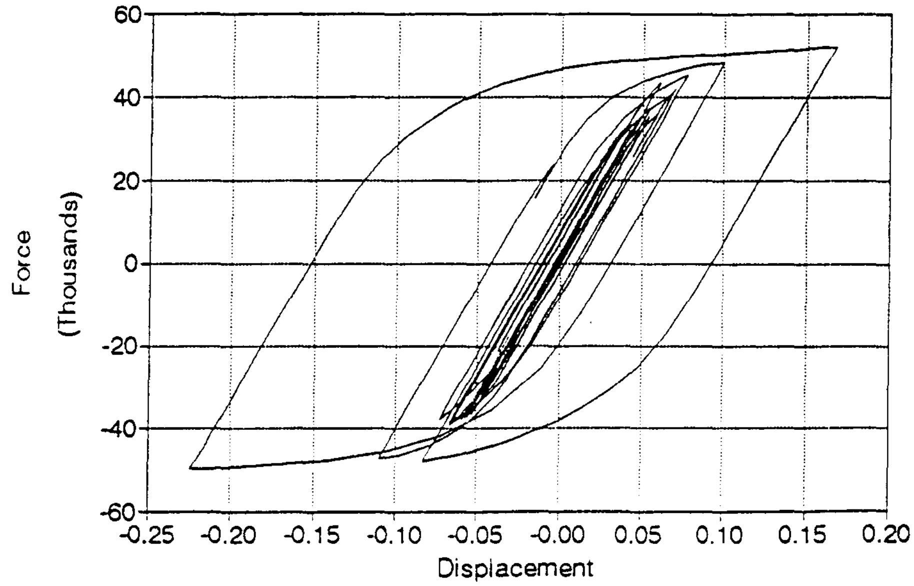

FIGURE 4-74 The Force-Displacement Relation of TPEA While the Structure is Subjected to the Peak AcceleRation of 900 Gal of San Fernando Ground Motion

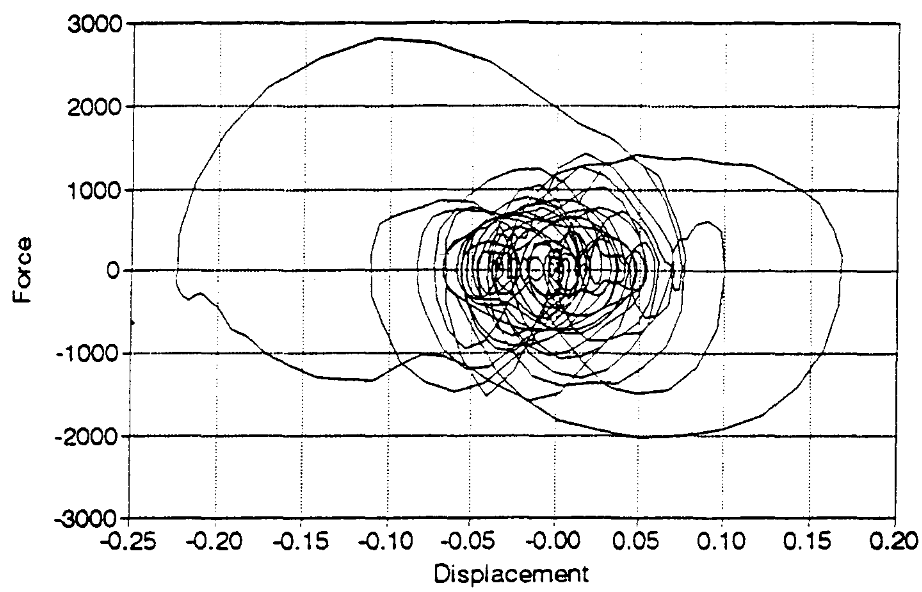

FIGURE 4-75 The Force-Displacement Relation of FD While the Structure is Subjected to the Peak AcceleRation of 900 Gal of San Fernando Ground Motion

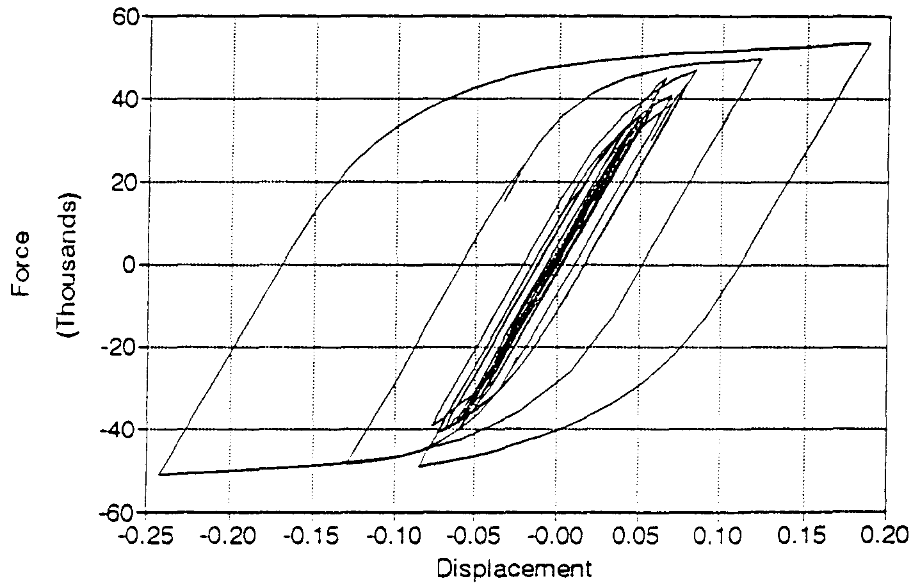

FIGURE 4-76 The Force-Displacement Relation of TPEA While the Structure is Subjected to the Peak AcceleRation of 1000 Gal of San Fernando Ground Motion

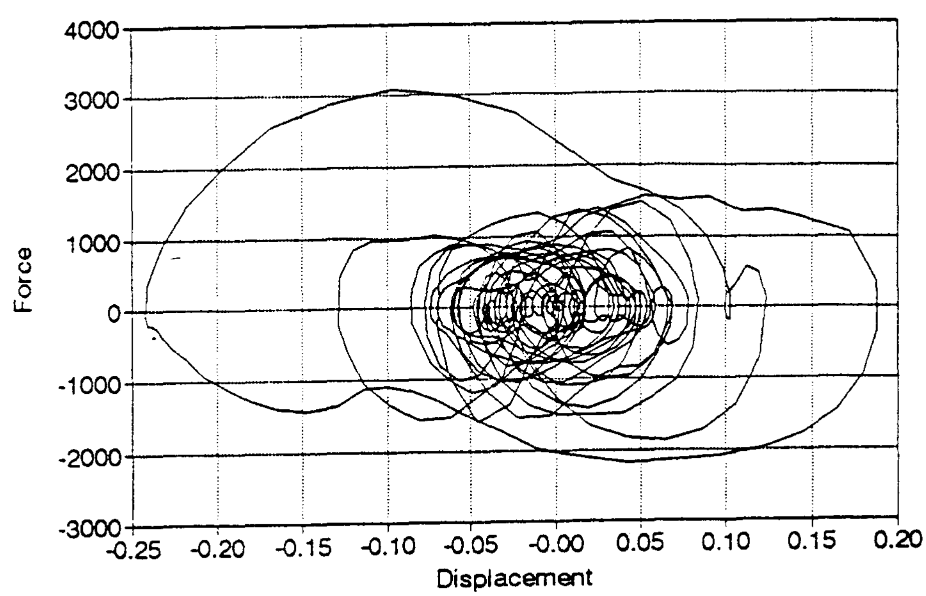

FIGURE 4-77 The Force-Displacement Relation of FD While the Structure is Subjected to the Peak AcceleRation of 1000 Gal of San Fernando Ground Motion

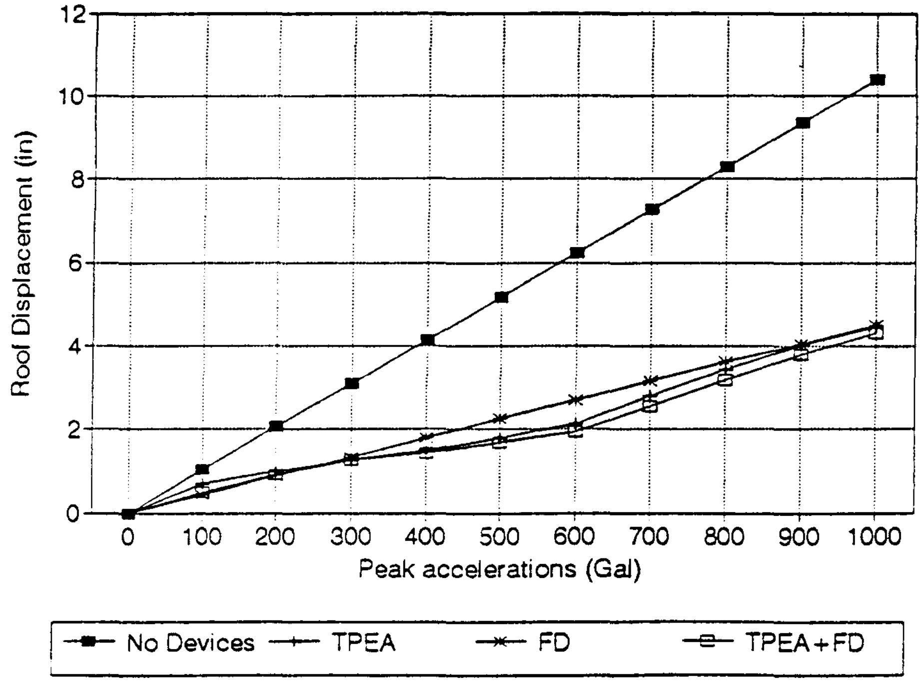

FIGURE 4-78 Comparison of Roof Displacement When the Structure is Subjected to the Peak AcceleRation of 100 Gal to 1000 Gal of San Fernando Ground Motion

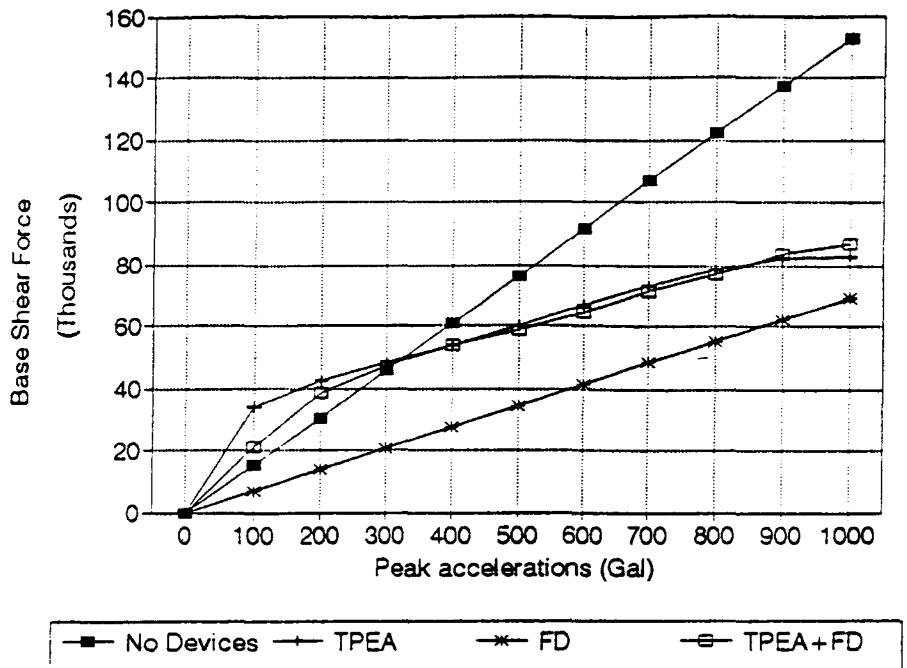

FIGURE 4-79 Comparison of Base Shear Force When the Structure is Subjected to the Peak AcceleRation of 100 Gal to 1000 Gal of San Fernando Ground Motion

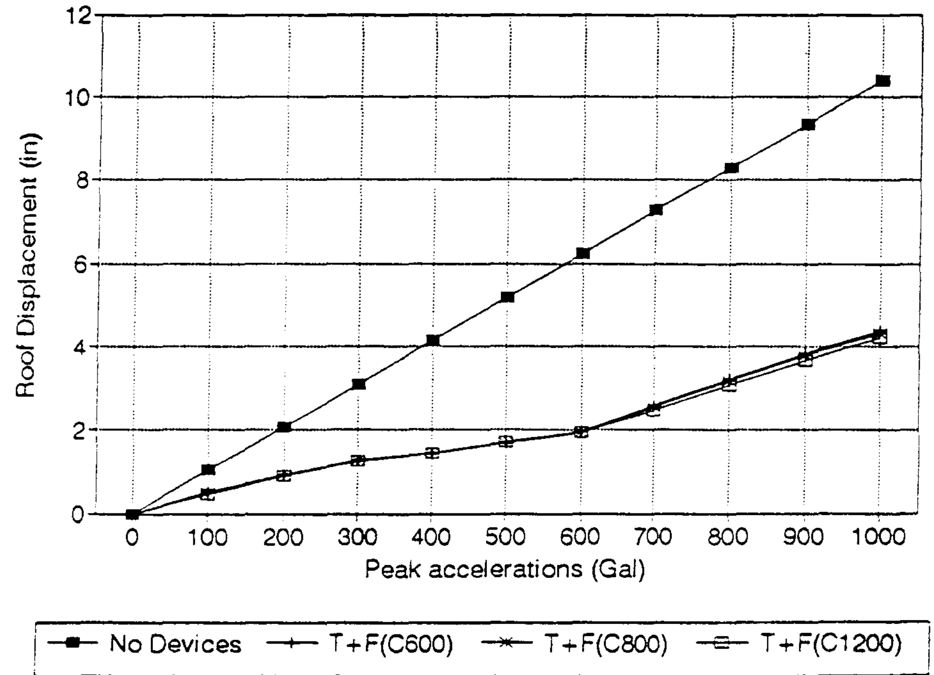

FIGURE 4-80 The Relation of Damping Coefficient and Roof Displacement When the Structure is Subjected to the Peak AcceleRation of 100 Gal to 1000 Gal of San Fernando Ground Motion

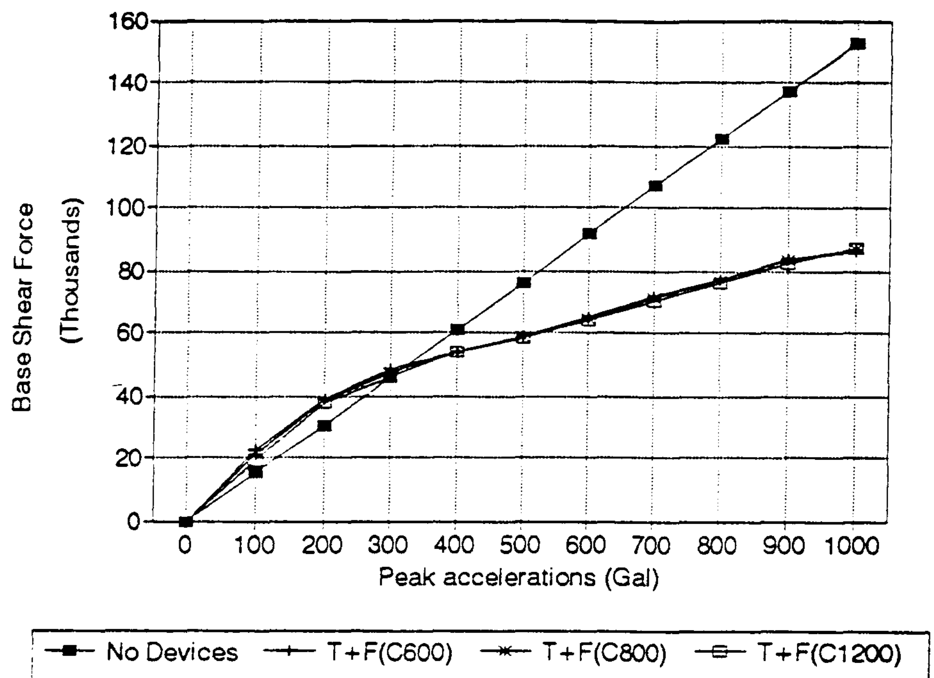

FIGURE 4-81 The Relation of Damping Coefficient and Base Shear Force When the Structure is Subjected to the Peak AcceleRation of 100 Gal to 1000 Gal of San Fernando Ground Motion

that the addition of TPEA to a structure increases the structure's stiffness and the TPEA operates in an elastic range at the lower peak acceleration of the San Fernando ground motion. Figures 4-82 and 4-83 show that the curves decay slowly when the fluid dampers are used jointly with TPEA. The results indicate that the value of the damping coefficient becomes less important in the reduction of base shear forces when TPEA and fluid dampers are jointly used on the structure.

The effects of SR ratios on roof displacement and base shear force were compared when the structure, with and without combined devices of TPEA and fluid dampers, was subjected to three selected ground motions. As shown in Figures 4-84 to 4-89, the number and the position of the fluid dampers have little influence in improving seismic resistance when the structure was equipped with TPEA and fluid dampers. All the curves have a similar pattern. It may be assumed that the TPEA is the governing device even when used jointly with fluid dampers. It can be said that the TPEA plays a more important role than the fluid dampers by taking a greater portion of shear force during stronger ground motions. Figures 4-84 and 4-88 illustrate that the curves have a similar pattern and decay slowly when SR is greater than 3. Figure 4-85 shows that SR=4 has the best performance in reducing base shear force when the structure is subjected to the El Centro ground motion. Figure 4-89 shows that SR=2 has the best performance when the structure is subjected to the Taft (ERSF=4) ground motion.

Finally, the time-history responses (roof displacement, column shear force at point B, and base shear force) of the structure, with and without combined devices, were compared when the structure was subjected to the El Centro and Taft (ERSF=4) ground motion. Figures 4-90 and 4-93 show that the roof displacement is reduced greatly overall and also is reduced once the earthquake occurs. The velocity dependence of fluid viscous dampers is avoided. Figure 4-90 shows that the natural frequency of the structure with combined devices is almost double of the structure without any devices because the structure's frequency is changed due to the addition of TPEA and fluid dampers. Figures 4-91 and 4-94 illustrate that the column takes only a very small portion of the base shear force which prevents the main load-carrying members from damage and lessens the energy dissipation demands on those members. Figures 4-92 and 4-95 indicate that the base shear force is reduced overall, although the base shear force is not reduced significantly in the early stage of the excitation. The reason is that the combination of TPEA and fluid dampers on a structure increases the structure's stiffness to change its natural frequencies. This may lead to an increase of the horizontal shear force accelerations. Most importantly, the TPEA operates in the elastic range in the early stage of the earthquake, therefore, the base shear force is not reduced greatly during that period. The combined devices provide not only additional stiffness, but also hysteretic damping to a structure.

The combined devices located at the lower floors of a building contribute more to energy absorption than those on other floors. Figures 4-96 to 4-101 show the relation of displacement and force of the TPEA and fluid dampers, respectively. They demonstrate that TPEA absorbs substantial amounts of the energy at the first floor while the TPEA still operates in the elastic range at tenth floor. They also illustrate that fluid dampers absorb more energy at the first floor than those at the tenth floor.

Finally, it can be concluded that the combination of TPEA and fluid dampers on a structure can be a very effective and promising energy-absorbing device because they compensate for

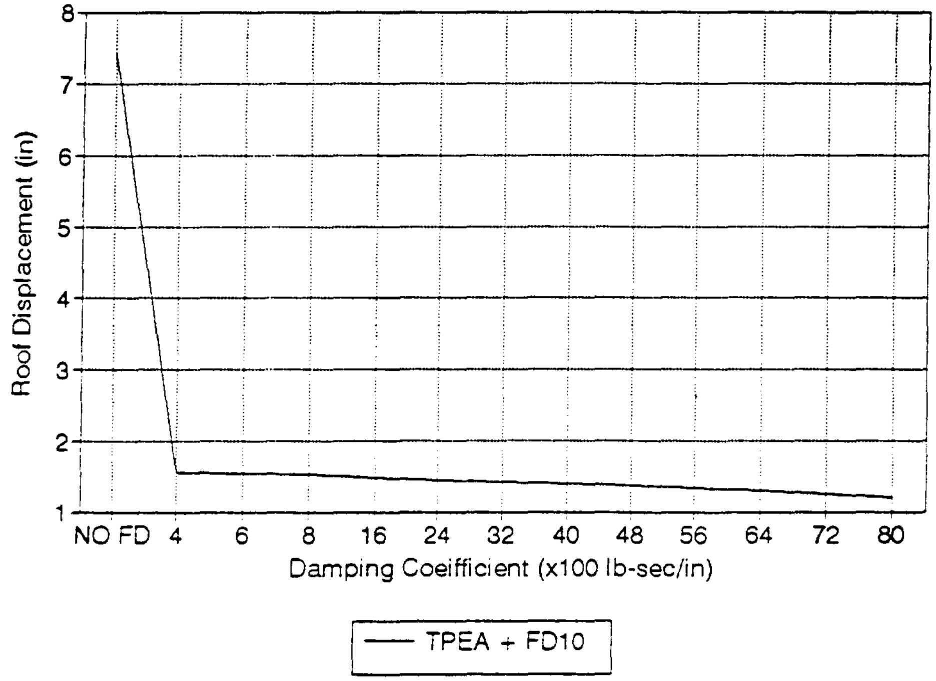

FIGURE 4-82 Comparison of Damping Coefficient and Roof Displacement When the Structure is Subjected to El Centro Ground Motion

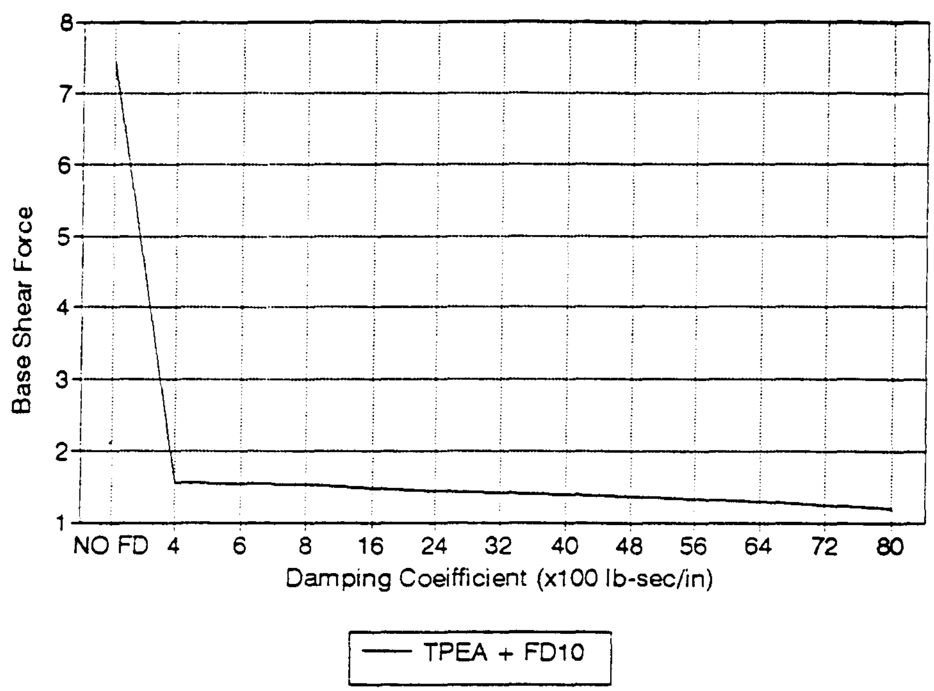

FIGURE 4-83 Comparison of Damping Coefficient and Base Shear Force When the Structure is Subjected to El Centro Ground Motion

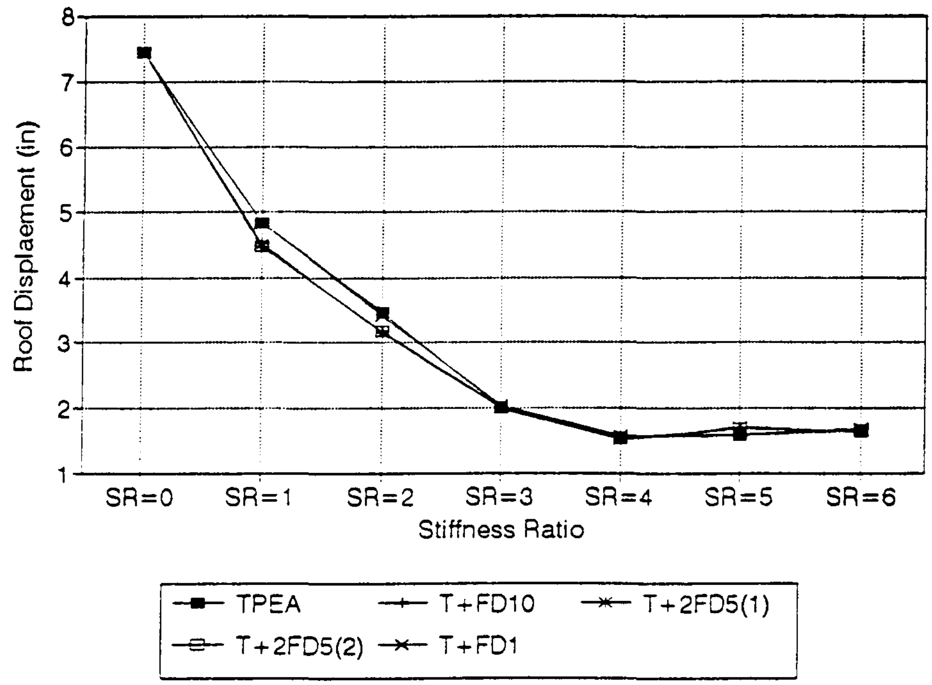

FIGURE 4-84 Comparison of SR Ratio and Roof Displacement When the Structure is Subjected to El Centro Ground Motion

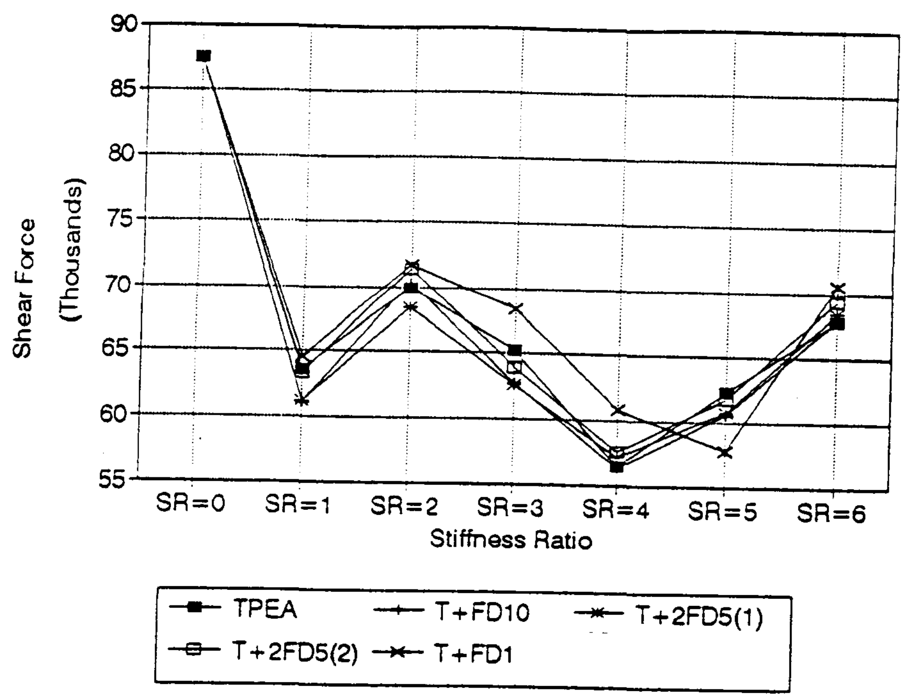

FIGURE 4-85 Comparison of SR Ratio and Base Shear Force When the Structure is Subjected to El Centro Ground Motion

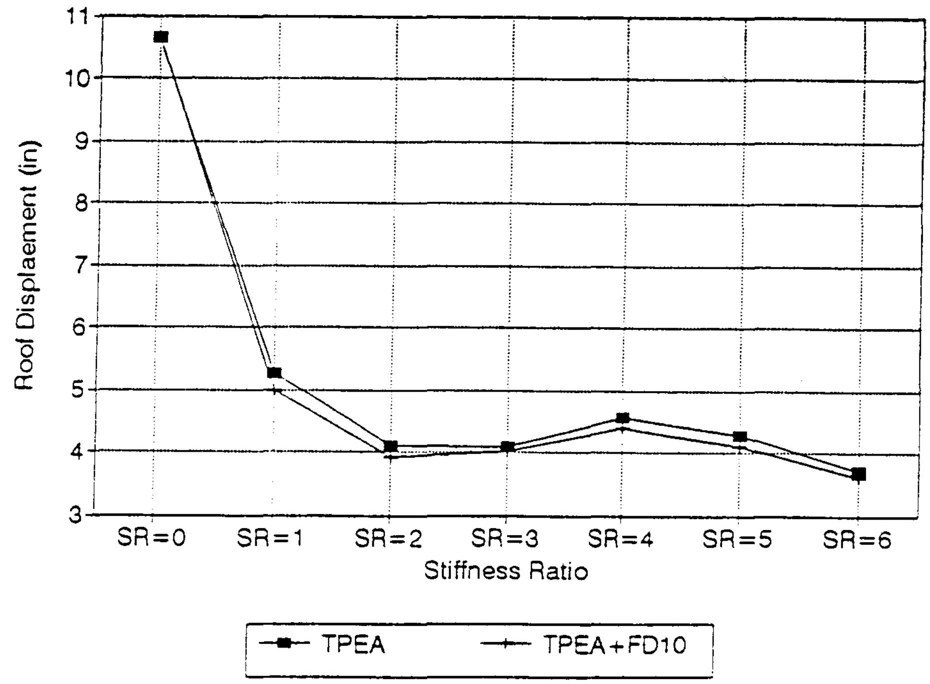

FIGURE 4-86 Comparison of SR Ratio and Roof Displacement When the Structure is Subjected to San Fernando Ground Motion

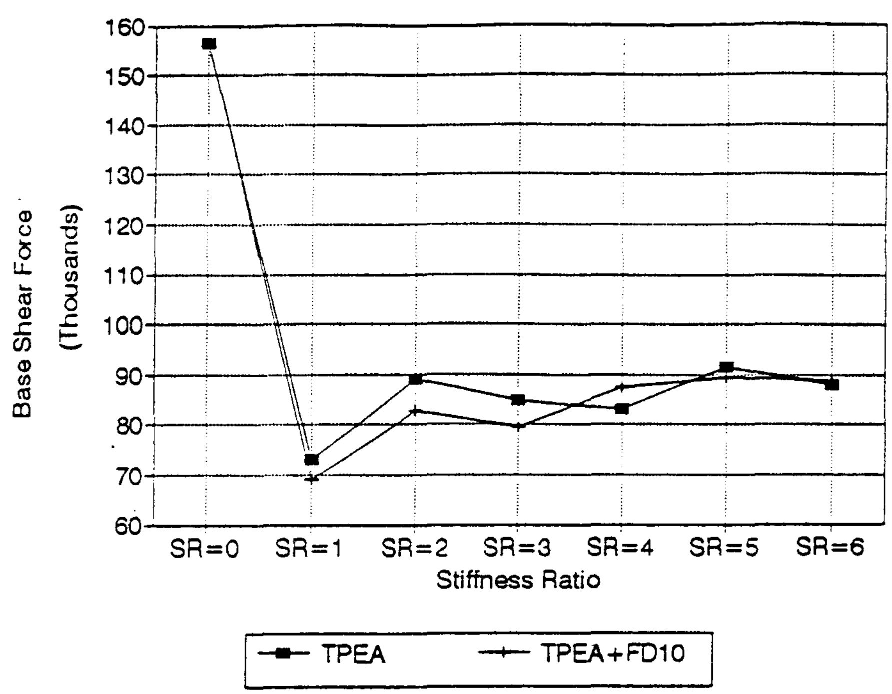

FIGURE 4-87 Comparison of SR Ratio and Base Shear Force When the Structure is Subjected to San Fearnando Ground Motion

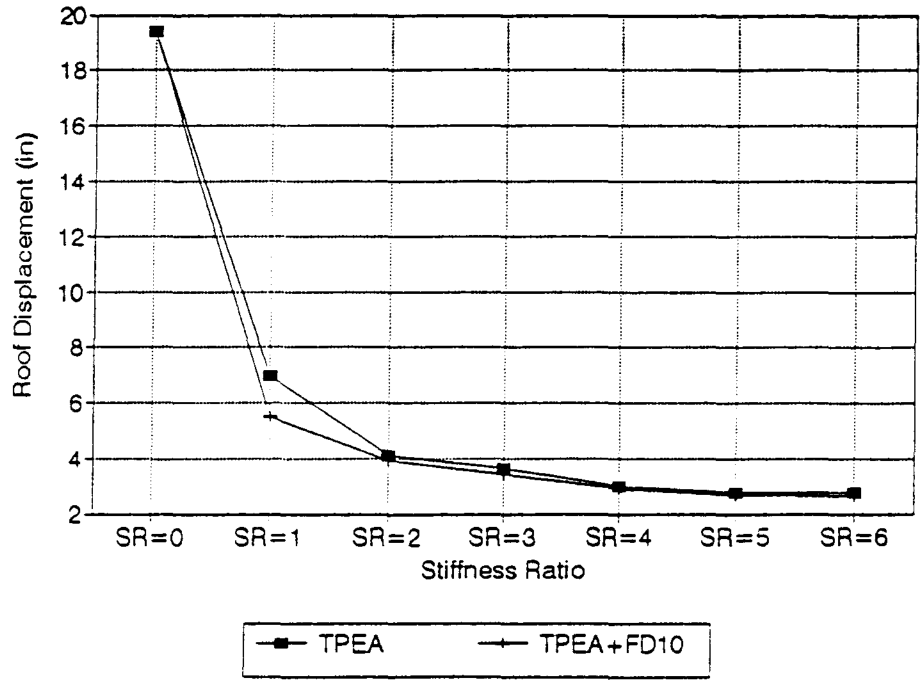

FIGURE 4-88 Comparison of SR Ratio and Roof Displacement When the Structure is Subjected to Taft (ERSF=4) Ground Motion

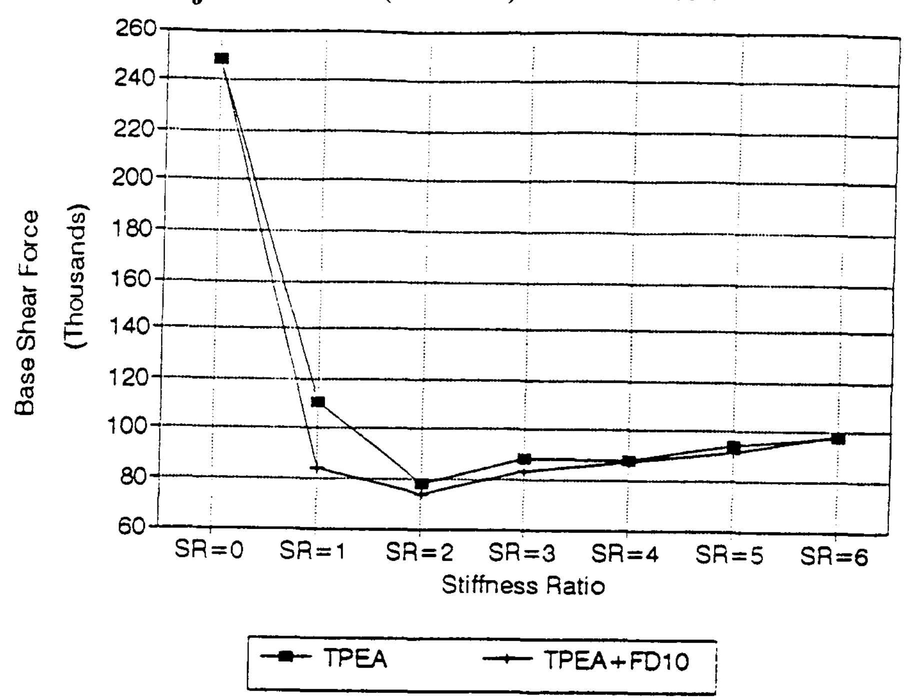

FIGURE 4-89 Comparison of SR Ratio and Base Shear Force When the Structure is Subjected to Taft (ERSF=4) Ground Motion

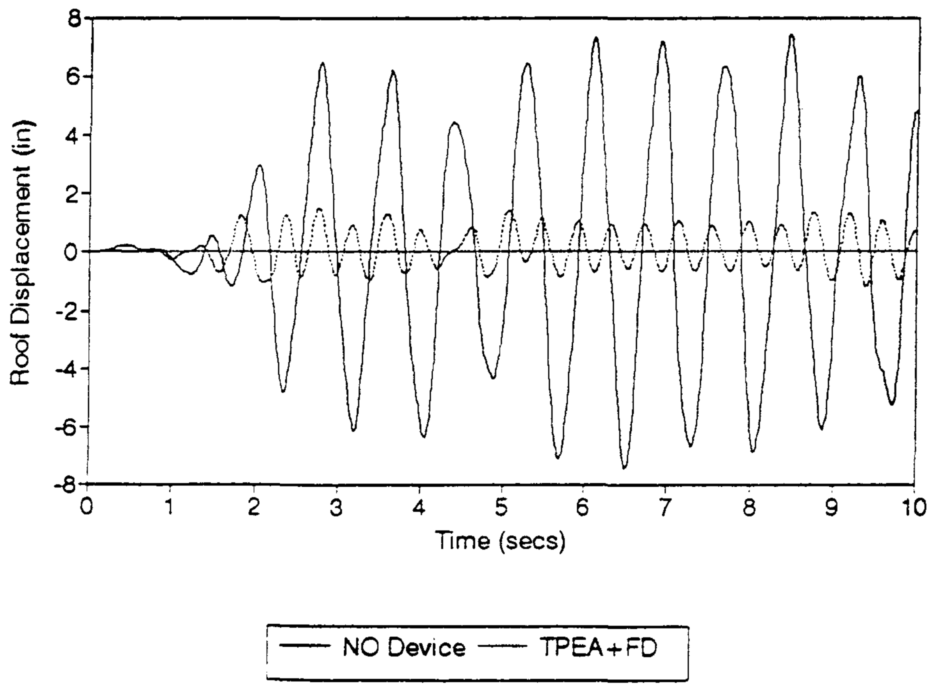

FIGURE 4-90 The Response of Roof Displacement of the Structure with TPEA and Fluid Dampers While the Structure is Subjected to El Centro Ground Motion

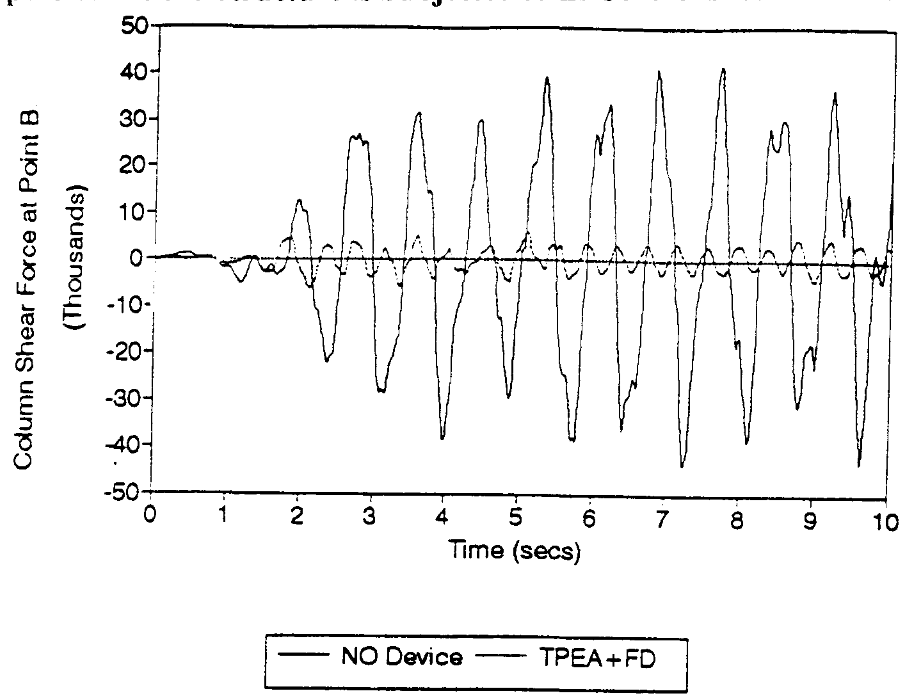

FIGURE 4-91 The Response of Column Shear Force at Point B of the Structure with TPEA and Fluid Dampers While the Structure is Subjected to El Centro Ground Motion

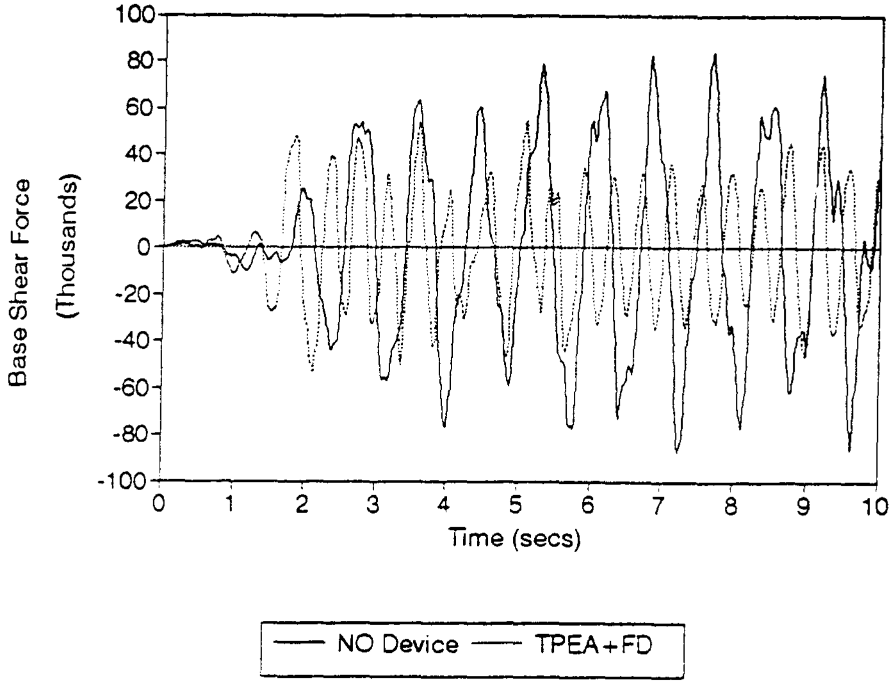

FIGURE 4-92 The Response of Base Shear Force of the Structure with TPEA and Fluid Dampers While the Structure is Subjected to El Centro Ground Motion

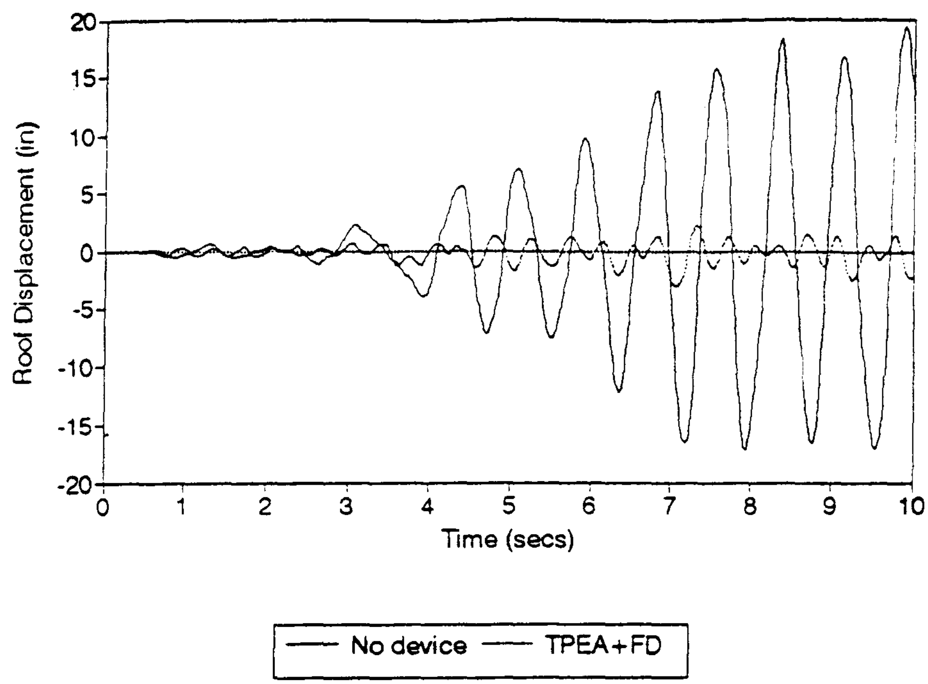

FIGURE 4-93 The Response of Roof Displacement of the Structure with TPEA and Fluid Dampers While the Structure is Subjected to Taft (ERSF=4) Ground Motion

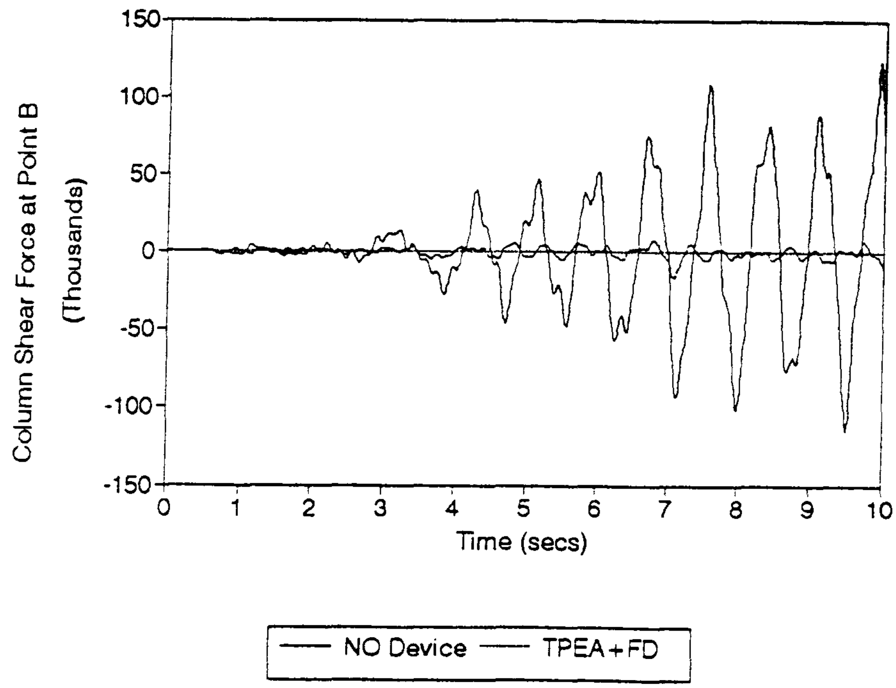

FIGURE 4-94 The Response of Column Shear Force at Point B of the Structure with TPEA and Fluid Dampers While the Structure is Subjected to Taft (ERSF=4) Ground Motion

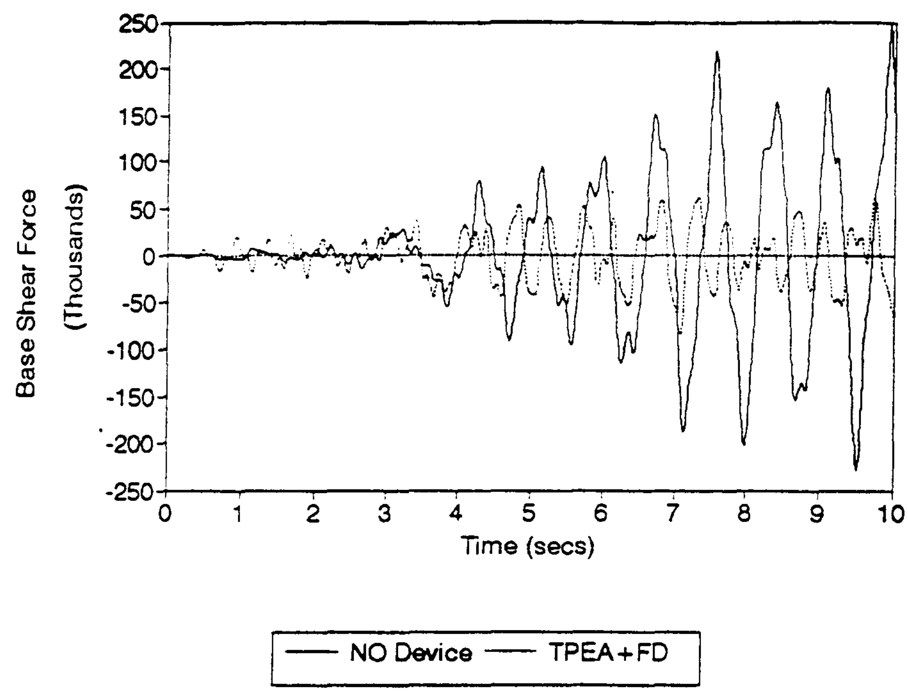

FIGURE 4-95 The Response of Base Shear Force of the Structure with TPEA and Fluid Dampers While the Structure is Subjected to Taft (ERSF=4) Ground Motion

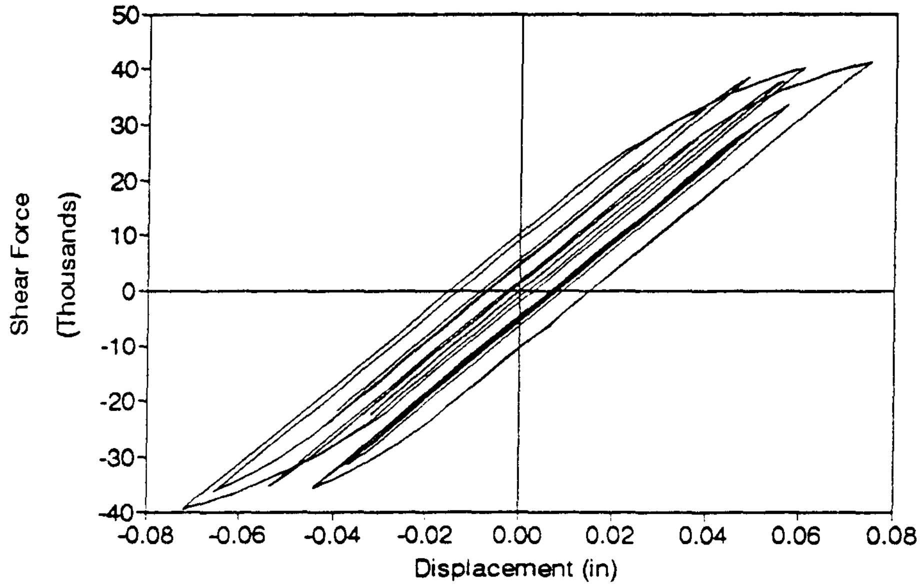

FIGURE 4-96 The Force-Displacement Relation of TPEA at 1st Floor While the Structure is Subjected to El Centro Ground Motion

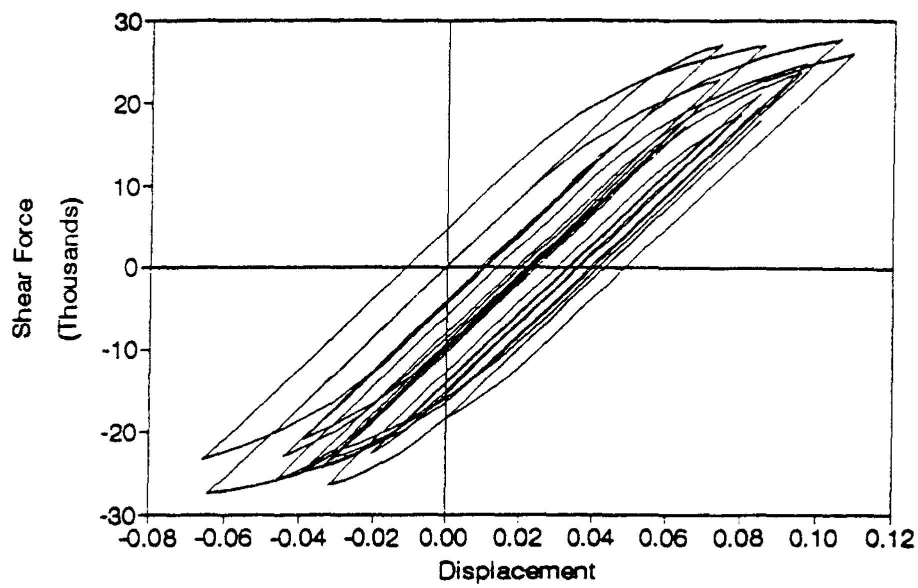

FIGURE 4-97 The Force-Displacement Relation of TPEA at 5th Floor While the Structure is Subjected to El Centro Ground Motion

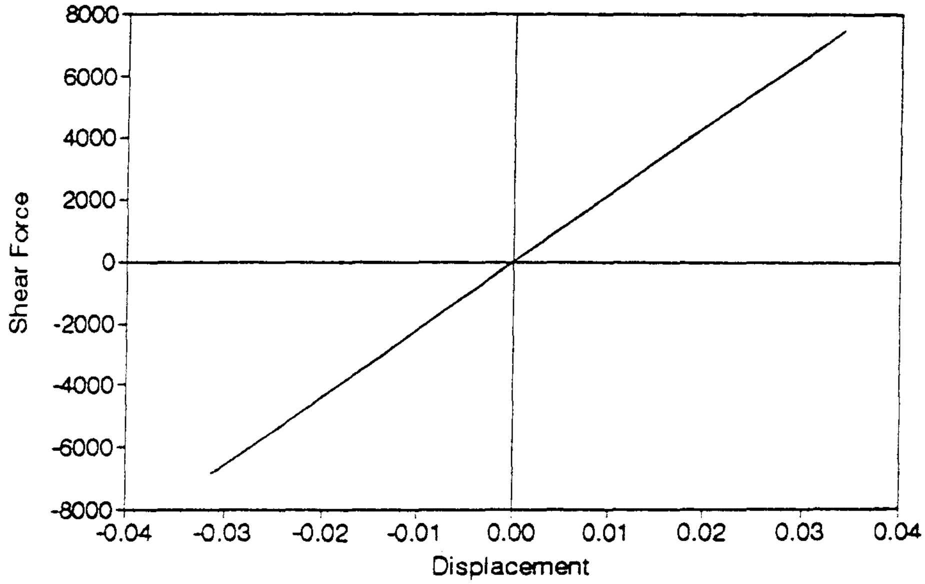

FIGURE 4-98 The Force-Displacement Relation of TPEA at 10th Floor While the Structure is Subjected to El Centro Ground Motion

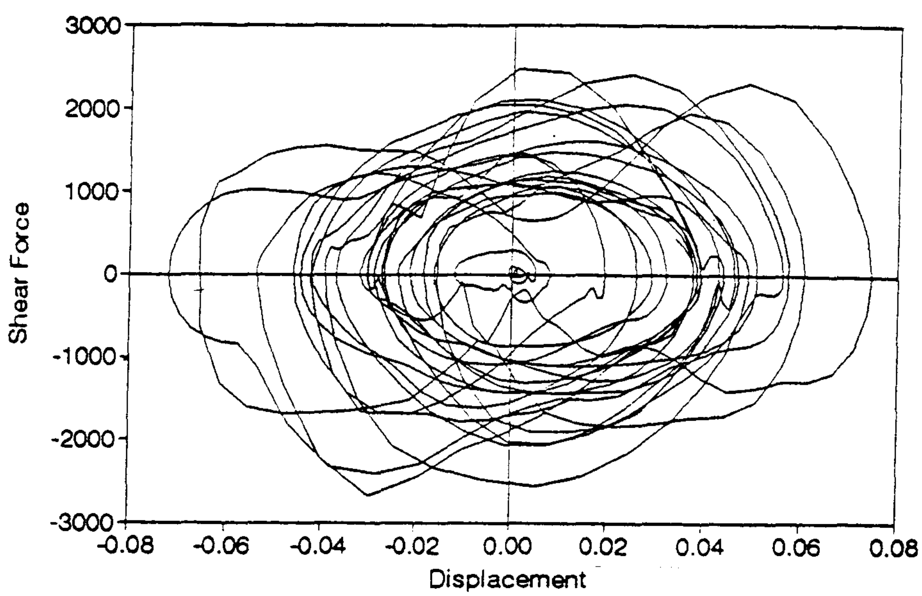

FIGURE 4-99 The Force-Displacement Relation of Fluid Dampers at 1st Floor While the Structure is Subjected to El Centro Ground Motion

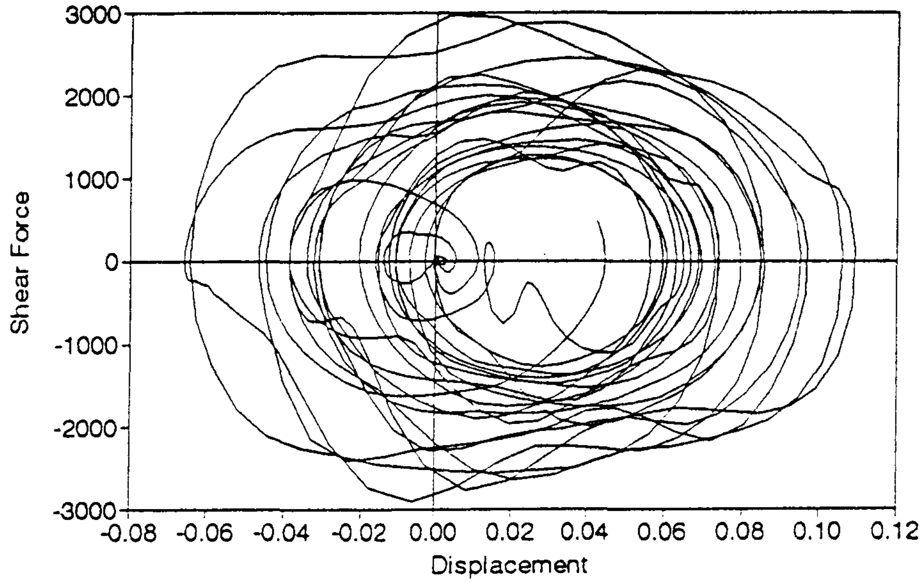

FIGURE 4-100 The Force-Displacement Relation of Fluid Dampers at 5th Floor While the Structure is Subjected to El Centro Ground Motion

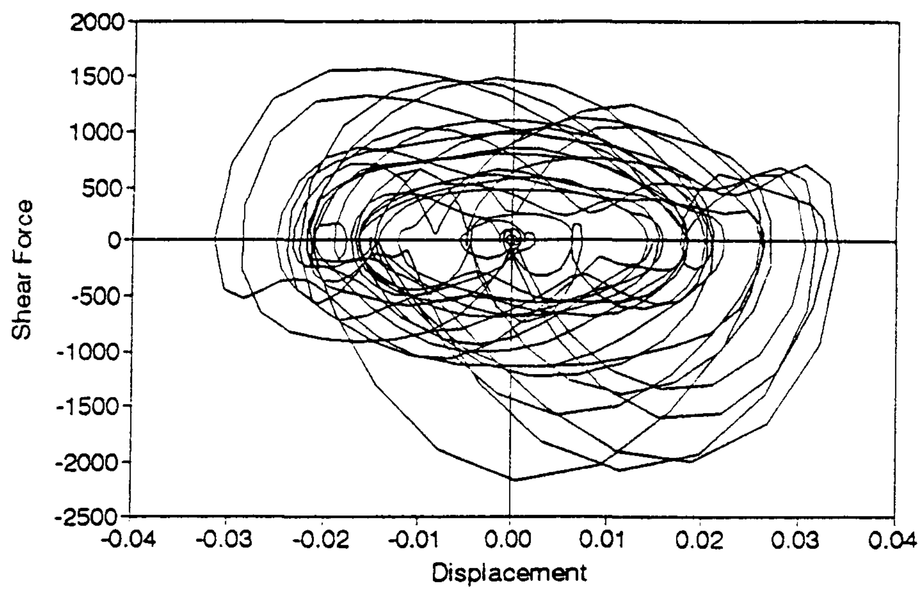

FIGURE 4-101 The Force-Displacement Relation of Fluid Dampers at 10th Floor While the Structure is Subjected to El Centro Ground Motion

each other's shortcomings to resist both earthquake and wind loads. Adding such devices to the structure may increase cost but it will increase the safety of the structure against earthquake and wind load. Moreover, adding energy-absorbing devices to the main load-carrying structural members could reduce the members' load carrying requirement and simplify the beam-column connections to offset the additional cost of the devices.

4.4 Design Implications

Based on the numerical results, some design implications can be concluded as follows:

(1) The damping coefficient of fluid dampers is a major factor for deciding damping force values. The results indicate that the structure with the high damping coefficient fluid dampers has better performance in seismic resistance. The damping value of 2400 lb-sec/in is a proper selection for this 10-story building in seismic resistance.

(2) According to the study of positional effects of fluid dampers, mounting a fluid damper on the first floor provides reliable performance for seismic resistance.

(3) If a proper damping coefficient is determined, the number of fluid dampers does not have a great influence in improving seismic resistance.

(4) Temperature has a minor effect on the behavior of the fluid dampers.

(5) Mounting viscoelastic dampers to all stories of the structure is not necessarily the most economical design. But adding a viscoelastic damper to the first floor will effectively reduce the response of the structure.

(6) It is recommended that the viscoelastic dampers be used in a relatively stable temperature environment.

(7) The thickness of the viscoelastic dampers should be carefully determined so that they will not be too small so as to induce large strain. At the same time, they should not be too large so as to reduce their performance and increase i their cost.

(8) There is no need to adopt large bracing members to support the TPEA because B/D ratios have little influence on improving seismic response. B/D ratios from 2 to 3 are recommended for the design of the TPEA devices.

(9) The bracing members should be strong enough to support the TPEA device without buckling in compression and yielding in tension.

(10) SR ratios from 2 to 4 are recommended for the design of the TPEA devices.

(11) The TPEA device's ductility ratios should be no larger than 6.

(12) The temperature effect becomes minor when combined devices are added to the structure.

(13) The TPEA devices play a governing role when the TPEA devices are jointly used with viscoelastic dampers or fluid dampers.

(14) The SR ratio =2 and B/D=2 are recommended for the combined devices.

(15) The damping value of fluid dampers can be reduced when fluid dampers and TPEA are jointly used.

(16) The property of viscoelastic dampers can be reduced when they are jointly used with the TPEA devices.

(17) The combined devices would provide a strong safe-failure mechanism and can compensate for each other device's shortcomings.

SECTION 5
Summary and Conclusion

5.1 Introduction

The concept behind passive vibration control is to add energy dissipating devices to a structure so that energy dissipation can be forced to occur at designated location in these passive control devices instead of the main load-carrying members [64]. These passive control devices can be easily replaced if extensively damaged during earthquakes. Adding energy-absorbing devices also provides additional damping to the structure. Moreover, adding energy-absorbing devices to the main load-carrying structural members could reduce the members' load carrying requirement and simplify the design of beam-column connections to offset the additional cost of the device [65].

The structural response of high-rise buildings mounted with three energy-absorbing devices, TPEA, viscoelastic dampers, fluid dampers, and two combined systems has been investigated in this study. The purposes of the investigation are to evaluate the performance of structures mounted with selected absorbing devices during three selected earthquake excitations and to identify the parameters that influence structural response so that a satisfactory design for seismic hazard mitigation of the structure with energy-absorbing devices can be achieved.

5.2 Limitations

The study considers only a typical 10-story frame in order to examine the relative merit of using single device vs. combined systems. No effort was given to consider the variations in effectiveness for a different number of devices and their locations. As pointed out earlier, this will require a significant effort on dynamic analyses of MDOF systems. The stiffness ratio of TPEA is defined as the ratio of the TPEA element initial stiffness to the structural story stiffness. Such a definition can be applied to multi-bay high-rise or low-rise structures. Therefore, SR ratios from 2 to 4 can be recommended not only for a one-bay 10-story structure but also for slender, high-rise structures. Generally speaking, the structural response of the low-rise building equipped with the added energy-absorbing devices can be reduced more significantly compared to that of the high-rise buildings equipped with the added energy-absorbing devices.

5.3 Computer Programs

Computer programs of the finite element formulations for TPEA, viscoelastic dampers, and fluid dampers are coded in Fortran language. They are on file in the structural dynamics laboratory at the State University of New York at Buffalo.

5.3.1 Computational Efficiency

The required CPU time in processing the computation on the viscoelastic dampers is less than three minutes for each job. It requires the longest time among the three systems considered.

The computational efficiency is considered satisfactory.

5.3.2 Structural Idealization of the 10-Story Building

The following approximations were made for the structural idealization of the 10-story frame which was used as a typical earthquake-resistant structure in this study. Each floor is modeled as a horizontal diaphragm. The diaphragm is assumed to have infinitely in-plane stiffness [77]. The out-of-plane stiffness of this diaphragm is neglected. Therefore, each column at every floor has two degrees of freedom, a vertical displacement and a rotation. In addition, there is one lateral degree of freedom at every floor level of the frame. Bending stiffness of the floors may be included approximately in the modeling of the individual frames. Floor level must be the same for all frames. Each floor acts as a rigid horizontal diaphragm in its own plane, so that the horizontal displacements of all points in the plane of the diaphragm are uniquely determined by two translations and one rotation of each floor. In accordance with this assumption, the beams are assumed to bend only normal to the floor slab, and to have no axial deformation [78].

5.3.3 Solution of Equilibrium Equations

The Newmark Method, one of the direct integration methods, was chosen as a numerical step-by-step procedure for the solution of equilibrium equations. The term "direct" means that prior to the numerical integration, no transformation of the equations into a different form is carried out [79]. The two parameters α and δ can be varied to obtain optimum stability and accuracy. The integration scheme is unconditionally stable provided that $\delta \geq 0.5$ and $\alpha \geq 0.25\,(\delta + 0.5)^2$. In this study, $\delta = 0.5$ and $\alpha = 0.25$ were chosen in order to have the most desirable accuracy of the results.

5.4 Conclusions

Energy-absorbing devices can be divided into static dampers and dynamic dampers. The TPEA devices are considered to be static dampers and the viscoelastic dampers and fluid dampers are considered to be dynamic dampers. TPEA devices are designed to yield earlier than the main load-carrying members during earthquakes so that the energy can be dissipated. On the other hand, viscoelastic dampers and fluid dampers are both made from strain-rate dependent material so their resisting force is proportional to the velocity. To absorb energy, a device must generate a resisting force, F, that acts over a certain displacement, s.

The energy absorbed, U, is given by [56]

$$U = \int_0^s F dx \tag{5.1}$$

If the resisting force is proportional to the velocity, the maximum force and maximum displacement will never be achieved at the same time. When the structural displacements approach the maximum, the structural velocities approach zero. The structural response cannot be reduced significantly in the early stages of an earthquake if fluid dampers and viscoelastic dampers are adopted as energy-absorbing devices.

Generally speaking, weight of the structure is a detriment in seismic design while weight is a favorable factor against wind forces [55]. To overcome the conflicts in structural design for wind loads and earthquake, a combination of TPEA and viscoelastic dampers and a combination of TPEA and fluid dampers are studied. TPEA has little effect on the reduction of structural accelerations induced by wind loads because it still typically operates in the elastic range when the structure is subjected to wind forces.

Controlling the acceleration of the structure is more important in the design against wind loads while controlling the displacement of the structure is more important in the design against earthquakes. Under the wind loads or minor earthquakes, adding TPEA to the structure does not change the acceleration of the structure. The reason can be explained by the following equations.

Assume an undamped SDOF system subjected to a harmonically impact load of amplitude P_0 as shown by the equation of motion [57]

$$m\ddot{v}(t) + k\dot{v}(t) = P_o u(t) \tag{5.2}$$

The response to the excitation of the undamped system becomes

$$v(t) = \frac{P_o}{k} R(t) \tag{5.3}$$

where R(t) is the response ratio. The acceleration can be expressed as

$$a(t) = w^2 v(t) = w^2 \frac{P_o}{k} R(t) \tag{5.4}$$

because

$$w^2 = \frac{k}{m} \tag{5.5}$$

therefore

$$a(t) = w^2 v(t) = \frac{k}{m}\frac{P_o}{k} R(t) = \frac{P_o}{m} R(t) \tag{5.6}$$

Eq. (5.6) shows that adding TPEA is equivalent to providing additional stiffness to the structure. Thus, it has little influence on controlling the acceleration of the structure. On the other hand, viscoelastic dampers and fluid dampers can provide additional damping to the structure under wind loads.

Under the limitations described earlier, using combined static dampers and dynamic dampers on the 10-story frame shows that the shortcomings of individual dampers can be minimized. Under wind loads, the weakness of the TPEA will be compensated for by the addition of viscoelastic dampers or fluid dampers to the structure. Under moderate or severe earthquakes, the weakness of dynamic dampers will be avoided by adding TPEA to the structure. By adding TPEA and fluid dampers or TPEA and viscoelastic dampers to the structure, a more economical design for each device is possible and better performance of the structure can be obtained. TPEA also provides a reliable safe-fail mechanism to the structure. Numerical results of this study show that the combined system can sustain a wider range of loadings, from wind load, minor earthquakes to severe ground motions, than single device can provide.

As pointed out in the section of limitations, an important future research area is to generalize the conclusions of this study. At present it is not possible to make general statement among the various schemes of different devices/combined systems without a better understanding of the dynamic responses of MDOF systems that may contain different number of added dampers/ devices at different locations.

A scaled-down model of the structure equipped with the combined devices of TPEA and fluid dampers or viscoelastic dampers tested on a shaking table will be an important research project to verify further the promising applications for seismic and wind load hazard mitigations.

SECTION 6
References

[1] Krinitzsky, E.L., Gould, J.P., and Edinger, P.H. (1993). "Fundamentals of earthquake resistant construction." John Wiley & Sons, Inc., New York.

[2] Uang, C.M. and Bertero, V.V. (1988). "Use of energy as a design criterion in earthquake-resistant design." Report No. UCB/EERC-88/18, Earthq. Engrg. Res. Ctr., Univ. of California at Berkeley, California.

[3] Soong, T.T. and Manolis, G.D. (1987). "Active structures." J. Struct. Engrg., ASCE, 113(11), 2290-2302.

[4] Soong, T.T. (1990). "Active structural control: Theory & Practice." John Wiley & Sons, Inc., New York.

[5] Warburton, G.B. (1992). "Reduction of vibrations." John Wiley & Sons, Inc., New York.

[6] Chung, L.L., Reinhorn, A.M., and Soong, T.T. (1988). "Experiments on active control of seismic structures." J. Engrg. Mechanics, ASCE, 114(2), 241-255.

[7] Kobori, T., Koshiska, N., and Yamada, Y. and Ikeda, Y. (1991). "Seismic-response-controlled structure with active mass driver system. Part 1: Design." Earthq. Engrg. Strct. Dyn., Vol. 20, 133-149.

[8] Kobori, T., Koshiska, N., and Yamada, Y. and Ikeda, Y. (1991). "Seismic-response-controlled structure with active mass driver system. Part 2: Verification." Earthq. Engrg. Strct. Dyn., Vol. 20, 151-166.

[9] Kobori, T. (1990). "Technology development and forecast of dynamic intelligent building (DIB)." Intelligent Structures. (Editors: Chong, K.P., Liu, S.C., and Li, J.C.), Elsevier Applied Science, London, 42-59.

[10] Skinner, R.I., Robinson, W.H., and McVervy, G.H. (1993). "An introduction to seismic isolation." John Wiley & Sons, Inc., New York.

[11] Buckle, I.G. (1986). "Development and application of base isolation and passive energy dissipation: A world overview." Proceedings of a seminar and workshop on base isolation and passive energy dissipation ATC-17. Applied Technology Council, San Francisco, California, 153-174.

[12] Kelly, J.M. (1993). "State-of-the-art and state-of-the practice in base isolation." Proceedings of seminar on seismic isolation, passive energy dissipation, and active control, ATC-17-1. Applied Technology Council, San Francisco, California.

[13] Pall, A.S., Marsh, C., (1982). "Response of friction damped braced frames." J. Strct. Engrg., ASCE, Vol. 108, No. ST6, 1313-1323.

[14] Aiken, I.D., Kelly, J.M. and Pall, A.S. (1988). "Seismic response of a nine-story steel frame with friction damped cross-bracing." Earthq. Engng. Res. Ctr., Univ. of California at Berkeley: 1988 (Report No. UCB/EERC-88-17), 1-7.

[15] Pall, A.S., Ghorayeb, F., and Pall, R. (1991). "Friction dampers for rehabilitation of Ecole Polyvalente at Sorel, Quebec." Proc., 6th Canadian Conf. on Earthq. Engng. Toronto, Canada, 389-396.

[16] Pekau, O.A., Guimond, R. (1991). "Controlling seismic response of eccentric structures by friction dampers." Earthq. Engng. Struct. Dyn., Vol. 20, 505-521.

[17] Skinner, R.I., Kelly, J.M. and Heine, A.J. (1975). "Hysteretic dampers for earthquake-resistant structures." Earthq. Engng. Struct. Dyn., Vol. 3, 287-296.

[18] Kelly, J.M. and Skinner, M.S.(1980). "The design of steel energy- absorbing restrainers and their incorporation into nuclear power plants for enhanced safety (vol.2): Development and testing of restraints for nuclear piping system." Report No. UCB/EERC-80/21, Earthq. Engng. Res. Ctr., Univ. of California at Berkeley, California.
[19] Stiemer, S.F. and Chow, F.L. (1984). "Curved plate energy absorbers for earthquake resistant structures." Proc., 8th World Conf. on Earthq. Engng. Earthq. Engng. Res. Institute, Oakland, California, Vol. V, 967-974.
[20] Whittaker, A.S., Bertero, V.V., Alonso, L.J. and Thompson, C. (1989). "Earthquake simulator testing of steel plate added damping and stiffness elements." Report No. UCB/EERC-89/02, Earthq. Engng. Res. Ctr., Univ. of California at Berkeley, California.
[21] Bergman, D.M. and Hanson, R.D. (1990). "Viscoelastic versus steel plate mechanical damping devices: An experimental comparison." Proc. 4th U.S. Nat. Conf. on Earthq. Engng., Earthq. Engng. Res. Institute, Oakland, California, Vol. III, 469-477.
[22] Tsai, K.C. and Hong, C.P. (1992). "Steel triangular plate energy absorbers for earthquake buildings." First World Conference on Construction Steel Design, Mexico.
[23] Constantionu, M.C. and Symans, M.D. (1992). "Experimental and analytical investigation of seismic of structures with supplemental fluid viscous dampers." Report No. NCEER-92-0032, National Center for Earthquake Engineering Research, SUNY at Buffalo, New York.
[24] Mahmoodi, P. (1972). "Structural Dampers." J. of the Structural Division, ASCE, 95(8), 1661-1672.
[25] Zhang, R.H., Soong, T.T. and Mahmoodi, P. (1989). "Seismic response of steel frame structures with added viscoelastic dampers." Earthq. Engng. Struct. Dyn., 18(3), 389-396.
[26] Aiken, I.D., Kelly, J.M. and Mahmoodi, P. (1990). "The application of viscoelastic dampers to seismically resistant structures." Proc., 4th U.S. Nat. Conf. on Earthq. Engng., Palm Springs, California, Vol. III, 459-468.
[27] Zhang, R.H. and Soong, T.T. (1992). "Seismic design of viscoelastic dampers for structural applications." J. Struct. Engng., ASCE, 118(5), 1375-1392.
[28] Tsai, C.S. (1993). "Innovative design of viscoelastic dampers for seismic mitigation." Nuclear Engineering and Design, 139, 83-106.
[29] Pall, A.S. and Marsh, C. (1984). "Response of friction damped buildings." Proceedings of the Eighth World Conference on Earthquake Engineering, San Francisco, Vol. V, 1007-1014.
[30] Pall, A.S. and Marsh, C. (1981). "Friction damped concrete shear walls." J. American Concrete Institute, No. 3, Vol. 78, 344-357.
[31] Pall, A.S., Marsh, C., and Fazio, P. (1980), "Friction joints for seismic control of large panel structures." J. Prestressed Concrete Institute, Vol. 25, No. 6, 38-61.
[32] Pall, A.S. (1986). "Energy-dissipation devices for aseismic design of buildings." Proceedings of a seminar and workshop on base isolation & passive energy dissipation, ACT-17, San Fransisco, California, March 12-14, 1986, 39-50.
[33] Filiatrault, A. and Cherry, S. (1985). "Performance evaluation of friction damped braced steel frames under simulated earthquake loads." Report of Earthquake Engineering Research Laboratory, Univ. of British Columbia, Vancouver, Canada.
[34] Aiken, I.D. and Kelly, J.M. (1988). "Experimental study of friction damping for steel frame structures." Proc. PVP Conference, ASME, Pittsburgh, PA, Vol. 133, 95-100.

[35] Fujita, K. and Kokubo, E. (1991). "Development of friction dampers as a aseimic support for the piping system in nuclear power plants." PVP Vol. 211, Active and Passive, ASME 1991, 57-62.
[36] Hanson, R.D. (1988)"Energy dissipation system." Structural Engineering Association of California Convention, October, Kona, Hawaii.
[37] Scholl, R.E. (1988). "Added damping and stiffness elements for earthquake damage and loss control." Proceeding of conference XLI: A review of earthquake research applications in the national earthquake hazards reduction program: 1977-1987. U.S. Geological Survey Open File, Report 88-13-A, San Diego, California.
[38] Ross, D., Ungar, E.E., and Kerwin, E.W. (1959). "Damping of plate flexural vibrations by means of viscoelastic laminar." Structural Damping. (Editor: Ruzicka, E.J.), ASME, New York, 49-97.
[39] Gehling, R.N. (1987). "Large space structure damping treatment performance: analytic and test results." Role of damping in vibration and noise control. ASME. 93-100.
[40] Morgenthaler, D.R. (1987). "Design and analysis of passive damped large space structures." Role of damping in vibration and noise control. ASME, New York, 1-8.
[41] Lin, R.C., Liang, Z., Soong, T.T. and Zhang, R.H. (1991). "An experimental study on seismic behavior of viscoelastic damped structures." Engineering Structures, Vol. 13. 75-84.
[42] Keel, C.J. and Mahmoodi, P. (1986). "Design of viscoelastic dampers for Columbia center building." Building motion in wind. (Editor: Isyumov, N. and Tschanz, T.) ASCE, New York, 66-82.
[43] Chang, K.C., Soong, T.T., Oh, S.T., and Lai, M.L. (1991). "Seismic response of 2/5 scale steel structure with added viscoelastic dampers." Report No. NCEER-91-0012, National Center for Earthquake Engineering Research, Buffalo, New York.
[44] Tseng, N.T. and Lee, G.C. (1983). "Simple plasticity model of two-surface." J. Engrg. Mech., ASCE, Vol. 109, No.3, 795-810.
[45] Chen, F.S. and Powell, H. (1982). "Generalized plastic hinge concepts for 3D beam-column elements." Report No. UCB/EERC-82/20. Earthq. Engrg. Res. Ctr., University of California, Berkerly, California.
[46] Tseng, N.T. (1981). "Inelastic finite strain analysis of structure metals subjected to nonproportional loadings." Ph.D. dissertation, State University of New York at Buffalo, New York.
[47] Bodeggwig, E. (1959). "Matrix Calculus." North-Holland Publishing Company. Amsterdam, Holland.
[48] Phillips, A. and Lee, C.W. (1979). "Yield surfaces and loading surfaces: experiments and recommendations." International Journal of Solids and Structures, Vol. 15, 715-729.
[49] Tsai, C.S. and Tsai, K.C. (1992). "ADAS devices for seismic mitigation of high-rise buildings." Workshop on base isolation and energy dissipation techniques for structures, Taipei, Taiwan, Oct. 2, 1992.
[50] Tsai, C.S. and Lee, G.C. (1993). "A new design of viscoelastic energy dissipaters." NCEER Bulletin, Vol. 7, No. 2, 6-9.
[51] Bagley, R.L. and Torvik, P.J. (1983). "A theoretical basis for the application of fractional calculus to viscoelasticity." Journal of Rheology, 27(3), 201-210.
[52] Bagley, R.L. and Torvik, P.J. (1983). "Fractional calculcus - a different approach to the analysis of viscoelastically damped structures." AIAA Journal, Vol. 21, No. 5, 741-748.
[53] Bird, R.B., Armstrong, R.C. and Hassager, O. (1987). "Dynamics of polymeric liquids." J. Wiley and Sons, New York.

[54] Markris, N. and Constantinou, M.C. (1991). "Fractional derivative Maxwell model for viscous dampers." J. Struct. Engrg., ASCE, 117(9), 2708-2724.
[55] Crawley, S.W. and Ward, D.B. (1990). "Seismic and wind loads in architectural design." The American Institute of Architects, Washington, D.C.
[56] Kelly, J.M. and Skinner, M.S. (1979). "A review of current uses of energy-absorbing devices." Report No. UCB/EERC-79/10, Earthq. Engrg. Res. Ctr. Univ. of California at Berkeley, California
[57] Clough, R.W. and Penzien, J. (1993). "Dynamics of Structures." McGraw-Hill, Inc.
[58] Aiken, I.D. and Kelly, J.M. (1990). "Earthquake simulator testing and analytical studies of two energy-absorbing systems for multistory structures." Report No. UCB/EERC-90/03, Earthq. Engrg. Res. Ctr. Univ. of California at Berkeley, California
[59] Wen, C.Y. (1988). "Vibration protection of inelastic structures by means of active and passive control." A dissertation submitted in partial fulfillment for the degree of Doctor of Philosophy, SUNY at Buffalo, New York.
[60] Malushte, S.R. and Singh, M.P. (1989). "A study of seismic response characteristics of structures with friction damping." Earthquake Engineering and Structural Dynamics. Vol. 18, 767-783.
[61] Stiemer, S.F. and Chow, F.L. (1984). "Curved plate energy absorbers for earthquake resistant structures." Proceedings of the Eighth World Conference on Earthquake Engineering. San Francisco, California. Prentice-Hall, Inc., Englewood Cliffs, New Jersey, Vol. V, 967-975.
[62] Symans, M.D. (1992). "Experimental and analytical investigation of seismic response of structures with supplemental fluid viscous dampers." A thesis submitted in partial fulfillment for the degree of master of science, SUNY at Buffalo.
[63] Tsai, C.S. and Lee, H.H. (1992). "Applications of viscoelastic dampers to bridges for seismic mitigation." ASME Pressure Vessels and Piping Conference, New Orleans PVP-Vol. 229, 113-118.
[64] Kelly, J.M., Skinner, R.I. and Heine, A.J. (1972). "Mechanisms of energy absorption in special devices for use in earthquake resistant structures." Bulletin of New Zealand National Society for Earthquake Engineering, Vol, 5, No. 3.
[65] Skinner, R.I., Kelly, J.M. and Heine, A.J. (1973). "Energy absorption devices for earthquake resistant structures." Proceedings of Fifth World Conference on Earthquake Engineering. Vol. 2, 2924-2933.
[66] Tsai, C.S. and Tsai, K.C. (1994). "TPEA device as seismic damper for high-rise buildings." Journal of Engineering Mechanics, ASCE in press.
[67] Tsai, C.S. and Lee, H.H. (1993). "Applications of viscoelastic dampers to high-rise buildings." Journal of Structural Engineering, ASCE, Vol. 119, No.4, 1222-1230.
[68] Cassaro, M.A. and Martinez-Romero, E. (1987). "The Mexico Earthquakes-1985: factors involved and lessons learned." Proceedings of the International Conference on 1985 Mexico Earthquake; Camino Real Hotel, Mexico City, September 19-21, 1986. ASCE, New York, v-vii.
[69] Tsai, C.S. and Lee, H.H. (1993). "Seismic mitigation of bridges by using viscoelastic dampers." Computers and Structures, 48(4), 719-727.
[70] Soong, T.T. and Reinhorn A.M. (1993). "Case studies of active control and implemental issues." Proceedings of seminar on seismic isolation, passive energy dissipation, and active control, ATC-17-1. Applied Technology Council, San Francisco, California.

[71] Tsai, C.S. (1994). "Temperature effect of viscoelastic dampers during earthquakes." Journal of Structural Engineering. ASCE, 120(2), 394-409.

[72] Soong, T.T. and Mahmoodi, P. (1990). "Seismic behavior of structures with added viscoelastic dampers." Proceedings of fourth U.S. National Conference on Earthquake Engineering. May 20-24, 1990, Palm Springs, California, Vol. 3. 499-506.

[73] Lee, G.C, Chang, K.C, Yao, G.C., Hao, D.S., and Yeh, Y.C. (1990). "Dynamic behavior of a prototype and a 2/5-scale steel frame structure." Proceedings of 4th U.S. National Conference on Earthquake Engineering, Vol. 2, 605-613.

[74] Oh, S.T. (1992) "Seismic behavior of a 2/5-scale steel structure with added viscoelastic dampers." A dissertation submitted in partial fulfillment for the degree of Doctor of Philosophy, SUNY at Buffalo, New York.

[75] Yao, G.C. (1991). "Diagnostic studies of steel structure through vibrational signature analysis." A dissertation submitted in partial fulfillment for the degree of Doctor of Philosophy, SUNY at Buffalo, New York.

[76] Zahrah, T.F. (1982). "Seismic energy absorption in simple structures." A dissertation submitted in partial fulfillment for the degree of Doctor of Philosophy, University of Illinois at Urbana-Champaign.

[77] Wilson, E.L., Dovey, H.H. and Habibullah, A. (1980). "Three dimensional analysis of building systems TABS80, Vol 1, Theoretical Manual." A report to the U.S. Army Engineer Waterways Experiment Station, Vicksburg, Mississippi.

[78] Guendelman-Israel, R. and Powell, G.B. (1977). "Drain-Tabs: A computerized program for inelastic earthquake response of three-dimensional buildings." Report No. UCB/EERC-77/08, Earthq. Engrg. Res. Ctr. Univ. of California at Berkeley, California.

[79] Bathe, K.J. (1982). "Finite Element Procedures in Engineering Analysis." Prentice-Hall, Inc. Englewood Cliffs, New Jersey.

NATIONAL CENTER FOR EARTHQUAKE ENGINEERING RESEARCH
LIST OF TECHNICAL REPORTS

The National Center for Earthquake Engineering Research (NCEER) publishes technical reports on a variety of subjects related to earthquake engineering written by authors funded through NCEER. These reports are available from both NCEER's Publications Department and the National Technical Information Service (NTIS). Requests for reports should be directed to the Publications Department, National Center for Earthquake Engineering Research, State University of New York at Buffalo, Red Jacket Quadrangle, Buffalo, New York 14261. Reports can also be requested through NTIS, 5285 Port Royal Road, Springfield, Virginia 22161. NTIS accession numbers are shown in parenthesis, if available.

NCEER-87-0001 "First-Year Program in Research, Education and Technology Transfer," 3/5/87, (PB88-134275).

NCEER-87-0002 "Experimental Evaluation of Instantaneous Optimal Algorithms for Structural Control," by R.C. Lin, T.T. Soong and A.M. Reinhorn, 4/20/87, (PB88-134341).

NCEER-87-0003 "Experimentation Using the Earthquake Simulation Facilities at University at Buffalo," by A.M. Reinhorn and R.L. Ketter, to be published.

NCEER-87-0004 "The System Characteristics and Performance of a Shaking Table," by J.S. Hwang, K.C. Chang and G.C. Lee, 6/1/87, (PB88-134259). This report is available only through NTIS (see address given above).

NCEER-87-0005 "A Finite Element Formulation for Nonlinear Viscoplastic Material Using a Q Model," by O. Gyebi and G. Dasgupta, 11/2/87, (PB88-213764).

NCEER-87-0006 "Symbolic Manipulation Program (SMP) - Algebraic Codes for Two and Three Dimensional Finite Element Formulations," by X. Lee and G. Dasgupta, 11/9/87, (PB88-218522).

NCEER-87-0007 "Instantaneous Optimal Control Laws for Tall Buildings Under Seismic Excitations," by J.N. Yang, A. Akbarpour and P. Ghaemmaghami, 6/10/87, (PB88-134333). This report is only available through NTIS (see address given above).

NCEER-87-0008 "IDARC: Inelastic Damage Analysis of Reinforced Concrete Frame - Shear-Wall Structures," by Y.J. Park, A.M. Reinhorn and S.K. Kunnath, 7/20/87, (PB88-134325).

NCEER-87-0009 "Liquefaction Potential for New York State: A Preliminary Report on Sites in Manhattan and Buffalo," by M. Budhu, V. Vijayakumar, R.F. Giese and L. Baumgras, 8/31/87, (PB88-163704). This report is available only through NTIS (see address given above).

NCEER-87-0010 "Vertical and Torsional Vibration of Foundations in Inhomogeneous Media," by A.S. Veletsos and K.W. Dotson, 6/1/87, (PB88-134291).

NCEER-87-0011 "Seismic Probabilistic Risk Assessment and Seismic Margins Studies for Nuclear Power Plants," by Howard H.M. Hwang, 6/15/87, (PB88-134267).

NCEER-87-0012 "Parametric Studies of Frequency Response of Secondary Systems Under Ground-Acceleration Excitations," by Y. Yong and Y.K. Lin, 6/10/87, (PB88-134309).

NCEER-87-0013 "Frequency Response of Secondary Systems Under Seismic Excitation," by J.A. HoLung, J. Cai and Y.K. Lin, 7/31/87, (PB88-134317).

NCEER-87-0014 "Modelling Earthquake Ground Motions in Seismically Active Regions Using Parametric Time Series Methods," by G.W. Ellis and A.S. Cakmak, 8/25/87, (PB88-134283).

NCEER-87-0015 "Detection and Assessment of Seismic Structural Damage," by E. DiPasquale and A.S. Cakmak, 8/25/87, (PB88-163712).

NCEER-87-0016 "Pipeline Experiment at Parkfield, California," by J. Isenberg and E. Richardson, 9/15/87, (PB88-163720). This report is available only through NTIS (see address given above).

NCEER-87-0017 "Digital Simulation of Seismic Ground Motion," by M. Shinozuka, G. Deodatis and T. Harada, 8/31/87, (PB88-155197). This report is available only through NTIS (see address given above).

NCEER-87-0018 "Practical Considerations for Structural Control: System Uncertainty, System Time Delay and Truncation of Small Control Forces," J.N. Yang and A. Akbarpour, 8/10/87, (PB88-163738).

NCEER-87-0019 "Modal Analysis of Nonclassically Damped Structural Systems Using Canonical Transformation," by J.N. Yang, S. Sarkani and F.X. Long, 9/27/87, (PB88-187851).

NCEER-87-0020 "A Nonstationary Solution in Random Vibration Theory," by J.R. Red-Horse and P.D. Spanos, 11/3/87, (PB88-163746).

NCEER-87-0021 "Horizontal Impedances for Radially Inhomogeneous Viscoelastic Soil Layers," by A.S. Veletsos and K.W. Dotson, 10/15/87, (PB88-150859).

NCEER-87-0022 "Seismic Damage Assessment of Reinforced Concrete Members," by Y.S. Chung, C. Meyer and M. Shinozuka, 10/9/87, (PB88-150867). This report is available only through NTIS (see address given above).

NCEER-87-0023 "Active Structural Control in Civil Engineering," by T.T. Soong, 11/11/87, (PB88-187778).

NCEER-87-0024 "Vertical and Torsional Impedances for Radially Inhomogeneous Viscoelastic Soil Layers," by K.W. Dotson and A.S. Veletsos, 12/87, (PB88-187786).

NCEER-87-0025 "Proceedings from the Symposium on Seismic Hazards, Ground Motions, Soil-Liquefaction and Engineering Practice in Eastern North America," October 20-22, 1987, edited by K.H. Jacob, 12/87, (PB88-188115).

NCEER-87-0026 "Report on the Whittier-Narrows, California, Earthquake of October 1, 1987," by J. Pantelic and A. Reinhorn, 11/87, (PB88-187752). This report is available only through NTIS (see address given above).

NCEER-87-0027 "Design of a Modular Program for Transient Nonlinear Analysis of Large 3-D Building Structures," by S. Srivastav and J.F. Abel, 12/30/87, (PB88-187950).

NCEER-87-0028 "Second-Year Program in Research, Education and Technology Transfer," 3/8/88, (PB88-219480).

NCEER-88-0001 "Workshop on Seismic Computer Analysis and Design of Buildings With Interactive Graphics," by W. McGuire, J.F. Abel and C.H. Conley, 1/18/88, (PB88-187760).

NCEER-88-0002 "Optimal Control of Nonlinear Flexible Structures," by J.N. Yang, F.X. Long and D. Wong, 1/22/88, (PB88-213772).

NCEER-88-0003 "Substructuring Techniques in the Time Domain for Primary-Secondary Structural Systems," by G.D. Manolis and G. Juhn, 2/10/88, (PB88-213780).

NCEER-88-0004 "Iterative Seismic Analysis of Primary-Secondary Systems," by A. Singhal, L.D. Lutes and P.D. Spanos, 2/23/88, (PB88-213798).

NCEER-88-0005 "Stochastic Finite Element Expansion for Random Media," by P.D. Spanos and R. Ghanem, 3/14/88, (PB88-213806).

NCEER-88-0006 "Combining Structural Optimization and Structural Control," by F.Y. Cheng and C.P. Pantelides, 1/10/88, (PB88-213814).

NCEER-88-0007 "Seismic Performance Assessment of Code-Designed Structures," by H.H-M. Hwang, J-W. Jaw and H-J. Shau, 3/20/88, (PB88-219423).

NCEER-88-0008 "Reliability Analysis of Code-Designed Structures Under Natural Hazards," by H.H-M. Hwang, H. Ushiba and M. Shinozuka, 2/29/88, (PB88-229471).

NCEER-88-0009 "Seismic Fragility Analysis of Shear Wall Structures," by J-W Jaw and H.H-M. Hwang, 4/30/88, (PB89-102867).

NCEER-88-0010 "Base Isolation of a Multi-Story Building Under a Harmonic Ground Motion - A Comparison of Performances of Various Systems," by F-G Fan, G. Ahmadi and I.G. Tadjbakhsh, 5/18/88, (PB89-122238).

NCEER-88-0011 "Seismic Floor Response Spectra for a Combined System by Green's Functions," by F.M. Lavelle, L.A. Bergman and P.D. Spanos, 5/1/88, (PB89-102875).

NCEER-88-0012 "A New Solution Technique for Randomly Excited Hysteretic Structures," by G.Q. Cai and Y.K. Lin, 5/16/88, (PB89-102883).

NCEER-88-0013 "A Study of Radiation Damping and Soil-Structure Interaction Effects in the Centrifuge," by K. Weissman, supervised by J.H. Prevost, 5/24/88, (PB89-144703).

NCEER-88-0014 "Parameter Identification and Implementation of a Kinematic Plasticity Model for Frictional Soils," by J.H. Prevost and D.V. Griffiths, to be published.

NCEER-88-0015 "Two- and Three- Dimensional Dynamic Finite Element Analyses of the Long Valley Dam," by D.V. Griffiths and J.H. Prevost, 6/17/88, (PB89-144711).

NCEER-88-0016 "Damage Assessment of Reinforced Concrete Structures in Eastern United States," by A.M. Reinhorn, M.J. Seidel, S.K. Kunnath and Y.J. Park, 6/15/88, (PB89-122220).

NCEER-88-0017 "Dynamic Compliance of Vertically Loaded Strip Foundations in Multilayered Viscoelastic Soils," by S. Ahmad and A.S.M. Israil, 6/17/88, (PB89-102891).

NCEER-88-0018 "An Experimental Study of Seismic Structural Response With Added Viscoelastic Dampers," by R.C. Lin, Z. Liang, T.T. Soong and R.H. Zhang, 6/30/88, (PB89-122212). This report is available only through NTIS (see address given above).

NCEER-88-0019 "Experimental Investigation of Primary - Secondary System Interaction," by G.D. Manolis, G. Juhn and A.M. Reinhorn, 5/27/88, (PB89-122204).

NCEER-88-0020 "A Response Spectrum Approach For Analysis of Nonclassically Damped Structures," by J.N. Yang, S. Sarkani and F.X. Long, 4/22/88, (PB89-102909).

NCEER-88-0021 "Seismic Interaction of Structures and Soils: Stochastic Approach," by A.S. Veletsos and A.M. Prasad, 7/21/88, (PB89-122196).

NCEER-88-0022 "Identification of the Serviceability Limit State and Detection of Seismic Structural Damage," by E. DiPasquale and A.S. Cakmak, 6/15/88, (PB89-122188). This report is available only through NTIS (see address given above).

NCEER-88-0023 "Multi-Hazard Risk Analysis: Case of a Simple Offshore Structure," by B.K. Bhartia and E.H. Vanmarcke, 7/21/88, (PB89-145213).

NCEER-88-0024 "Automated Seismic Design of Reinforced Concrete Buildings," by Y.S. Chung, C. Meyer and M. Shinozuka, 7/5/88, (PB89-122170). This report is available only through NTIS (see address given above).

NCEER-88-0025 "Experimental Study of Active Control of MDOF Structures Under Seismic Excitations," by L.L. Chung, R.C. Lin, T.T. Soong and A.M. Reinhorn, 7/10/88, (PB89-122600).

NCEER-88-0026 "Earthquake Simulation Tests of a Low-Rise Metal Structure," by J.S. Hwang, K.C. Chang, G.C. Lee and R.L. Ketter, 8/1/88, (PB89-102917).

NCEER-88-0027 "Systems Study of Urban Response and Reconstruction Due to Catastrophic Earthquakes," by F. Kozin and H.K. Zhou, 9/22/88, (PB90-162348).

NCEER-88-0028 "Seismic Fragility Analysis of Plane Frame Structures," by H.H-M. Hwang and Y.K. Low, 7/31/88, (PB89-131445).

NCEER-88-0029 "Response Analysis of Stochastic Structures," by A. Kardara, C. Bucher and M. Shinozuka, 9/22/88, (PB89-174429).

NCEER-88-0030 "Nonnormal Accelerations Due to Yielding in a Primary Structure," by D.C.K. Chen and L.D. Lutes, 9/19/88, (PB89-131437).

NCEER-88-0031 "Design Approaches for Soil-Structure Interaction," by A.S. Veletsos, A.M. Prasad and Y. Tang, 12/30/88, (PB89-174437). This report is available only through NTIS (see address given above).

NCEER-88-0032 "A Re-evaluation of Design Spectra for Seismic Damage Control," by C.J. Turkstra and A.G. Tallin, 11/7/88, (PB89-145221).

NCEER-88-0033 "The Behavior and Design of Noncontact Lap Splices Subjected to Repeated Inelastic Tensile Loading," by V.E. Sagan, P. Gergely and R.N. White, 12/8/88, (PB89-163737).

NCEER-88-0034 "Seismic Response of Pile Foundations," by S.M. Mamoon, P.K. Banerjee and S. Ahmad, 11/1/88, (PB89-145239).

NCEER-88-0035 "Modeling of R/C Building Structures With Flexible Floor Diaphragms (IDARC2)," by A.M. Reinhorn, S.K. Kunnath and N. Panahshahi, 9/7/88, (PB89-207153).

NCEER-88-0036 "Solution of the Dam-Reservoir Interaction Problem Using a Combination of FEM, BEM with Particular Integrals, Modal Analysis, and Substructuring," by C-S. Tsai, G.C. Lee and R.L. Ketter, 12/31/88, (PB89-207146).

NCEER-88-0037 "Optimal Placement of Actuators for Structural Control," by F.Y. Cheng and C.P. Pantelides, 8/15/88, (PB89-162846).

NCEER-88-0038 "Teflon Bearings in Aseismic Base Isolation: Experimental Studies and Mathematical Modeling," by A. Mokha, M.C. Constantinou and A.M. Reinhorn, 12/5/88, (PB89-218457). This report is available only through NTIS (see address given above).

NCEER-88-0039 "Seismic Behavior of Flat Slab High-Rise Buildings in the New York City Area," by P. Weidlinger and M. Ettouney, 10/15/88, (PB90-145681).

NCEER-88-0040 "Evaluation of the Earthquake Resistance of Existing Buildings in New York City," by P. Weidlinger and M. Ettouney, 10/15/88, to be published.

NCEER-88-0041 "Small-Scale Modeling Techniques for Reinforced Concrete Structures Subjected to Seismic Loads," by W. Kim, A. El-Attar and R.N. White, 11/22/88, (PB89-189625).

NCEER-88-0042 "Modeling Strong Ground Motion from Multiple Event Earthquakes," by G.W. Ellis and A.S. Cakmak, 10/15/88, (PB89-174445).

NCEER-88-0043 "Nonstationary Models of Seismic Ground Acceleration," by M. Grigoriu, S.E. Ruiz and E. Rosenblueth, 7/15/88, (PB89-189617).

NCEER-88-0044 "SARCF User's Guide: Seismic Analysis of Reinforced Concrete Frames," by Y.S. Chung, C. Meyer and M. Shinozuka, 11/9/88, (PB89-174452).

NCEER-88-0045 "First Expert Panel Meeting on Disaster Research and Planning," edited by J. Pantelic and J. Stoyle, 9/15/88, (PB89-174460).

NCEER-88-0046 "Preliminary Studies of the Effect of Degrading Infill Walls on the Nonlinear Seismic Response of Steel Frames," by C.Z. Chrysostomou, P. Gergely and J.F. Abel, 12/19/88, (PB89-208383).

NCEER-88-0047 "Reinforced Concrete Frame Component Testing Facility - Design, Construction, Instrumentation and Operation," by S.P. Pessiki, C. Conley, T. Bond, P. Gergely and R.N. White, 12/16/88, (PB89-174478).

NCEER-89-0001 "Effects of Protective Cushion and Soil Compliancy on the Response of Equipment Within a Seismically Excited Building," by J.A. HoLung, 2/16/89, (PB89-207179).

NCEER-89-0002 "Statistical Evaluation of Response Modification Factors for Reinforced Concrete Structures," by H.H-M. Hwang and J-W. Jaw, 2/17/89, (PB89-207187).

NCEER-89-0003 "Hysteretic Columns Under Random Excitation," by G-Q. Cai and Y.K. Lin, 1/9/89, (PB89-196513).

NCEER-89-0004 "Experimental Study of 'Elephant Foot Bulge' Instability of Thin-Walled Metal Tanks," by Z-H. Jia and R.L. Ketter, 2/22/89, (PB89-207195).

NCEER-89-0005 "Experiment on Performance of Buried Pipelines Across San Andreas Fault," by J. Isenberg, E. Richardson and T.D. O'Rourke, 3/10/89, (PB89-218440). This report is available only through NTIS (see address given above).

NCEER-89-0006 "A Knowledge-Based Approach to Structural Design of Earthquake-Resistant Buildings," by M. Subramani, P. Gergely, C.H. Conley, J.F. Abel and A.H. Zaghw, 1/15/89, (PB89-218465).

NCEER-89-0007 "Liquefaction Hazards and Their Effects on Buried Pipelines," by T.D. O'Rourke and P.A. Lane, 2/1/89, (PB89-218481).

NCEER-89-0008 "Fundamentals of System Identification in Structural Dynamics," by H. Imai, C-B. Yun, O. Maruyama and M. Shinozuka, 1/26/89, (PB89-207211).

NCEER-89-0009 "Effects of the 1985 Michoacan Earthquake on Water Systems and Other Buried Lifelines in Mexico," by A.G. Ayala and M.J. O'Rourke, 3/8/89, (PB89-207229).

NCEER-89-R010 "NCEER Bibliography of Earthquake Education Materials," by K.E.K. Ross, Second Revision, 9/1/89, (PB90-125352).

NCEER-89-0011 "Inelastic Three-Dimensional Response Analysis of Reinforced Concrete Building Structures (IDARC-3D), Part I - Modeling," by S.K. Kunnath and A.M. Reinhorn, 4/17/89, (PB90-114612).

NCEER-89-0012 "Recommended Modifications to ATC-14," by C.D. Poland and J.O. Malley, 4/12/89, (PB90-108648).

NCEER-89-0013 "Repair and Strengthening of Beam-to-Column Connections Subjected to Earthquake Loading," by M. Corazao and A.J. Durrani, 2/28/89, (PB90-109885).

NCEER-89-0014 "Program EXKAL2 for Identification of Structural Dynamic Systems," by O. Maruyama, C-B. Yun, M. Hoshiya and M. Shinozuka, 5/19/89, (PB90-109877).

NCEER-89-0015 "Response of Frames With Bolted Semi-Rigid Connections, Part I - Experimental Study and Analytical Predictions," by P.J. DiCorso, A.M. Reinhorn, J.R. Dickerson, J.B. Radziminski and W.L. Harper, 6/1/89, to be published.

NCEER-89-0016 "ARMA Monte Carlo Simulation in Probabilistic Structural Analysis," by P.D. Spanos and M.P. Mignolet, 7/10/89, (PB90-109893).

NCEER-89-P017 "Preliminary Proceedings from the Conference on Disaster Preparedness - The Place of Earthquake Education in Our Schools," Edited by K.E.K. Ross, 6/23/89, (PB90-108606).

NCEER-89-0017 "Proceedings from the Conference on Disaster Preparedness - The Place of Earthquake Education in Our Schools," Edited by K.E.K. Ross, 12/31/89, (PB90-207895). This report is available only through NTIS (see address given above).

NCEER-89-0018 "Multidimensional Models of Hysteretic Material Behavior for Vibration Analysis of Shape Memory Energy Absorbing Devices, by E.J. Graesser and F.A. Cozzarelli, 6/7/89, (PB90-164146).

NCEER-89-0019 "Nonlinear Dynamic Analysis of Three-Dimensional Base Isolated Structures (3D-BASIS)," by S. Nagarajaiah, A.M. Reinhorn and M.C. Constantinou, 8/3/89, (PB90-161936). This report is available only through NTIS (see address given above).

NCEER-89-0020 "Structural Control Considering Time-Rate of Control Forces and Control Rate Constraints," by F.Y. Cheng and C.P. Pantelides, 8/3/89, (PB90-120445).

NCEER-89-0021 "Subsurface Conditions of Memphis and Shelby County," by K.W. Ng, T-S. Chang and H-H.M. Hwang, 7/26/89, (PB90-120437).

NCEER-89-0022 "Seismic Wave Propagation Effects on Straight Jointed Buried Pipelines," by K. Elhmadi and M.J. O'Rourke, 8/24/89, (PB90-162322).

NCEER-89-0023 "Workshop on Serviceability Analysis of Water Delivery Systems," edited by M. Grigoriu, 3/6/89, (PB90-127424).

NCEER-89-0024 "Shaking Table Study of a 1/5 Scale Steel Frame Composed of Tapered Members," by K.C. Chang, J.S. Hwang and G.C. Lee, 9/18/89, (PB90-160169).

NCEER-89-0025 "DYNA1D: A Computer Program for Nonlinear Seismic Site Response Analysis - Technical Documentation," by Jean H. Prevost, 9/14/89, (PB90-161944). This report is available only through NTIS (see address given above).

NCEER-89-0026 "1:4 Scale Model Studies of Active Tendon Systems and Active Mass Dampers for Aseismic Protection," by A.M. Reinhorn, T.T. Soong, R.C. Lin, Y.P. Yang, Y. Fukao, H. Abe and M. Nakai, 9/15/89, (PB90-173246).

NCEER-89-0027 "Scattering of Waves by Inclusions in a Nonhomogeneous Elastic Half Space Solved by Boundary Element Methods," by P.K. Hadley, A. Askar and A.S. Cakmak, 6/15/89, (PB90-145699).

NCEER-89-0028 "Statistical Evaluation of Deflection Amplification Factors for Reinforced Concrete Structures," by H.H.M. Hwang, J-W. Jaw and A.L. Ch'ng, 8/31/89, (PB90-164633).

NCEER-89-0029 "Bedrock Accelerations in Memphis Area Due to Large New Madrid Earthquakes," by H.H.M. Hwang, C.H.S. Chen and G. Yu, 11/7/89, (PB90-162330).

NCEER-89-0030 "Seismic Behavior and Response Sensitivity of Secondary Structural Systems," by Y.Q. Chen and T.T. Soong, 10/23/89, (PB90-164658).

NCEER-89-0031 "Random Vibration and Reliability Analysis of Primary-Secondary Structural Systems," by Y. Ibrahim, M. Grigoriu and T.T. Soong, 11/10/89, (PB90-161951).

NCEER-89-0032 "Proceedings from the Second U.S. - Japan Workshop on Liquefaction, Large Ground Deformation and Their Effects on Lifelines, September 26-29, 1989," Edited by T.D. O'Rourke and M. Hamada, 12/1/89, (PB90-209388).

NCEER-89-0033 "Deterministic Model for Seismic Damage Evaluation of Reinforced Concrete Structures," by J.M. Bracci, A.M. Reinhorn, J.B. Mander and S.K. Kunnath, 9/27/89.

NCEER-89-0034 "On the Relation Between Local and Global Damage Indices," by E. DiPasquale and A.S. Cakmak, 8/15/89, (PB90-173865).

NCEER-89-0035 "Cyclic Undrained Behavior of Nonplastic and Low Plasticity Silts," by A.J. Walker and H.E. Stewart, 7/26/89, (PB90-183518).

NCEER-89-0036 "Liquefaction Potential of Surficial Deposits in the City of Buffalo, New York," by M. Budhu, R. Giese and L. Baumgrass, 1/17/89, (PB90-208455).

NCEER-89-0037 "A Deterministic Assessment of Effects of Ground Motion Incoherence," by A.S. Veletsos and Y. Tang, 7/15/89, (PB90-164294).

NCEER-89-0038 "Workshop on Ground Motion Parameters for Seismic Hazard Mapping," July 17-18, 1989, edited by R.V. Whitman, 12/1/89, (PB90-173923).

NCEER-89-0039 "Seismic Effects on Elevated Transit Lines of the New York City Transit Authority," by C.J. Costantino, C.A. Miller and E. Heymsfield, 12/26/89, (PB90-207887).

NCEER-89-0040 "Centrifugal Modeling of Dynamic Soil-Structure Interaction," by K. Weissman, Supervised by J.H. Prevost, 5/10/89, (PB90-207879).

NCEER-89-0041 "Linearized Identification of Buildings With Cores for Seismic Vulnerability Assessment," by I-K. Ho and A.E. Aktan, 11/1/89, (PB90-251943).

NCEER-90-0001 "Geotechnical and Lifeline Aspects of the October 17, 1989 Loma Prieta Earthquake in San Francisco," by T.D. O'Rourke, H.E. Stewart, F.T. Blackburn and T.S. Dickerman, 1/90, (PB90-208596).

NCEER-90-0002 "Nonnormal Secondary Response Due to Yielding in a Primary Structure," by D.C.K. Chen and L.D. Lutes, 2/28/90, (PB90-251976).

NCEER-90-0003 "Earthquake Education Materials for Grades K-12," by K.E.K. Ross, 4/16/90, (PB91-251984).

NCEER-90-0004 "Catalog of Strong Motion Stations in Eastern North America," by R.W. Busby, 4/3/90, (PB90-251984).

NCEER-90-0005 "NCEER Strong-Motion Data Base: A User Manual for the GeoBase Release (Version 1.0 for the Sun3)," by P. Friberg and K. Jacob, 3/31/90 (PB90-258062).

NCEER-90-0006 "Seismic Hazard Along a Crude Oil Pipeline in the Event of an 1811-1812 Type New Madrid Earthquake," by H.H.M. Hwang and C-H.S. Chen, 4/16/90(PB90-258054).

NCEER-90-0007 "Site-Specific Response Spectra for Memphis Sheahan Pumping Station," by H.H.M. Hwang and C.S. Lee, 5/15/90, (PB91-108811).

NCEER-90-0008 "Pilot Study on Seismic Vulnerability of Crude Oil Transmission Systems," by T. Ariman, R. Dobry, M. Grigoriu, F. Kozin, M. O'Rourke, T. O'Rourke and M. Shinozuka, 5/25/90, (PB91-108837).

NCEER-90-0009 "A Program to Generate Site Dependent Time Histories: EQGEN," by G.W. Ellis, M. Srinivasan and A.S. Cakmak, 1/30/90, (PB91-108829).

NCEER-90-0010 "Active Isolation for Seismic Protection of Operating Rooms," by M.E. Talbott, Supervised by M. Shinozuka, 6/8/9, (PB91-110205).

NCEER-90-0011 "Program LINEARID for Identification of Linear Structural Dynamic Systems," by C-B. Yun and M. Shinozuka, 6/25/90, (PB91-110312).

NCEER-90-0012 "Two-Dimensional Two-Phase Elasto-Plastic Seismic Response of Earth Dams," by A.N. Yiagos, Supervised by J.H. Prevost, 6/20/90, (PB91-110197).

NCEER-90-0013 "Secondary Systems in Base-Isolated Structures: Experimental Investigation, Stochastic Response and Stochastic Sensitivity," by G.D. Manolis, G. Juhn, M.C. Constantinou and A.M. Reinhorn, 7/1/90, (PB91-110320).

NCEER-90-0014 "Seismic Behavior of Lightly-Reinforced Concrete Column and Beam-Column Joint Details," by S.P. Pessiki, C.H. Conley, P. Gergely and R.N. White, 8/22/90, (PB91-108795).

NCEER-90-0015 "Two Hybrid Control Systems for Building Structures Under Strong Earthquakes," by J.N. Yang and A. Danielians, 6/29/90, (PB91-125393).

NCEER-90-0016 "Instantaneous Optimal Control with Acceleration and Velocity Feedback," by J.N. Yang and Z. Li, 6/29/90, (PB91-125401).

NCEER-90-0017 "Reconnaissance Report on the Northern Iran Earthquake of June 21, 1990," by M. Mehrain, 10/4/90, (PB91-125377).

NCEER-90-0018 "Evaluation of Liquefaction Potential in Memphis and Shelby County," by T.S. Chang, P.S. Tang, C.S. Lee and H. Hwang, 8/10/90, (PB91-125427).

NCEER-90-0019 "Experimental and Analytical Study of a Combined Sliding Disc Bearing and Helical Steel Spring Isolation System," by M.C. Constantinou, A.S. Mokha and A.M. Reinhorn, 10/4/90, (PB91-125385).

NCEER-90-0020 "Experimental Study and Analytical Prediction of Earthquake Response of a Sliding Isolation System with a Spherical Surface," by A.S. Mokha, M.C. Constantinou and A.M. Reinhorn, 10/11/90, (PB91-125419).

NCEER-90-0021 "Dynamic Interaction Factors for Floating Pile Groups," by G. Gazetas, K. Fan, A. Kaynia and E. Kausel, 9/10/90, (PB91-170381).

NCEER-90-0022 "Evaluation of Seismic Damage Indices for Reinforced Concrete Structures," by S. Rodriguez-Gomez and A.S. Cakmak, 9/30/90, PB91-171322).

NCEER-90-0023 "Study of Site Response at a Selected Memphis Site," by H. Desai, S. Ahmad, E.S. Gazetas and M.R. Oh, 10/11/90, (PB91-196857).

NCEER-90-0024 "A User's Guide to Strongmo: Version 1.0 of NCEER's Strong-Motion Data Access Tool for PCs and Terminals," by P.A. Friberg and C.A.T. Susch, 11/15/90, (PB91-171272).

NCEER-90-0025 "A Three-Dimensional Analytical Study of Spatial Variability of Seismic Ground Motions," by L-L. Hong and A.H.-S. Ang, 10/30/90, (PB91-170399).

NCEER-90-0026 "MUMOID User's Guide - A Program for the Identification of Modal Parameters," by S. Rodriguez-Gomez and E. DiPasquale, 9/30/90, (PB91-171298).

NCEER-90-0027 "SARCF-II User's Guide - Seismic Analysis of Reinforced Concrete Frames," by S. Rodriguez-Gomez, Y.S. Chung and C. Meyer, 9/30/90, (PB91-171280).

NCEER-90-0028 "Viscous Dampers: Testing, Modeling and Application in Vibration and Seismic Isolation," by N. Makris and M.C. Constantinou, 12/20/90 (PB91-190561).

NCEER-90-0029 "Soil Effects on Earthquake Ground Motions in the Memphis Area," by H. Hwang, C.S. Lee, K.W. Ng and T.S. Chang, 8/2/90, (PB91-190751).

NCEER-91-0001 "Proceedings from the Third Japan-U.S. Workshop on Earthquake Resistant Design of Lifeline Facilities and Countermeasures for Soil Liquefaction, December 17-19, 1990," edited by T.D. O'Rourke and M. Hamada, 2/1/91, (PB91-179259).

NCEER-91-0002 "Physical Space Solutions of Non-Proportionally Damped Systems," by M. Tong, Z. Liang and G.C. Lee, 1/15/91, (PB91-179242).

NCEER-91-0003 "Seismic Response of Single Piles and Pile Groups," by K. Fan and G. Gazetas, 1/10/91, (PB92-174994).

NCEER-91-0004 "Damping of Structures: Part 1 - Theory of Complex Damping," by Z. Liang and G. Lee, 10/10/91, (PB92-197235).

NCEER-91-0005 "3D-BASIS - Nonlinear Dynamic Analysis of Three Dimensional Base Isolated Structures: Part II," by S. Nagarajaiah, A.M. Reinhorn and M.C. Constantinou, 2/28/91, (PB91-190553).

NCEER-91-0006 "A Multidimensional Hysteretic Model for Plasticity Deforming Metals in Energy Absorbing Devices," by E.J. Graesser and F.A. Cozzarelli, 4/9/91, (PB92-108364).

NCEER-91-0007 "A Framework for Customizable Knowledge-Based Expert Systems with an Application to a KBES for Evaluating the Seismic Resistance of Existing Buildings," by E.G. Ibarra-Anaya and S.J. Fenves, 4/9/91, (PB91-210930).

NCEER-91-0008 "Nonlinear Analysis of Steel Frames with Semi-Rigid Connections Using the Capacity Spectrum Method," by G.G. Deierlein, S-H. Hsieh, Y-J. Shen and J.F. Abel, 7/2/91, (PB92-113828).

NCEER-91-0009 "Earthquake Education Materials for Grades K-12," by K.E.K. Ross, 4/30/91, (PB91-212142).

NCEER-91-0010 "Phase Wave Velocities and Displacement Phase Differences in a Harmonically Oscillating Pile," by N. Makris and G. Gazetas, 7/8/91, (PB92-108356).

NCEER-91-0011 "Dynamic Characteristics of a Full-Size Five-Story Steel Structure and a 2/5 Scale Model," by K.C. Chang, G.C. Yao, G.C. Lee, D.S. Hao and Y.C. Yeh," 7/2/91, (PB93-116648).

NCEER-91-0012 "Seismic Response of a 2/5 Scale Steel Structure with Added Viscoelastic Dampers," by K.C. Chang, T.T. Soong, S-T. Oh and M.L. Lai, 5/17/91, (PB92-110816).

NCEER-91-0013 "Earthquake Response of Retaining Walls; Full-Scale Testing and Computational Modeling," by S. Alampalli and A-W.M. Elgamal, 6/20/91, to be published.

NCEER-91-0014 "3D-BASIS-M: Nonlinear Dynamic Analysis of Multiple Building Base Isolated Structures," by P.C. Tsopelas, S. Nagarajaiah, M.C. Constantinou and A.M. Reinhorn, 5/28/91, (PB92-113885).

NCEER-91-0015 "Evaluation of SEAOC Design Requirements for Sliding Isolated Structures," by D. Theodossiou and M.C. Constantinou, 6/10/91, (PB92-114602).

NCEER-91-0016 "Closed-Loop Modal Testing of a 27-Story Reinforced Concrete Flat Plate-Core Building," by H.R. Somaprasad, T. Toksoy, H. Yoshiyuki and A.E. Aktan, 7/15/91, (PB92-129980).

NCEER-91-0017 "Shake Table Test of a 1/6 Scale Two-Story Lightly Reinforced Concrete Building," by A.G. El-Attar, R.N. White and P. Gergely, 2/28/91, (PB92-222447).

NCEER-91-0018 "Shake Table Test of a 1/8 Scale Three-Story Lightly Reinforced Concrete Building," by A.G. El-Attar, R.N. White and P. Gergely, 2/28/91, (PB93-116630).

NCEER-91-0019 "Transfer Functions for Rigid Rectangular Foundations," by A.S. Veletsos, A.M. Prasad and W.H. Wu, 7/31/91.

NCEER-91-0020 "Hybrid Control of Seismic-Excited Nonlinear and Inelastic Structural Systems," by J.N. Yang, Z. Li and A. Danielians, 8/1/91, (PB92-143171).

NCEER-91-0021 "The NCEER-91 Earthquake Catalog: Improved Intensity-Based Magnitudes and Recurrence Relations for U.S. Earthquakes East of New Madrid," by L. Seeber and J.G. Armbruster, 8/28/91, (PB92-176742).

NCEER-91-0022 "Proceedings from the Implementation of Earthquake Planning and Education in Schools: The Need for Change - The Roles of the Changemakers," by K.E.K. Ross and F. Winslow, 7/23/91, (PB92-129998).

NCEER-91-0023 "A Study of Reliability-Based Criteria for Seismic Design of Reinforced Concrete Frame Buildings," by H.H.M. Hwang and H-M. Hsu, 8/10/91, (PB92-140235).

NCEER-91-0024 "Experimental Verification of a Number of Structural System Identification Algorithms," by R.G. Ghanem, H. Gavin and M. Shinozuka, 9/18/91, (PB92-176577).

NCEER-91-0025 "Probabilistic Evaluation of Liquefaction Potential," by H.H.M. Hwang and C.S. Lee," 11/25/91, (PB92-143429).

NCEER-91-0026 "Instantaneous Optimal Control for Linear, Nonlinear and Hysteretic Structures - Stable Controllers," by J.N. Yang and Z. Li, 11/15/91, (PB92-163807).

NCEER-91-0027 "Experimental and Theoretical Study of a Sliding Isolation System for Bridges," by M.C. Constantinou, A. Kartoum, A.M. Reinhorn and P. Bradford, 11/15/91, (PB92-176973).

NCEER-92-0001 "Case Studies of Liquefaction and Lifeline Performance During Past Earthquakes, Volume 1: Japanese Case Studies," Edited by M. Hamada and T. O'Rourke, 2/17/92, (PB92-197243).

NCEER-92-0002 "Case Studies of Liquefaction and Lifeline Performance During Past Earthquakes, Volume 2: United States Case Studies," Edited by T. O'Rourke and M. Hamada, 2/17/92, (PB92-197250).

NCEER-92-0003 "Issues in Earthquake Education," Edited by K. Ross, 2/3/92, (PB92-222389).

NCEER-92-0004 "Proceedings from the First U.S. - Japan Workshop on Earthquake Protective Systems for Bridges," Edited by I.G. Buckle, 2/4/92, (PB94-142239, A99, MF-A06).

NCEER-92-0005 "Seismic Ground Motion from a Haskell-Type Source in a Multiple-Layered Half-Space," A.P. Theoharis, G. Deodatis and M. Shinozuka, 1/2/92, to be published.

NCEER-92-0006 "Proceedings from the Site Effects Workshop," Edited by R. Whitman, 2/29/92, (PB92-197201).

NCEER-92-0007 "Engineering Evaluation of Permanent Ground Deformations Due to Seismically-Induced Liquefaction," by M.H. Baziar, R. Dobry and A-W.M. Elgamal, 3/24/92, (PB92-222421).

NCEER-92-0008 "A Procedure for the Seismic Evaluation of Buildings in the Central and Eastern United States," by C.D. Poland and J.O. Malley, 4/2/92, (PB92-222439).

NCEER-92-0009 "Experimental and Analytical Study of a Hybrid Isolation System Using Friction Controllable Sliding Bearings," by M.Q. Feng, S. Fujii and M. Shinozuka, 5/15/92, (PB93-150282).

NCEER-92-0010 "Seismic Resistance of Slab-Column Connections in Existing Non-Ductile Flat-Plate Buildings," by A.J. Durrani and Y. Du, 5/18/92.

NCEER-92-0011 "The Hysteretic and Dynamic Behavior of Brick Masonry Walls Upgraded by Ferrocement Coatings Under Cyclic Loading and Strong Simulated Ground Motion," by H. Lee and S.P. Prawel, 5/11/92, to be published.

NCEER-92-0012 "Study of Wire Rope Systems for Seismic Protection of Equipment in Buildings," by G.F. Demetriades, M.C. Constantinou and A.M. Reinhorn, 5/20/92.

NCEER-92-0013 "Shape Memory Structural Dampers: Material Properties, Design and Seismic Testing," by P.R. Witting and F.A. Cozzarelli, 5/26/92.

NCEER-92-0014 "Longitudinal Permanent Ground Deformation Effects on Buried Continuous Pipelines," by M.J. O'Rourke, and C. Nordberg, 6/15/92.

NCEER-92-0015 "A Simulation Method for Stationary Gaussian Random Functions Based on the Sampling Theorem," by M. Grigoriu and S. Balopoulou, 6/11/92, (PB93-127496).

NCEER-92-0016 "Gravity-Load-Designed Reinforced Concrete Buildings: Seismic Evaluation of Existing Construction and Detailing Strategies for Improved Seismic Resistance," by G.W. Hoffmann, S.K. Kunnath, A.M. Reinhorn and J.B. Mander, 7/15/92, (PB94-142007, A08, MF-A02).

NCEER-92-0017 "Observations on Water System and Pipeline Performance in the Limón Area of Costa Rica Due to the April 22, 1991 Earthquake," by M. O'Rourke and D. Ballantyne, 6/30/92, (PB93-126811).

NCEER-92-0018 "Fourth Edition of Earthquake Education Materials for Grades K-12," Edited by K.E.K. Ross, 8/10/92.

NCEER-92-0019 "Proceedings from the Fourth Japan-U.S. Workshop on Earthquake Resistant Design of Lifeline Facilities and Countermeasures for Soil Liquefaction," Edited by M. Hamada and T.D. O'Rourke, 8/12/92, (PB93-163939).

NCEER-92-0020 "Active Bracing System: A Full Scale Implementation of Active Control," by A.M. Reinhorn, T.T. Soong, R.C. Lin, M.A. Riley, Y.P. Wang, S. Aizawa and M. Higashino, 8/14/92, (PB93-127512).

NCEER-92-0021 "Empirical Analysis of Horizontal Ground Displacement Generated by Liquefaction-Induced Lateral Spreads," by S.F. Bartlett and T.L. Youd, 8/17/92, (PB93-188241).

NCEER-92-0022 "IDARC Version 3.0: Inelastic Damage Analysis of Reinforced Concrete Structures," by S.K. Kunnath, A.M. Reinhorn and R.F. Lobo, 8/31/92, (PB93-227502, A07, MF-A02).

NCEER-92-0023 "A Semi-Empirical Analysis of Strong-Motion Peaks in Terms of Seismic Source, Propagation Path and Local Site Conditions, by M. Kamiyama, M.J. O'Rourke and R. Flores-Berrones, 9/9/92, (PB93-150266).

NCEER-92-0024 "Seismic Behavior of Reinforced Concrete Frame Structures with Nonductile Details, Part I: Summary of Experimental Findings of Full Scale Beam-Column Joint Tests," by A. Beres, R.N. White and P. Gergely, 9/30/92, (PB93-227783, A05, MF-A01).

NCEER-92-0025 "Experimental Results of Repaired and Retrofitted Beam-Column Joint Tests in Lightly Reinforced Concrete Frame Buildings," by A. Beres, S. El-Borgi, R.N. White and P. Gergely, 10/29/92, (PB93-227791, A05, MF-A01).

NCEER-92-0026 "A Generalization of Optimal Control Theory: Linear and Nonlinear Structures," by J.N. Yang, Z. Li and S. Vongchavalitkul, 11/2/92, (PB93-188621).

NCEER-92-0027 "Seismic Resistance of Reinforced Concrete Frame Structures Designed Only for Gravity Loads: Part I - Design and Properties of a One-Third Scale Model Structure," by J.M. Bracci, A.M. Reinhorn and J.B. Mander, 12/1/92, (PB94-104502, A08, MF-A02).

NCEER-92-0028 "Seismic Resistance of Reinforced Concrete Frame Structures Designed Only for Gravity Loads: Part II - Experimental Performance of Subassemblages," by L.E. Aycardi, J.B. Mander and A.M. Reinhorn, 12/1/92, (PB94-104510, A08, MF-A02).

NCEER-92-0029 "Seismic Resistance of Reinforced Concrete Frame Structures Designed Only for Gravity Loads: Part III - Experimental Performance and Analytical Study of a Structural Model," by J.M. Bracci, A.M. Reinhorn and J.B. Mander, 12/1/92, (PB93-227528, A09, MF-A01).

NCEER-92-0030 "Evaluation of Seismic Retrofit of Reinforced Concrete Frame Structures: Part I - Experimental Performance of Retrofitted Subassemblages," by D. Choudhuri, J.B. Mander and A.M. Reinhorn, 12/8/92, (PB93-198307, A07, MF-A02).

NCEER-92-0031 "Evaluation of Seismic Retrofit of Reinforced Concrete Frame Structures: Part II - Experimental Performance and Analytical Study of a Retrofitted Structural Model," by J.M. Bracci, A.M. Reinhorn and J.B. Mander, 12/8/92, (PB93-198315, A09, MF-A03).

NCEER-92-0032 "Experimental and Analytical Investigation of Seismic Response of Structures with Supplemental Fluid Viscous Dampers," by M.C. Constantinou and M.D. Symans, 12/21/92, (PB93-191435).

NCEER-92-0033 "Reconnaissance Report on the Cairo, Egypt Earthquake of October 12, 1992," by M. Khater, 12/23/92, (PB93-188621).

NCEER-92-0034 "Low-Level Dynamic Characteristics of Four Tall Flat-Plate Buildings in New York City," by H. Gavin, S. Yuan, J. Grossman, E. Pekelis and K. Jacob, 12/28/92, (PB93-188217).

NCEER-93-0001 "An Experimental Study on the Seismic Performance of Brick-Infilled Steel Frames With and Without Retrofit," by J.B. Mander, B. Nair, K. Wojtkowski and J. Ma, 1/29/93, (PB93-227510, A07, MF-A02).

NCEER-93-0002 "Social Accounting for Disaster Preparedness and Recovery Planning," by S. Cole, E. Pantoja and V. Razak, 2/22/93, (PB94-142114, A12, MF-A03).

NCEER-93-0003 "Assessment of 1991 NEHRP Provisions for Nonstructural Components and Recommended Revisions," by T.T. Soong, G. Chen, Z. Wu, R-H. Zhang and M. Grigoriu, 3/1/93, (PB93-188639).

NCEER-93-0004 "Evaluation of Static and Response Spectrum Analysis Procedures of SEAOC/UBC for Seismic Isolated Structures," by C.W. Winters and M.C. Constantinou, 3/23/93, (PB93-198299).

NCEER-93-0005 "Earthquakes in the Northeast - Are We Ignoring the Hazard? A Workshop on Earthquake Science and Safety for Educators," edited by K.E.K. Ross, 4/2/93, (PB94-103066, A09, MF-A02).

NCEER-93-0006 "Inelastic Response of Reinforced Concrete Structures with Viscoelastic Braces," by R.F. Lobo, J.M. Bracci, K.L. Shen, A.M. Reinhorn and T.T. Soong, 4/5/93, (PB93-227486, A05, MF-A02).

NCEER-93-0007 "Seismic Testing of Installation Methods for Computers and Data Processing Equipment," by K. Kosar, T.T. Soong, K.L. Shen, J.A. HoLung and Y.K. Lin, 4/12/93, (PB93-198299).

NCEER-93-0008 "Retrofit of Reinforced Concrete Frames Using Added Dampers," by A. Reinhorn, M. Constantinou and C. Li, to be published.

NCEER-93-0009 "Seismic Behavior and Design Guidelines for Steel Frame Structures with Added Viscoelastic Dampers," by K.C. Chang, M.L. Lai, T.T. Soong, D.S. Hao and Y.C. Yeh, 5/1/93, (PB94-141959, A07, MF-A02).

NCEER-93-0010 "Seismic Performance of Shear-Critical Reinforced Concrete Bridge Piers," by J.B. Mander, S.M. Waheed, M.T.A. Chaudhary and S.S. Chen, 5/12/93, (PB93-227494, A08, MF-A02).

NCEER-93-0011 "3D-BASIS-TABS: Computer Program for Nonlinear Dynamic Analysis of Three Dimensional Base Isolated Structures," by S. Nagarajaiah, C. Li, A.M. Reinhorn and M.C. Constantinou, 8/2/93, (PB94-141819, A09, MF-A02).

NCEER-93-0012 "Effects of Hydrocarbon Spills from an Oil Pipeline Break on Ground Water," by O.J. Helweg and H.H.M. Hwang, 8/3/93, (PB94-141942, A06, MF-A02).

NCEER-93-0013 "Simplified Procedures for Seismic Design of Nonstructural Components and Assessment of Current Code Provisions," by M.P. Singh, L.E. Suarez, E.E. Matheu and G.O. Maldonado, 8/4/93, (PB94-141827, A09, MF-A02).

NCEER-93-0014 "An Energy Approach to Seismic Analysis and Design of Secondary Systems," by G. Chen and T.T. Soong, 8/6/93, (PB94-142767, A11, MF-A03).

NCEER-93-0015 "Proceedings from School Sites: Becoming Prepared for Earthquakes - Commemorating the Third Anniversary of the Loma Prieta Earthquake," Edited by F.E. Winslow and K.E.K. Ross, 8/16/93.

NCEER-93-0016 "Reconnaissance Report of Damage to Historic Monuments in Cairo, Egypt Following the October 12, 1992 Dahshur Earthquake," by D. Sykora, D. Look, G. Croci, E. Karaesmen and E. Karaesmen, 8/19/93, (PB94-142221, A08, MF-A02).

NCEER-93-0017 "The Island of Guam Earthquake of August 8, 1993," by S.W. Swan and S.K. Harris, 9/30/93, (PB94-141843, A04, MF-A01).

NCEER-93-0018 "Engineering Aspects of the October 12, 1992 Egyptian Earthquake," by A.W. Elgamal, M. Amer, K. Adalier and A. Abul-Fadl, 10/7/93, (PB94-141983, A05, MF-A01).

NCEER-93-0019 "Development of an Earthquake Motion Simulator and its Application in Dynamic Centrifuge Testing," by I. Krstelj, Supervised by J.H. Prevost, 10/23/93.

NCEER-93-0020 "NCEER-Taisei Corporation Research Program on Sliding Seismic Isolation Systems for Bridges: Experimental and Analytical Study of a Friction Pendulum System (FPS)," by M.C. Constantinou, P. Tsopelas, Y-S. Kim and S. Okamoto, 11/1/93, (PB94-142775, A08, MF-A02).

NCEER-93-0021 "Finite Element Modeling of Elastomeric Seismic Isolation Bearings," by L.J. Billings, Supervised by R. Shepherd, 11/8/93, to be published.

NCEER-93-0022 "Seismic Vulnerability of Equipment in Critical Facilities: Life-Safety and Operational Consequences," by K. Porter, G.S. Johnson, M.M. Zadeh, C. Scawthorn and S. Eder, 11/24/93.

NCEER-93-0023 "Hokkaido Nansei-oki, Japan Earthquake of July 12, 1993, by P.I. Yanev and C.R. Scawthorn, 12/23/93.

NCEER-94-0001 "An Evaluation of Seismic Serviceability of Water Supply Networks with Application to the San Francisco Auxiliary Water Supply System," by I. Markov, Supervised by M. Grigoriu and T. O'Rourke, 1/21/94.

NCEER-94-0002 "NCEER-Taisei Corporation Research Program on Sliding Seismic Isolation Systems for Bridges: Experimental and Analytical Study of Systems Consisting of Sliding Bearings, Rubber Restoring Force Devices and Fluid Dampers," Volumes I and II, by P. Tsopelas, S. Okamoto, M.C. Constantinou, D. Ozaki and S. Fujii, 2/4/94.

NCEER-94-0003 "A Markov Model for Local and Global Damage Indices in Seismic Analysis," by S. Rahman and M. Grigoriu, 2/18/94.

NCEER-94-0004 "Proceedings from the NCEER Workshop on Seismic Response of Masonry Infills," edited by D.P. Abrams, 3/1/94.

NCEER-94-0005 "The Northridge, California Earthquake of January 17, 1994: General Reconnaissance Report," edited by J.D. Goltz, 3/11/94.

NCEER-94-0006 "Seismic Energy Based Fatigue Damage Analysis of Bridge Columns: Part I - Evaluation of Seismic Capacity," by G.A. Chang and J.B. Mander, 3/14/94.

NCEER-94-0007 "Seismic Isolation of Multi-Story Frame Structures Using Spherical Sliding Isolation Systems," by T.M. Al-Hussaini, V.A. Zayas and M.C. Constantinou, 3/17/94.

NCEER-94-0008 "The Northridge, California Earthquake of January 17, 1994: Performance of Highway Bridges," edited by I.G. Buckle, 3/24/94.

NCEER-94-0009 "Proceedings of the Third U.S.-Japan Workshop on Earthquake Protective Systems for Bridges," edited by I.G. Buckle and I. Friedland, 3/31/94.

NCEER-94-0010 "3D-BASIS-ME: Computer Program for Nonlinear Dynamic Analysis of Seismically Isolated Single and Multiple Structures and Liquid Storage Tanks," by P.C. Tsopelas, M.C. Constantinou and A.M. Reinhorn, 4/12/94.

NCEER-94-0011 "The Northridge, California Earthquake of January 17, 1994: Performance of Gas Transmission Pipelines," by T.D. O'Rourke and M.C. Palmer, 5/16/94.

NCEER-94-0012 "Feasibility Study of Replacement Procedures and Earthquake Performance Related to Gas Transmission Pipelines," by T.D. O'Rourke and M.C. Palmer, 5/25/94.

NCEER-94-0013 "Seismic Energy Based Fatigue Damage Analysis of Bridge Columns: Part II - Evaluation of Seismic Demand," by G.A. Chang and J.B. Mander, 6/1/94, to be published.

NCEER-94-0014 "NCEER-Taisei Corporation Research Program on Sliding Seismic Isolation Systems for Bridges: Experimental and Analytical Study of a System Consisting of Sliding Bearings and Fluid Restoring Force/Damping Devices," by P. Tsopelas and M.C. Constantinou, 6/13/94.

NCEER-94-0015 "Generation of Hazard-Consistent Fragility Curves for Seismic Loss Estimation Studies," by H. Hwang and J-R. Huo, 6/14/94.

NCEER-94-0016 "Seismic Study of Building Frames with Added Energy-Absorbing Devices," by W.S. Pong, C.S. Tsai and G.C. Lee, 6/20/94.